universität wien

DISSERTATION

Titel der Dissertation

Marine nematode-bacteria symbiosis: New species and unexpected bacterial reproduction strategies.

verfasst von

Mag. rer. nat. Nikolaus Leisch

angestrebter akademischer Grad

Doctor of Philosophy (PhD)

Wien, 2014

Studienkennzahl lt. Studienblatt:	A 794 685 437
Dissertationsgebiet lt. Studienblattt:	Biologie
Betreut von:	Univ-Prof. Dr. Christa Schleper

"There are some oddities in the perspective with which we see the world. The fact that we live at the bottom of a deep gravity well, on the surface of a gas covered planet going around a nuclear fireball 90 million miles away and think this to be normal is obviously some indication of how skewed our perspective tends to be..."

Douglas Adams

Table of Contents

Thesis Outline

The material and data for this thesis were collected since September 2011 and resulted in six manuscripts so far, four of them published, one under review and one "ready for submission". In the following section I provide a short summary for each chapter and briefly describe the questions addressed and the results achieved of the individual manuscripts (Chapter 2-7). The central work of this thesis is presented in the Chapters 5-7. At the start of each chapter a statement detailing my contribution to the manuscript is provided.

Chapter 1 – Introduction is a short introduction into the history of bacteriology and presents an overview on the research in the field of bacterial cell biology. Additionally, the concepts underlying prokaryotic-eukaryotic relationships are explored and the subject of this thesis, the marine sub-family of the Stilbonematinae and its symbionts is introduced.

Electron microscopy was an important method for the analysis of the stilbonematid ectosymbionts. In **Chapter 2 - Preserving ultrastructure and morphology of tissue under laboratory and field conditions using PHEM buffered fixatives**, we adapted a buffer, originally proposed for the extraction of eukaryotic cytoskeleton, for the immersion fixation of specimen for electron microscopy. In comparative studies we could show that samples fixed with this PHEM-buffer resulted in superior ultrastructural preservation in both marine invertebrates and vertebrates. Most of the electron microscopy in the following chapters was done using this method.

During the sampling of stilbonematids of the genus *Eubostrichus*, we discovered a new species of both nematode host and gammaproteobacterial symbiont, which turned out to be suitable in terms of reliability of sampling and ease of handling during the experiments. **Chapter 3 - *Eubostrichus fertilis* sp. n., a new marine nematode (Desmodoridae, Stilbonematinae) with an extraordinary reproductive potential from Belize, Central America** is the formal description of the host, which was necessary to exclude any confusion with similar species that occur in the same habitat (e.g. *Eubostrichus parasitiferus*). In a similar manner, **Chapter 4 - Phylogenetic confirmation of the genus *Robbea***

GERLACH, 1956 (Nematoda Desmodoridae, Stilbonematinae) with the description of three new species represents the formal description of *Robbea hypermnestra* and two additional species of the genus *Robbea*. The genus *Robbea* was previously under dispute (Bayer et al. 2009), but the single-worm approach used for the PCR-based gene assay in this chapter corroborates it.

In **Chapter 5 - Growth in width and FtsZ ring longitudinal positioning in a gammaproteobacterial symbiont** I characterize the growth and division mode of the *Laxus oneistus* symbiont (Los). Using morphometric measurements of thousands cells, scanning electron microscopy of whole cells and transmission electron microscopy of whole cells and purified sacculi, I could show that the symbiont predominantly grows in width; by correlating morphology with FtsZ localization pattern I could show that longitudinal division is its default reproduction mode.

Co-occurring in the same habitat as *Laxus oneistus* is the nematode *Robbea hypermnestra*. Its symbiont (Rhs) forms a similar arrangement as that of *L. oneistus*. However, as I show in **Chapter 6 - Non-ring FtsZ-mediated cell constriction in a longitudinal dividing gammaproteobacterial symbiont**, the division in Rhs progresses asynchronously, starting at the apical, nematode-attached pole. This is mediated by a non-ring accumulation of FtsZ, and only when the apical pole has invaginated, a Z-ring forms and constriction occurs on both poles.

Chapter 7 - Size-independent symmetric division in extraordinarily long cells is addressing how non-septated filamentous bacteria with a length of up to 45 µm (in case of the *Eubostrichus fertilis* symbiont Efs) or 120 µm (in the case of the *Eubostrichus dianeae* symbiont Eds) divide. We show that both species divide by binary fission but Efs does so at virtually any length between 4 and 45 µm while Eds positions a single Z-ring in the middle of up to 120 µm long cells.

In **Chapter 8 – Conclusion and outlook**, selected characteristics of the symbionts and their division modes are discussed and an outlook for future research is given.

Appendix

A summary of the dissertation in English and German is provided in the appendix, as well as the acknowledgements and my *curriculum vitae*.

Chapter 1

Introduction

1.1. Bacteria and their discovery

Despite being the oldest known form of life (~3.5 billion years), microorganisms were only discovered in the late 17th century by the Dutch tradesman and scientist Antonie van Leeuwenhoek (Bulloch 1960, Noffke et al. 2013). Nevertheless, not until the second half of the 19th century did the existence and importance of microbes become universally accepted. The discovery of disease agents in this first golden age of microbiology gave rise to the field of immunology and the development of the first vaccines. The second golden age of microbiology during the first half of the 20th century, saw the birth of molecular genetics, the identification of the structure of DNA, the concept of the gene and the biochemical background of genetics (Maloy and Schaechter 2006, Madigan et al. 2008).

The seminal work of Woese and colleagues (Woese and Fox 1977) not only pointed out the existence of a third domain of life, the Archaea, but by developing a sequence-based phylogenetic framework for the identification of species, it spurred rapid advancement of sequencing and phylogenetic techniques in the years thereafter. The improvements in amplifying, sequencing and analyzing prokaryotic genes, as well as in labelling and imaging culminated in the development of the full cycle rRNA approach (Pace et al. 1986). This technique allowed the study of microbial diversity and distribution in the environment in greater detail and revealed that only 1% of the overall microbial biomass is reflected by cultivable organisms (Amann et al. 1995).

1.2. Bacterial cell biology

Bacteria come in a plethora of shapes and sizes and have evolved a variety of strategies to reproduce (e.g. budding, hyphal growth, daughter cell formation) (Angert 2005, Young 2006, Pinho et al. 2013). The seminal work of Bi and Lutkenhaus (1991) showed that the protein FtsZ forms a ring structure at the site of cell division in most bacteria. The discovery of a protein machinery that assembles at a certain sub-cellular location during the cell division process eventually gave rise to the field of bacterial cell biology as we know it today (Errington 2003). Many of the key components of the bacterial cell division

machinery and their function have been elucidated using model organism like *Escherichia coli, Bacillus subtilis* and *Caulobacter crescentus*. In the last two decades, the detailed study of growth and reproduction has also been extended to a few other model organisms like e.g. *Streptomyces,* gram-positive Actinobacteria, or *Staphylococcus aureus,* a gram positive bacterium of the phylum Firmicutes. Coinciding with this renewed interest in bacteria came rapid advances in technology. Whole genome sequencing became widely available major improvements were made in the field of fluorescent microscopy, pushing resolution beyond the diffraction limit, and GFP as marker for a protein of interest allowed the visualization of molecules in live cells (Chalfie et al. 1994, Gustafsson 2005, Betzig et al. 2006). These techniques, combined with the increasing capabilities of digital imaging and computational image analysis, allowed for more systematic and quantitative approaches (Myers 2012).

Binary fission is the most common strategy for bacterial cell division and, until now, also the best understood. In rod-shaped bacteria like *E. coli* or *B. subtilis*, the cell doubles in mass, places a septum at the division site and divides into two equal-sized daughter cells. Despite the apparent simplicity of this mechanism, binary fission is a highly orchestrated series of interdependent events. It requires that the cell doubles in mass and that the division machinery localizes to the correct place within the cell. Additionally, each daughter cell needs to receive a complete copy of the genome along with any other components, which are necessary for the functionality and viability of the offspring. Therefore, it needs to be well coordinated with the growth of the cell, the duplication of its genome and its segregation (Figure 1). The major mechanisms by which this coordination is achieved will be outlined in the rest of this chapter.

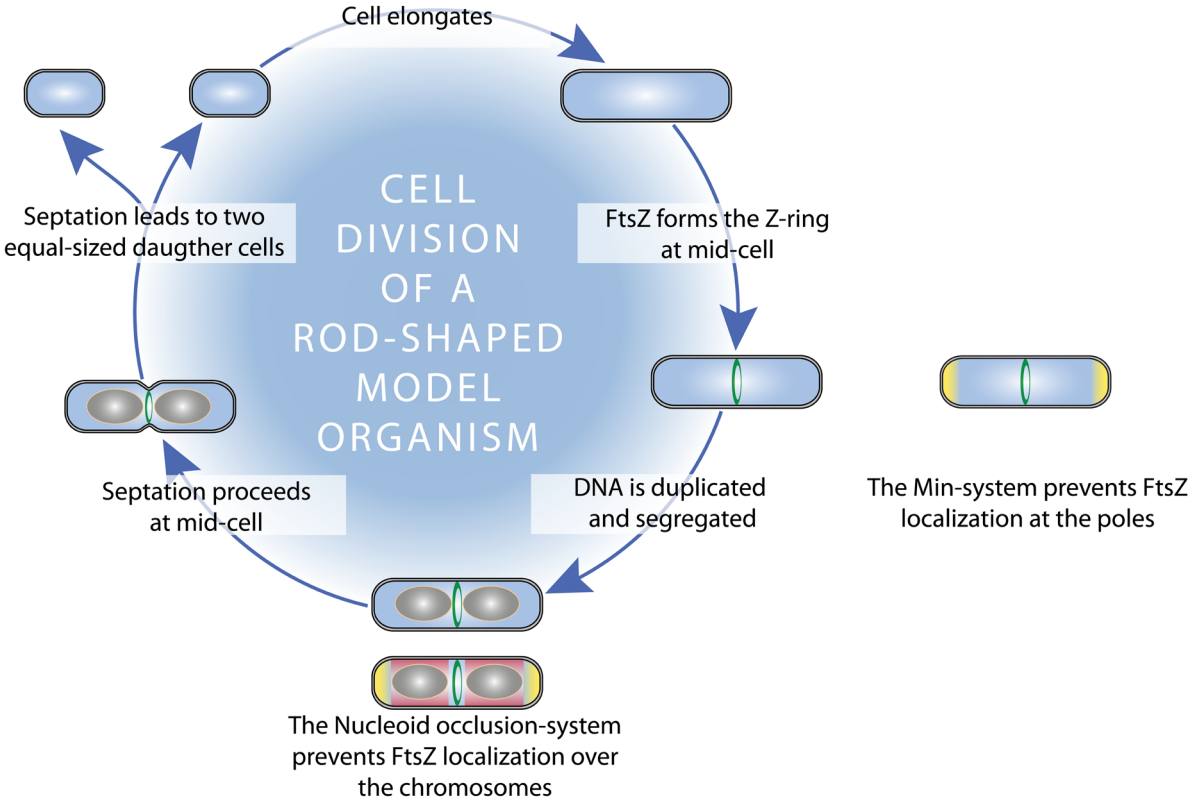

Figure 1: Simplified cell cycle of a model rod-shaped bacterium. The different stages of the cell cycle are shown in sequential form here, but many of the processes happen simultaneously. Min system-mediated inhibition of FtsZ is shown in yellow, nucleoid occlusion-mediated inhibition of FtsZ is shown in red.

1.2.1. Cell growth

Cell length can vary by two orders of magnitude between bacterial species, but the members of a single population of a bacterial species differ very little in length (e.g. *E. coli* cells show a difference of 1-4% in cell length at the time of cell division, depending on strain and growth conditions (reviewed in Young 2010)). Rod-shaped bacteria have two modes of growth.

On the one hand, cell elongation which happens as dispersed growth over the bulk of the cell cylinder and is coordinated by MreB (reviewed in Carballido-López 2006). MreB is the bacterial actin homologue, which forms filaments and interacts with inner membrane proteins and lipid synthesis enzymes (Teeffelen et al. 2011). When MreB is inhibited, cells do not elongate but increase their diameter and grow into spherical cells, indicating its role in maintaining the rod-like shape (reviewed in Typas et al. 2012, Ursell et al. 2014).

A recent study also demonstrated that MreB interacts with FtsZ, most likely delivering protein factors from the cell-wall elongation complex to mid-cell for the subsequent division event (Fenton and Gerdes 2013).

On the other hand, synthesis of the preseptal peptidoglycan (Nanninga 1991, Potluri et al. 2012) and the new cell poles (den Blaauwen et al. 2008), controlled by FtsZ which redirects peptidoglycan-synthesizing enzymes to mid-cell.

Nutrient availability strongly influences cell size as well, with cells growing longer under nutrient-rich conditions. Both *B. subtilis* and *E. coli* encode proteins that function as metabolic sensors (UgtP in *B. subtilis* and OpgH in *E. coli*), delaying cell division under nutrient rich conditions (Weart et al. 2007, Hill et al. 2013) and implying that cell length is under the control of the division apparatus.

1.2.2. FtsZ and the Z-ring

The central cell division protein is FtsZ, a guanosine triphosphatase which is the bacterial homolog of tubulin. FtsZ is highly conserved in bacteria and archaea but also found in chloroplasts and mitochondria of some eukaryotes (Gilson and Beech 2001, Osteryoung 2001, Vaughan et al. 2004, Margolin 2005). By hydrolyzing GTP, FtsZ polymerizes into linear protofilaments and forms the Z-ring underneath the cytoplasmic membrane (Bi and Lutkenhaus 1991, reviewed in Adams and Errington 2009). After assembling at the future division site, the Z-ring recruits additional proteins (the “divisome”) (Aarsman et al. 2005) and re-directs peptidoglycan synthesis to mid-cell (den Blaauwen et al. 2008, Potluri et al. 2012) before constriction is initiated. How constriction and septation is achieved in detail still requires further study, but FtsZ-based constriction and division of liposomes was shown in vitro (Osawa et al. 2008, Mingorance et al. 2010, Osawa and Erickson 2013), demonstrating that the Z-ring can generate a constricting force.

1.2.3. Positioning of the Z-ring

In rod-shaped bacteria, the Z-ring is positioned with high precision at the cell center

(Yu and Margolin 1999) and two key mechanisms that ensure its placement have been identified.

Min system: The *E. coli* Min system is a negative regulatory system, comprised of the three proteins MinC, D and E that prevents Z-ring formation at the cell pole (Figure 1, indicated in yellow) (de Boer et al. 1989). MinC is the effector protein in this system which prevents Z-ring assembly by binding to FtsZ and destabilizing and disrupting polymerized FtsZ (Hu and Lutkenhaus 2000, Shen and Lutkenhaus 2010). MinD is an ATPase (de Boer et al. 1991) which, in its ATP-bound form, binds to the cell membranes at the poles and recruits MinC (Hu and Lutkenhaus 2003). MinE acts as antagonist in this system: it competes with MinC for binding MinD and stimulates its ATPase activity, leading to the hydrolyzing of the bound ATP and thus causing MinD to dissociate from the membrane (Hu et al. 2003, Lackner et al. 2003). Consequently, in *E. coli* MinCD oscillate rapidly from pole to pole (Raskin and de Boer 1997, Raskin and de Boer 1999), binding and inhibiting Z-ring formation at each cell pole (reviewed in Lutkenhaus 2007). In contrast, the *B. subtilis* Min system lacks MinE and does not oscillate. Instead, MinCD is bound statically to the protein DivIVA which localizes to the cell poles, via the protein MinJ (Marston et al. 1998, Marston and Errington 1999, Bramkamp et al. 2008, Joyce and Daniel 2008).

Nucleoid occlusion: The second mechanism, nucleoid occlusion (NO), inhibits Z-ring formation in the vicinity of the chromosomal DNA (also called nucleoids) (Figure 1, indicated in red) (reviewed in Wu and Errington 2012). The non-homologous proteins SlmA in *E. coli* (Bernhardt and de Boer 2005) and Noc in *B. subtilis* (Wu and Errington 2004) localize over the nucleoid by binding to the DNA. Their exact way of preventing Z-ring formation is not entirely clear, but they seem to work differently in the respective organisms (Wu and Errington 2012).

Additional mechanisms: Recent data from *B. subtilis* and *E. coli* mutants lacking functional Min and NO systems show that these cells still position the Z-ring preferentially at mid-cell (Rodrigues and Harry 2012, Bailey et al. 2014). It has therefore been proposed

that there are additional factors that influence Z-ring positioning. In *E. coli* the protein MatP, which binds to the terminus region of the bacterial chromosome, is indicated to be a positive factor that influences cell division proteins to localize to the future division site (Bailey et al. 2014). The work on *B. subtilis* implies additional, so far unknown, positive factors (Moriya et al. 2010, Rodrigues and Harry 2012).

In the multinucleated sporulating cells of *Streptomyces coelicolor* the first positive factor – SsgB - has been identified. SsgB, which in turn is controlled by SsgA, localizes between the nucleoids prior to FtsZ and recruits FtsZ by direct interaction. During sporulation, multiple Z-rings are formed in a synchronized manner. It was suggested that a "conventional" Z-ring placement system (placement at one point in the cell) is insufficient to achieve this, while the SsgAB system allows for multiple FtsZ localization foci (Willemse et al. 2011).

In the Deltaproteobacterium *Myxococcus xanthus,* the protein PomZ localizes to the division site prior to FtsZ and is important for the correct positioning of the Z-ring (Treuner-Lange et al. 2013).

Additionally, the conformation of the cell membrane and its constituting lipids can influence protein localization and activity (Mileykovskaya and Dowhan 2005, Matsumoto et al. 2006).

1.3. Symbiosis

With the increase in awareness of the distribution and diversity of microbial life, understanding the interactions between different species became a field of growing interest (McFall-Ngai 2008, McFall-Ngai et al. 2013). The "living together of unlike organisms" is called symbiosis, a term coined by the German researcher Heinrich Anton de Bary working on lichen in the late 19th century (based on the Greek words "sýn" = with or together and "bíōsis" = living).

Symbiotic associations are divided into three main types: mutualism (both partners benefit from the association), commensalism (one partner benefits with the other not

being affected) and parasitism (one partner benefits on the expense of the other partner). Furthermore, it can be classified by the spatial localization of the symbiont (usually the smaller partner, often a microorganism) in relation to its host (usually the bigger partner, often a metazoan). In an ectosymbiosis, the symbiont is located on the outside of the host organism while in an endosymbiosis it resides within the host's body. Endosymbiosis can be further categorized as either intracellular or extracellular. Perhaps the most extreme examples of intracellular endosymbionts are the mitochondria and the plastids (reviewed in Dyall et al. 2004) of the eukaryotic cell. Due to their tight integration into the eukaryotic cell (e.g. gene loss, transfer of genes to the host nucleus) they are by now classified as cell-organelles.

Last but not least, it is necessary to distinguish how the interaction is maintained over multiple host generations. Vertically transmitted symbioses are considered permanent associations and show either little or no aposymbiotic phase (the phase where the two partners live separated from each other) during the host's lifecycle. The symbionts are often transmitted through the female germ line and thus passed on from one generation to the next. In vertically transmitted symbioses often co-speciation can be observed, as well as reduction of the symbionts genome, since any evolutionary pressure is influencing the whole association and the symbiont loses "non-essential" genes (reviewed in Bright and Bulgheresi 2010).

On the other hand, if the host needs to re-acquire the symbiont from the environment every generation anew, it is called horizontal transmission. In such cases, the aposymbiotic phase can be longer than in vertical transmitted symbioses, and a host-symbiont recognition mechanism needs to be in place. This is often mediated by host-secreted mucus and bacterial surface appendages (e.g. pili). In such symbioses, co-speciation and genome reduction are less common as both partners need to cope with an aposymbiotic phase (reviewed in Bright and Bulgheresi 2010).

Mutualistic interactions allow partners with different capabilities to increase the fitness

of both partners and to extend their range of suitable habitats (Boucher et al. 1982). Such an interaction can for example improve nutritional capabilities (e.g. aphids, plant sap-feeding insects, carry endosymbionts that complement their carbohydrate-rich diet by synthesizing essential amino acids (reviewed in Douglas 2011)). It can provide the host with bioluminescence for camouflage purposes; for example the bobtail squid *E. scolopes* develops a special symbiont housing organ in which the symbiont *V. fisheri* resides and generates bioluminescence (reviewed inMcFall-Ngai 2014). It can also be of a defensive nature, e.g. the symbiont of the marine bryozoan *Bugula neritina* produces compounds that protect its host from biofouling and grazing, and the host's larva from predation (Sharp et al. 2007).

1.3.1. Chemoautotrophic symbioses

While photoautotrophic organisms play an important role in the oceans, they are restricted to the upper 200 meters of the water column, and few millimeters in sediments. In many habitats where photosynthesis is restricted or not possible, microorganisms perform chemosynthesis instead. These primary producers use the energy gained from the oxidation of reduced inorganic compounds (e.g. sulfide, ammonium or methane) to fix carbon. Conditions that favor such a lifestyle are usually found around hot vents or around decomposing organic matter.

Symbioses with chemosynthetic microbes were first described from the hydrothermal vent fields at the Galapagos Rift. The giant (up to 2m in length) tubeworm *Riftia pachyptila* has no mouth or gut; instead, it has a special organ which houses its endosymbiont, the trophosome. The host provides the symbiont with both oxygen and sulfide to fuel its chemoautotrophic metabolism and in return receives fixed carbon (Cavanaugh et al. 1981, Felbeck et al. 1981, for overview see Bright et al. 2013). Since the discovery of *Riftia*, animals of many taxa, living in symbiosis with chemoautotrophic symbionts, have been described (see Figure 2); many of them are members of the meiofauna in shallow-water sediments (reviewed in Dubilier et al. 2008).

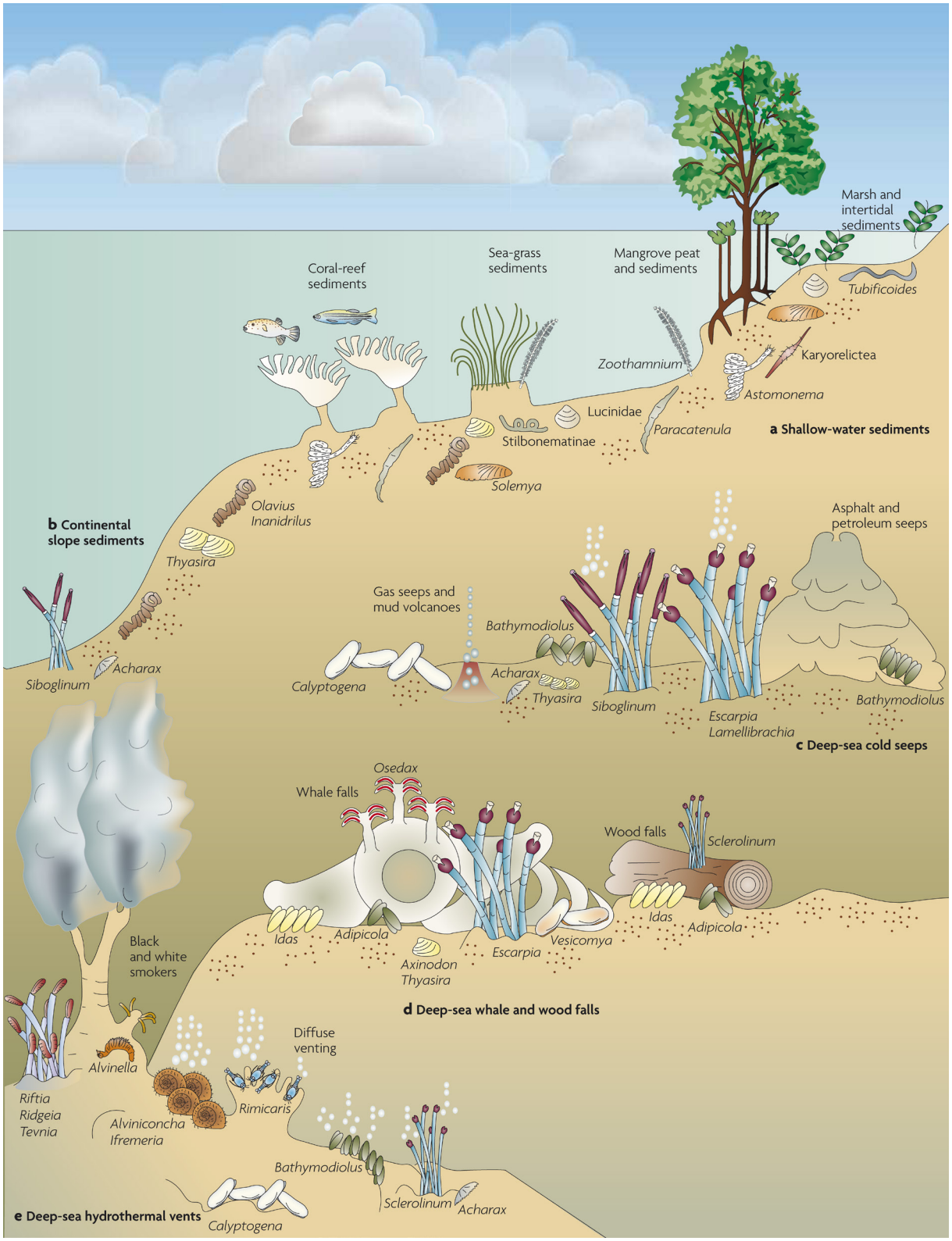

Figure 2: Overview of marine chemoautotrophic symbioses in different marine habitats. This kind of associations are found in all depths in the ocean, from (a) shallow water sediments, (b) continental slope sediments, (c) cold seeps, (d) whale and wood falls to (e) hydrothermal vents. Species are not drawn in scale (from Dubilier et al. 2008).

1.3.2. Stilbonematids

Among the symbiotic meiofauna are the free-living desmodorid nematodes of the subfamily Stilbonematinae, which occur worldwide in sulfidic sediments (reviewed in Ott et al. 2004, Tchesunov 2013). The cuticle of each species is covered by a specific sulfur-oxidizing symbiont (Polz et al. 1994, Bayer et al. 2009, Bulgheresi et al. 2011, Pende et al. 2014). By migrating between the oxygenated sediment layers and the anoxic, sulfide rich sediment layers, the nematodes provide their symbionts with the electron acceptor (oxygen) and donor (e.g. hydrogen sulfide, thiosulfate) they need to fuel their chemoautotrophic lifestyle (Ott et al. 1991). Stable isotope analysis indicates that the organic carbon compounds synthesized by the symbiont are transferred to the host. However, how this nutritional transfer takes place is still under investigation (Ott et al. 1991). Additionally, the symbiont, by taking up e.g. hydrogen sulfide, may play a role in protecting the worm from toxic compounds (Hentschel et al. 1999).

Located underneath the worms cuticle are complex glandular sense organs, which so far are only found in members of the Stilbonematinae (Nebelsick et al. 1992, Bauer-Nebelsick et al. 1995). They secrete mucus to the outside of the worm via hollow setae, covering the symbiont. Along with the mucus, they secret a family of calcium-dependent lectins, called the Mermaids, which mediate specific symbiont attachment (Bulgheresi et al. 2006, Bulgheresi et al. 2011).

All of the symbionts characterized so far are basal *Gammaproteobacteria* (Polz et al. 1994, Bayer et al. 2009, Bulgheresi et al. 2011, Pende et al. 2014) and belong to the "**M**arine **O**ligochaete and **N**ematode **T**hiotropic **S**ymbionts" cluster (MONTS). This cluster also includes endosymbionts of gutless nematodes and oligochaetes (Bayer et al. 2009). Under incident light, the worm appears bright white, which is attributed to the symbionts sulfur inclusions (Polz et al. 1992, Himmel et al. 2009).

In this thesis, the following four species were investigated (Figure 3).The species ***Laxus oneistus*** (Figure 3A) and ***Robbea hypermnestra*** (Figure 3B) are both covered by a monolayer of rod-shaped bacteria (termed **Los** (*Laxus oneistus* symbiont) and **Rhs** (*Robbea hypermnestra* symbiont) (Figure 3E and 3I, 3F and 3J respectively)), arranged like a columnar epithelium. The anterior region of both species is free of symbionts and the length of this symbiont-free region depends on the sex of the worm. Both species co-occur in the same habitat in coarse back reef sediments of the Belizean Barrier reef.

The species ***Eubostrichus fertilis*** (Figure 3C) and ***Eubostrichus dianeae*** (Figure 3D) carry filamentous bacteria which colonize their cuticle. The *E. fertilis* symbiont (**Efs**) is crescent shaped and attaches with both poles to the cuticle (Figure 3G and 3K), while the symbiont of *E. dianeae* (**Eds**) attaches with one pole to the cuticle (Figure 3H and 3L). Both worms are found in the fine sediments overlaying mangrove peat.

The Stilbonematids form the only metazoan sub-family in which all members engage in a binary ectosymbiosis with bacteria. Although none of the symbionts are cultivable so far, it is possible to harvest a virtually pure culture of symbionts from each nematode host.

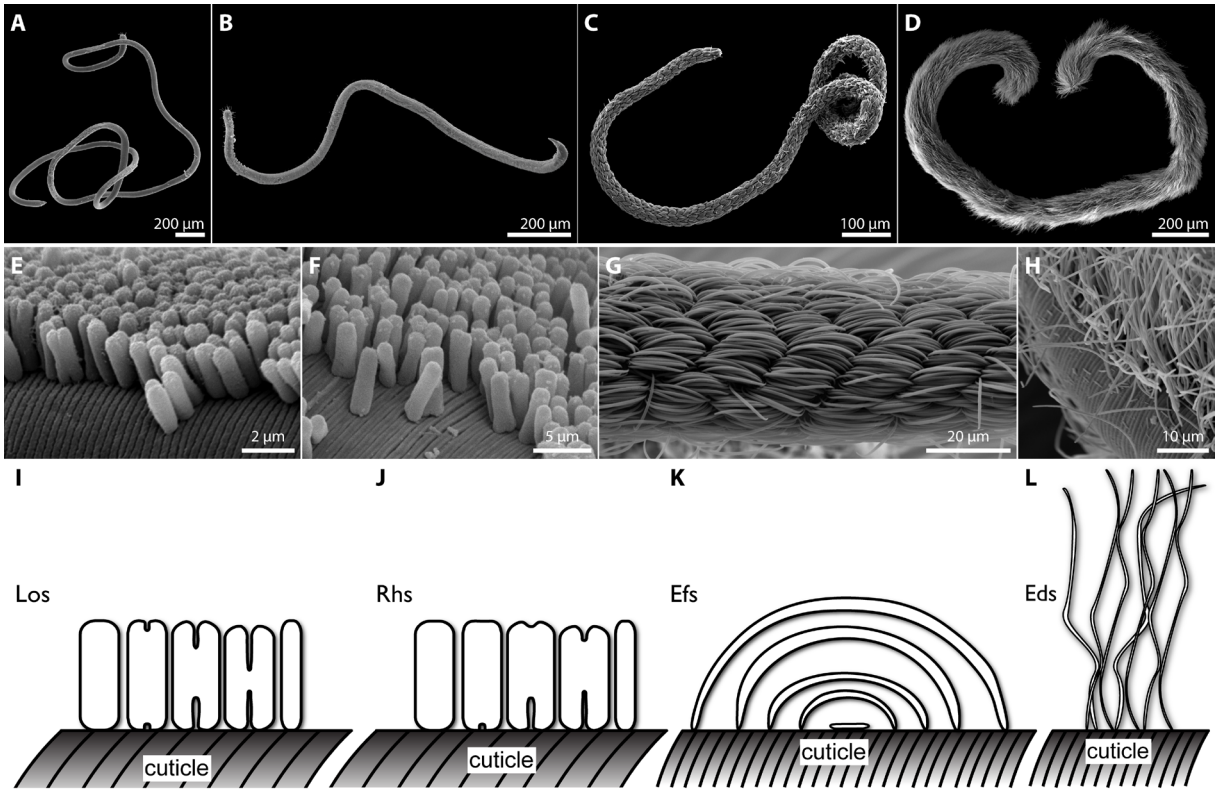

Figure 3: Scanning electron micrographs of the stilbonematid nematodes, their symbionts and simplified drawings of the arrangement of each symbiont on its host. (A) and (E) show *Laxus oneistus* and its symbionts attached to the cuticle, (B) and (F) show *Robbea hypermnestra* and its symbiont, (C) and (G) show *Eubostrichus fertilis* and its symbiont and (D) and (H) show *Eubostrichus dianeae* and its symbiont. (I-L) are simplified drawings of the attachment of the respective symbionts to their hosts.

Major Goals

Although bacterial cell division has been intensely studied, especially in the last two decades, the main focus has been on few model organisms. However, recently a number of plant and animal-associated bacteria have been found to grow and reproduce abnormally. Therefore, we decided to investigate the fundamental process of cell division in the ectosymbionts of the free living marine nematodes of the sub-family Stilbonematinae. These symbionts belong to the *Gammaproteobacteria,* just like the model organism of bacterial cell biology, *E. coli*.

The overall goal of my Ph.D. was to increase the knowledge of bacterial cell biology of

non-model organisms. By comparing the cellular and molecular mechanisms underlying cell division in these basal gammaproteobacterial ectosymbionts with those in the model organism *E. coli* I aim to understand the conserved motifs of bacterial cell division.

The first goal was to characterize the growth and division mode of two rod-shaped symbionts, Los and Rhs, whose hosts co-occur in the same habitat. This was done using automated image analysis which resulted in morphometric measurements of thousands of cells, as well as electron microscopy-based analyses. Additionally, the sub-cellular localization of the cell division protein FtsZ was recorded and analyzed.

The second goal was the analysis of two filamentous symbionts (Efs and Eds) and their growth and division pattern. As these symbionts were not yet described, a first step was to confirm that both symbionts form a monoculture using fluorescence *in-situ* hybridization. Morphometric data was recorded using light and electron microscopy. Furthermore, FtsZ and DNA localization patterns of these extraordinarily long cells were analyzed and their implications discussed.

The description of the nematode hosts was an additional goal. Many of the species are not yet described and a proper identification was needed. To address this, four new species of stilbonematid worms were formally described, using light and electron microscopy as well as PCR-based molecular phylogeny.

An additional goal was the optimal preservation of specimen in the field for electron microscopy, as this technique played a crucial role in the analysis of stilbonematid ectosymbionts. A buffer was adapted for immersion fixation and extensive comparative studies showed that its application resulted in superior ultrastructural preservation.

Chapter 2

Preserving ultrastructure and morphology of tissue using PHEM buffered fixatives

Authors Jacqueline Montanaro* and Nikolaus Leisch*, Daniela Gruber, Aleksandra Inic-Kanada, Sandra Belij, Elizabeth Stein, Nora Bintner, Angela Ladurner and Talin Barisani-Asenbauer

*these authors contributed equally

Keywords electron microscopy, immersion fixation, marine invertebrates, vertebrates, kidney

Publication status Manuscript since 2014-11-06 under review at Journal of Microscopy

Detailed description of NL's contribution

a. designed the study together with JM

b. performed the osmolarity measurements

c. performed electron microscopy of the marine invertebrates

d. analyzed the data and prepared the figures

e. wrote the manuscript together with JM

Abstract

Chemical fixation is widely used for the preparation of electron microscopy samples. This crucial step can strongly influence the quality of the final result, and depends on the buffer and fixative. In this study, we adapted the non-toxic PHEM buffer (PIPES, HEPES, EGTA and MgCl2) to form an isotonic fixative in combination with glutaraldehyde, for immersion fixation. We compared the resulting ultrastructure of both mammalian (mouse kidney tubules) and marine invertebrate (acoel) tissue when fixed with either the PHEM-fixative combinations or conventional fixatives. The use of PHEM buffer resulted in excellent structural preservation (e.g. enhanced membrane visibility). Importantly, using this isosmotic fixative, neither the mammalian nor the marine sample showed shrinkage artifacts. These isotonic PHEM-glutaraldehyde fixatives, when compared to standard methods, resulted in equal or better ultrastructural preservation.

Introduction

The first and most crucial step for successful EM analysis is the fixation of the specimen to preserve the ultrastructure of cells with minimal alteration from the living state (Hayat 2000). There are currently two methods regularly used for sample fixation. On the one hand high-pressure freezing which relies on rapid cooling to vitrify the water in the sample and is followed by dehydration at ultra-low temperatures (freeze-substitution) and on the other hand chemical fixation (Kuo 2007). Chemical fixation remains the most widely used method for preserving biological specimens for electron microscopy. Cellular components and ultrastructural details are adequately preserved, whilst the technique itself is easy to apply and requires minimal equipment and expertise (Hayat 2000).

Chemical immersion fixation is conventionally based on aldehydes such as glutaraldehyde

(GA) or formaldehyde (FA) or a combination of both (e.g. Karnovskys (Karnovsky 1965)) (Hayat 2002, Dykstra and Reuss 2003). Regardless of which fixative is used, any artifact or structural changes introduced during the fixation step (e.g. due to changes of pH or osmolarity), cannot be corrected in later stages and may lead to poor preservation. Particularly, changes in osmolarity can cause shrinkage or swelling of tissue and such artifacts hinder the interpretation of ultrastructural morphology or can even lead to wrong interpretations.

The most commonly used buffers for ultrastructure fixation are cacodylate buffer and phosphate buffer (Dykstra and Reuss 2003). For fixation of marine invertebrates, diluted seawater can be used, otherwise sucrose is often added to buffers to increase their osmolarity (Dykstra and Reuss 2003, Ettensohn et al. 2004). The buffer needs to act as solvent for the fixative, maintain a specific pH and convey tonicity to the final fixative solution. All of the above buffers come with trade-offs; e.g. phosphate buffer can cause precipitation artifacts in the tissue (Przysiezniak and Spencer 1989, Hayat 2000). Seawater is, by nature, isotonic to marine samples but has little buffering capacity. Cacodylate buffer contains arsenic and can have a toxic effect on the sample prior to fixation, which can alter membrane permeability and affect subcellular preservation. Additionally, arsenic gas can be produced in presence of acids, posing a health hazard. According to the Globally Harmonized System of Classification and Labeling of Chemicals, it must be disposed of as hazardous waste (Electron Microscopy Sciences 08/2013). Some toxic components are essential for electron microscopy (e.g. fixative for immersion fixation) however, there has been a concerted effort to reduce the toxic materials used (e.g.: replacing uranyl acetate with either gadolinium or samarium (Nakakoshi et al. 2011)).

The non-toxic PHEM buffer has a wide pH range, good buffering capacity and causes no

precipitations with any reagents used during sample processing. It is a combination of the two zwitterionic chemicals PIPES and HEPES with EGTA and MgCl2 and was proposed by Schliwa and van Blerkom in (1981). HEPES seems to stabilize the lipid components of cell membranes and PIPES causes retention of cellular material, reduces lipid loss in the cells and facilitates extensive cross-linking of cellular material (Hayat 2000). The addition of EGTA, a chelating agent with a high affinity for calcium ions, as well as magnesium chloride enhances the preservation of microtubules and membranes. Therefore, PHEM would seem an ideal electron microscopy buffer. However, until now, its traditional use has been limited to extraction stabilization of eukaryotic cytoskeleton, immunofluorescence applications (in e.g. *Dictyostelium discoideum* (Koonce and Gräf 2010), embryos of *Danio rerio* (reviewed in Schieber et al. 2010)) as well as immuno-electron microscopy (in e.g. *Saccharomyces cerevisiae* (Griffith et al. 2008)) of either single cell organisms or cell culture monolayers.

In this study we explored the potential of PHEM buffered fixation for both mammalian and marine samples. Kidney tissue is a dense and heterogeneous complex of different cells, where a four times range of osmolarities can be present between the cells. This renders optimal fixation of all cells in this tissue very difficult (Hayat 1981, Kriz and Kaissling 2012). In this fixative comparison study, we focused on both distal convoluted tubules (DCT) and proximal tubules (PT) to assess the quality of fixation at the ultrastructural level. The lumenal cell membranes of DCT and PT cells differ by the presence (in PT) or absence (in DCT) of the apical brush border microvilli (Kriz and Kaissling 2012). At the base of these tubule cells, both types have large, elongated mitochondria encased by deep folds of the plasma membrane. These membrane infoldings, together with the interdigitating basal ridges, collectively form the basal labyrinth structure (Pavelka and Roth 2010).

The marine invertebrate *Convolutriloba longifissura* Bartolomaeus and Balzer, 1997 (Xenacoelomorpha, Acoela) is ~3-5mm long, occurs in shallow coral reefs and harbors symbiotic photosynthetic algae within its body as well as extrusomes, the sagittocysts. These needle-shaped secretory products are often surrounded by a muscle mantle and are used for copulation, defense and probably capture of prey for nutrition (Gschwentner et al. 1999, Gschwentner et al. 2002).

The aim of this study was to explore the usage of PHEM buffer in combination with glutaraldehyde for the fixation of different tissue samples (mammalian and marine) and suggest it as a viable alternative to established fixatives, such as Karnovskys. We measured the osmolarity of the different buffers and fixatives, adapted the concentration of the PHEM buffer and formulated new isosmotic buffer-fixative combinations. These new formulations were compared to established buffer-fixative combinations using either mouse kidney tissue or the marine invertebrate C. longifissura.

Methods

Ethics Statement

All animal work has been conducted according to relevant national and international guidelines.

Eight-week-old BALB/c female mice were used in the mammalian experiments. The mouse tissue used in this study was excess of other ongoing experiments at the Institute of Virology, Vaccines and Sera - Torlak, Serbia. All experiments were approved by the "Ethics Committee for the Welfare of Experimental Animals" and by the Torlak committee section and conformed to the Serbian laws and European regulations on animal welfare (Approval No. 011-00-00510/2011-05/2).

Specimens of *Convolutriloba longifissura*, were provided by the public aquarium Haus des Meeres - Vienna.

Osmolarity measurements and buffer preparations

Osmolarity of seawater (salinity 35 PSU), buffer and fixative solutions was measured using either an Osmomat 030 (Gonotec, Germany) or an Advanced Micro Osmometer Model 3MO Plus (Advanced Instruments, USA). All samples were tested in duplicate and measured independently three times. Mean values of sample readings were used for further calculations.

A 10X stock solution of the PHEM buffer was prepared according to (Schliwa and van Blerkom 1981) by dissolving 18.14 g (600 mM) PIPES (Merck, Germany), 5.96 g (250 mM) HEPES (Merck, Germany), 3.805 g (100 mM) EGTA (VWR, USA) and 0.41 g (20 mM) MgCl2 (Merck, Germany) in 100 ml of ddH2O. When mixing the components the pH needed to be raised above 7.0 with KOH for them to dissolve. Final pH was adjusted to 7.4. Our studies showed, that this stock solution can be stored frozen for at least a year without any obvious detrimental effect. All fixatives solutions were prepared from freshly made 20% paraformaldehyde or 25% glutaraldehyde solutions, according to Table 1.

Sampling and specimen preparations

Mouse kidney was dissected and immediately plunged into a pool of either modified Karnovsky's or isotonic PHEM-GA fixative solution (Table 1) while being minced into smaller pieces of 1 x 0.5 x 0.5 mm. Tissues remained in fixative for 1 h at RT with agitation, and then stored overnight at 4°C before processing to resin. The tissue was washed in the respective buffer (0.1M cacodylate buffer or 1.5X PHEM), and then post-fixed with 0.5% aqueous osmium tetroxide (Electron Microscopy Sciences, USA) for 1 h. After briefly rinsing in water, tissue was dehydrated in 70% acetone for 10 min, followed by 3 times 10

min changes of absolute acetone. Tissues were infiltrated with 1:1 acetone- Low Viscosity Resin (Agar Scientific, United Kingdom) mixtures for 5 min, changed into fresh mixture 1:1 acetone-resin for further 25 min before infiltration with pure resin for 2 times 1 h at room temperature. Tissue samples were then changed into fresh resin and polymerized 48 h at 60°C.

C. longifissura specimens were fixed with isotonic PHEM-GA, a modified Karnovsky's variant or seawater-GA fixative (Table 1) for 1 h at room temperature. After washing with the corresponding buffer (4.25X PHEM, 0.1M cacodylate buffer with 10% sucrose added or filtered seawater) three times, they were post-fixed with 1% osmium tetroxide in ddH2O for 1 h. The samples were then dehydrated in a graded ethanol series (50 %, 70 %, 100 % twice), transferred into 100 % dry acetone, and infiltrated with a 50/50 mixture of acetone and Low Viscosity Resin for 30 min. After 2 h of infiltration in pure LVR resin the samples were then polymerized at 60°C in the oven for 12 h.

80 nm ultra-thin sections were cut with an Ultracut S (Leica Microsystem, Austria), mounted on formvar coated slot grids (Agar Scientific, United Kingdom) and contrasted with 0.5 % aqueous uranyl acetate (Leica Microsystem, Austria) for 20 min and with 2 % Reynold's lead citrate (Leica Microsystems, Austria) for 6 min. Ultrathin sections for Figures 1-4 were imaged at 120 kV on a Libra 120 transmission electron microscope (Zeiss, Germany). Ultrathin sections for Figure 5 and Supplementary figures were imaged at 80 kV on an EM 902 transmission electron microscope (Zeiss, Germany). Images were recorded with a SharpEye camera system (Olympus, Japan) using the AnalySIS 5.0 program (Olympus, Japan). Images were processed using Photoshop CS6 and Illustrator CS6 (Adobe Systems, Inc., USA).

Results and Discussion

Osmolarity measurements and buffer compositions

We measured the osmolarity of the fixative (2.5 % glutaraldehyde (Carl Roth, Germany) in ddH2O), sterile filtered seawater and a dilution series of the PHEM buffer (Table 1, highlighted in yellow) as well as the working solutions of buffer and fixatives for marine (Table 1, highlighted in blue) and vertebrate tissue (Table 1, highlighted in green). To allow for easier adaptation to other organisms and/or other techniques, we have provided additional osmolarity measurements of PHEM buffer with a wider range of GA and FA combinations (Supplementary Table 1).

For the mammalian tissue the low PHEM buffer concentration of 0.06X with 2.5% glutaraldehyde (**mamP**) was isosmotic to plasma and the kidney cortex (Table 1). We compared this fixation with the standard modified Karnovsky's containing 2.5 % GA and 2 % FA in 0.1 M cacodylate buffer (**mamK**).

For marine samples, our measurements showed that 2.5 % GA combined with 3X PHEM (**marP**) was isosmotic to seawater (Table 1). We compared marP with the two most commonly used fixatives for marine invertebrates in our lab (e.g. (Klepal et al. 2010)). A Karnovsky's fixative variant with 2.5 % GA and 4 % FA (Carl Roth, Germany) in 0.1 M cacodylate (Electron Microscopy Sciences, USA) buffer with 10 % sucrose (Sigma-Aldrich, USA) added, (**marK**) And diluted filtered seawater (80 %) with 2.5 % GA (**fsG**).

Replacement of toxic solutions with non-toxic alternatives in electron microscopy samples preparation protects the researchers' health and reduces toxic waste. It is however important that non-toxic alternatives provide equal or better ultrastructural morphology. The innate toxicity of cacodylate buffer has been viewed as beneficial, preventing contamination and degradation due to microorganisms during prolonged

sample storage. However, routine EM work often goes from initial sampling all the way to resin embedding within 1 or 2 days. Moreover, protective agents can be added for long-term storage if required. By using PHEM buffer as an alternative to cacodylate buffer, less hazardous waste for disposal is produced.

Comparing PHEM-buffered fixation with standard fixation in mammalian tissue

Mouse kidney tissue was subjected to either mamK or mamP fixation and the ultrastructure of the DCT or PT cells was explored.

The distal convoluted tubule cells of the mouse kidney

The DCT cells showed overall good fixation in both the mamK (Figure 1) and the mamP fixative (Figure2). The nucleus (n) of the mamK cell was well preserved (Figure 1 A). The nuclear pores appeared very prominent (Figure 1 B) due to a separation of the nuclear membranes, visible as a gap between the nucleus (Figure 1 B) and the cytoplasm. The numerous elongated mitochondria (m) (Figure 1 A and C) were well-preserved with many parallel, fine cristae. The interdigitations of the basal labyrinth (bl) showed clear spaces between the membranes (Figure 1 A and C) and the basement membrane (bm) (Figure 1 D) showed minor variation in density.

The mamP fixed DCT cell (Figure 2 A) showed very good preservation with well-defined cell membranes. The nucleus (n) (Figure 2 A and B) had parallel nuclear membranes and clearly defined, small nuclear pores. The mitochondria (m) (Figure 2 A and C) showed clear parallel cristae and visible membranes outlined them. The membranes of the basal labyrinth (bl) revealed no gaps between them and the extracellular basal membrane (bm) was homogenous (Figure 2 A and D).

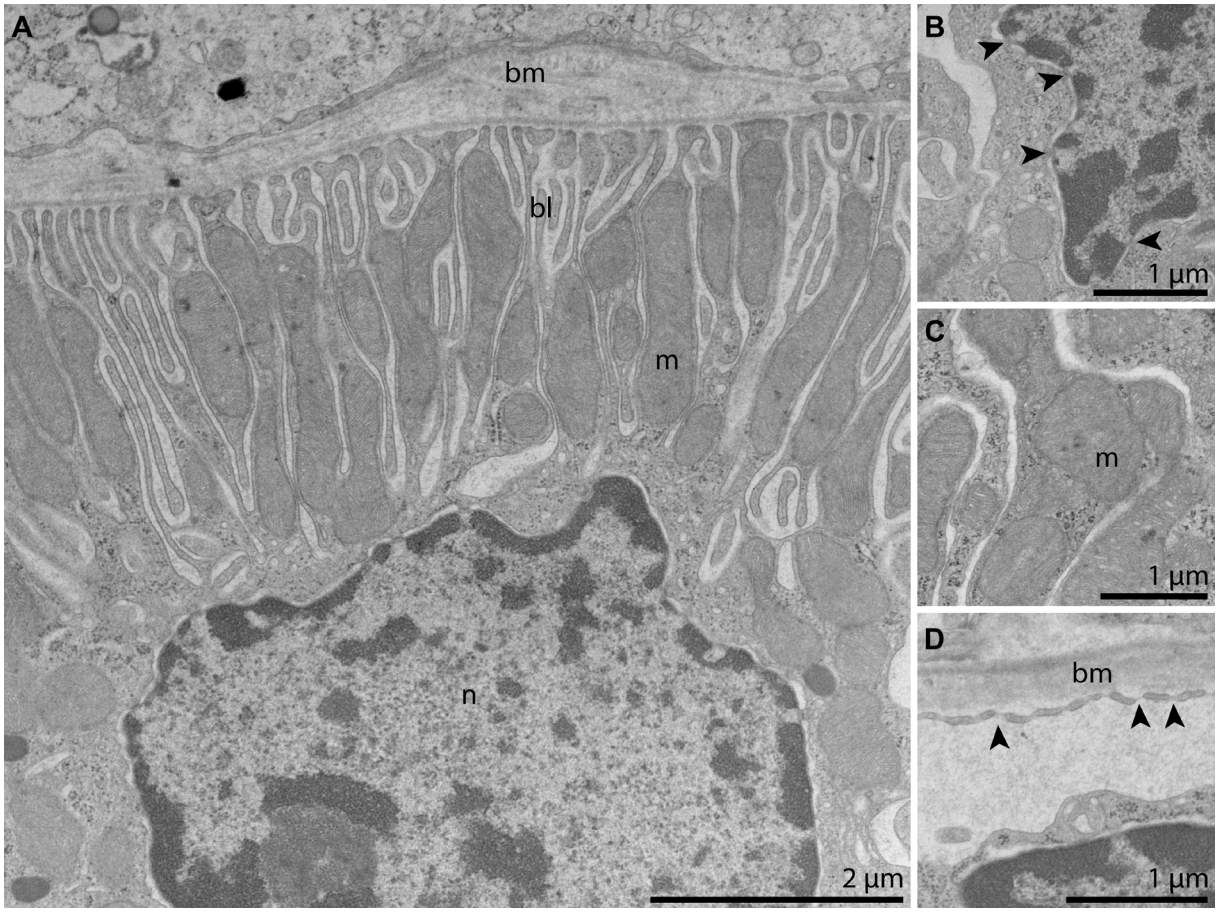

Figure 1: Overview and details of a distal convoluted tubule cell of the mouse kidney fixed with modified Karnovsky's.
(A) shows an overview with the nucleus (n), mitochondria (m) the basal labyrinth (bl) and the basement membrane (bm). (B) shows a detail of the nucleus (n) with the nuclear pores (arrowheads). (C) is a higher magnification of the mitochondria (m) a nd (D) a higher magnification of the basement membrane (bm) with arrowheads pointing to fenestrated capillary epithelial cells.

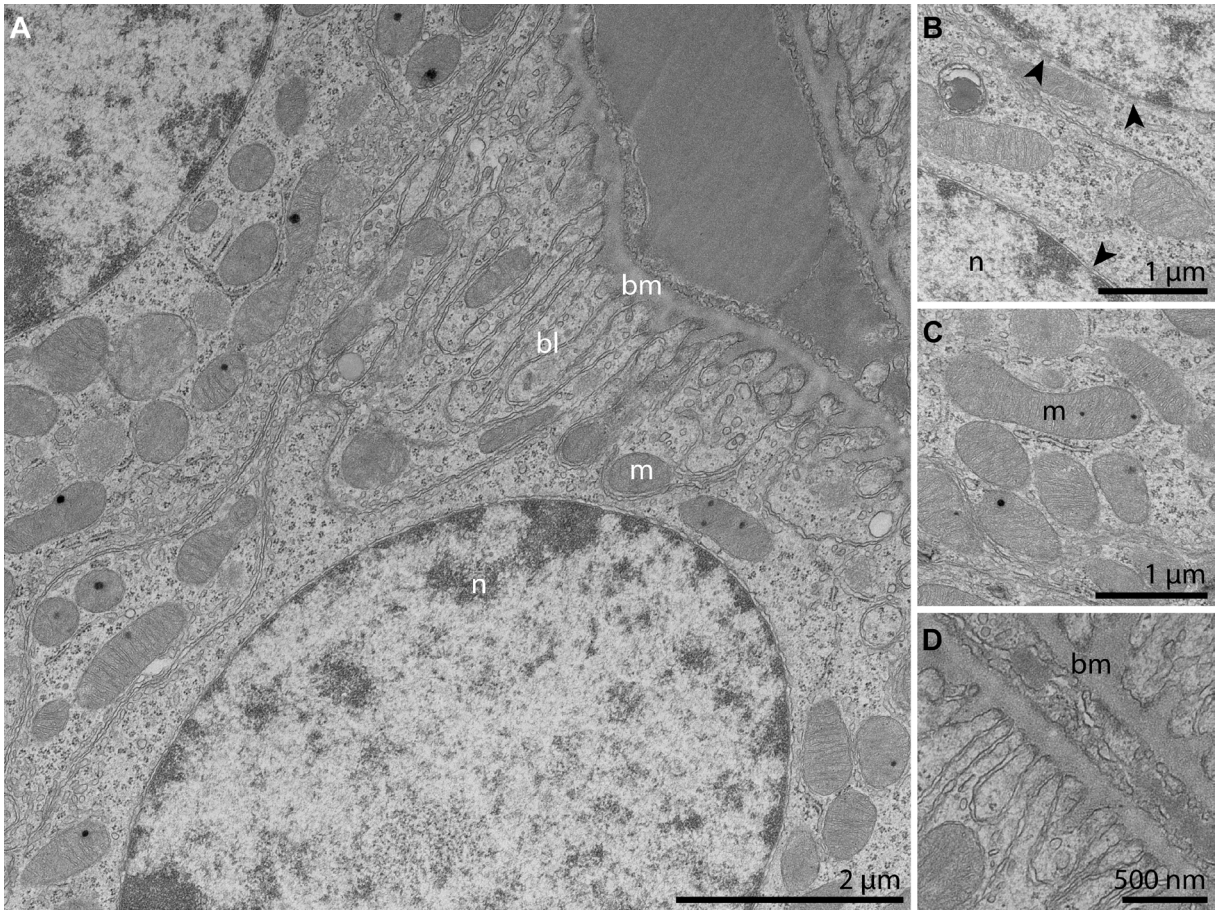

Figure 2: Overview and details of a distal convoluted tubule cell of the mouse kidney fixed with mammalian PHEM-GA.
(A) shows an overview with the nucleus (n), mitochondria (m) the basal labyrinth (bl) and the basement membrane (bm). (B) shows a detail of the nucleus (n) with the nuclear pores (arrowheads). (C) shows details of the mitochondria (m) and (D) details of the basement membrane (bm).

The proximal tubule cells of the mouse kidney

The PT cell fixed with mamK (Figure 3) exhibited a well-defined nucleus (n) with prominent nuclear pores (Figure 3 A), and a very dense brush border (bb). The elongated mitochondria (m) showed slight separation of the cristae (Figure 3 A and B), the infoldings of the membranes of the basal labyrinth (bl) were slightly separated and the basement membrane was homogenous (Figure 3 C).

The PT cells fixed with mamP had well-defined nuclei (n) with small distinct nuclear pores (Figure 4 A), and the membranes of the brush border (bb) were easily distinguishable

(Figure 4 A and B). At the base of the brush border, a tight junction (tj) was visible (Figure 4 A and B). The mitochondria (m) and their cristae were well preserved (Figure 4 A and B). The basal labyrinth (bl) showed no separation between the membranes and the extracellular basement membrane (bm) was homogenous (Figure 4 C).

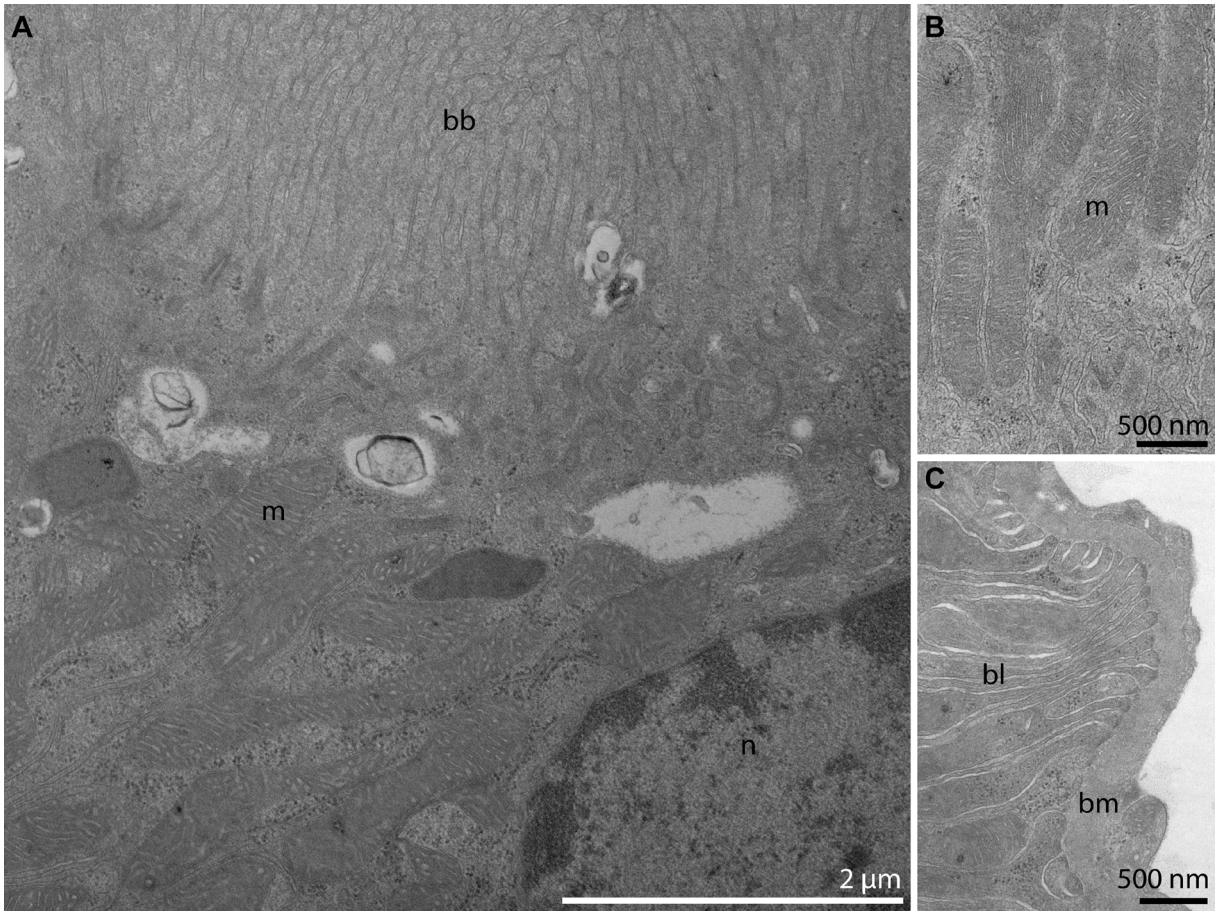

Figure 3: Overview and details of a proximal tubule cell of the mouse kidney fixed with modified Karnovsky's.
(A) shows an overview with the nucleus (n), the brush border (bb, highlighted in yellow) and the mitochondria (m). (B) shows details of the mitochondria (m). (C) is a high magnification of the basement membrane (bm) and the basal labyrinth (bl).

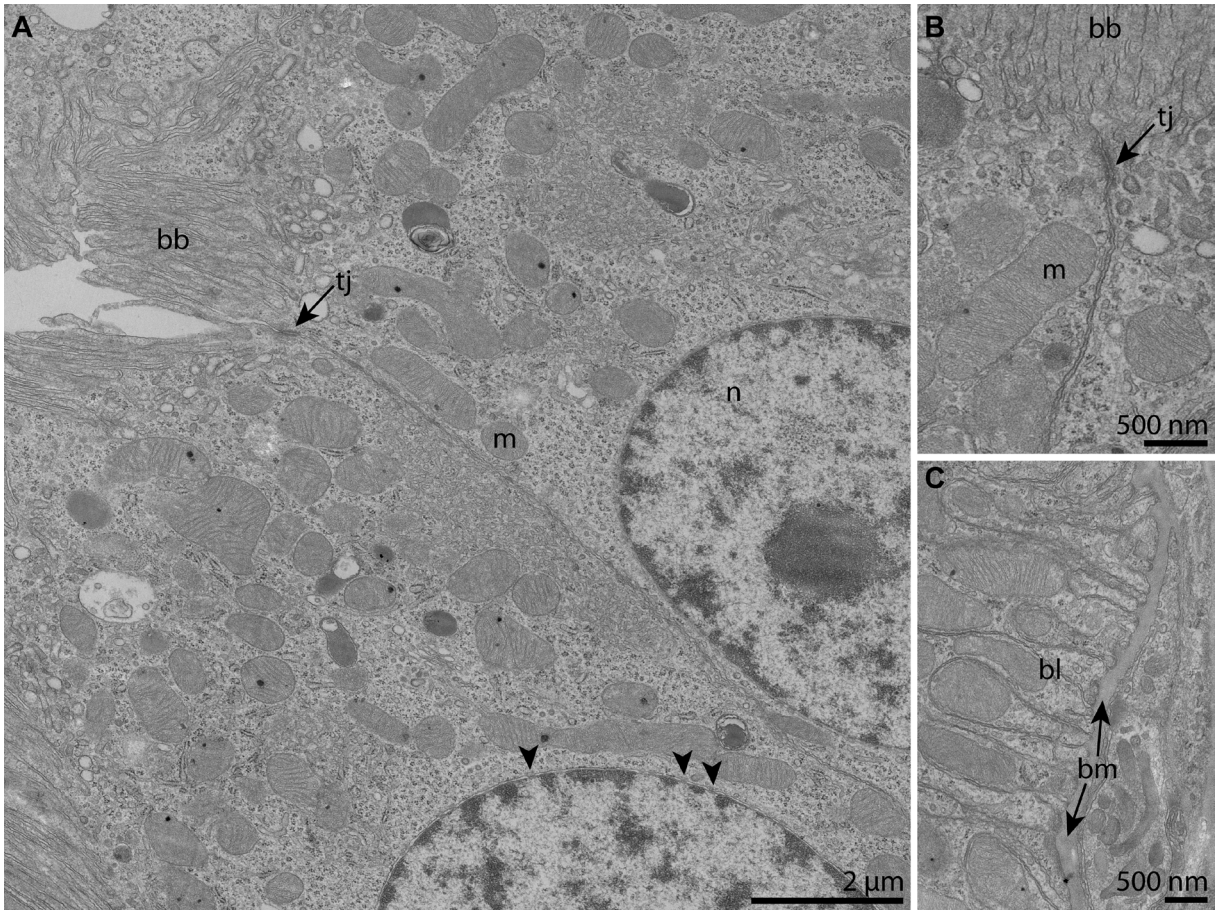

Figure 4: Overview and details of a proximal tubule cell of the mouse kidney fixed with mammalian PHEM-GA.
(A) shows an overview with the nucleus (n), nuclear pores (arrowhead) mitochondria (m), a tight junction (tj) and the brush border (bb, highlighted in yellow). (B) shows a detail of the brush border (bb) and mitochondria (m) and a tight junction (tj). (C) is a high magnification image of the basement membrane (bm) and the basal labyrinth (bl).

Overall, both fixations showed excellent tissue preservation; however, the mamK fixed tissue showed separation between membranes (e.g. basal labyrinth, nucleus) in the form of prominent gaps, which is consistent with shrinking artifacts. Additionally, the cytoplasm of the mamK fixed material looked denser than the mamP fixed tissue, which might be partly due to compression caused by cell shrinkage. On the other hand, the cytoplasmic elements of the mamP fixed cells were evenly distributed. The nuclei in both fixatives were well-preserved but the nuclear membranes of the mamK fixed material had separated and emphasized the location of the nuclear pores. In comparison the mamP

fixed nuclear membranes were very fine, parallel and the nuclear pores displayed areas of membrane fusion. The mitochondria exhibited fine parallel cristae in both fixatives, but were less defined in the mamK fixed tissue. The mitochondria in the mamK fixed PT cell revealed slight separation of the cristae membranes while the mitochondrial cristae of the same cells fixed with mamP remained parallel. The basal membrane of all cells examined was homogenous, except for the DCT fixed with mamK. The interdigitation of the basal labyrinth of all mamP fixed cells was clearly delineated without gaps, which we interpreted as evidence of excellent fixation. In contrast, the basal labyrinth of the mamK fixed DCT cells showed wide gaps, which seemed to be a shrinkage artifact. Similar effects were also noted, although to a lesser extent, in the PT cells. Individual microvilli of the PT brush border of the mamK fixed cells could not be resolved due to the low contrast and their tight clumping. In contrast, the mamP fixed PT, showed clearly delineated brush border microvilli.

Despite the dense tissue samples and using an immersion fixation method, both fixatives gave consistently good results. Textbooks recommend fixation by vascular perfusion for kidney ultrastructure to overcome fixative diffusion gradients (Hayat 1981). As the focus of this work was immersion fixation, we avoided this issue by mincing the tissue into very small pieces in a pool of fixative. Kidney tissue is notoriously difficult to fix because it varies in osmolarity across a four-fold range in different structural and functional elements (Hayat 1981). Thus, a compromise in osmolarity is required for good immersion fixation to ensure the preservation of the chosen cell of interest. Some of the shrinkage we observed in the basal labyrinth could be attributed to the high osmolarity of the mamK fixative (1322 mOsm), compared to the 300 mOsm of the mamP fixative, similar to what has been previously observed (Yun and Kenney 1976).

The direct comparison of the routinely used mamK fixative and the mamP fixative showed that excellent fixation results could be achieved with both fixatives on kidney tubule cortex tissue. The differences observed between the fixatives were subtle but distinct; however the minimal shrinkage artifact and enhanced membrane contrast with the isotonic PHEM makes it our preferred buffer for future works.

Comparing PHEM buffered fixation with standard fixation methods for marine invertebrates

We simultaneously fixed the marine acoel *C. longifissura* in either marK, marP of fsG fixative. To facilitate easy comparison we chose the following regions of interest: nucleus, Golgi apparatus, cilia, chloroplasts (with a focus on the membrane stacks) and the sagittocysts' muscle mantle (focusing on details such as muscle alignment and desmosomes between the layers). We also selected representative images of these details at higher magnification. Fixation with fsG (Figure 5 A-D) showed good fixation of cilia including basal bodies (Figure 5 A, arrowhead), however in the underlying tissue many empty vacuoles were seen. The membrane stacks of the chloroplast (Figure 5 B, arrowhead) were moderately preserved but some content of the algal cytosol seemed to be missing. The sagittocysts and the surrounding muscle mantle (Figure 5 C) were overall well preserved but the desmosomes (arrowhead) were expanded and there were gaps between the individual layers of muscles which, indicating shrinkage during sample preparation. This might have been due to the poor buffering capacity of seawater. At higher magnification the membranes of the cilia (Figure 5 D, arrowhead) were visible and parallel.

The marK fixation (Figure 5 E-H) showed well-preserved cilia (Figure 5 E) and the basal root of the cilia (arrowhead) can be seen. The tissue underlying the cilia appeared washed

out and vacuolated. The membrane stacks of the chloroplast (Figure 5 F) disrupted (arrowhead) and were the least well-preserved compared to the other two fixatives. The desmosomes (Figure 5 G and H, arrowheads) of the sagittocyst muscle mantle appeared less expanded than the ones of the seawater fixed samples and the individual fibers were more defined than in (Figure 5 C), but the muscle sheath layers still were separated. The desmosomes (Figure 5 H, arrowhead) in the higher magnification image were well-preserved but no individual muscle fibers could be distinguished and the chloroplast membrane stacks next to it were disheveled. In this image set (Figure 5 E-H), the formvar support film was visible with variation in thickness resulting in small round lighter areas in the background.

Using the marP fixation (Figure 5 I-L) all structures were very well preserved. Figure 5 I showed Golgi complexes (arrowhead) with parallel cisternae. The nucleus was well-maintained and no signs of shrinkage of the nucleic membrane were observed. The chloroplast (Figure 5 J) was best preserved with the marP fixative, with the membrane stacks (arrowhead) intact, the nuclear chromatin homogenous and the membranes well defined and parallel. The sagittocysts muscle mantle (Figure 5 K) had the least separation between the muscle sheath layers, the desmosomes (arrowhead) were clearly visible and individual muscle fibers were easily discernable. At higher magnification (Figure 5 L), the algal symbiont showed parallel chloroplast membrane stacks, a well-defined nucleus and a pair of flagellal basal bodies (arrowhead).

Overall, the individual thylakoid membranes of all chloroplasts were preserved. However, the structural organization of the membrane stacks varied considerably. While the marP fixed sample showed the best preservation, samples fixed in fsG appeared intact but slightly compressed, while those fixed in marK lost cohesion. The best preserved sagittocyst was

the one fixed with the marP fixative. We observed bigger spaces between the muscle layers of both the marK and fsG fixed sagittocysts, which we again attributed to shrinkage. Taken together, this experiment demonstrated that PHEM is a viable alternative to established buffers used for electron microscopy of a marine invertebrate.

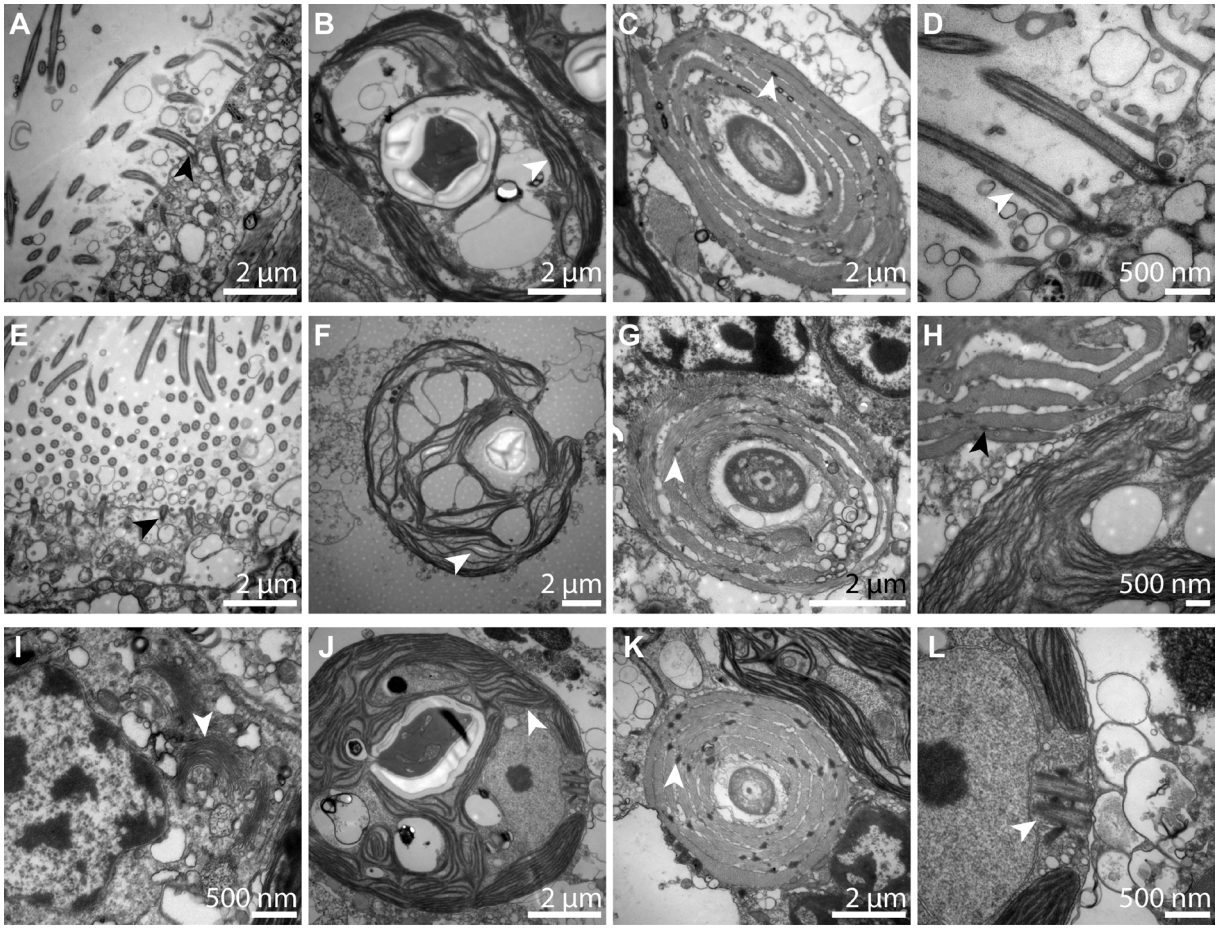

Figure 5: Comparative overview of Convolutriloba longifissura fixed with the three different fixative solutions.
Details of Convolutriloba longifissura fixed with 2.5 % glutaraldehyde in filtered seawater (A-D), 2 % glutaraldehyde and 4 % formaldehyde in sodium cacodylate buffer (E-H) and marine PHEM-GA fixative (I-L). (A, D and E) show epidermis and cilia, (B,F, J and L) show the symbiotic algae, (C,G,H and K) show the sagittocyst and (I) shows part of a nucleus and multiple golgi. Arrowheads indicate cilial root in (A and E), chloroplast membrane stacks in (B,F and J), desmosomes in (C, G, H, and K), the cilium membrane in (D), golgi complexes in (I) and flagellal basal bodies in (L).

Additional applications of PHEM buffered fixation

Applying PHEM-buffered fixation to mammalian conjunctiva

We tested mamP fixation with the conjunctival tissue of mice (Supplementary Figure 1). The striated muscle underneath the substantia propria (Supplementary Figure 1 A) were well preserved and the single muscle fibers and the classical A, I, H, M and Z-bands were easily discernable. The epithelial keratinocyte cells (Supplementary Figure 1 B) showed very dense nuclear chromatin along the membrane, even cytoplasm and well defined deep processes (arrowhead) to adjacent cells. This shows that mamP performs well with other tissues as well.

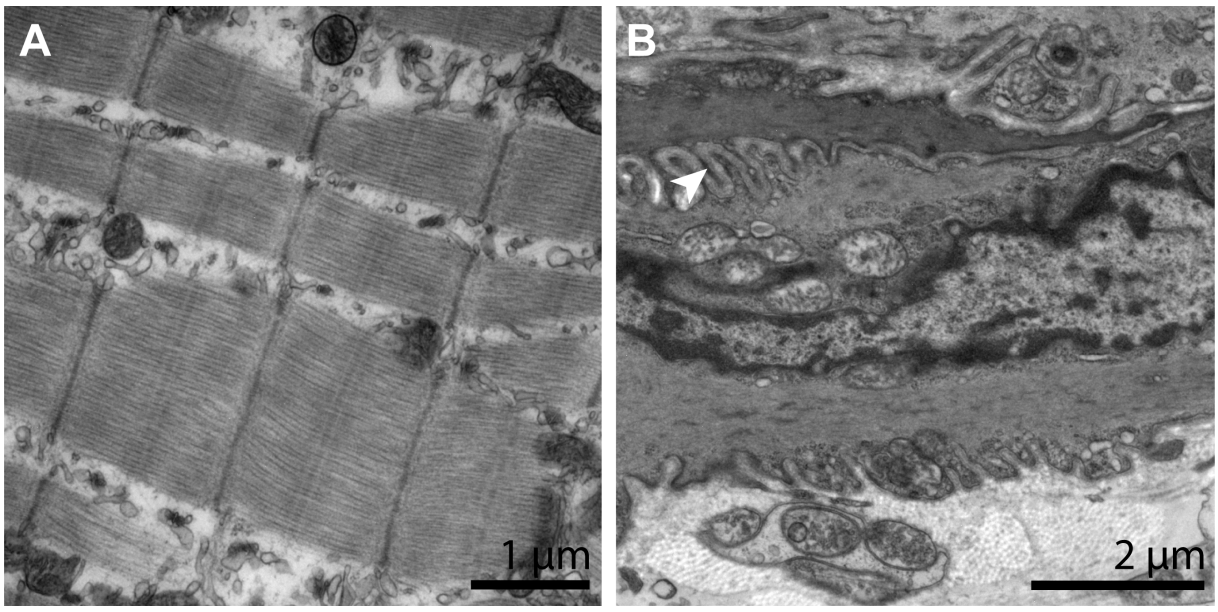

Supplementary Figure 1: Mouse eye lid tissue fixed with mammalian PHEM fixative. Details of mouse eye lid (A-B) fixed with 2.5 % glutaraldehyde and 0.03X PHEM buffer. The sections show (A) muscle tissue from mouse eye lid and (B) shows keratinocytes of the conjunctival epithelium with the arrowhead indicating deep cell process.

PHEM buffered formaldehyde fixation of marine invertebrates

We explored the tissue preservation of C. longifissura using formaldehyde alone as a primary fixative in combination with PHEM buffer. Potentially, this would allow for a wider range of techniques, e.g. immuno-electron microscopy. While the FA fixed organism, as expected,

showed overall inferior fixation to the marP ones, the cells of Convolutriloba longifissura (Supplementary Figure 2) showed a well-preserved nucleus (Supplementary Figure 2 A, arrowhead), chloroplast (Supplementary Figure 2 B, arrowhead) and cilia (Supplementary Figure 2 C, arrowhead), but the surrounding tissues were vacuolated. These results are a good basis for using this buffer-fixative combination for immunolabelling studies in the future.

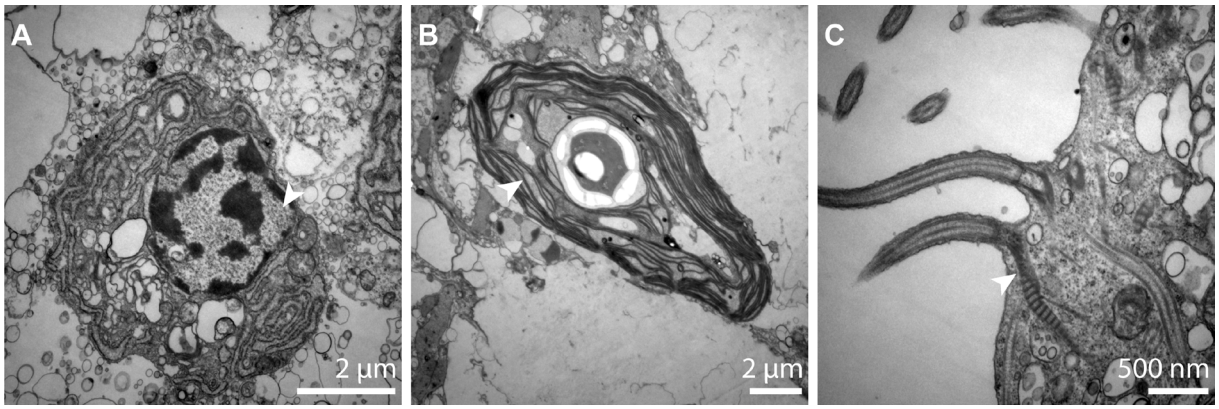

Supplementary Figure 2: Overview of Convolutriloba longifissura fixed with 2.2X PHEM and 2 % formaldehyde.
Details of Convolutriloba longifissura. (A) shows nucleus and surrounding cell, (B) the membrane stacks of the symbiotic algae and (C) shows a close up of a cilia and it's rootlet. Arrowheads indicate a nucleus in (A), a thylakoid membrane in (B) and the root of a cilium in (C).

Combining PHEM-buffered fixation in the field with HPF and FS in the lab for improved ultrastructure

The marine free-living nematode *Laxus oneistus* Ott 1995 cannot be cultivated and requires collection and fixation at a remote field station. Based on literature that reported an improved ultrastructural preservation when chemical fixed samples were processed with cryo-techniques (Sosinsky et al. 2008, Yamaguchi et al. 2011), we did a proof-of-concept experiment, combining marP fixation in the field with cryo-techniques for sample processing. Due to sample size high pressure freezing was chosen as the most appropriate

cryo-immobilization technique. The sample was further processed by freeze-substitution dehydration and epoxy resin embedding.

The resulting longitudinal section in (Supplementary Figure 3 A) depicts the rod-shaped bacteria (ba) lined up on the cuticle (cu), the glandular sense organ (GSO) underneath the cuticle and the gut epithelium (ge) with the gut lumen (gl). This experiment resulted in excellent preservation with straight, parallel membranes, consistent spatial relationships and no discernable tissue losses due to extraction. With this method, ultrastructural elements that are traditionally difficult to preserve like e.g. the Golgi complex (Supplementary Figure 3 B) were very well-preserved. The overview of the gut lumen and the associated epithelial cells (Supplementary Figure 3C) showed no sign of shrinkage and all cells were well preserved. The high magnification detail of the cell membrane (Supplementary Figure 3D) exhibited highly parallel membranes including a zonula adherens (arrowhead), consistent with excellent fixation.

With this approach we could combine our routine immersion fixation protocol in the field with modern cryo-preparation techniques. Applying HPF enabled us to dehydrate the sample at ultra-low temperatures which minimized the extraction and shrinkage during the processing. These results highlight how much ultrastructural morphological detail is potentially available after “conventional” chemical immersion fixation. As a side note, we emphasize that this processing experiment was conducted 6 months after initial collection and fixation in the field.

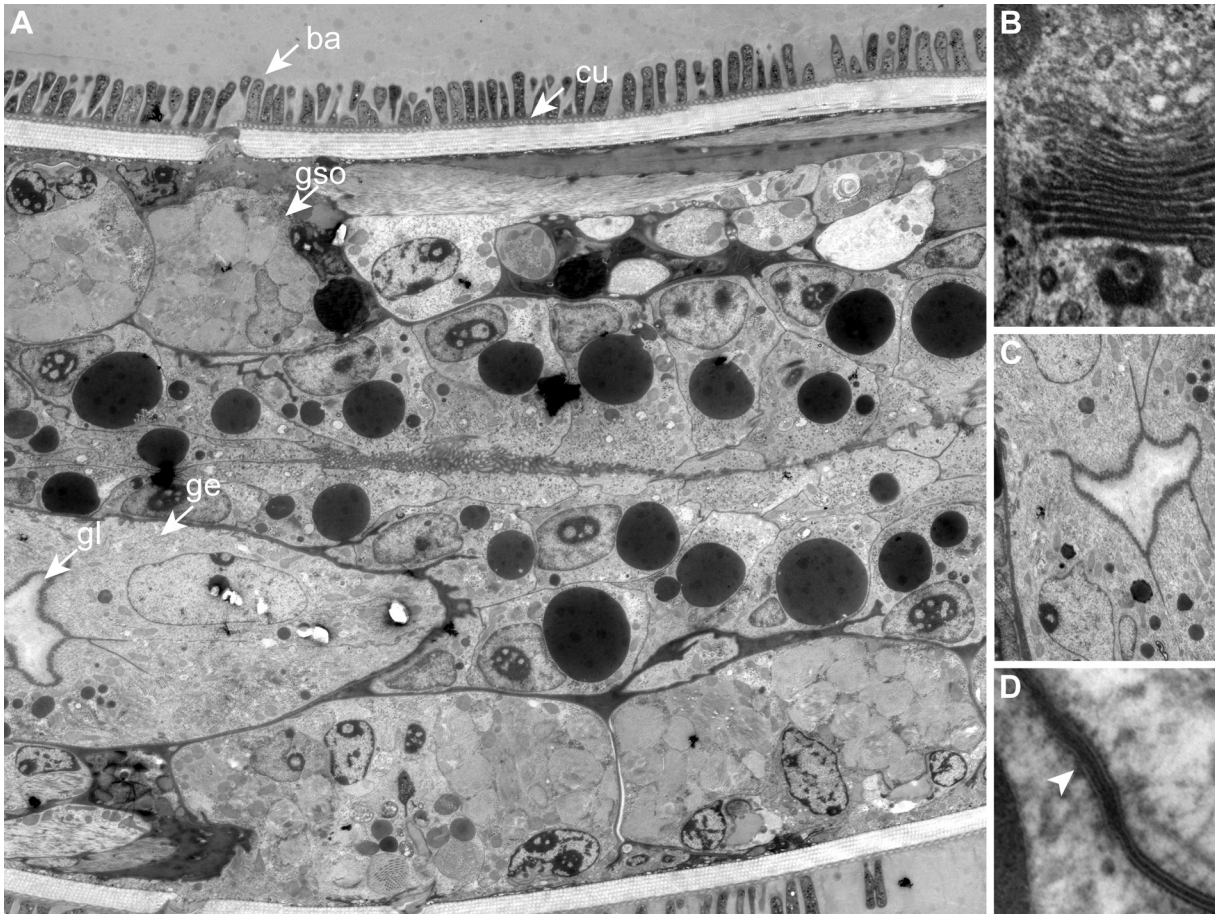

Supplementary figure 3: Overview and details of Laxus oneistus fixed with marine PHEM-GA fixative.
Longitudinal section (A) showing the symbiotic bacteria (ba) on the nematodes cuticle (cu), the glandular sense organs (gso) underlying the cuticle, the gut lumen (gl) and the surrounding epithelial cells of the gut (ge) of the nematode. High magnification image of the Golgi apparatus (B). Overview of the gut epithelial and lumen (C) and detail of cell membrane (D).

Since the start of this study, both mamP and marP fixative has been used in our lab to investigate multiple marine organisms (Platyhelminthes (*Paracatenula* sp.), Nematodes, Oligochaetes (*Olavius* sp.), unicellular (*Kentrophorus* sp.) and colonial (*Zoothamnium* sp.) ciliates), marine and terrestrial bacteria (data not shown) and archaea (Stieglmeier et al. 2014) for both scanning and transmission electron microscopy, with satisfying results.

Conclusion

In this study we show the effectiveness of an isosmotic non-toxic PHEM buffer in combination with aldehydes when applied as immersion fixative. We have adapted this buffer-fixative combination for ultrastructural fixation of both mammalian tissue and marine invertebrates. The individual components of PHEM buffer seem to enhance ultrastructural detail, reduce extraction and preserve membrane integrity. Both the mammalian and the marine samples showed no evidence of shrinkage, excellent structural preservation and, due to their contrast, easily discernable membranes. In addition, we have shown excellent tissue preservation by combining chemical immersion fixation in the field with high-pressure freezing and freeze substitution processing. Taken together, our comparative studies showed that isotonic PHEM buffered fixation resulted in equal or better fixation and subsequent ultrastructural preservation. We highly recommend PHEM buffer with glutaraldehyde as an electron microscopy fixative solution for both routine lab and field use.

Acknowledgements

The authors wish to thank M. Stojanovic for providing mouse tissue and J. Cerovic for excellent technical assistance. The authors also wish to thank W. Klepal, A. Ellinger and S. Bulgheresi for careful review and A. Klingl and H.R. Gruber-Vodicka for editorial advice. We are very grateful to the Core Facility Cell Imaging and Ultrastructure Research of the University of Vienna for technical support, to J. Ott for providing field samples and D. Abed-Navandi from the public aquarium Haus des Meeres aquarium for providing the Convolutriloba longifissura specimens. This work is contribution XXX from the Carrie Bow Cay Laboratory, Caribbean Coral Reef Ecosystem Program, National Museum of Natural

History, Washington, DC.

Funding

This research was funded by the Laura Bassi Centers of Expertise (FFG Project Number: 822768, http://www.ffg.at/en) and the Republic of Austria. N.L. was supported by the Austrian Science Fund (FWF) grant P22470-B17 (S. Bulgheresi, PI) and the Ph.D. completion grant 2014 of the University of Vienna.

Table 1: Osmolarity measurements of the buffers, fixative agents and the combined buffer/fixative solutions at different concentrations.

Abbreviation	buffer concentration	buffer type / additions	% Formaldehyde [vol/vol]	% Glutaraldehyde [vol/vol]	Mean osmolarity [mOsm]	s.d.
-	-	-	-	2.5	287	± 6.9
-	-	Filtered seawater	-	-	1100	± 8.0
-	0.06X	PHEM-buffer	-	-	19	± 1.2
-	1X	PHEM buffer	-	-	219	± 1.2
-	2X	PHEM buffer	-	-	444	± 2.6
-	2.5X	PHEM buffer	-	-	558	± 6.3
-	3.33X	PHEM buffer	-	-	765	± 2.4
-	5X	PHEM buffer	-	-	1204	± 23.0
mamK	0.1M	cacodylate buffer	2	2.5	1322	± 3.8
mamP	0.06X	PHEM buffer	-	2.5	300	± 3.6
mamP washing buffer	1.5X	PHEM buffer	-	-	323	± 1.4
marK	0.1M	cacodylate buffer + 10% sucrose	4	2.5	1694	± 16.7
marK washing buffer	0.1M	Cacodylate +10 % sucrose	-	-	339	± 4.5
fsG	-	80% seawater	-	2.5	1246	± 15.2
marP	3X	PHEM buffer	-	2.5	1071	± 6.9
marP washing buffer	4.25	PHEM buffer	-	-	1010	± 12.2

Components are highlighted in yellow, fixative and washing buffer used for mammalian samples in green, and those used for marine samples in blue.

Supplementary Table 1: Osmolarity measurements of additional buffer / fixative combinations.

Buffer concentration	Buffer type	% Formaldehyde [vol / vol]	% Glutaraldehyde [vol / vol]	Mean osmolarity [mOsm]	s.d.
-	-	1	-	287	±15.3
-	-	2	-	571	±9.3
-	-	4	-	1132	±3.6
2.2X	PHEM buffer	2	-	1118	±12.6
0.03X	PHEM buffer	1	-	314	±1.5
0.06X	PHEM buffer	1	-	325	±11.4
0.03X	PHEM buffer	2	-	590	±7.0
0.06X	PHEM buffer	2	-	598	±4.4
0.03X	PHEM buffer	4	-	1138	±22.4
0.06X	PHEM buffer	4	-	1193	±1.0
0.03X	PHEM buffer	1	0.2	348	±5.5
0.06X	PHEM buffer	1	0.2	345	±7.5
0.03X	PHEM buffer	4	0.5	1450	±50.5
0.03X	PHEM buffer	2	2	776	±7.9
0.06X	PHEM buffer	2	2	778	±1.3

The FA-PHEM solution used for Supp. Figure 2 is highlighted in light blue.

Supplementary Methods

Mouse conjunctiva

Mouse eyelid tissue was excised, immediately immersed in a mammalian PHEM-GA fixative solution and then sliced into 2x1x1 mm pieces through the epithelial layers. Tissue was processed further as described for the mouse kidney tissue. Tissues remained in fixative for 1 h at RT with agitation, and then stored overnight at 4°C before processing to resin. The tissue was washed in 1.5X PHEM washing buffer, and then post-fixed with 0.5% aqueous osmium tetroxide for 1 h. After briefly rinsing in water, tissue was dehydrated in 70% acetone for 10 min, followed by 3 times 10 min changes of absolute acetone. Tissues were infiltrated with 1:1 acetone- Low Viscosity Resin mixtures for 5 min, changed into fresh mixture 1:1 acetone-resin for further 25 min before infiltration with pure resin for 2 times 1 h at room temperature. Tissue samples were then changed into fresh resin and polymerized 48 h at 60°C.

Marine invertebrates

Our measurements showed that the combination of 2.2X PHEM with 2% formaldehyde was isosmotic to seawater (Supplementary Table 1). *C. longifissura* specimens were fixed with this combination for 1 h at room temperature. After washing with 4.25X PHEM washing buffer three times, they were post-fixed with 1% osmium tetroxide (vol/vol) in ddH2O for 1 h. The samples were then dehydrated in a graded ethanol series (50 %, 70 %, 100 % twice), transferred into 100 % dry acetone, and infiltrated with a 50/50 mixture of acetone and Low Viscosity Resin for 30 min. After 2 h of infiltration in pure LVR resin the samples were then polymerized at 60°C in the oven for 12 h.

Permission for the collection and export of invertebrate animals (*Laxus oneistus*) from Belize (Central America) was issued by the Ministry of Agriculture and Fisheries of Belize. *Laxus oneistus* specimens were collected at 1 m depth from a sand patch off Carrie Bow Cay (16°48'11"N 88° 4'54"W). The nematodes were extracted from the sand by stirring the sediment gently and pouring the supernatant through a 63 µm-pore-size mesh sieve. The content of the sieve was transferred into a petri dish and single worms were selected using a pipette under a dissecting microscope. Samples were fixed in marine PHEM- GA for 12 h at 4°C, washed thrice and stored in washing buffer. After high-pressure freezing with a HPM 100 (Leica Microsystems, Austria) they were processed in the freeze substitution unit AFS2 (Leica Microsystems, Austria). Substitution was performed at -90°C for 110 h using dry acetone containing 2 % (vol/vol) osmium tetroxide as substitution medium. Afterwards, the samples were rinsed twice with pure acetone, slowly warmed up to room temperature and embedded in Epon resin (Electron Microscopy Science, USA).

References

Bartolomaeus, T. and I. Balzer (1997). "*Convolutriloba longifissura* nov. spec.(Acoela) - the first case of longitudinal fission in Plathelminthes." Microfauna Mar. 11: 7-18.

Dykstra, M. J. and L. E. Reuss (2003). Biological electron microscopy: theory, techniques and troubleshooting. Springer, New York.

Electron Microscopy Sciences. (08/2013). "Sodium Cacodylate buffer Material Data Safety Sheet." Retrieved 08, 2014, from https://www.emsdiasum.com/microscopy/technical/msds/11654.pdf.

Ettensohn, C. A., G. A. Wray and G. M. Wessel (2004). Development of Sea Urchins, Ascidians, and Other Invertebrate Deuterostomes: Experimental Approaches. Elsevier Academic Press, San Diego.

Griffith, J., M. Mari, A. De Mazière and F. Reggiori (2008). "A cryosectioning procedure for the ultrastructural analysis and the immunogold labelling of yeast Saccharomyces cerevisiae." Traffic 9(7): 1060-1072.

Gschwentner, R., S. Baric and R. Rieger (2002). "New model for the formation and function of sagittocysts: *Symsagittifera corsicae* n. sp. (Acoela)." Invertebr. Biol. 121(2): 95-103.

Gschwentner, R., P. Ladurner, W. Salvenmoser and S. Tyler (1999). "Fine structure and evolutionary significance of sagittocysts of *Convolutriloba longifissura* (Acoela, Platyhelminthes)." Invertebr. Biol. 118(4): 332-345.

Hayat, M. (1981). Fixation for electron microscopy. Academic Press, Inc., New York.

Hayat, M. (2000). Principles and techniques of electron microscopy: biological applications. Cambridge University Press, Cambridge.

Hayat, M. (2002). Fixation and Embedding. Microscopy, Immunohistochemistry, and Antigen Retrieval Methods. pp. 53-69. Springer US, New York.

Karnovsky, M. J. (1965). "A formaldehyde-glutaraldehyde fixative of high osmolarity for use in electron microscopy." J. Cell Biol. 27: 137-138A.

Klepal, W., C. Rentenberger, V. Zheden, S. Adam and D. Gruber (2010). "Structural peculiarities of the penis of *Semibalanus balanoides* (Linnaeus, 1767) and Chthamalus stellatus (Poli, 1791)(Crustacea: Cirripedia: Thoracica)." J. Exp. Mar. Biol. Ecol. 392(1): 228-233.

Koonce, M. P. and R. Gräf (2010). *Dictyostelium discoideum*: A Model System for Ultrastructural Analyses of Cell Motility and Development. Methods in Cell Biology - Electron Microscopy of Model Systems.(ed. by T. Müller-Reichert). pp. 197-216. Academic Press, San Diego.

Kriz, W. and B. Kaissling (2012). Structural Organization of the Mammalian Kidney. Seldin and Giebisch's The Kidney (ed. by R. Alpert, M. Caplan and O. Moe). pp. 595-691. Academic Press, Oxford.

Kuo, J. (2007). Electron microscopy: methods and protocols. Humana Press, New Jersey.

Nakakoshi, M., H. Nishioka and E. Katayama (2011). "New versatile staining reagents for biological transmission electron microscopy that substitute for uranyl acetate." J. Electron Microsc. 60(6): 401-407.

Ott, J. A., M. Bauer-Nebelsick and V. Novotny (1995). "The genus *Laxus* Cobb, 1894 (Stilbonematinae: Nematoda): Description of two new species with ectosymbiotic chemoautotrophic bacteria." Proc. Biol. Soc. Wash. 108(3): 508-527.

Pavelka, M. and J. Roth (2010). Functional ultrastructure: atlas of tissue biology and pathology. Springer, Wien.

Przysiezniak, J. and A. N. Spencer (1989). "Primary culture of identified neurones from a cnidarian." J. Exp. Biol. 142(1): 97-113.

Schieber, N. L., S. J. Nixon, R. I. Webb, V. M. J. Oorschot and R. G. Parton (2010). Modern Approaches for Ultrastructural Analysis of the Zebrafish Embryo. Methods in Cell Biology - Electron Microscopy of Model Systems.(ed. by T. Müller-Reichert). pp. 425-442. Elsevier Academic Press, San Diego.

Schliwa, M. and J. van Blerkom (1981). "Structural interaction of cytoskeletal components." J. Cell Biol. 90(1): 222-235.

Sosinsky, G. E., et al. (2008). "The combination of chemical fixation procedures with high pressure freezing and freeze substitution preserves highly labile tissue ultrastructure for electron tomography applications." J. Struct. Biol. 161(3): 359-371.

Stieglmeier, M., A. Klingl, R. J. Alves, S. K. Rittmann, M. Melcher, N. Leisch and C. Schleper (2014). "*Nitrososphaera viennensis* sp. nov., an aerobic and mesophilic ammonia-oxidizing archaeon from soil and member of the archaeal phylum Thaumarchaeota." Int. J. Syst. Evol. Microbiol. 64(8): 2783-2752.

Yamaguchi, M., Y. Namiki, H. Okada, K. Uematsu, A. Tame, T. Maruyama and Y. Kozuka (2011). "Improved preservation of fine structure of deep-sea microorganisms by freeze-substitution after glutaraldehyde fixation." J. Electron Microsc. 60(4): 283-287.

Yun, J. and R. A. Kenney (1976). "Preparation of Cat Kidney Tissue for Ultrastructural Studies." J. Electron Microsc. 25(1): 11-23.

Chapter 3

Eubostrichus fertilis sp. n., a new marine nematode (Desmodoridae, Stilbonematinae) with an extraordinary reproductive potential from Belize, Central America.

Authors Jörg A. Ott, Nikolaus Leisch and Harald R. Gruber-Vodicka

Keywords Caribbean Sea, description, Eubostrichus gerlachi nom. nov., meiofauna, molecular, morphology, morphometrics, new name, new species, sulphide system, symbiosis, taxonomy, thiotrophic bacteria.

Publication status Article published in Nematology **16**(7): 777-787

Detailed description of NL's contribution

a. designed the study together with JAO

b. collected material on two field trips to Carrie Bow Caye (Belize)

c. sequenced the 18S rRNA genes

d. performed the electron microscopy

e. digitized the drawings and prepared the figures

f. wrote the manuscript together with JAO and HGV

BRILL

Nematology 16 (2014) 777-787

Nematology
brill.com/nemy

Eubostrichus fertilis sp. n., a new marine nematode (Desmodoridae: Stilbonematinae) with an extraordinary reproductive potential from Belize, Central America

Jörg A. Ott [1,*], Nikolaus Leisch [2] and Harald R. Gruber-Vodicka [3]

[1] *Department of Limnology and Bio-Oceanography, University of Vienna, Althanstrasse 14, 1090 Vienna, Austria*
[2] *Department of Ecogenomics and Systems Biology, University of Vienna, Althanstrasse 14, 1090 Vienna, Austria*
[3] *Department of Symbiosis, Max-Planck Institute for Marine Microbiology, Celsiusstrasse 1, 28359 Bremen, Germany*

Received: 26 December 2013; revised: 7 May 2014
Accepted for publication: 7 May 2014; available online: 25 June 2014

Summary – *Eubostrichus fertilis* sp. n. is described from fine subtidal sands in the Belize Barrier Reef system using LM and SEM illustrations and the sequence of the 18S rRNA gene. The new species is one of the smallest (mature specimens ranging from 1.88 to 3.03 mm) and the stoutest (a = 36-80) of all previously described *Eubostrichus* species. The closest relatives are *E. parasitiferus* and *E. hopperi*. It differs from the former in the more posterior position of the vulva and the postanal porids, and from the latter in the smaller size of the amphids, the shorter cephalic setae and the shape of the tail. Furthermore, it is remarkable for the prominent extent of the female genital system. Females have up to 18 eggs of similar size in their uteri. The body of the worm is covered by large (up to 45 μm long) crescent-shaped bacteria attached with both poles to the cuticle of the worm in a spiral pattern. The genus *Eubostrichus* is phylogenetically well supported on the basis of the 18S rRNA gene sequence. *Eubostrichus gerlachi* nom. nov. (= *E. parasitiferus apud* Gerlach, 1963 *nec* Chitwood, 1936) is proposed.

Keywords – Caribbean Sea, description, *Eubostrichus gerlachi* nom. nov., meiofauna, molecular, morphology, morphometrics, new name, new species, sulphide system, symbiosis, taxonomy, thiotrophic bacteria.

The subtidal porous back-reef sediments of the Belize Barrier Reef system harbour a rich meiofauna in which the subfamily Stilbonematinae (Desmodoridae) plays a prominent role, occasionally dominating the nematode fauna (Ott & Novak, 1989). Stilbonematinae are remarkable for their symbiosis with sulphur-oxidising Gammaproteobacteria, which cover the body cuticle in an often regular pattern (Ott *et al.*, 1991; Polz *et al.*, 1992; Hentschel *et al.*, 1999). In all cases where the identity of the symbiotic bacteria has been established, the coat proved to be a monospecific biofilm specific to each host species (Polz *et al.*, 1994; Bayer *et al.*, 2009; Bulgheresi *et al.*, 2011). The mechanism of symbiont/host recognition has been attributed to lectins secreted by the worms from unique hypodermal glands (glandular sensory organs, gso) (Bauer-Nebelsick *et al.*, 1995) interacting with sugars in the bacterial cell wall in a specific fashion (Nussbaumer *et al.*, 2004; Bulgheresi *et al.*, 2006, 2011).

In *Eubostrichus* Greeff, 1869, the symbiotic bacteria grow to exceptionally large sizes, forming non-septate filaments. In *E. dianeae* Hopper & Cefalu, 1973 these filaments may exceed 100 μm in length (Polz *et al.*, 1999; Ott *et al.*, 2004) and are attached by only one pole to the host cuticle. In all other so far described species of *Eubostrichus*, the bacteria are crescent-shaped, up to 30 μm long and usually attached by both poles. The symbionts are arranged in a spiral pattern along the anterior/posterior axis of the host giving the worm a rope-like appearance (Ott *et al.*, 2004).

To date, nine *Eubostrichus* species have been described, two of which are regarded as *species inquirendae*. Except for *E. hortulanus* Leduc, 2013, which has been retrieved from a depth of 350 m, all other species have been found in intertidal or shallow subtidal sediments. Here we describe *Eubostrichus fertilis* sp. n., which shows a remarkable expansion of the female genital system

* Corresponding author, e-mail: joerg.ott@univie.ac.at

 DOI:10.1163/15685411-00002807

and occurs in fine subtidal sands in the Belize Barrier Reef, occasionally in very high numbers. The new taxonomic name is registered in ZooBank (publication ID Zoobank: urn:lsid:zoobank.org:pub:69B84D1E-1560-4233-88F0-AEAC8911B5FE).

Materials and methods

Nematode collection

Specimens of *E. fertilis* sp. n. were collected in December 2011 and January 2012 at the type locality. The nematodes were extracted by stirring the sand in seawater and pouring the supernatant through a 63 μm pore sieve. The contents of the net were transferred into a Petri dish and single individuals were then picked by hand under a dissecting microscope.

Microphotographs of live animals were taken with a Canon EOS 500D camera mounted on a Zeiss microscope. For permanent slides, animals fixed in methanol were slowly transferred to and mounted in pure glycerin. Drawings from permanent mounts were made using a Reichert Diavar equipped with a *camera lucida*.

For genomic DNA extraction, nematodes were fixed in methanol and stored deep-frozen for transportation and storage. For scanning electron microscopy (SEM), nematodes were fixed with 2.5% glutaraldehyde and stored and transported in buffer at 4°C.

Scanning electron microscopy (SEM)

Worms were post-fixed with 1% osmium tetroxide for 2 h at room temperature and then dehydrated in a graded ethanol series, transferred into pure acetone and critical point dried with a CPD 300 unit (Leica). After mounting on stubs they were gold-sputter coated with an AGAR B7340 sputter-coater unit. Images were taken with a XL20 (Philips) using the Microscope control program (v. 7.00, FEI).

Genomic DNA extraction and PCR amplification of the nematode 18S rRNA genes

DNA was extracted from two single *E. fertilis* sp. n. individuals as previously described (Schizas *et al.*, 1997). Two μl of DNA were used as template in each 50 μl PCR reaction. An almost complete (*ca* 1800 bp) fragment of the 18S rRNA-gene was amplified by PCR with the general eukaryotic primers, 1f (5′-CTGGTTGATYCTGCC AGT-3′) (Winnepenninckx *et al.*, 1998) and 2023r (5′-GGTTCACCTACGGAAACC-3′) (Pradillon *et al.*, 2007). Cycling conditions for the 18S rRNA-gene amplification were as follows: 95°C for 3 min followed by 35 cycles of 95°C for 45 s, 48°C for 45 s and 72°C for 120 s, and a final elongation of 72°C for 10 min. The PCR products were cleaned using the MinElute PCR purification kit (Qiagen) and directly sequenced using the PCR primers.

18S rRNA phylogenetic analysis

The two *E. fertilis* sp. n. 18S rRNA sequences and all sequences from the Stilbonematinae available in GenBank, as well as two Draconematidae sequences as outgroup representatives, were aligned using MAFFT Q-INS-I, which considers the predicted secondary structure of the RNA for the alignment (Katoh *et al.*, 2005). Alignments were manually inspected and 5′- and 3′-end-trimmed using Geneious software version 6 (Drummond *et al.*, 2011). The optimal substitution model was assessed using the Akaike information criterion as implemented in MEGA 5.3 (Tamura *et al.*, 2011) and the GTR + G + I model was chosen. Phylogenetic trees were reconstructed using maximum likelihood- (PHYML) (Guindon *et al.*, 2010) and Bayesian inference-based (MrBayes) (Ronquist & Huelsenbeck, 2003) methods. MrBayes was run for 2×10^6 generations using four chains. Convergence was evaluated by plotting the generations *vs* log L and the burn-in was set to 5×10^5 generations. Node stability was evaluated using posterior probabilities (pp, Bayesian inference) and aLRT (maximum likelihood) (Anisimova & Gascuel, 2006) with values above 0.80 (pp), 80 (aLRT) considered significant.

Results

Eubostrichus fertilis[*] sp. n.
(Figs 1-5)

Measurements

See Table 1.

Description

Adults

Body stout, cylindrical, tapering only slightly towards anterior end, head diam. at level of cephalic setae =

[*] Specific epithet formed from the Latin *fertilis* = fertile, and referring to the high number of eggs in the female gonads.

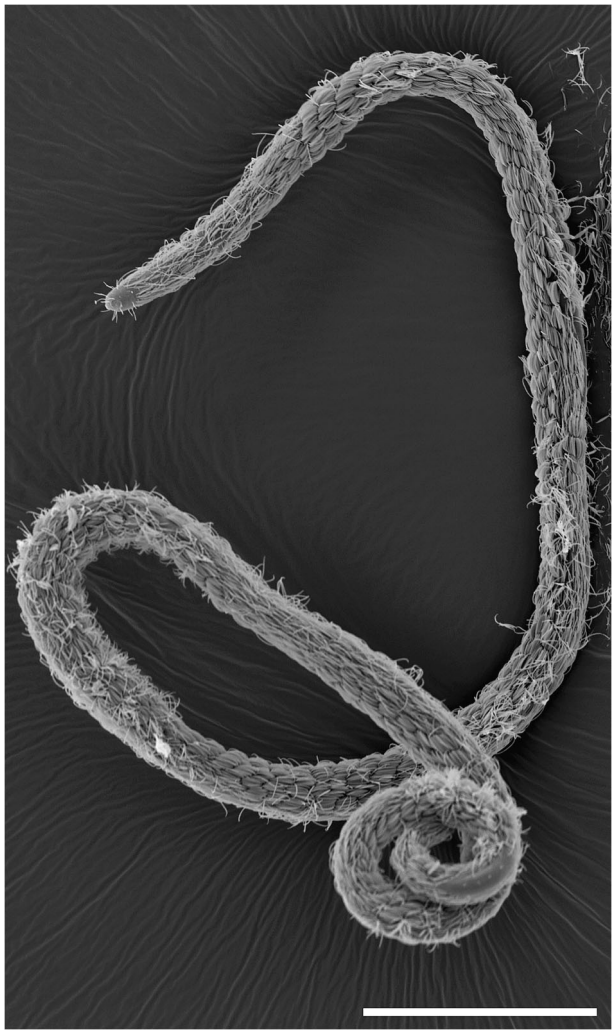

Fig. 1. *Eubostrichus fertilis* sp. n. SEM of entire female. (Scale bar = 200 μm.)

15-18 μm, at level of centre of amphid = 17-20 μm. Tail conical, cuticle finely annulated except for anterior part of head and tail tip, annulation beginning at level of centre of amphid, annuli in pharyngeal region 0.4-0.5 μm wide (20-25 annuli 10 μm^{-1}), in mid-body region 0.30-0.35 μm (28-32 annuli 10 μm^{-1}), non-annulated tail tip 2-3 μm long. Somatic setae short (1.2 μm), arranged in eight longitudinal rows in submedian and sublateral position. Distance between setae within a row 10-11 μm in pharyngeal region, 18-22 μm in mid-body region. One or two pairs of small (<2 μm) terminal setae on non-annulated tail tip. Mouth surrounded by a circle of six papilliform outer labial sensilla, in lateral, laterodorsal and lateroventral position, whether there is an inner circle of labial sensilla could not be ascertained, four cephalic setae close to anterior margin of amphid, in some specimens setae on ventral side are double, two circles of eight subcephalic setae each, first at level of amphid with sublateral setae bordering amphid, submedian setae in a slightly more anterior position, length variable within same specimen. Second circle 15-25 μm from anterior end. Amphids situated close to anterior end, spiral with 1.5 turns, indistinct in live animals and glycerin whole mounts, in SEM preparations conspicuous because of *corpus gelatum* filling fovea. Mouth opening in some specimens slightly protruding, forming a 'snout', buccal cavity minute, conical, pharynx with a cylindrical elongated corpus slightly thicker than isthmus, isthmus surrounded by nerve ring. Terminal bulb slightly wider than long, weakly muscular. No ventral gland. Gso in eight rows in cervical region, subcentral rows merging in posterior body region. Gso opening through the somatic setae.

Male

Monorchic, testis on right side of intestine; spicule cephalate, curved, gubernaculum simple, directed anteriodorsal, with small lateral flanges, proximal end with small hook. One pair of precloacal porids (thorn-like setae), 10 μm anterior to cloacal aperture, and three pairs of postcloacal porids, first of which situated at 33-46% of tail length, last at level where annulation ends. Porids 5-8 μm long. One symbiont-free male showing two pairs of long subventral setae in pharyngeal region, at 45 and 80% of pharynx length. Unfortunately these are obscured by bacterial coat in specimens used for drawings.

Female

Didelphic, amphidelphic, ovaries reflexed, position in relation to gut not determined unambiguously, at point of reflexion a *receptaculum seminis* filled with sperm. Ripe eggs *ca* 30 × 30 μm in size, one most distal from ovary up to 40 μm long. Always several (up to ten) eggs of similar size in each branch of uterus, apparently produced almost at same time and accumulating proximally to point of flexure of female gonad, which they seem to pass simultaneously *en route* to vulva. Long uteri leading to vagina, distal 50-60 μm of uterus branches consisting of large vesicular cells and never containing eggs. Vulva and vagina strongly cuticularised. Female genital system occupying up to two-thirds of body length.

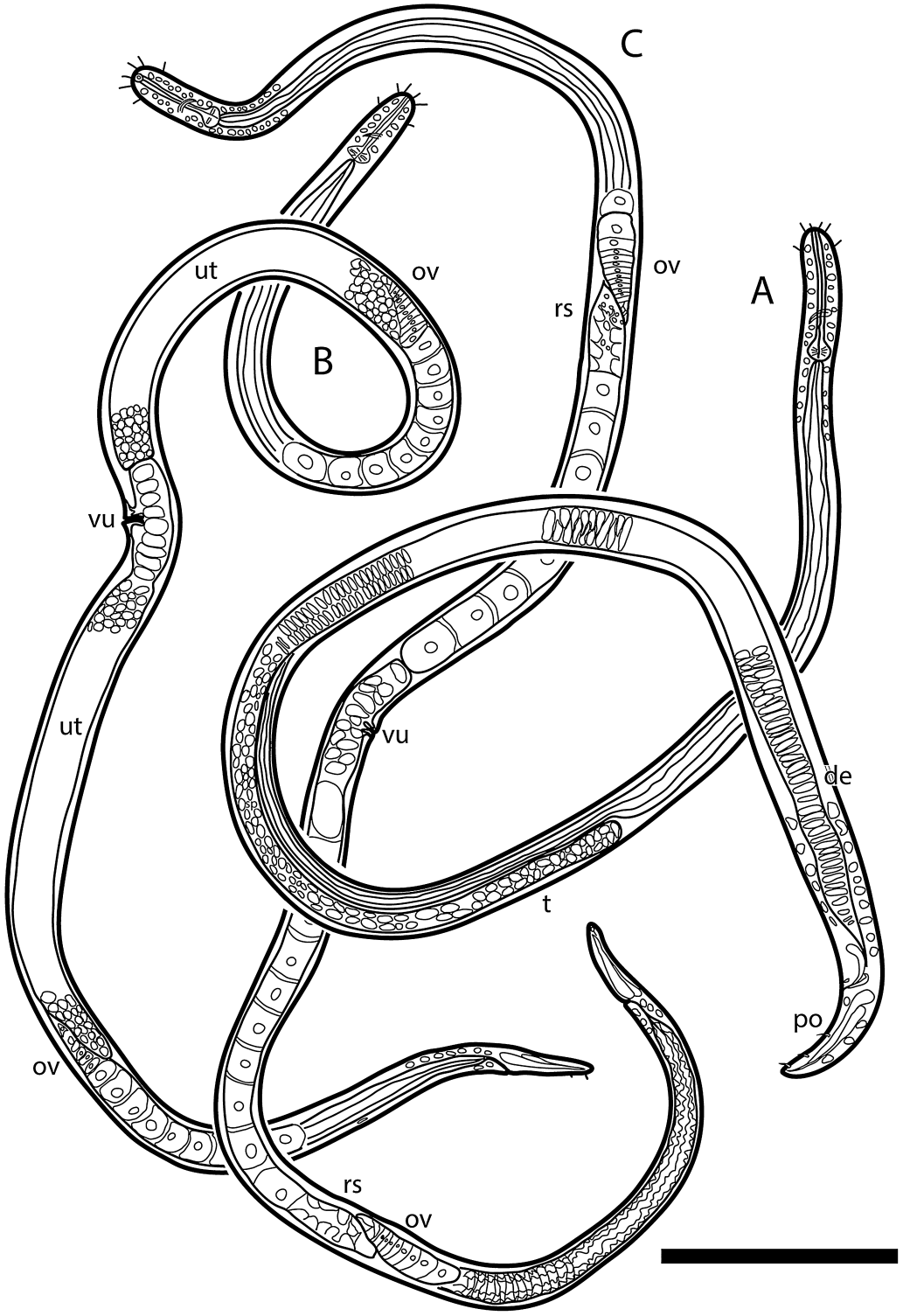

Fig. 2. *Eubostrichus fertilis* sp. n., entire view. A: Male, holotype. B: Female, paratype. C: Female, paratype. (Abbreviations: de = *ductus ejaculatorius*; ov = ovary; po = porid; rs = *receptaculum seminis*; t = testis; ut = uterus; vu = vulva.) (Scale bar = 200 μm.)

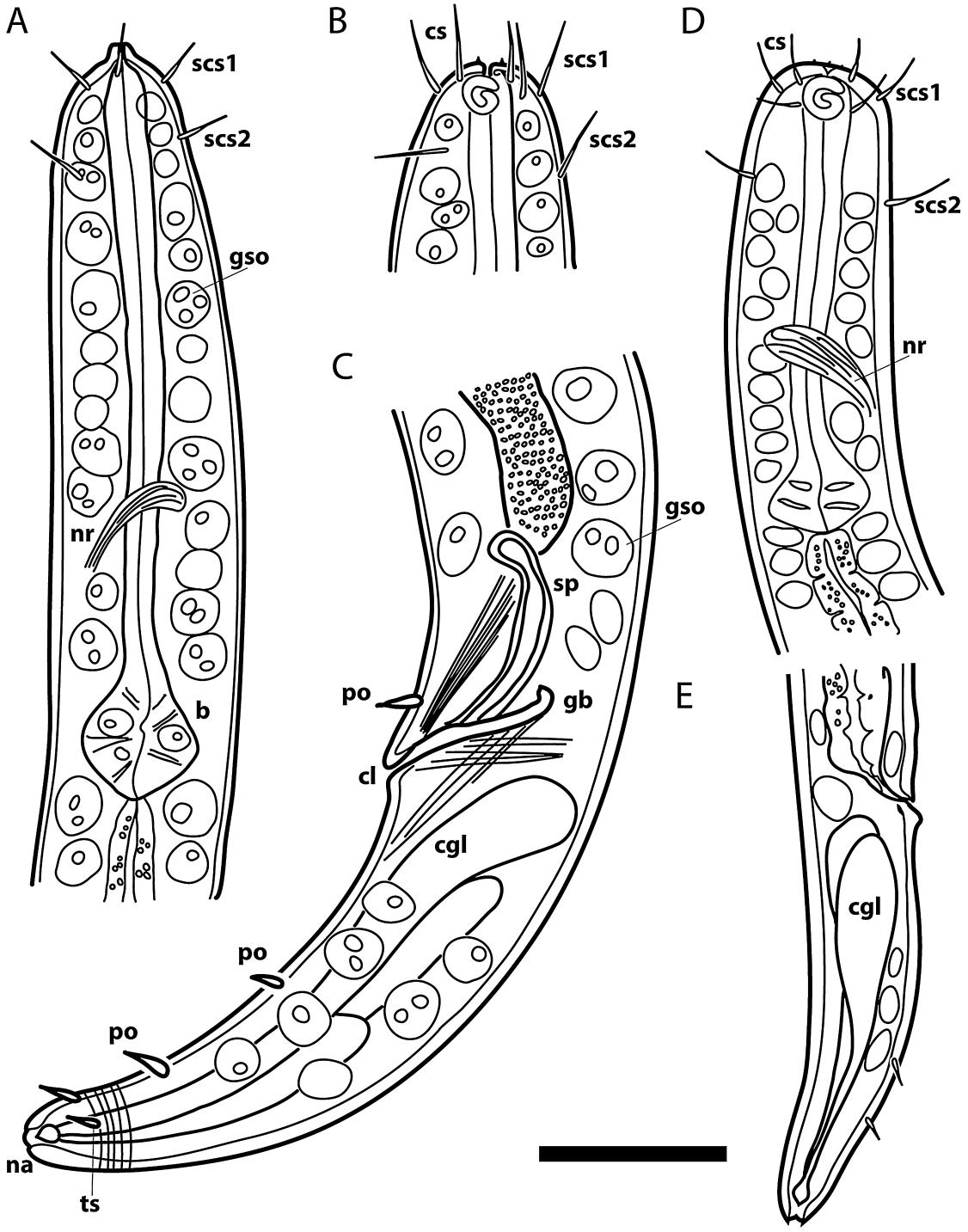

Fig. 3. *Eubostrichus fertilis* sp. n. A: Male holotype, anterior region; B: Male paratype, head; C: Male holotype, tail and spicular apparatus; D: Female paratype, anterior region; E: Female paratype, tail. (Abbreviations: b = *bulbus*; cgl = caudal gland; cl = cloacal aperture; cs = cephalic seta; gb = gubernaculum; gso = glandular sensory organ; na = non-annulated tail tip; nr = nerve ring; po = porid; scs1 = first circle of subcephalic setae; scs2 = second circle of subcephalic setae; sp = spiculum; ts = terminal seta.) (Scale bar = 30 μm.)

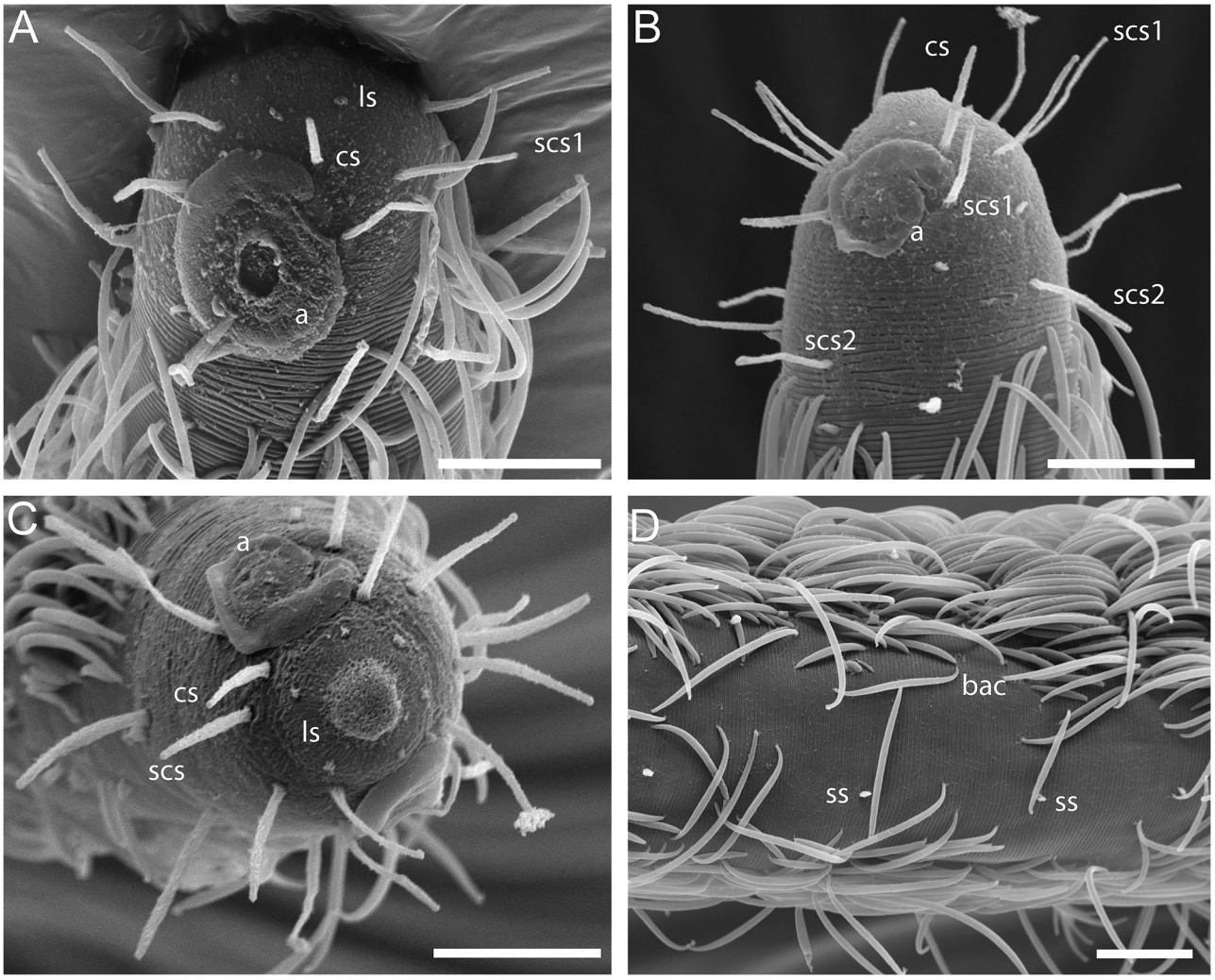

Fig. 4. *Eubostrichus fertilis* sp. n., SEM. A: Male, lateral view of head region; B: Female, lateral view of head region; C: Male, *en face* view of anterior end; D: Female, mid-body region, symbiotic bacteria partly removed. (Abbreviations: a = amphid; bac = bacteria; cs = cephalic seta; ls = labial sensilla; scs = subcephalic seta; scs1 = first circle of subcephalic setae; scs2 = second circle of subcephalic setae; ss = somatic seta.) (Scale bars = 10 μm.)

Type habitat and locality

Subtidal fine calcareous sand at depth of 1 m adjacent to the Fisheries Department Warden Station on Twin Cayes, Belize ('Fisheries Beach'; 16°49′25″N, 88°06′21″W).

Other habitat and locality

Also been found in intertidal and shallow subtidal sand north of the main channel entrance ('Candy's Trail'; 16°49′47.96″N, 88°6′29.67″W).

Type material

Holotype male, three paratype males and four paratype females (accession numbers: 1231525-1231532) deposited at the National Museum of Natural History, Washington, USA. Two female paratypes from the type locality and one female from the additional locality are in the collection of the first author (J.A.O.).

Diagnosis and relationships

Eubostrichus fertilis sp. n. is among the smallest and the stoutest *Eubostrichus* species described so far. Mature

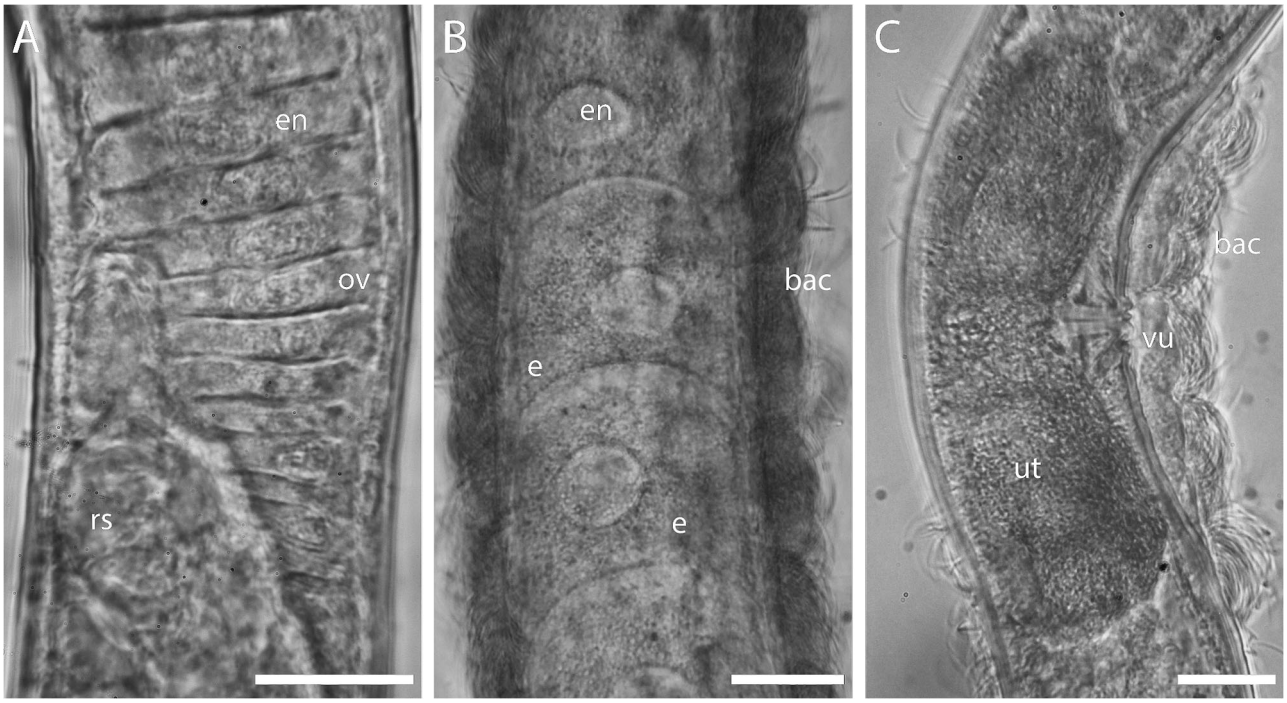

Fig. 5. *Eubostrichus fertilis* sp. n., LM. A: Anterior ovary of female paratype 2; B: Eggs in uterus of female paratype 2; C: Vulva and uterus of female paratype 1. (Abbreviations: bac = bacteria; e = egg; en = egg nucleus; ov = ovary; rs = *receptaculum seminis*; ut = uterus; vu = vulva.) (Scale bars = 20 μm.)

specimens vary considerably in body length, which ranges in males from 2.00 to 2.41 mm and in females from 1.87 to 3.03 mm. Long specimens tend to be more slender, with a values above 70, whereas short specimens are stouter (a = 36-70). Cephalic setae 6-11 μm long, amphids in male 8-10 μm (50-65% of corresponding diam. wide), in female 6-8 μm (38-50%), respectively. Tail short, 2.6-3.1 cloacal diam. long in male, 3.2-3.9 anal body diam. in female. Males with three pairs of thorn-like setae (porids) on ventral side of tail, the first pair at 33-48% of tail length. Female V = 51-57, both ovaries containing up to nine oocytes maturing at the same time and being simultaneously transferred to the uterus. Body covered by large (up to 45 μm long) crescent-shaped symbiotic bacteria arranged in a spiral pattern around the nematode's body.

The new species is similar to the two species previously described from the West Atlantic, *E. parasitiferus* Chitwood, 1936 and *E. hopperi* (Hopper & Cefalu, 1973) Muthumbi, Verschelde & Vincx, 1995. It differs from the former in the position of the vulva (V = 53-57 *vs* 43). Chitwood (1936) does not depict porids; however, the type specimen deposited in the USNM and material collected by one of the authors (J.A.O.) close to the type locality, including males, show that the first pair of postcloacal porids is at >50% of tail length. *Eubostrichus hopperi* has larger amphids, longer cephalic setae and a longer, more slender, tail (Table 1). The small species that Gerlach (1963) identified as *E. parasitiferus* has only two pairs of porids on the tail, the first of which is at 44% of the tail length. It should therefore be regarded as a separate species, for which we propose herein *E. gerlachi* nom. nov. (= *E. parasitiferus apud* Gerlach, 1963) *nec* Chitwood, 1936). The female individual that Gerlach (1964) reported from the Red Sea most probably also belongs to that species.

Molecular sequences

The sequences of the 18S rRNA genes of two individuals are available from GenBank and under accession numbers KF453617 and KF453618.

Bionomics

A remarkable feature in the biology of the new species is the high number of eggs that are presumably produced

Table 1. Morphometric data for *Eubostrichus fertilis* sp. n. and the two most similar species, *E. parasitiferus* Chitwood, 1936 and *E. hopperi* (Hopper & Cefalu, 1973) Muthumbi, Verschelde & Vincx, 1995. For *E. fertilis*, ranges are given for the male and female types and for all measured individuals, including three additional females from the collection of the first author (see *Other material*). All measurements are in μm.

Character	*E. fertilis* sp. n.				*E. parasitiferus*	*E. hopperi*
	Male		Female	All measured individuals		
	Holotype	Paratypes	Paratypes			
n	–	3	4	11	n.a.	n.a.
L	2010	2077-2412	2000-3032	1876-3032	2800-2920	2140-2680
a	36.5	65.5-69.0	40.0-79.7	36.5-79.7	75.0-100.0	78.0-90.0
b	17.0	24.0-27.0	20.0-34.4	17.0-34.4	30.0-33.0	20.0-25.4
c	21.1	27.7-28.4	24.7-33.6	21.1-33.6	26.0-30.0	25.0-29.0
V	n.a.	n.a.	51-57	51-57	43*	50-53
Max. diam.	55	30-37	38-50	30-55	n.d.	22-34
Pharynx length	118	77-100	76-100	70-118	82	85-108
Tail length	98	75-85	70-85	65-98	85	75-107
Nerve ring (% pharynx length)	59	58-59	56-59	56-59	61	65
Corresponding body diam. (cbd)	30	25-30	28-30	25-30	32	n.d.
Bulbus length/diam.	18/18	14-18/16-18	12-16/18-20	12-18/16-20	13/20**	13-16/18-21
Bulbus cbd	30	24-30	27-30	24-30	31	n.d.
Vulval cbd	n.a.	n.a.	40-45	40-45	n.d.	n.d.
Anal (cloacal) body diam.	32	25-33	18-28	18-33	35	21-24
Tail length: anal diam. male/female	3.1	2.6-3.1	3.2-3.9	2.6-3.1/3.2-3.9	2.4/n.d.	3.4-3.9/4.5-4.9*
Spicule length arc/chord	50/40	45-50/38-42	n.a.	45-50/38-42	50/40**	37-53/28-41
Gubernaculum length	30	23-29	n.a.	23-30	25**	19-22
Amphid males width/% cbd	10/50	8-10/60-65	n.a.	8-10/50-65	n.d.	13-15/73*
Amphid females width/% cbd	n.a.	n.a.	6-8/38-50	6-8/38-50	n.d.	6-8/n.d.*
Cephalic setae number/length	4/7-8	4/10-11	4/9-11	4/6-11	4/11	4/13-15*
Subcephalic setae 1 number/length	8/9	8/10-15	8/9-15	8/9-15	8/8**	8/12-16
Subcephalic setae 2 number/length	8/8-11	8/10-14	8/10-13	8/8-14	8/10**	8/10-16
Subventral elongated setae number of pairs/length	n.d.	2/12	n.a.	2/12	2/10**	2/8-10 and 6-8
Postanal thorn-like setae (porids) number of pairs	3	3	n.a.	3	3**	3
Position of first postanal porid pair (% tail length)	46	33-48	n.a.	33-48	61*,**	50

Abbreviations: n.d. = not determined; n.a. = not applicable.

* Diagnostically significant morphometric features.

** Data obtained from the holotype and a co-type of *E. parasitiferus* deposited in the US National Museum.

simultaneously in both ovaries. In all other *Eubostrichus* species the eggs are – when described – fewer in number (maximum of seven eggs per animal in *E. topiarius*) and much larger (up to 320 μm long in *E. hortulanus*). The high egg number in *E. fertilis* sp. n. can be interpreted as an indication of a high reproduction rate and presumably an r-strategist life history. This agrees well with the observation that *E. fertilis* sp. n. was only a rare member of the nematode community at the Candy's trail locality, which has been intensively sampled for many years, during which this habitat has remained nearly unchanged. The subtidal fine sand deposit at Fisheries beach, however, has been recently formed due to changes in coastal morphology associated with the development of the ranger station. Here the new species is abundant and conspicuous. It is also here where the smallest mature specimens

are found. A combination of early sexual maturity and high reproduction rate would make *E. fertilis* sp. n. an ideal colonising species.

Discussion

A diagnosis of the genus *Eubostrichus* was recently given by Tchesunov (2013) and has subsequently been modified by Leduc (2013) to accommodate *E. hortulanus* Leduc, 2013. All species so far described belong to the FA (faintly annulated) group *sensu* Urbancik *et al.* (1996a), in which the annulation involves <50% of the cuticle thickness. In *E. topiarius*, for example, the basal layer of the cuticle contributes 70% of the cuticle and is composed exclusively of longitudinal fibres. The annuli extend far anterior and enclose the posterior half of the amphid. The cuticle of the anterior end (cephalic cuticle) shows no reinforcement (Urbancik *et al.*, 1996b). The arrangement of the cephalic sensilla follows a consistent pattern. The first circle of six inner labial sensilla is hard to see and requires SEM. In *E. topiarius* they are represented by finger-like papillae within the mouth opening (Berger *et al.*, 1996) in mediolateral and subdorsal and subventral positions. Nipple-like papillae or small setae in the lateral and laterodorsal and lateroventral position constitute the second circle of six outer labial sensilla. A circle of four cephalic setae is generally situated close to the anterior margin of the amphid. A first circle of eight subcephalic setae occurs at the general level of the amphids, a second one a short distance posterior to the amphid. The somatic setae are the outlets of complex hypodermal glands (gso) that are characteristic for the Stilbonematinae and are 'porids' in the sense of Cobb (1925). Hopper & Cefalu (1973) used this term in the description of *E. dianeae*, pointing out that in males there are special thorn-like pairs developed close to the ventral line in the cloacal and tail region. In subsequent descriptions of new *Eubostrichus* species the term 'porid' has been used just for these. There is one pair situated a short distance anterior to the cloacal aperture and 2-3 pairs on the tail. In addition there are one or two pairs of terminal setae on the non-annulated tip of the tail. Pairs of subventral elongated setae in the pharyngeal region have been reported for *E. dianeae*, *E. hopperi* and *E. topiarius*, for the specimen of *E. africanus* described by Tchesunov (2013), and for the current new species. They are also visible in a co-type for *E. parasitiferus* deposited by Chitwood. It is unclear whether they occur in all *Eubostrichus* species since the symbionts make observation of setae very difficult.

According to the 18S rRNA gene sequences so far available, the genus *Eubostrichus* is phylogenetically well-supported (Fig. 6). It appears to be the sister group to all other genera of Stilbonematinae for which genomic data exist. The genus probably split off early in the evolution of the Stilbonematinae.

In addition to the morphological similarities and the genomic relationship, the species of *Eubostrichus* share the association with large bacteria, which are non-septate filaments with several to many nucleoids. The filaments are attached by one (*E. dianeae*) or both poles (all other

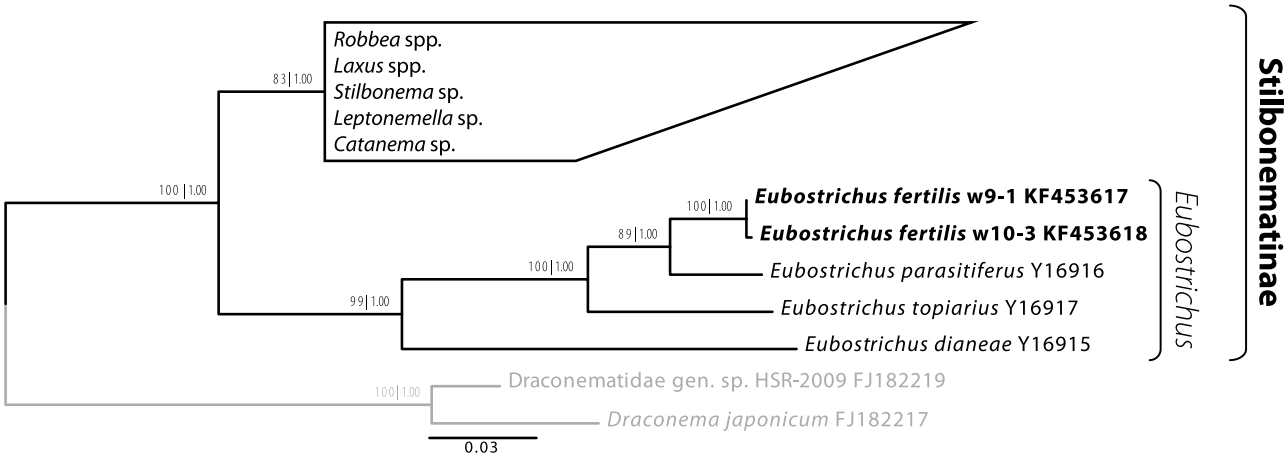

Fig. 6. Phylogenetic relationship of the *Eubostrichus* clade within the Stilbonematinae based on the 18S rRNA gene. The tree shown was calculated using maximum likelihood (PHYML) and node support is given as aLRT as well as Bayesian posterior probabilities. (Scale bar = 0.03 nucleotide substitutions per site.)

species) in a highly ordered fashion. The symbionts of *E. fertilis* sp. n. are the longest so far observed of the latter type. There are two other genera of Stilbonematinae, *Adelphos* Ott, 1997 and *Squanema* Gerlach, 1963 that bear similar symbionts. Whether they fall into the same clade as the *Eubostrichus* species could be explored with 18S rRNA data from members of the two genera.

Acknowledgements

We thank Silvia Bulgheresi and Nika Pende for collaboration in the collection of material, the CCRE Program and the staff of the Carrie Bow Cay Laboratory for their support. We are grateful to the Core Facility Cell Imaging and Ultrastructure Research of the University of Vienna for technical support. N.L. was supported by an Austrian Science Fund (FWF) grant P22470-B17 (S. Bulgheresi, PI) and H.R.G.-V. by a Marie-Curie Intra-European Fellowship PIEF-GA-2011-301027 CARISYM. This is CCRE contribution Number 960 from the Smithsonian National Museum of Natural History Carrie Bow Cay Field Station.

References

Anisimova, M. & Gascuel, O. (2006). Approximate likelihood-ratio test for branches: a fast, accurate, and powerful alternative. *Systematic Biology* 55, 539-552.

Bauer-Nebelsick, M., Blumer, M., Urbancik, W. & Ott, J.A. (1995). The glandular sensory organ of Desmodoridae (Nematoda) – ultrastructure and phylogenetic implications. *Invertebrate Biology* 114, 211-219.

Bayer, C., Heindl, N.R., Rinke, C., Lücker, S., Ott, J.A. & Bulgheresi, S. (2009). Molecular characterization of the symbionts associated with marine nematodes of the genus *Robbea*. *Environmental Microbiology Reports* 1, 136-144.

Berger, E., Urbancik, W. & Ott, J. (1996). *Eubostrichus topiarius* sp. n., a new free-living, marine species of Stilbonematinae (Nematoda: Desmodoridae) from a shallow subtidal sand bottom. *Nematologica* 42, 521-536.

Bulgheresi, S., Schabussova, I., Chen, T., Mullin, N.P., Maizels, R.M. & Ott, J.A. (2006). A new C-type lectin similar to the human immunoreceptor DC-SIGN mediates symbiont acquisition by a marine nematode. *Applied and Environmental Biology* 72, 2950-2956.

Bulgheresi, S., Gruber-Vodicka, H.R., Heindl, N.R., Dirks, U., Kostadinova, M., Breiteneder, H. & Ott, J.A. (2011). Sequence variability of the pattern recognition receptor Mermaid mediates specificity of marine nematode symbioses. *ISME Journal* 5, 986-998.

Chitwood, B. (1936). Some marine nematodes from North Carolina. *Proceedings of the Helminthological Society of Washington* 3, 1-16.

Cobb, N.A. (1925). Notes on nemas. 1. Repetitive lateral organs. 2. Axids and porids. 3. Differentiations of intestinal cells. 4. Structure and position of amphids. 5. Birifringents in *Sphaerolaimus*. 6. Innervation of the anterior portion of the nema body. *Journal of Parasitology* 11, 221-223.

Drummond, A., Ashton, B., Buxton, S., Cheung, M., Cooper, A., Duran, C., Field, M., Heled, J., Kearse, M., Markowitz, S. *et al.* (2011). Geneious v5.5, available online at http://www.geneious.com/.

Gerlach, S.A. (1963). *Robbea tenax* sp. n., ein merkwürdiger mariner Nematode von den Malediven. *Internationale Revue der gesamten Hydrobiologie und Hydrographie* 48, 153-158.

Gerlach, S.A. (1964). Freilebende Nematoden aus dem Roten Meer. *Kieler Meeresforschungen* 20, 18-34.

Greeff, R. (1869). Untersuchungen über einige merkwürdige Formen des Arthropoden und Wurm-Typus. *Archiv für die Geschichte der Naturwissenschaften und der Technik* 35, 71-121.

Guindon, S., Dufayard, J.-F., Lefort, V., Anisimova, M., Hordijk, W. & Gascuel, O. (2010). New algorithms and methods to estimate maximum-likelihood phylogenies: assessing the performance of PhyML 3.0. *Systematic Biology* 59, 307-321.

Hentschel, U., Berger, E.C., Bright, M., Felbeck, H. & Ott, J.A. (1999). Metabolism of nitrogen and sulfur in ectosymbiotic bacteria of marine nematodes (Nematoda, Stilbonematinae). *Marine Ecology Progress Series* 183, 149-158.

Hopper, B.E. & Cefalu, R.C. (1973). Free-living marine nematodes from Biscayne Bay, Florida V. Stilbonematinae: contributions to the taxonomy and morphology of the genus *Eubostrichus* Greeff and related genera. *Transactions of the American Microscopical Society* 92, 578-591.

Katoh, K., Kuma, K.-i., Toh, H. & Miyata, T. (2005). MAFFT version 5: improvement in accuracy of multiple sequence alignment. *Nucleic Acids Research* 33, 511-518.

Leduc, D. (2013). One new genus and two new deep-sea nematode species (Desmodoridae, Stilbonematinae) from phosphorite nodule deposits on Chatham Rise, Southwest Pacific Ocean. *Marine Biodiversity* 43, 421-428.

Muthumbi, A., Verschelde, D. & Vincx, M. (1995). New Desmodoridae (Nematoda: Desmodoroidea): three new species from *Ceriops* mangrove sediments (Kenya) and one related new species from the North Sea. *Cahiers de Biologie Marine* 36, 181-195.

Nussbaumer, A.D., Bright, M., Baranyi, C., Beisser, C.J. & Ott, J.A. (2004). Attachment mechanism in a highly specific association between ectosymbiotic bacteria and marine nematodes. *Aquatic Microbial Ecology* 34, 239-246.

Ott, J. (1997). A new symbiotic marine nematode, *Adelphos rolandi* gen. n. sp. n. (Stilbonematinae), from the Caribbean Sea. *Annalen des Naturhistorischen Museums in Wien Serie B Botanik und Zoologie* 99, 417-422.

Ott, J.A. & Novak, R. (1989). Living at an interface: Meiofauna at the oxygen/sulfide boundary of marine sediments. In: Ryland, J.S. & Tyler, P.A. (Eds). *23rd European Marine Biology Symposium*. Fredensborg, Denmark, Olsen & Olsen.

Ott, J.A., Novak, R., Schiemer, F., Hentschel, U., Nebelsick, M. & Polz, M. (1991). Tackling the sulfide gradient: a novel strategy involving marine nematodes and chemoautotrophic ectosymbionts. *Pubblicazioni Stazione Zoologica Napoli I: Marine Ecology* 12, 261-279.

Ott, J.A., Bright, M. & Bulgheresi, S. (2004). Symbioses between marine nematodes and sulfur-oxidizing chemoautotrophic bacteria. *Symbiosis* 36, 103-126.

Polz, M.F., Felbeck, H., Novak, R., Nebelsick, M. & Ott, J.A. (1992). Chemoautotrophic, sulfur-oxidizing symbiotic bacteria on marine nematodes: morphological and biochemical characterization. *Microbial Ecology (Historical Archive)* 24, 313-329.

Polz, M.F., Distel, D.L., Zarda, B., Amann, R., Felbeck, H., Ott, J.A. & Cavanaugh, C.M. (1994). Phylogenetic analysis of a highly specific association between ectosymbiotic, sulfur-oxidizing bacteria and a marine nematode. *Applied and Environmental Microbiology* 60, 4461-4467.

Polz, M.F., Harbison, C. & Cavanaugh, C.M. (1999). Diversity and heterogeneity of epibiotic bacterial communities on the marine nematode *Eubostrichus dianae*. *Applied and Environmental Microbiology* 65, 4271-4275.

Pradillon, F., Schmidt, A., Peplies, J. & Dubilier, N. (2007). Species identification of marine invertebrate early stages by whole-larvae *in situ* hybridisation of 18S ribosomal RNA. *Marine Ecology Progress Series* 333, 103-116.

Ronquist, F. & Huelsenbeck, J.P. (2003). MrBayes 3: Bayesian phylogenetic inference under mixed models. *Bioinformatics* 19, 1572-1574.

Schizas, N.V., Street, G.T., Coull, B.C., Chandler, G.T. & Quattro, J.M. (1997). An efficient DNA extraction method for small metazoans. *Molecular Marine Biology and Biotechnology* 6, 381-383.

Tamura, K., Peterson, D., Peterson, N., Stecher, G., Nei, M. & Kumar, S. (2011). MEGA5: molecular evolutionary genetics analysis using maximum likelihood, evolutionary distance, and maximum parsimony methods. *Molecular Biology and Evolution* 28, 2731-2739.

Tchesunov, A.V. (2013). Marine free-living nematodes of the subfamily Stilbonematinae (Nematoda, Desmodoridae): taxonomic review with descriptions of a few species from the Nha Trang Bay, Central Vietnam. *Meiofauna Marina* 20, 71-94.

Urbancik, W., Bauer-Nebelsick, M. & Ott, J.A. (1996a). The ultrastructure of the cuticle of Nematoda. *Zoomorphology* 116, 51-64.

Urbancik, W., Novotny, V. & Ott, J.A. (1996b). The ultrastructure of the cuticle of Nematoda. II. The cephalic cuticle of Stilbonematinae (Adenophorea, Desmodoridae). *Zoomorphology* 116, 65-75.

Winnepenninckx, B.M.H., Van de Peer, Y. & Backeljau, T. (1998). Metazoan relationships on the basis of 18S rRNA sequences: a few years later. *American Zoologist* 38, 888-906.

Chapter 4

Phylogenetic confirmation of the genus *Robbea* GERLACH, 1956 (Nematoda Desmodoridae, Stilbonematinae) with the description of three new species.

Authors Jörg A. Ott, Harald R. Gruber Vodicka, Nikolaus Leisch and Judith Zimmermann

Keywords Belize Barrier Reef, Caribbean Sea, chemosynthetic symbiosis, marine nematodes, molecular phylogeny, SSU rRNA, ectosymbionts, systematics, taxonomy

Publication status Article published in Systematics and Biodiversity **12**(4): 434-455

Detailed description of NL's contribution

a. sequenced 18S rRNA genes

b. performed electron microscopic analysis

c. prepared parts of the figures

d. wrote parts of the manuscript, edited and approved the manuscript

Systematics and Biodiversity (2014), 1–22

Taylor & Francis
Taylor & Francis Group

Research Article

Phylogenetic confirmation of the genus *Robbea* (Nematoda: Desmodoridae, Stilbonematinae) with the description of three new species

JÖRG A. OTT[1], HARALD R. GRUBER-VODICKA[2], NIKOLAUS LEISCH[3] & JUDITH ZIMMERMANN[2]

[1]Department of Limnology and Biooceanography, University of Vienna, Althanstr. 14, A-1090 Vienna, Austria
[2]Department of Symbiosis, Max Planck Institute for Marine Microbiology, Celsiusstr. 1, D-28359 Bremen, Germany
[3]Department of Ecogenomics and System Biology, University of Vienna, Althanstr. 14, A-1090 Vienna, Austria

(Received 13 February 2014; accepted 12 June 2014)

The Stilbonematinae are a monophyletic group of marine nematodes that are characterized by a coat of thiotrophic bacterial symbionts. Among the ten known genera of the Stilbonematinae, the genus *Robbea* GERLACH 1956 had a problematic taxonomic history of synonymizations and indications of polyphyletic origin. Here we describe three new species of the genus, *R. hypermnestra* sp. nov., *R. ruetzleri* sp. nov. and *R. agricola* sp. nov., using conventional light microscopy, interference contrast microscopy and SEM. We provide 18S rRNA gene sequences of all three species, together with new sequences for the genera *Catanema* and *Leptonemella*. Both our morphological analyses as well as our phylogenetic reconstructions corroborate the genus *Robbea*. In our phylogenetic analysis the three species of the genus *Robbea* form a distinct clade in the Stilbonematinae radiation and are clearly separated from the clade of the genus *Catanema*, which has previously been synonymized with *Robbea*. Surprisingly, in *R. hypermnestra* sp. nov. all females are intersexes exhibiting male sexual characters. Our extended dataset of Stilbonematinae 18S rRNA genes for the first time allows the identification of the different genera, e.g. in a barcoding approach.

http://zoobank.org/urn:lsid:zoobank.org:pub:D37C3F5A-CF2B-40E6-8B09-3C72EEED60B0

Key words: Belize Barrier Reef, Caribbean Sea, chemosynthetic symbiosis, marine nematodes, molecular phylogeny, SSU rRNA, ectosymbionts, systematics, taxonomy

Introduction

Stilbonematinae are a marine subfamily within the nematode family Desmodoridae (order Desmodorida) and occur worldwide in sulphidic sediments (reviewed in Tchesunov, 2013). They are characterized by an ectosymbiosis with sulphur-oxidizing bacteria that covers their cuticle in a genus- and sometimes even species-characteristic manner (Polz *et al.*, 1992, 1994; Ott *et al.*, 2004). Although the family Desmodoridae is probably polyphyletic (van Megen *et al.*, 2009), molecular data (Kampfer *et al.*, 1998; van Megen *et al.*, 2009) suggest a monophyly of the subfamily Stilbonematinae. A distinct morphological synapomorphy of the subfamily is the complex glandular sense organ (GSO) described by Nebelsick *et al.* (1992) and Bauer-Nebelsick *et al.* (1995), that has so far only been found in members of the Stilbonematinae. This organ produces a special set of lectins (sugar-binding proteins) that seem to be involved in sustaining the specificity of the symbiosis (Bulgheresi *et al.*, 2006, 2011). Otherwise very few common features unite the group, such as the lack of a buccal armature and the weak development of the pharynx (Ott *et al.*, 2004). Some characters appear to have developed independently more than once. For example, there is a tendency towards the development of an enlarged muscular portion of the anterior part of the pharynx (corpus), which is conspicuous in all species of the genera *Robbea* and *Catanema*, and has been described for the single species of *Parabostrichus* (Tchesunov *et al.*, 2012), whereas in other genera (*Laxus*, *Leptonemella*, *Eubostrichus*) it is present only in a few species. Other examples are the reduction of the amphidial fovea or the presence of a stiff corpus gelatum protruding from the amphidial fovea (*Stilbonema*, *Catanema, Leptonemella* partim) (Tchesunov, 2013). This complicates the

Correspondence to: Jörg A. Ott. Email: joerg.ott@univie.ac.at

ISSN 1477-2000 print / 1478-0933 online

http://dx.doi.org/10.1080/14772000.2014.941038

assessment of the relationships between the various genera described until now.

In addition, the type species of several genera are either inadequately described or have features which are the exception rather than the rule in the subsequently described members of the genus. Liberal synonymization has added further confusion.

The genus *Robbea*, introduced by Gerlach (1956), is characterized by the clear separation of a muscular anterior corpus from a mostly glandular isthmus and posterior bulbus which make up the remaining portion of the pharynx. In some species the males have peculiar papillae in the ventromedian line of the cervical and post-cervical region, which resemble suction cups and have a stout conical setae in its centre. These appear to be unique for the genus *Robbea* and have not been described from other stilbonematine genera.

The aim of this study was to reinvestigate morphological characters that are shared by all species of the genus *Robbea* but clearly distinguish those from other stilbonematine nematode genera. We describe three new species of *Robbea* from shallow subtidal sands around the island Carrie Bow Cay on the Belize Barrier Reef (Caribbean Sea). We combine morphological and molecular analyses to clarify the status of the genus and support our findings by providing additional phylogenetic information on previously under-sampled genera.

Materials and methods

Sediment samples containing *Robbea* species were collected in the vicinity of the island of Carrie Bow Cay, Belize from shallow subtidal sand patches and from turtle grass (*Thalassia testudinum*) beds using buckets or cores. Samples for sequencing were obtained at the following coordinates: *R. hypermnestra*: 16° 48′ 47″N, 88° 04′ 58″W; *R. agricola:* 16° 52′ 58″N, 88° 07′ 11″W; *R. ruetzleri:* 16° 47′ 19″N, 88° 04′ 48″W (Fig. 1). Subtidal sediment containing *Catanema* sp. was collected in the bay off Capo di Sant' Andrea, Elba, Italy (42° 48′ 26″N, 10° 08′ 28″E) from sand patches surrounding sea grass beds of *Posidonia oceanica* in 4−8 m water depth (Fig. 1). *Leptonemella vicina* was collected off the island of Sylt,

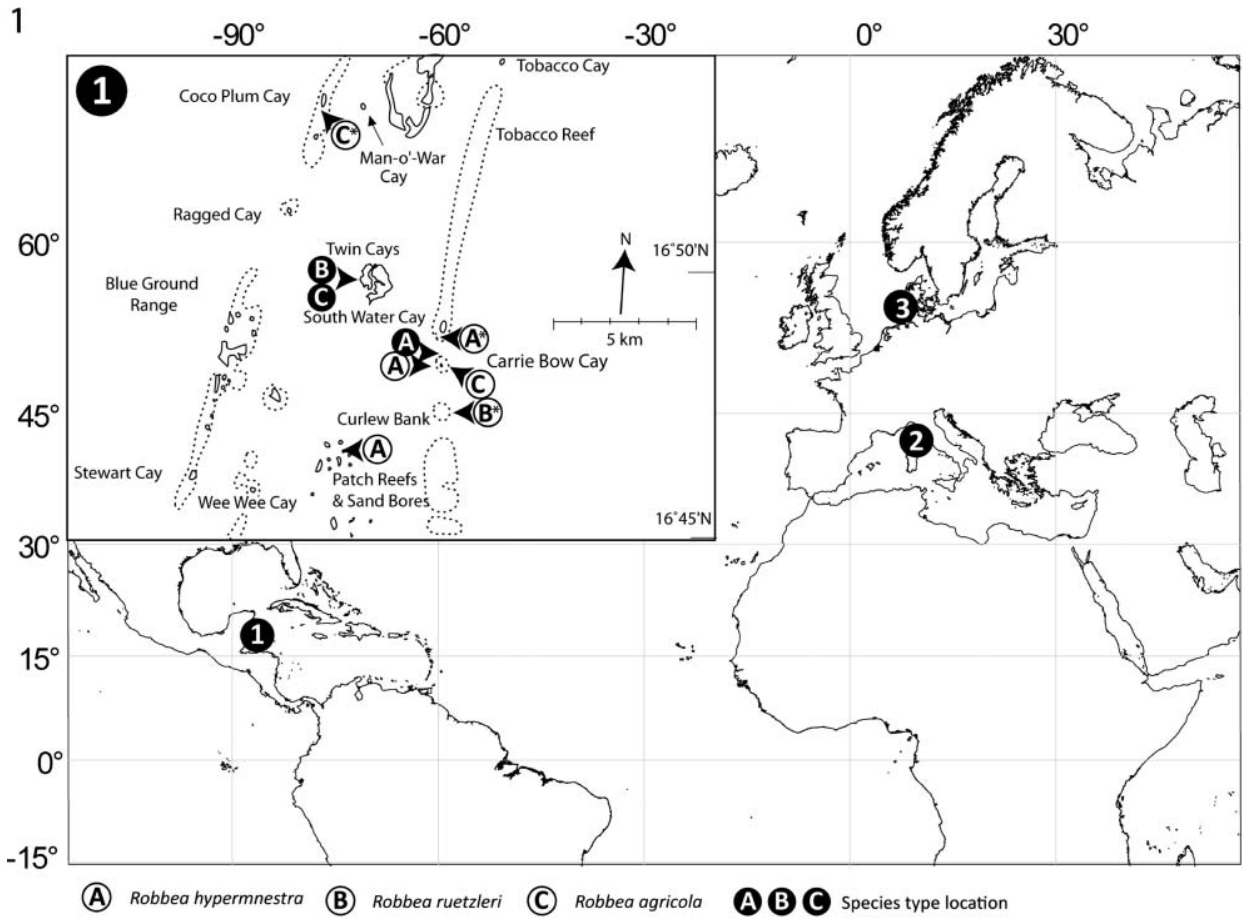

Fig. 1. Map showing sampling locations for the nematodes used in this study. 1, Carrie Bow Cay, Belize; 2, Elba, Italy; and 3, Sylt, Germany. Insert shows detailed locations in the vicinity of Carrie Bow Cay where the three new *Robbea* species were found. Asterisks mark the sampling locations of the individuals that were used for sequencing.

Germany (55° 00′ 54″N, 08° 26′ 16″E) with sediment cores from an intertidal sand flat (Fig. 1). Worms were extracted from the sand after anaesthesia with $MgCl_2$, shaking and decanting or simply shaking and decanting through a 32 μm mesh sieve. The live animals were sorted using a dissecting microscope and immediately fixed in 4% formaldehyde (for taxonomic preparations) or 2.5% glutaraldehyde in 0.1 sodium cacodylate buffer and post-fixed in 2% OsO_4 (for SEM and semi-thin sections). For light microscopy the worms were placed into glycerol: water 1:9, slowly evaporated and finally mounted in pure glycerol; for SEM specimens were critical point-dried and coated with gold. Specimens for sequencing of the 18S rRNA gene were preserved in 70% ethanol or methanol.

Drawings were done using a *camera lucida* on a Reichert Diavar or a Leitz Ortholux. Nomarsky interference contrast photos were taken on a Reichert Polyvar; SEM on a JEOL JSM-35 CF and a Phillips XL20; semi-thin sections were cut on a Reichert Ultracut and photographed in a Reichert Polyvar.

DNA extraction, PCR amplification and sequencing of the 18S rRNA gene

DNA for all sampled species was extracted and purified from single nematode specimens as described before (Schizas *et al.*, 1997). The partial 18S rRNA gene (~1800 bp) was amplified by PCR with the general eukaryotic primers 1F (5′-GGTTGATYCTGCCAGT-3′) (modified from Winnepenninckx *et al.*, 1995) and 2023R (5′-GGTTCACCTACGRAAA-3′) (modified from Pradillon *et al.*, 2007) using the Phusion® DNA polymerase (Finnzymes, Finland). Cycling conditions were as follows: initial denaturation at 96 °C for 5 min, followed by 35 cycles of 96 °C for 1 min, 55 °C for 1.5 min, 72 °C for 2 min and final elongation at 72 °C for 10 min. The purified PCR products (PCR Purification Kit; Qiagen, Hilden, Germany) were sequenced bidirectionally with the PCR primers and an internal reverse primer (5′-CAGACAAATCGCTCC-3′) 1272 nucleotides downstream of the 1F primer. All sequencing reactions were performed with an ABI PRISM 3100 genetic analyser (Applied Biosystems, Foster City, CA, USA).

The generated 18S rRNA gene sequences and all sequences from the Stilbonematinae available in GenBank, as well as four Draconematinae sequences as outgroup were aligned using MAFFT Q-INS-I, which considers the predicted secondary structure of the RNA for the alignment (Katoh *et al.*, 2005). Alignments were manually inspected and 5′ and 3′ end-trimmed using Geneious software version 6 (Drummond *et al.*, 2011). The optimal substitution model was assessed using the Akaike information criterion as implemented in MEGA 5.3 (Tamura *et al.*, 2011) and the GTR+G+I model was chosen. Phylogenetic trees were reconstructed using maximum likelihood- (RAxML) (Stamatakis, 2006) and Bayesian inference-based (MrBayes) (Ronquist & Huelsenbeck, 2003) methods. The dataset was screened for chimeric sequences by calculating maximum likelihood-based trees on three partitions of the alignments (0−600 bp, 601−1200 bp and 1201−1799 bp). The Stilbonematinae sequences Y16915 (designated *Eubostrichus dianae*) and Y16921 (designated *Robbea hypermnestra*) had statistically supported positions in 2 (Y16915) and 3 (Y16921) different genus level clades across all three partitions and were excluded from the final analysis. MrBayes was run for four Mio generations using four chains. Convergence was evaluated by plotting the generations versus logL and the burn-in was set to 1 Mio generations. Node stability was evaluated using posterior probabilities (pp, Bayesian inference) and bootstrap support (200 RAxML rapid bootstrap runs, maximum likelihood) (Stamatakis *et al.*, 2008) with values above .80 considered significant.

Nucleotide sequence accession numbers

The 18S rRNA sequences from this study were submitted to GenBank under accession numbers KJ414464 (*Robbea agricola*), KJ414465 (*Robbea ruetzleri*), KJ414466-7 (*Robbea hypermnestra*), KJ414468 (*Leptonemella vicina*) and KJ414469 (*Catanema* sp.).

Results

Class Chromadorea Inglis, 1983
Subclass Chromadoria Pearse, 1942
Order Desmodorida De Coninck, 1965
Suborder Desmodorina De Coninck, 1965
Superfamily Desmodoroidea Filipjev, 1922
Family Desmodoridae Filipjev, 1922
Subfamily Stilbonematinae Chitwood, 1936
Robbea Gerlach 1956

Diagnosis. (Modified from Tchesunov, 2013): Stilbonematinae. Cuticle transversely striated, except for the head region and the tip of the tail. Cephalic capsule when present with a block-layer; cephalic setae as long or longer than the subcephalic setae, usually directed straight forward. Amphidial fovea well developed, spirally coiled or loop-shaped. Pharynx distinctly tripartite, corpus muscular and clearly set off from the narrow isthmus. Pharynx bulbus largely glandular. Gubernaculum variable in shape, with or without dorso-caudal apophysis. The males of *R. tenax* Gerlach 1963 and the three new species have cup-shaped ventral papillae in the post-pharyngeal region. These species share also a stout body with *a* not exceeding 100. The species *R. gerlachi* Boucher 1975 from which

only a female has been described may also belong to this group. Symbiotic bacteria rod shaped, corn-kernel shaped or coccoid, usually covering the body as a monolayer.

Robbea hypermnestra sp. nov.
http://zoobank.org/urn:lsid:zoobank.org:act:505DEA0B-614A-4086-A52F-62BA8A68F474

Synonymy. *Robbea* sp. in: Ott & Novak (1989), Schiemer *et al*. (1990), Ott *et al*. (1991), Polz *et al*. (1992), Bauer-Nebelsick *et al*. (1995), Urbancik *et al*. (1996a, 1996b), Polz *et al*. (2000); *Robbea* sp. 3 in: Bayer *et al*. (2009), Heindl *et al*. (2011); *Robbea hypermnestra* nomen nudum in: Kampfer *et al*. (1998), Polz *et al*. (2000).

Type material. Holotype (male), 4 paratypes (male), 4 paratypes (female/intersex).

Measurements. See Table 1.

Additional material. Several specimens in the author's collection and those used for SEM.

The sequences of the 18S rRNA gene are available from GenBank and have the accession numbers KJ414466-7.

Type locality. Subtidal sand bar in 10–50 cm depth at the north end of Carrie Bow Cay, Belize in coarse, poorly sorted calcareous sand with rubble (Fig. 1).

Distribution. This robust species is extremely common in the above sand bar (compare Ott & Novak, 1989) and a similar sand bar at the south end of neighbouring South Water Cay. Other localities are open sand patches between *Thalassia testudinum* beds and patch reefs to the west and north of Carrie Bow Cay in up to 1.5 m depth and medium, poorly sorted sand at the base of 'sand bores' south of Carrie Bow Cay in 5–6 m depth (Fig. 1).

Etymology. Named after Hypermnestra, the only one of the 50 daughters of the king of Argos, Danaos, who did not kill her husband in the wedding night as requested by her father although she was armed with a dagger. This refers to the presence of a spiculum in females (intersexes).

Table 1. Morphometric data for *Robbea hypermnestra* sp. nov. Ranges are given for the male and female paratypes. All measurements are in μm.

	Holotype	Paratypes (male) n = 4	Paratypes (female intersexes) n = 4
Length	3125	2765–3535	3020–3985
a	44.5	41.4–58.9	44.4–64.3
b	30.6	23.6–37.2	27.5–36.2
c	17.9	17.4–23.6	23.0–26.9
maximum width	70	55–65	65–82
pharynx length	102	92–100	90–117
tail length	174	140–162	120–150
nerve ring (% pharynx length)	50	48–54	46–58
corresponding body diameter (cbd)	45	45–52	48–55
bulbus length/width	25/32	20–28/29–30	25–38/32–45
bulbus cbd	48	47–50	48–55
V	n.a.	n.a.	41–45
vulva cbd	n.a.	n.a.	65–82
anal (cloacal) body diameter	68	55–65	50–60
tail length:anal diameter	2.6	2.3–2.9	2.3–2.5
spiculae length arc/chord	105/88	98–102/80–85	62–70/53–60
gubernaculum length/apophysis length	20/25	20–30/25–34	10–15/10–15
amphid width	15	16–20	9–12
cephalic setae number/length	4/38	4/32–40	4/30–38
subcephalic setae 1 number/length	8/37	8/30–38	8/28–32
subcephalic setae 2 number/length	8/30	8/28–32	8/28–32
Sucker-like papillae, number	17	16–18	n.a.
Position of first/last papilla	85/501	65–95/440–480	n.a.

n.a. = not applicable.

Description

Body cylindrical (Figs 2, 3), head diameter at level of cephalic setae 20−23 μm, diameter at level of posterior margin of amphidial fovea 40−54 μm in males, 33−42 μm in females, at end of pharynx 47−55 μm, maximum body diameter 55−82 μm, anal diameter 55−68 μm in males, 50−60 μm in females. Tail conical, 140−174 μm long in males and 120−150 μm in females (Figs 7, 8).

Cuticle finely transversely striated except for the first 28−36 μm of the head (Figs 5−8, 14) and the last 35−50 μm of the tail (Fig. 15), annules 0.45 to 0.55 μm wide (18−22 annuli/10 μm); non-striated head cuticle reinforced (cephalic capsule). The anteriormost circle of head sensillae (inner labial sensillae) is represented by 6 finger-like papillae, 2 μm long in lateral, subventral and subdorsal position surrounding the mouth opening (Fig. 19). The second circle consists of 6 short outer labial sensillae, 3−6 μm long, on the margin of the membranous buccal field; 4 cephalic setae flanking the anterior margin of the amphidial fovea, 32−38 μm long; 3 circles of 8 subcephalic setae each, 28−38 μm long, on the non-striated part of the head region, the posteriormost at the level of the posterior margin of the amphidial fovea (Figs 11, 17); 8 rows of somatic setae along the whole length of the body, 20−35 μm long somatic setae alternating with only 5−12 μm long bristles (Fig. 4). In males, there is a distinct field of about 7−10 stout, conical setae, 5 μm long on the ventral side in front of the cloacal opening (Figs 8, 25, 26). Non-striated part of the tail in females with 2 pairs of stout setae, the first pair 7 μm long, shortly behind the end of the annulation; the second pair of 3−4 μm long, close to the tip of the tail (Fig. 15); in males with a small velum ventrally (Fig. 23). Three caudal glands with separate openings at the tail tip (Fig. 16). Males have a 380−450 μm long row of 16−19 (mean 17.2, n = 16) conspicuous cuticular papillae along the mid-ventral line beginning at a distance of 65−95 μm from the anterior end at the level of the posterior bulbus of the pharynx (Figs 4, 20). Papillae cup-shaped, with a diameter of 11−15 μm, on short annulated stalks, bearing a conical seta in its centre (Figs 21, 22). Amphidial foveas situated at the anterior end bordering the buccal field, showing a distinct sexual dimorphism: small, slightly oval spirals with 1.25 turns in females, 13−18 μm long and 9−12 μm wide; in males much larger, elongated loops, 28−38 μm long and 16−20 μm wide (Figs 5, 6, 12, 18, 28, 29).

Pharynx (Figs 4, 27) 90−117 μm long, with a minute tubular buccal cavity, 7−12 μm long and 4 μm in diameter, leading into a conspicuous pyriform muscular corpus, 34−40 μm long and 18−25 μm wide, which is clearly set off from the following 32−40 μm long isthmus. Posterior bulbus subspherical, 20−38 μm long, 30−45 μm wide, largely glandular, containing only weak muscles. No cardia.

Nerve ring 50−65 μm from anterior end; no secretory-excretory pore or ventral gland seen; 8 rows of glandular sense organs (two in each lateral and each median line) connect to the small somatic setae.

Males monorchic, testis on the left side of the intestine, beginning at about 35% of body length; sperm spherical, 10 μm in diameter; spicula (Figs 8, 10, 31) strong, arcuate, slightly cephalate proximally, with blunt tips (Fig. 24), 80−88 μm (chord) or 98−105 μm (arc) long; gubernaculum massive, corpus embracing spicules, 20−30 μm long, with strong dorsocaudal apophysis, 28−34 μm long).

Females didelphic, ovaries reflexed, long uteri leading to a strongly cuticularized vagina; vulva (Fig. 13) at 41−45% of body length. Large eggs (190 × 50 μm) are often present in one or both uteri, which also contain usually many sperm cells of the same shape and size as seen in males. All females are intersexes, having spicula and a gubernaculum in the anal region (Figs 7, 9, 30). Spicula and gubernaculum much smaller and of simpler construction than in males: length of the female spicula, 53−60 μm (chord) or 62−70 μm (arc); gubernaculum, 10−15 μm long with a similar sized apophysis. No traces of other parts of a male genital apparatus were found. A weakly cuticularized vulva primordium but no other female or male characteristic features could be seen in 7 of 11 large (probably 4th stage) juveniles.

The bacteria covering the cuticle of the worms (Fig. 14) are distributed over the whole body, leaving only the tip of the tail and the cephalic capsule uncovered. On the ventral side the bacteria rarely reach the basis of the cephalic capsule. The bacteria are rod shaped and are usually attached with their longitudinal axis perpendicular to the cuticle surface. In a few cases, however, bacteria were seen lying parallel to the cuticular annuli of the worm (Fig. 14). The thiotrophic bacterial ectosymbionts have been previously characterized (Bayer *et al.*, 2009) and belong to the MONTS clade of Gammaproteobacteria (Heindl *et al.*, 2011) that also contains the symbionts of the mouthless nematode genus Astomonema and of gutless oligochaetes. The GenBank accession number for their 16S rRNA gene is EU711428.

Diagnosis. Species with a distinct cephalic capsule with block-layer; 16−19 cup-shaped stalked ventral papillae in the post pharyngeal region; pharynx almost equally divided into corpus, isthmus and bulbus; all females are intersexes; spicula weakly cephalate, gubernaculum with dorsocaudal apophysis, pronounced sexual dimorphism of the amphidial fovea. Symbiotic bacteria rod-shaped.

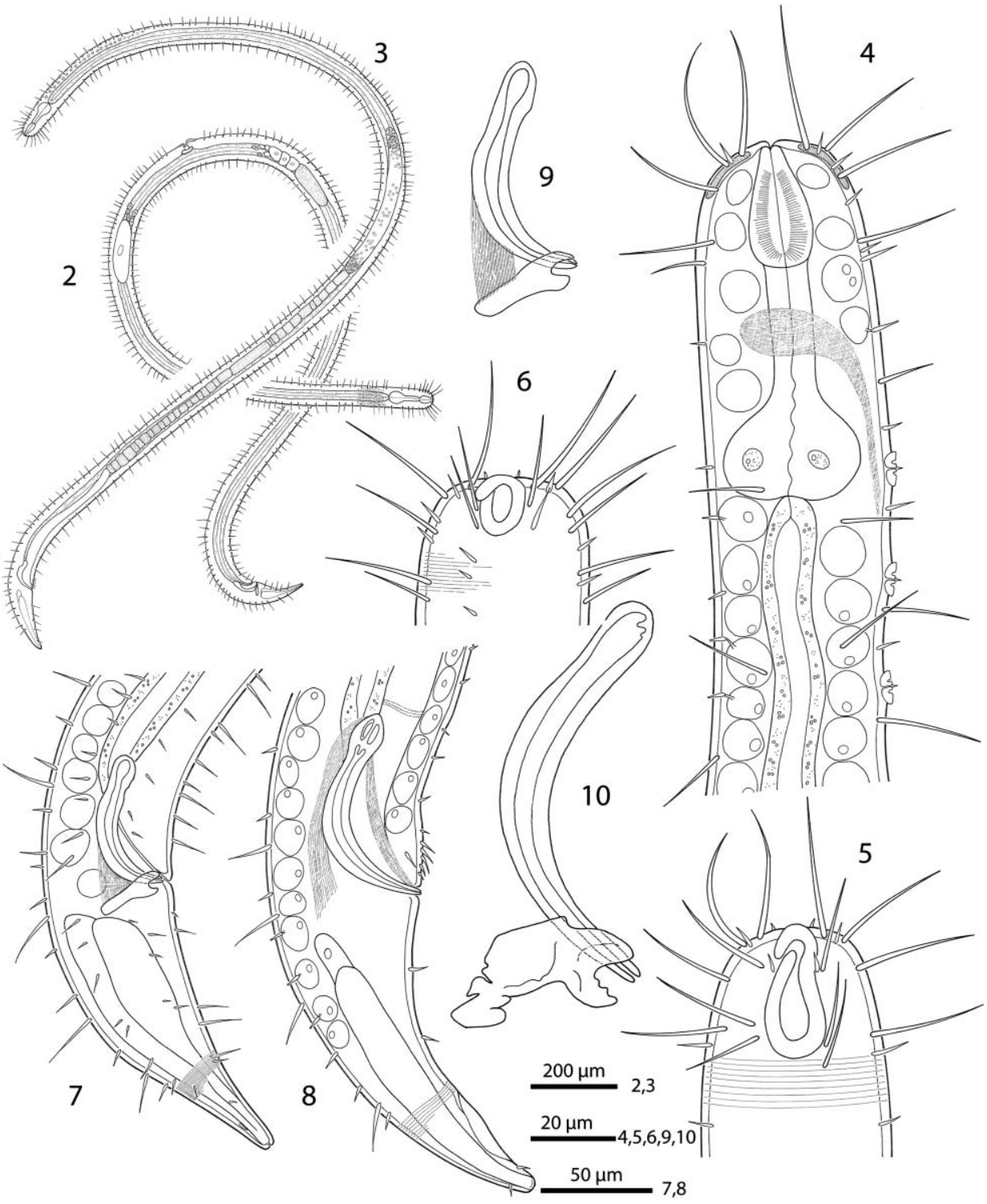

Figs. 2–10. *Robbea hypermnestra* sp. nov. **2**. Female, whole; **3**. Male, whole; **4**. Male, anterior body region; **5**. Male, head, surface view; **6**. Female, head, surface view; **7**. Female, tail; **8**. Male, tail (gubernaculum not drawn); **9**. Female, spiculum; **10**. Male, spiculum.

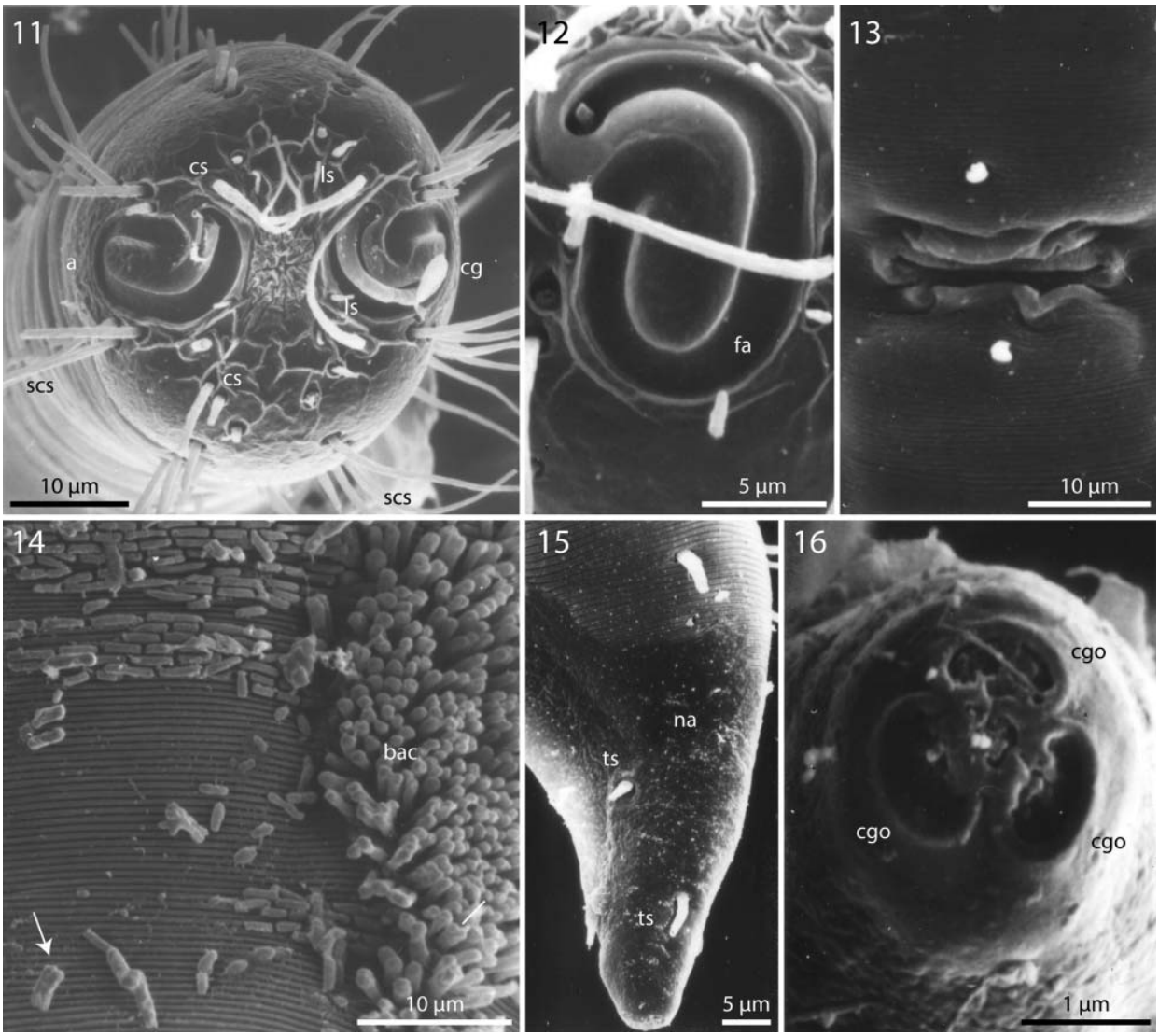

Figs. 11–16. *Robbea hypermnestra* sp. nov. Female. **11**. Head, in face view; **12**. Amphidial fovea; **13**. Vulva; **14**. Annulation and bacterial coat in midbody region; **15**. Tip of tail, non-striated portion; **16**. Openings of the caudal glands. SEM.

Robbea ruetzleri sp. nov.
http://zoobank.org/urn:lsid:zoobank.org:act:92A7E898-62D0-452D-A6A3-9A622CBD4599

Type material. Holotype (male), 3 paratypes (male), 3 paratypes (female).

Measurements. See Table 2.

Additional material. Several specimens in the authors' collection and those used for SEM.

The sequence of the 18S rRNA gene is available from GenBank and has the accession number KJ414465.

Type locality. West side of Twin Cayes, Belize; shallow fine sand among *Rhizophora mangle* stilt roots and *Thalassia testudinum* beds (Fig. 1).

Distribution. Rare, in fine to medium subtidal sand samples (Fig. 1).

Etymology. Named in honour of Klaus Ruetzler, CCRE programme director, friend and generous host on Carrie Bow Cay.

Description

Body slender, cylindrical (Fig. 32), head diameter at level of cephalic setae 20–25 μm, diameter at level of posterior margin of amphidial fovea 25–30 μm at end of pharynx 33–39 μm, maximum body diameter 40–60 μm, anal diameter 32–45 μm. Tail conical, 60–88 μm long (Figs 35, 36).

Cuticle finely transversely striated except for the first 32–44 μm of the head and the last 30–42 μm of the tail,

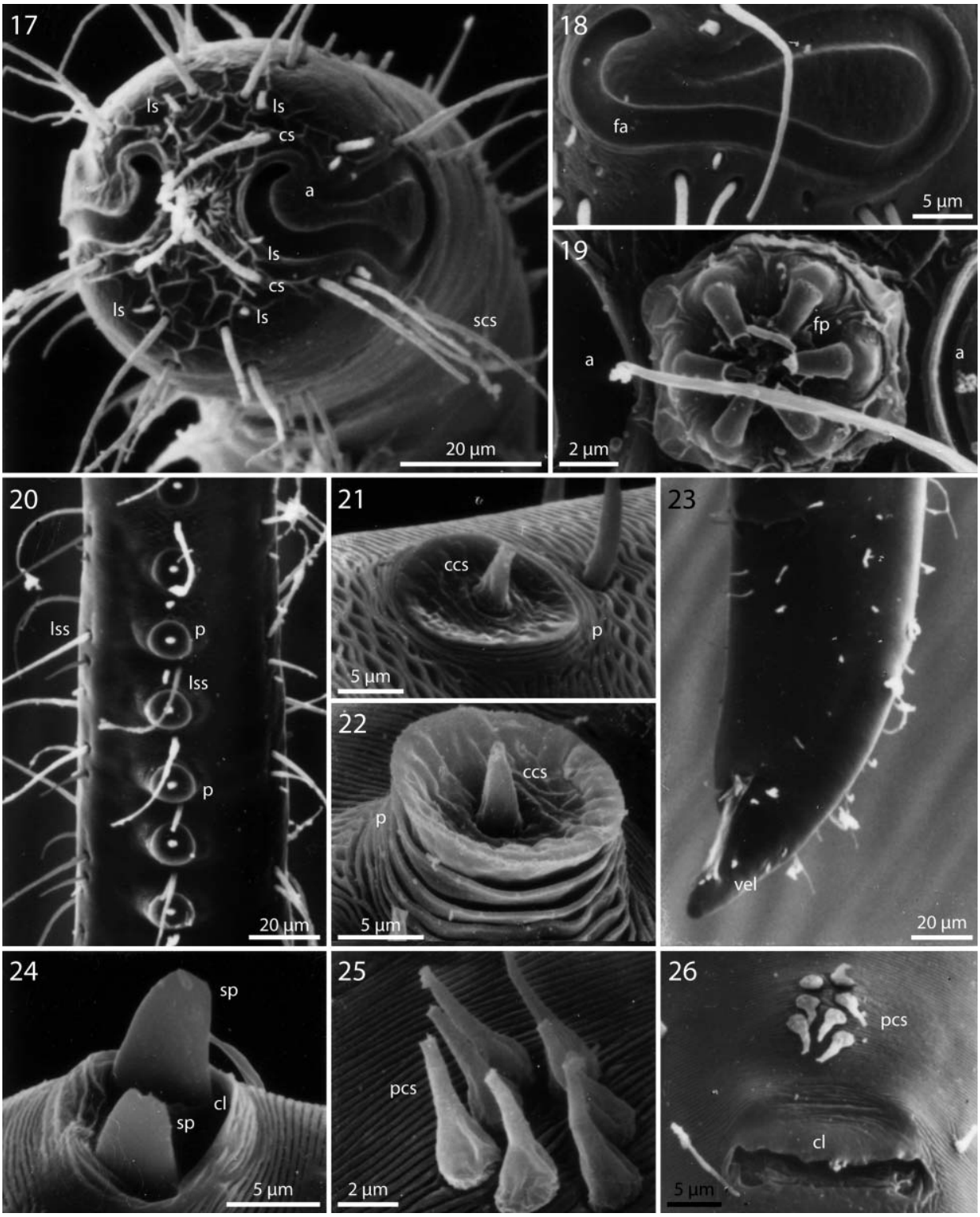

Figs. 17–26. *Robbea hypermnestra* sp. nov. Male. **17**. Head, in face view; **18**. Amphidial fovea; **19**. Mouth opening with fingerlike papillae; **20**. Row of ventral sucker-shaped papillae; **21**. Papilla withdrawn; **22**. Papilla extended; **23**. Tail; **24**. Tips of spicule protruding from cloaca; **25**. Group of precloacal setae; **26**. Cloaca and precloacal setae. SEM.

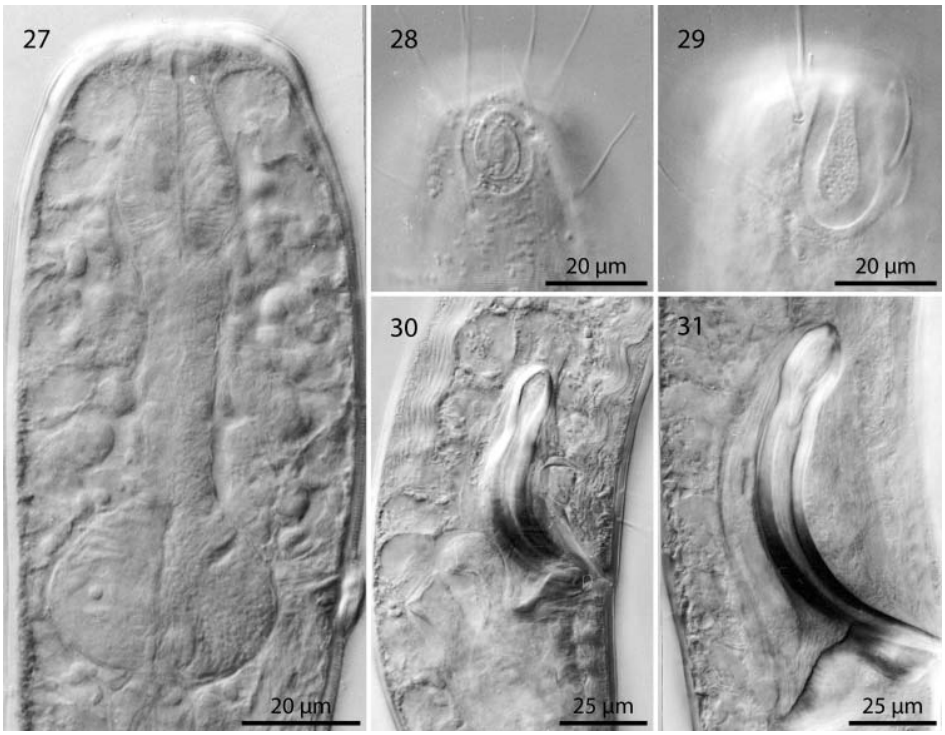

Figs. 27–31. *Robbea hypermnestra* sp. nov. **27**. Pharyngeal region, optical section; **28**. Female, amphidial fovea; **29**. Male, amphidial fovea; **30**. Female, spiculum; **31**. Male, spiculum. LM Interference contrast.

annules 0.5–0.65 µm wide (15–20 annuli/10 µm) (Figs 39, 42); head with a circle of 6 finger-like inner labial papillae surrounding the mouth opening (Fig. 38); 6 short outer labial sensillae, 2.5–4 µm long, at the margin of the membranous buccal field; 4 cephalic setae, flanking the anterior margin of the amphidial fovea, 21–27 µm long (Figs 33, 34, 37); a first circle of 8 subcephalic setae at the level of the amphidial fovea, a second circle approximately in the middle, a third circle at the posterior margin of the cephalic capsule; subcephalic setae, 18–27 µm long, 8 rows of somatic setae along the whole length of the body. Somatic setae of males in the region of the row of ventral papillae stout, 12–17 µm long, the following body setae thinner and shorter (8–13 µm). There is a transverse row of precloacal setae a short distance anterior to the cloacal opening (Figs 36, 42, 43). Somatic setae of females in cervical region 12–15 µm long, the following body setae 17–20 µm long. Males with a 250–320 µm long row of 15–17 conspicuous mid-ventral cuticularized papillae (Figs 34, 40), first papilla situated a short distance posterior to the end of the pharynx. Papillae with short annulated stalks, bearing central conical setae (Fig. 41). The non-striated part of the tail bears no terminal setae, in males there is a velum present (Figs 42, 44). Loop-shaped amphidial foveas (7–12 µm long, 10–12 µm wide), situated at the anterior end bordering the buccal field, with only slight sexual dimorphism.

Pharynx 72–90 µm long; minute tubular buccal cavity, 10–15 µm long and 2–4 µm in diameter, leading into a conspicuous pyriform muscular corpus, 22–30 µm long and 16–18 µm wide, clearly set off from the following 24–41 µm long isthmus. Spherical bulb, 12–18 µm long and 17–20 µm wide, mainly glandular and containing only weak muscles. No cardia (Figs 33, 34, 45).

Nerve ring 42–60 µm from anterior end; no secretory-excretory pore or ventral gland seen; there are 8 rows of glandular sense organs (two in each lateral and each median line) connecting to the small somatic setae.

Males monorchic, testis on the left side of the intestine, beginning at about 35% of body length; spicula strong, arcuate, distinctly cephalate proximally, 60–66 µm (chord) or 72–85 µm (arc) long, without velum; gubernaculum simple, embracing the distal part of the spicula laterally, with dorsally directed apophysis (35–37 µm long) (Figs 36, 47). Females didelphic, ovaries reflexed, long uteri leading to the vagina; vulva at 52–54 of body length.

A dense monolayer of rod-shaped symbiotic bacteria (Fig. 39) covers almost the whole body, beginning at the level of the pharyngeal terminal bulb or at the level of the posterior region of the cup-shaped cervical papillae (Fig. 46) and terminating with the cuticle striation at the tail tip or already at the level of the cloacal opening.

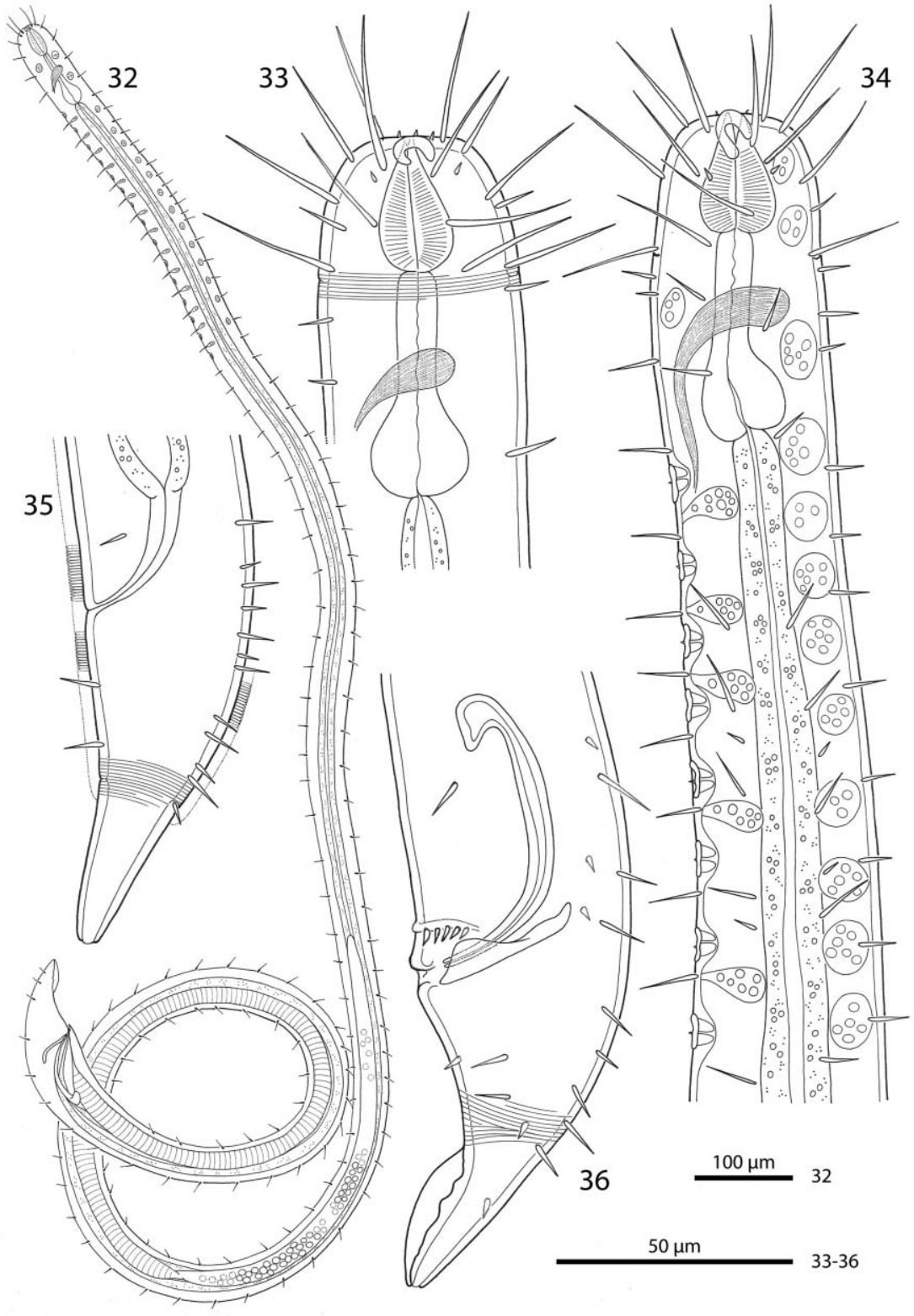

Figs. 32–**36.** *Robbea ruetzleri* sp. nov. **32**. Male, whole; **33**. Female, anterior body region; **34**. Male, anterior body region; **35**. Female, tail; **36**. Male, tail and spicular apparatus.

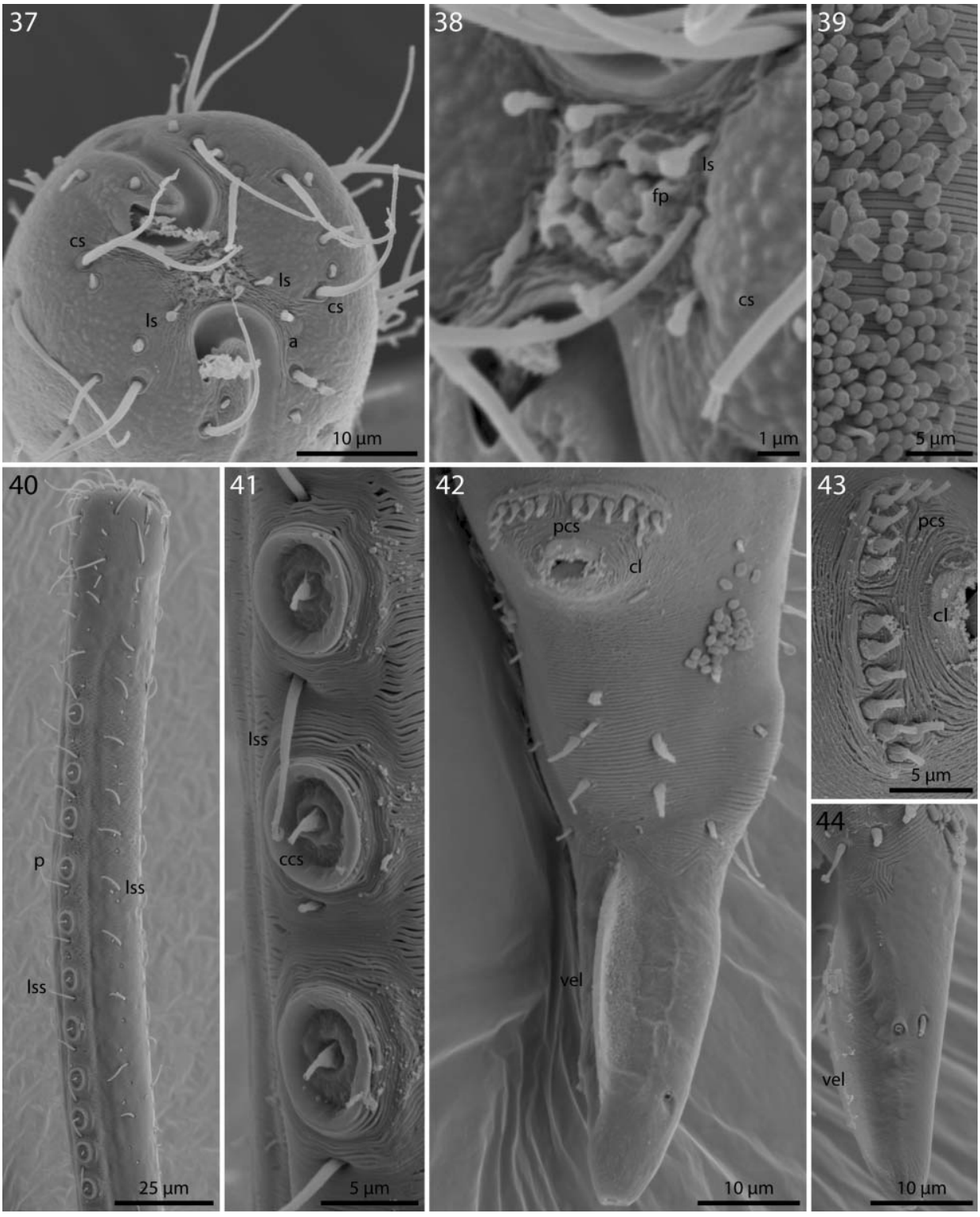

Figs. 37–44. *Robbea ruetzleri* sp. nov. **37**. Male, head in face view; **38**. Mouth opening with fingerlike papillae and circle of outer labial sensillae; **39**. Annulation and bacterial coat in midbody region; **40**. Male, anterior body region with row of sucker-shaped papillae; **41**. Male, detail of papillae; **42**. Male, tail, cloaca and precloacal setae; **43**. Precloacal setae; **44**. Male, Tip of tail with velum. SEM.

Table 2. Morphometric data for *Robbea ruetzleri* sp. nov. Ranges are given for the male and female paratypes. All measurements are in μm.

	Holotype	Paratypes (male) n = 3	Paratypes (female) n = 3
Length	2320	2280–3150	2750–3790
a	58.0	57.0–78.8	54.6–70.2
b	30.9	27.8–31.5	33.5–45.1
c	18.9	23.8–47.0	37.2–40.8
maximum width	40	40–45	50–60
pharynx length	75	72–90	72–78
tail length	72	70–88	69–75
nerve ring (% pharynx length)	53	55–60	55–58
corresponding body diameter (cbd)	38	35–40	38–42
bulbus length/width	12/17	15–17/19–20	12–18/18–20
bulbus cbd	35	34–39	33 –39
V	n.a.	n.a.	52–54
vulva cbd	n.a.	n.a.	50–60
anal (cloacal) body diameter	40	40–45	32–40
tail length:anal diameter	1.8	1.8–2.0	1.7–2.2
spiculae length arc/chord	75/60	72–85/60–66	n.a.
gubernaculum length	35	36–39	n.a.
amphid width	10	10–12	10–12
cephalic setae number/length	4/23	4/21–27	4/22–27
subcephalic setae 1 number/length	8/26	8/25–26	8/23–27
subcephalic setae 2 number/length	8/23	8/20–22	8/18–22
Sucker-like papillae, number	15	15–17	n.a.
Position of first/last papilla	72/315	80–105/305–415	n.a.

n.a. = not applicable.

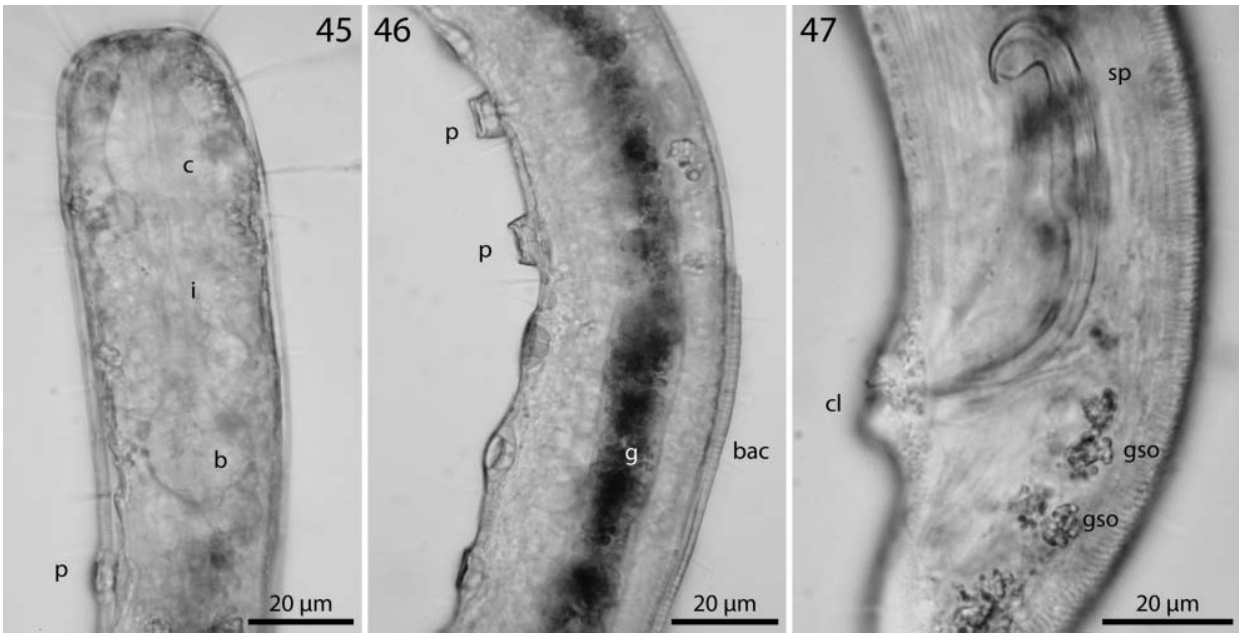

Figs. 45–47. *Robbea ruetzleri* sp. nov. **45**. Pharyngeal region, optical section; **46**. Male, sucker-shaped papillae and begin of bacterial coat; **47**. Male, spiculum. LM of live animals.

Rows or plaques of smaller cocci stretch forward up to the anterior bulbus of the pharynx, but not up to the non-striated part of the head.

Diagnosis. Species with indistinct cephalic capsule; 14−17 cup-shaped stalked ventral papillae in the post pharyngeal region; pharynx almost equally divided into corpus, isthmus and bulbus; spicula strongly cephalate, gubernaculums without apophysis; amphidial fovea in both sexes open loop-shaped. Symbiotic bacteria rod shaped.

Robbea agricola sp. nov.
http://zoobank.org/urn:lsid:zoobank.org:act:97995BAA-7914-4578-A4DE-64ED0DEF761B

Type material. Holotype (male), 3 paratypes (male), 3 paratypes (female).

Additional material. Several specimens in the authors' collection and those used for SEM.

Measurements. See Table 3.
The sequence of the 18S rRNA gene is available from GenBank and has the accession number KJ414464.

Type locality. West side of Twin Cayes, Belize; shallow fine sand among *Rhizophora mangle* stilt roots and *Thalassia testudinum* beds (Fig. 1).

Distribution. Regularly in fine sand samples at several locations in the vicinity of the CBC laboratory (Fig. 1).

Etymology. Agricola (lat.) = farmer (German 'Bauer'), named after Monika Bright (then Monika Bauer) who provided the first specimens.

Description

Body slender, cylindrical (Figs 48, 49), tapering only slightly towards anterior end, head diameter at level of cephalic setae 18−25 μm, diameter at level of posterior margin of amphidial fovea 20−29 μm, at end of pharynx 25−33 μm, maximum body diameter 33−42 μm, anal diameter 24−35 μm. Tail conical, 70−105 μm long; non-striated tail tip 17−19 μm long in males and 23−30 μm in females (Figs 52, 53, 62).

Cuticle finely transversely striated except 24−28 μm of the anterior part of the head (cephalic capsule) and the tail tip, annules 0.6 to 0.7 μm wide (14−17 annuli/10 μm) (Fig. 57). Mouth opening surrounded by 6 finger-like inner labial papillae in lateral, subventral and subdorsal position (Fig. 56) followed by a circle of 6 short labial sensillae, 3−4 μm long, surrounding the membranous buccal field; a circle of 4 cephalic setae flanking the anterior margin of the amphidial fovea, 20−22 μm long; closely followed by a circle of 8 subcephalic setae, 16−26 μm long, a second circle near the end of the cephalic capsule (Figs 50, 51, 55); 8 rows of somatic setae along the whole length of the body, 5−8 μm long; a pair of 6−8 μm long setae at the begin of the non-striated part of the tail. No special precloacal setae. Mid-ventral line of males with a 150−170 μm long row of 8−9 conspicuous cup-shaped papillae (diameter 7 μm) positioned on short stalks. Papillae with central setae (1.5 μm long) (Figs 51, 59, 60). The first of these papillae is situated at a distance of 70−110 μm from the anterior end at the level of the pharyngeal terminal bulb. Amphidial foveas spiral with 2.5 turns, slight sexual dimorphism: in females oval, 12−13 μm long and 8−12 μm wide, situated directly at the anterior end bordering the buccal field; in males larger, somewhat elongated, 15−16 μm long, 12−14 μm wide, 1−4 μm from the anterior end (Figs 50, 51, 64).

A minute tubular buccal cavity, 7−10 μm long and 2−3 μm in diameter, leading into a tripartite, 60−95 μm long pharynx consisting of an anterior pyriform muscular corpus (19−30 μm long, 12−18 μm wide), the following isthmus (30−50 μm long) and the terminal bulb (12−18 μm long, 17−20 μm wide). Terminal bulb largely glandular, containing only weak muscles. No cardia (Figs 50, 51, 63, 69).

Nerve ring 44−67 μm from anterior end; no secretory-excretory pore or ventral gland seen; 8 rows of glandular sense organs (two in each lateral and each median line) connecting to the small somatic setae.

Males monorchic, testis on the left side of the intestine, beginning at about 35% of body length; spicula strong, arcuate, slightly cephalate proximally, 35−45 μm (chord) or 55−58 μm (arc) long, with a velum; gubernaculum with a strong dorso-caudal directed apophysis (13−15μm long) ending in a spherical swelling (Figs 53, 54, 65).

Females didelphic, ovaries reflexed, long uteri leading to the vagina, ventral gso enlarged in the region of the uteri; vulva at 52−55% of body length.

Epigrowth of symbiotic bacteria starting at a defined line at a distance from the anterior end (Figs 66, 67) showing a sexual dimorphism: in males the bacterial coat begins at 220−340 μm (2.7−3.5 pharynx length), in females at 155−195 μm (2−2.3 pharynx length). A monolayer of corn-kernel shaped bacteria (1.5 × 0.8 μm) (Figs 57, 58) covers the remaining body except the non-striated tip of the tail. At the start of the coat the body diameter abruptly becomes smaller to accommodate the thickness of the bacterial layer without increasing the consortium's diameter (Fig. 67). In some specimens patches of bacteria occur around the cup-shaped papillae; here rods lie parallel to the cuticle surface (Fig. 61). Occasionally larger coccoid bacteria are found on the normally symbiont-free anterior body part (Fig. 68). The role of these bacteria is unknown.

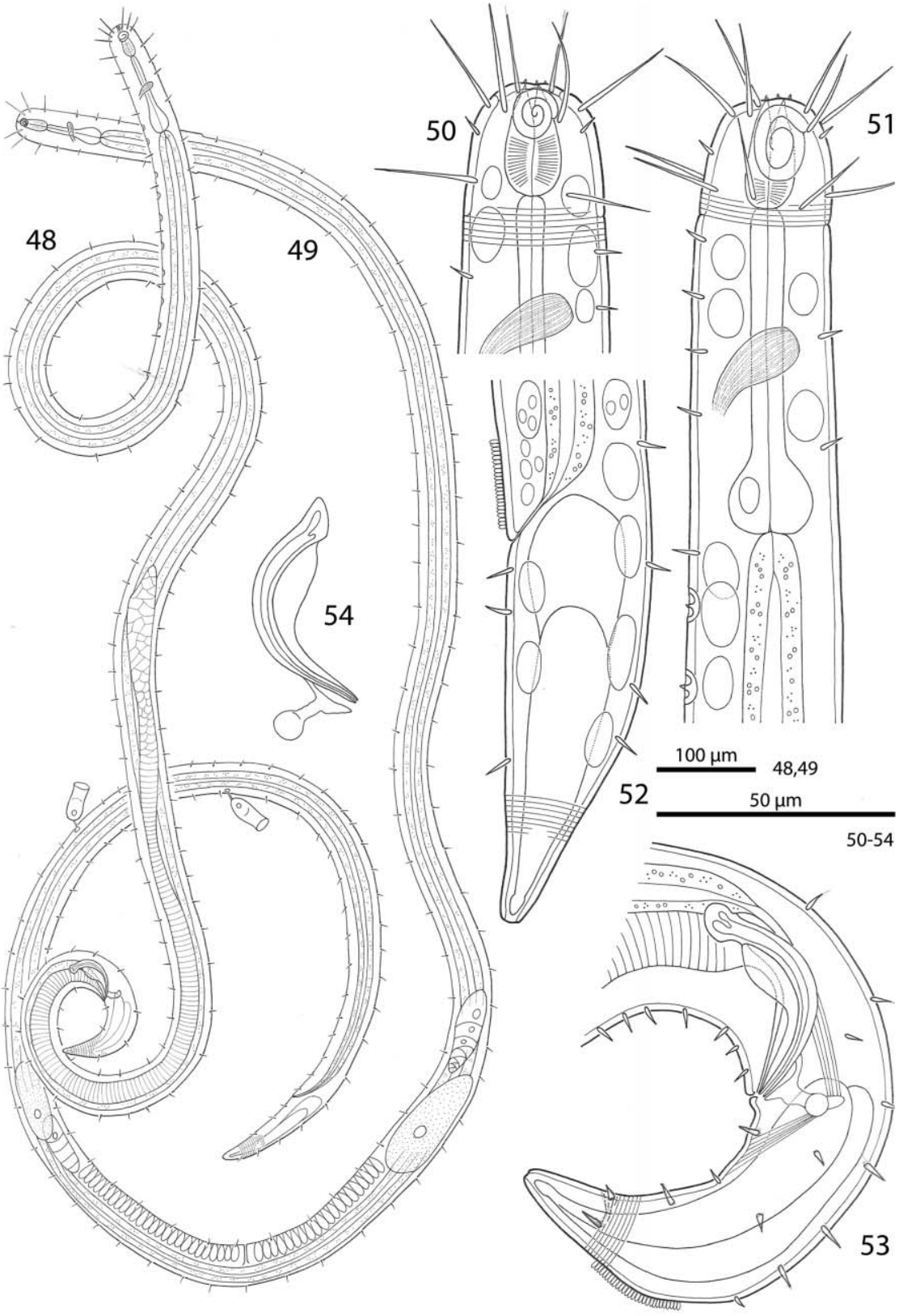

Figs. 48–**54.** *Robbea agricola* sp. nov. **48**. Male, total; **49**. Female, total; **50**. Female, head region; **51**. Male, anterior body region; **52**. Female, tail; **53**. Male, tail; **54**. Spicular apparatus.

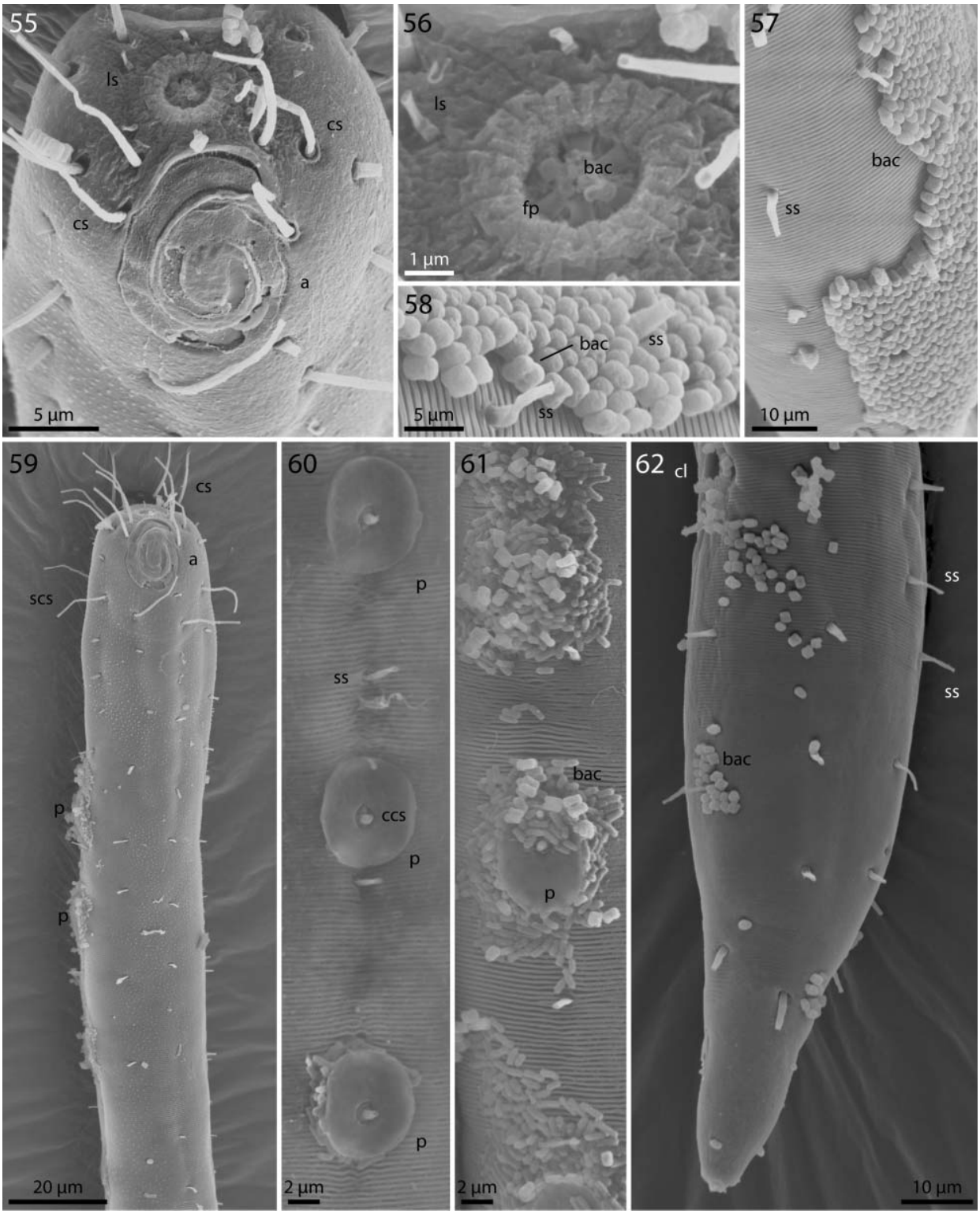

Figs. 55–62. *Robbea agricola* sp. nov. **55**. Male, head in face view; **56**. Mouth opening with fingerlike papillae; **57**. Annulation and bacterial coat in midbody region; **58**. Coat of corn-kernel shaped bacteria; **59**. Male, anterior body region with the first part of the row of sucker-shaped papillae; **60**. Papillae; **61**. Papillae surrounded by bacterial growth; **62**. Female, tail. SEM.

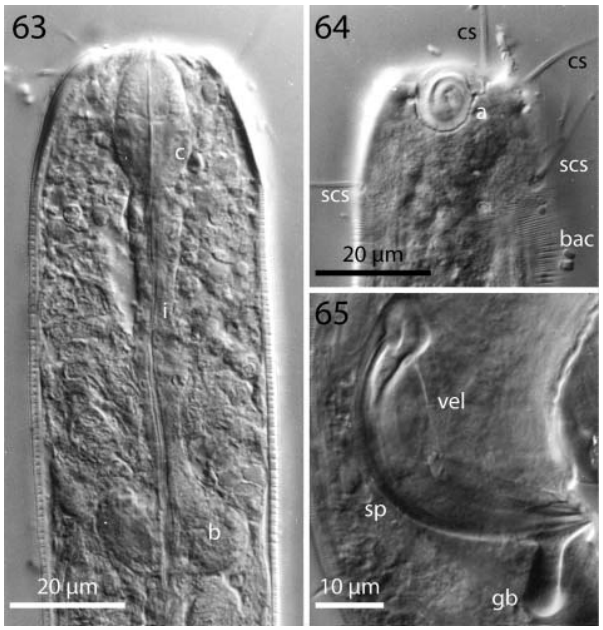

Figs. 63–65. *Robbea agricola* sp. nov. 63. Pharyngeal region, optical section; **64**. Male, amphidial fovea; **65**. Male, spiculum. LM Interference contrast.

Suctorians are frequently attached to the cuticle in the posterior body region (Fig. 49).

Diagnosis. Species with indistinct cephalic capsule; 8–9 cup-shaped ventral papillae in post-pharyngeal region; isthmus occupies more than 50% of pharynx length; spicula cephalate with velum, gubernaculums with dorso-caudal apophysis ending in a spherical swelling; amphidial fovea spiral in both sexes, larger in males. Symbiotic bacteria corn-kernel shaped, bacterial coat starting at a defined line 2 to 3.5 pharynx lengths from the anterior end.

Discussion

Systematics

Gerlach (1956) erected the genus *Robbea* for a male animal collected on the coast of Brazil, which he named *Robbea caelestis*. A second species was subsequently described from the Maldive Islands by the same author, *Robbea tenax* Gerlach (1963). The material consisted of one female and three males, the latter showing conspicuous cervical papillae. Both *Robbea* species were later placed into the genus *Catanema* Cobb, 1920 by Platt & Zhang (1982). Recently Tchesunov (2013) proposed diagnoses for both *Robbea* and *Catanema* in which the major distinguishing character is the shape of the amphidial fovea, which is distinct in *Robbea* but is reduced to a small apical opening in *Catanema*. Other characters such as the degree to which the pharyngeal corpus is set off from the isthmus, 'clearly' in *Robbea*, 'distinctly' in *Catanema* (see Fig. 70 for the situation in *Robbea hypermnestra*), and the presence (*Robbea*) or absence (*Catanema*) of a cephalic capsule are less clear and not all descriptions published so far contain explicit statements regarding these characters. According to Tchesunov's criteria, the

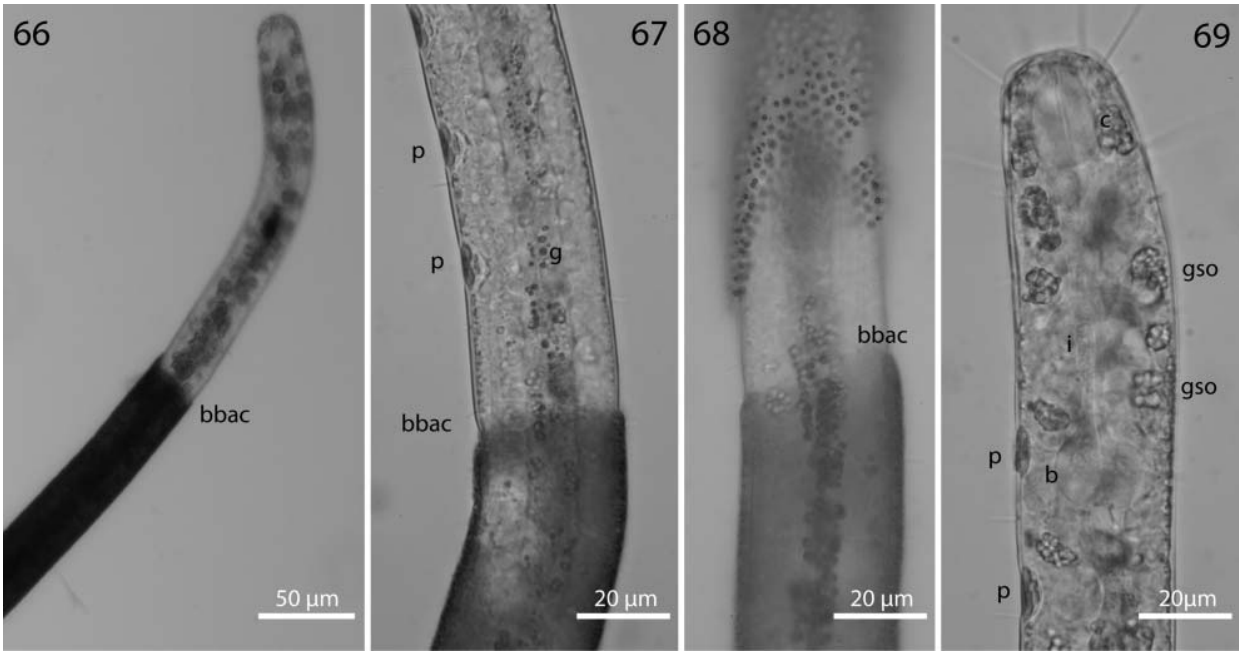

Figs. 66–69. *Robbea agricola* sp. nov. **66**. Anterior body region and beginning of bacterial coat; **67**. Beginning of bacterial coat, detail; **68**. Large cocci on anterior body region; **69**. Glandular sensory organs. LM of live animals.

Table 3. Morphometric data for *Robbea agricola* sp. n. Ranges are given for the male and female paratypes. All measurements are in μm.

	Holotype	Paratypes (male) n = 3	Paratypes (female) n = 3
Length	1880	1780–2550	2280–2550
a	47.0	40.0–54.3	57.0–68.2
b	19.8	19.6–28.7	28.0–37.4
c	22.1	18.8–21.3	27.3–29.6
maximum width	40	33–38	35–42
pharynx length	95	60–75	80–90
tail length	85	78–105	70–85
nerve ring (% pharynx length)	57	53–60	53–62
corresponding body diameter (cbd)	30	28–35	30–32
bulbus length/width	15/20	12–15/17–18	12–15/18–20
bulbus cbd	30	25–32	28–33
V	n.a.	n.a.	52–55
vulva cbd	n.a.	n.a.	35–42
anal (cloacal) body diameter	30	30–35	24–30
tail length:anal diameter	2.8	2.6–3.3	2.3–3.5
spiculae length arc/chord	55/40	45–58/35–45	n.a.
gubernaculum length/apophysis length	15/15	10–12/10–13	n.a.
amphid width	16	12–14	8–12
cephalic setae number/length	4/21	4/20–21	4/21–22
subcephalic setae 1 number/length	8/20	8/16 –20	8/20–26
subcephalic setae 2 number/length	8/16–18	8/13–16	8/18–22
Sucker-like papillae, number	9	9	n.a.
Position of first/last papilla	90/260	70–98/225–268	n.a.

n.a. = not applicable.

following species belong to the genus *Robbea*: *R. caelestis* Gerlach 1956, *R. tenax* Gerlach 1963, *R. gallica* Vitiello 1974, R. (*Catanema*) *porosum* Hopper & Cefalu 1973, *R.* (*Catanema*) *macintyrei* Platt & Zhang 1982, *R.* (*Catanema*) *smo* Platt & Zhang 1982, furthermore the animal that Hopper & Cefalu (1973) described as *R. tenax* from Florida and the three new species described herein. *R. gerlachi* Boucher 1975 has only been described from a female, but according to the shape of its amphidial fovea it should be placed into the genus *Robbea.* One additional species of *Robbea* has been suggested by Tchesunov (2013), but due to the lack of male specimens the species has not been described in detail yet.

In the genus *Catanema* only two formally described species remain, the type species *C. exile* Cobb 1920 and *C. dambayensis* Tchesunov 2013. *Catanema cobbi* Inglis 1967 has been placed into the genus *Laxus* by Ott *et al.* (1995), *Catanema gerlachi sensu* Hopper & Cefalu 1973 most probably belongs to *Laxus cosmopolitus* (Ott *et al.*, 1995).

To consolidate the taxonomic descriptions of the three newly described *Robbea* species on a molecular level we used phylogenetic 18S rRNA analyses. The tree shows a clear separation between the clade containing the three new *Robbea* species and the other Stilbonematinae (Fig. 71). We also provide additional 18S rRNA gene sequences for the genera *Catanema* and *Leptonemella* that only had a single 18S rRNA gene deposited prior to this study. The morphological characters of the three yet undescribed *Catanema* species included in the phylogenetic analyses conform to the diagnosis given by Tchesunov (2013). Our data confirm that both *Robbea* and *Catanema*, as well as all other genera of Stilbonematinae with available sequence data are represented by statistically supported genus level clades in 18S rRNA gene based phylogenetic analyses. This high resolution of the 18S rRNA gene finally allows to assign or to re-evaluate the correct taxonomic affiliation at the genus level for new or already deposited sequences.

For the moment this ends the confusion around these two genera to which we have added by assigning two stilbonematine species to the genus *Robbea* (namely *Robbea* sp. 1 and 2) in Bayer *et al.* (2009). We have reinvestigated the nematode material used in that paper where possible. In the case of *Robbea* sp. 1 from Calvi (Corse), there obviously had been a mix-up during the sample sorting, and

Fig. 70. *Robbea hypermnestra* sp. nov. Semi-thin longitudinal section through pharynx showing separation of corpus from isthmus and glandular bulbus.

two different nematode species were present in the sample analysed: a *Laxus* sp. that is morphologically indistinguishable from *Laxus cosmopolitus* described from the Adriatic (Ott *et al*., 1995) and a yet undescribed *Catanema* species. Judging from the phylogenetic position of the deposited 18S rRNA gene, a specimen of the former species was probably sequenced. *Robbea* sp. 2 from the Cayman Islands is a member of the *Catanema* clade (Fig. 71). *Robbea* sp. 3 is morphologically and phylogenetically identical to the newly sequenced *Robbea hypermnestra* sp. nov. specimens (Fig. 71). The 18S sequences for *Robbea hypermnestra* sensu Kampfer 1998 (*nomen nudum*) that were formerly deposited under Y19621 were identified as chimeric but the last 600 bp are identical to the correct *Robbea hypermnestra* sp. nov. sequences from this study as well as to the *Robbea* sp. 3 sequence published by Bayer *et al*. (2009). The sequences in the Kampfer *et al*. (1998) paper were generated from pools of up to 50 nematodes that likely were contaminated by other nematode species. Thus, the chimeric nature of the published sequences could likely be attributed to different priming bias in the forward and reverse primers used. In contrast, all sequences generated in the present work come from single nematode specimens. This has been made possible with high-yield DNA extraction methods based on GeneReleaser (Bioventures) (Schizas *et al*., 1997) or the Blood and Tissue kit (Qiagen) combined with highly sensitive and efficient polymerases such as the Phusion® DNA polymerase (Finnzymes). Successful PCR based sequencing of multiple genes from the DNA of a single meiofauna individual has been performed without amplification using specimens as small as 500 μm long microturbellarians (Gruber-Vodicka *et al*., 2011). We thus emphasize that, wherever possible, single individuals should be used for PCR-based gene assays.

While the diagnoses given by Tchesunov (2013) currently hold true for the genera *Robbea* and *Catanema*, they are based on characters such as the reduction of the amphidial foveas. However, these characters are also present in some species of other genera, such as *Stilbonema* and *Leptonemella* (e.g. in the type species *L. cincta* COBB 1920). Findings of new species may make emendation of diagnoses that were based on morphology alone necessary. Our results clearly indicate the necessity to provide molecular data to confirm the morphological identification and that larger taxon sampling is an important factor to be able to validate sequencing results and enable for example barcoding approaches.

Intersexes

Cases of intersexuality have been described from various terrestrial, parasitic or marine nematodes (e.g. Zhuo *et al*., 2009; Moura *et al*., 2014). In the latter, intersexes are most commonly reported as females with a functional reproductive system and rudimentary male sexual characters (e.g. Gourbault & Vincx, 1990; Riemann *et al*., 2003; Zhuo *et al*., 2009; Miljutina *et al*., 2013; Moura *et al*., 2014), just as observed in our newly described *R. hypermnestra*. However, only few intersex individuals are usually found within nematode populations (Gourbault & Vincx, 1990). As driving factor for intersexuality in nematodes, unfavourable environmental conditions (Davide & Triantaphyllou, 1968), hybridization between closely related species (Steiner, 1923; Krall, 1972) or genetic or chromosomal disorder (Roy & Gupta, 1975; Jairajpuri *et al*., 1977) have been hypothesized. Considering the clean and stable environment around Carrie Bow Cay and the fact that all females of *R. hypermnestra* are intersexes, environmental sex determination appears unlikely. We cannot exclude

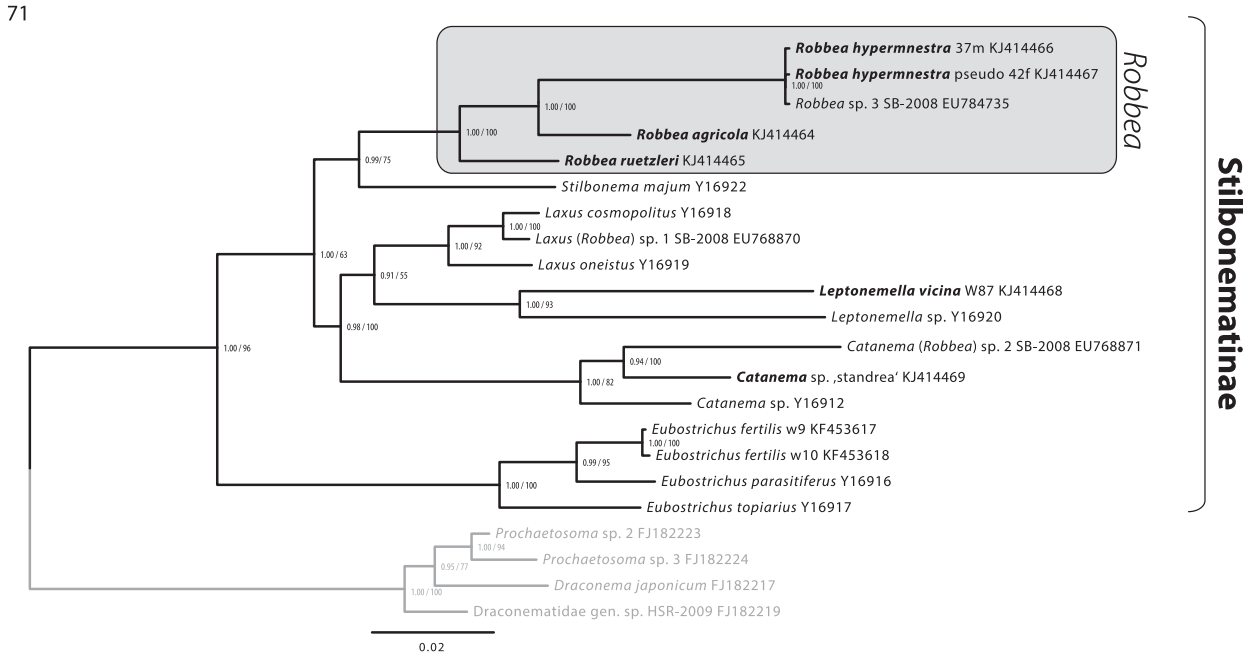

Fig. 71. Phylogenetic relationships of the genera of the Stilbonematinae based on the 18S rRNA gene. The tree shown was calculated using maximum likelihood (RAxML) and node support is given as aLRT as well as Bayesian posterior probabilities. The scale bar indicates 0.02 nucleotide substitutions per site.

hybridization events with closely related species in the past. It is difficult to assign any specific function to the spicula observed in *R. hypermnestra* intersexes and the *R. hypermnestra* chromosome set has not been determined, thus our hypotheses will remain rather speculative. The spicula could be remnants from a previously hermaphroditic lifestyle, but since no hermaphroditic lifestyle is known from stilbonematine nematodes, the interpretations that *R. hypermnestra* females are in a transition to a hermaphroditic stage, is more likely. In fact, individuals of the well-studied terrestrial nematodes *C. elegans* and *C. briggsae* are either male or hermaphrodites where the hermaphrodites are descendants from male or female ancestors and mutations in two independent pathways were sufficient for *C. elegans* to develop self-fertile hermaphrodites (Baldi *et al.*, 2009). This indicates a high plasticity and flexibility in the expression of sexual phenotypes in nematodes in general. Hermaphroditism could be favourable at low effective population densities to ensure reproduction in the absence of a mating partner (Pires-DaSilva, 2007). To test whether this is the case, the distribution patterns and gender ratios of the *R. hypermnestra* populations need to be monitored systematically.

Ecological notes

The shallow subtidal sands around Carrie Bow Cay harbour a diverse interstitial meiofauna. Among these are representatives of several taxa known to harbour bacterial symbionts. These include the ciliate genus *Kentrophoros*, the mouthless nematode genus *Astomonema* (authors' unpublished observation), several species of the mouthless catenulid flatworm genus *Paracatenula* (Dirks *et al.*, 2011; Gruber-Vodicka *et al.*, 2011) and the gutless marine oligochaete genera *Inanidrilus* and *Olavius* (Erséus, 1990). So far, stilbonematid nematode species of several genera have been described from shallow water habitats around Carrie Bow Cay. These include *Laxus oneistus*, *Stilbonema majum*, *Adelphus rolandi*, *Eubostrichus dianae*, *E.parasitiferus* and *E. fertilis* (Ott *et al.*, 1995, 2014; Ott, 1997; Kampfer *et al.*, 1998; Polz *et al.*, 1999). We add to this diversity with our description of three new *Robbea* species that live in vicinity of Carrie Bow Cay (Fig. 1). Available physiological and molecular evidence shows that all (*Paracatenula*, Stilbonematinae) or the majority of bacterial symbionts (oligochaetes) are sulphur-oxidizing chemoautotrophs (SOBs) (Dubilier *et al.*, 2006; Bayer *et al.*, 2009; Gruber-Vodicka *et al.*, 2011). Associations of SOBs with motile hosts appear to be beneficial when oxygen-containing surface layers are spatially separated from sulphidic deeper layers and vertical migration by the host can alternately supply the symbiotic bacteria with sulphide and oxygen (Giere *et al.*, 1991; Ott *et al.*, 1991).

Shallow sandbars in the immediate back reef area of Carrie Bow Cay consist of coarse to medium, unsorted carbonate sand of local origin that has been deposited under sheltered conditions and has a spacious interstitium with reduced, sulphidic conditions in layers several

centimetres below the sediment surface (Ott & Novak, 1989). Here large species of Stilbonematinae (*Laxus oneistus*, *Stilbonema majum*) and also *R. hypermnestra* are found in high densities (Ott & Novak, 1989). In contrast, a diverse assemblage of smaller Stilbonematinae species such as *E. dianae*, *E. fertilis*, *R. agricola* and *R. ruetzleri* inhabit the fine sands in the vicinity of lagunal mangrove islands and *Thalassia testudinum* seagrass beds (Ott *et al.*, 2014). Additionally to the described species, several undescribed species and possibly genera of stilbonematine nematodes can be found in the shallow water habitats in the vicinity of Carrie Bow Cay (authors' pers. observation).

Acknowledgements

We thank Werner Urbancik, Veronica Novotny and Monika Bright for providing several micrographs and Sigrid Neulinger for executing the ink drawings. We gratefully acknowledge the generous help of Klaus Ruetzler and the staff of the Carrie Bow Cay Laboratory.

Funding

We are grateful to the Core Facility Cell Imaging and Ultrastructure Research of the University of Vienna for technical support and the Max Planck Society for funding. This is contribution # 962 from the Carrie Bow Cay Laboratory (CCRE Program of the National Museum of Natural History, Washington, DC). N.L. was supported by an Austrian Science Fund (FWF) grant P22470-B17 (S. Bulgheresi, PI) and H.R. G.-V. by a Marie-Curie Intra-European Fellowship PIEF-GA-2011-301027 CARISYM.

References

Baldi, C., Cho, S. & Ellis, R.E. 2009. Mutations in two independent pathways are sufficient to create hermaphroditic nematodes. *Science* **326**, 1002–1005.

Bauer-nebelsick, M., Blumer, M., Urbancik, W. & Ott, J.A. 1995. The glandular sensory organ of Desmodoridae (Nematoda) – ultrastructure and phylogenetic implications. *Invertebrate Biology* **114**, 211–219.

Bayer, C., Heindl, N.R., Rinke, C., Lücker, S., Ott, J.A. & Bulgheresi, S. 2009. Molecular characterization of the symbionts associated with marine nematodes of the genus *Robbea*. *Environmental Microbiology Reports* **1**, 136–144.

Boucher, G. 1975. Nématodes des sables fins infralittoraux de la Pierre Noire (Manche occidentale). I. Desmodorida. *Bulletin du Muséum National d'Histoire Naturelle, Paris 3e série* **285**, 101–128.

Bulgheresi, S., Schabussova, I., Chen, T., Mullin, N.P., Maizels, R.M. & Ott, J.A. 2006. A new C-type lectin similar to the human immunoreceptor DC-SIGN mediates symbiont acquisition by a marine nematode. *Applied and Environmental Microbiology* **72**, 2950–2956.

Bulgheresi, S., Gruber-vodicka, H.R., Heindl, N.R., Dirks, U., Kostadinova, M., Breiteneder, H. & Ott, J.A. 2011. Sequence variability of the pattern recognition receptor Mermaid mediates specificity of marine nematode symbioses. *International Society of Microbial Ecology Journal* **5**, 986–998.

Cobb, N. 1920. One hundred new nemas (type species of 100 new genera). *Contributions to a Science of Nematology* **9**.

Davide, R. & Triantaphyllou, A. 1968. Influence of the environment on development and sex differentiation of root-knot nematodes. *Nematologica* **14**, 37–46.

Dirks, U., Gruber-vodicka, H.R., Leisch, N., Sterrer, W. & Ott, J.A. 2011. A new species of symbiotic flatworms, *Paracatenula galateia* sp. nov. (Platyhelminthes: Catenulida: Retronectidae) from Belize (Central America). *Marine Biology Research* **7**, 769–777.

Drummond, A., Ashton, B., Buxton, S., Cheung, M., Cooper, A., Duran, C., Field, M., Heled, J., Kearse, M., Markowitz, S., Moir, R., Stones-havas, S., Sturrock, S., Thierer, T. & Wilson, A. 2011. *Geneious* v5.5. http://www.geneious.com/ (accessed 18 June 2014).

Dubilier, N., Blazejak, A. & Rühland, C. 2006. Symbioses between bacteria and gutless marine Oligochaetes. In: Overmann, J., Ed., *Molecular Basis of Symbiosis*. Springer Berlin, Heidelberg, Germany, pp. 251–275.

Erséus, C. 1990. The marine Tubificidae (Oligochaeta) of the barrier reef ecosystems at Carrie Bow Cay, Belize, and other parts of the Caribbean Sea, with descriptions of twenty-seven new species and revision of Heterodrilus, Thalassodrilides and Smithsonidrilus. *Zoologica Scripta* **19**, 243–303.

Gerlach, S.A. 1956. Die Nematodenbesiedlung des tropischen Brandungsstrandes von Pernambuco. Brasilianische Meeres-Nematoden II, *Kieler Meeresforschungen* **12**, 202–218.

Gerlach, S.A. 1963. *Robbea tenax* sp. n., ein merkwürdiger mariner Nematode von den Malediven. *Internationale Revue der gesamten Hydrobiologie und Hydrographie* 48, 153–158.

Giere, O., Conway, N., Gastrock, G. & Schmidt, C. 1991. "Regulation" of gutless annelid ecology by endosymbiotic bacteria. *Marine Ecology Progress Series* **68**, 287–299.

Gourbault, N. & Vincx, M. 1990. Chromadorida (Nematoda) from Guadeloupe and Polynesia with evidence of intersexuality. *Zoologica Scripta* **19**, 31–37.

Gruber-vodicka, H.R., Dirks, U., Leisch, N., Baranyi, C., Stoecker, K., Bulgheresi, S., Heindl, N.R., Horn, M., Lott, C., Loy, A., Wagner, M. & Ott, J. 2011. *Paracatenula*, an ancient symbiosis between thiotrophic Alphaproteobacteria and catenulid flatworms. *Proceedings of the National Academy of Sciences USA* **108**, 12078–12083.

Heindl, N.R., Gruber-vodicka, H.R., Bayer, C., Lücker, S., Ott, J.A. & Bulgheresi, S. 2011. First detection of thiotrophic symbiont phylotypes in the pelagic marine environment. *Federation of European Microbiological Society Microbiology Ecology* **77**, 223–227.

Hopper, B.E. & Cefalu, R.C. 1973. Free-living marine nematodes from Biscayne Bay, Florida V. Stilbonematinae: contributions to the taxonomy and morphology of the genus *Eubostrichus* Greeff and related genera. *Transactions of the American Microscopical Society* **92**, 578–591.

Inglis, W. 1967. Interstitial nematodes from St Vincent's Bay New Caledonia. *Editions de la Fondation Singer-Polignac, Paris, France*, 29–74.

Jairajpuri, M., Ahmad, I. & Ahmad, M. 1977. Record of an intersex of *Aquatides thornei* with remarks on the phenomenon of intersexuality in nematodes. *Indian Journal of Nematology* **7**, 177–181.

Kampfer, S., Sturmbauer, C. & Ott, J.A. 1998. Phylogenetic analysis of rDNA sequences from Adenophorean nematodes

and implications for the Adenophorea-Secernentea controversy. *Invertebrate Biology* **117**, 29–36.

Katoh, K., Kuma, K.-I., Toh, H. & Miyata, T. 2005. MAFFT version 5: improvement in accuracy of multiple sequence alignment. *Nucleic Acids Research* **33**, 511–518.

Krall, E. 1972. On the biological background of the intersexuality in the genus *Aphelenchoides* (Nematoda: Tylenchida). *Indian Journal of Nematology* **2**, 206–207.

Miljutina, M.A., Miljutin, D.M. & Tchesunov, A.V. 2013. Seven *Acantholaimus* (Chromadoridae: Nematoda) species from one deep-sea sediment sample (Angola Basin, south-east Atlantic). *Journal of the Marine Biological Association of the United Kingdom* **93**, 935–953.

Moura, J.D.R., da Silva, M.C. & Esteves, A.M. 2014. Four new species of Desmodora (Nematoda) from the deep south-east Atlantic, and a case of intersexuality in Desmodoridae. *Journal of the Marine Biological Association of the United Kingdom* **94**, 85–104.

Nebelsick, M., Blumer, M., Novak, R. & Ott, J.A. 1992. A new glandular sensory organ in *Catanema* sp. (Nematoda, Stilbonematinae). *Zoomorphology* **112**, 17–26.

Ott, J. 1997. A new symbiotic marine nematode, *Adelphos rolandi* gen. n. sp. n.(Stilbonematinae), from the Caribbean Sea. *Annalen des Naturhistorischen Museums in Wien Serie B Botanik und Zoologie* **99**, 417–422.

Ott, J.A. & Novak, R. 1989. Living at an interface: meiofauna at the oxygen/sulfide boundary of marine sediments. In: Ryland, J.S. & Tyler, P.A., Eds., *23rd European Marine Biology Symposium*. Olsen & Olsen, Fredensborg, Denmark, pp. 415–422.

Ott, J.A., Novak, R., Schiemer, F., Hentschel, U., Nebelsick, M. & Polz, M. 1991. Tackling the sulfide gradient: a novel strategy involving marine nematodes and chemoautotrophic ectosymbionts. *Pubblicazioni Stazione Zoologica Napoli I: Marine Ecology* **12**, 261–279.

Ott, J.A., Bauer-nebelsick, M. & Novotny, V. 1995. The genus *Laxus* Cobb, 1894 (Stilbonematinae: Nematoda): description of the two species with ectosymbiotic chemoautotrophic bacteria. *Proceedings of the Biological Society of Washington* **108**, 508–527.

Ott, J.A., Bright, M. & Bulgheresi, S. 2004. Symbioses between marine nematodes and sulfur-oxidizing chemoautotrophic bacteria. *Symbiosis* **36**, 103–126.

Ott, J., Leisch, N. & Gruber-vodicka, H.R. 2014. *Eubostrichus fertilis* sp. n., a new marine nematode (Desmodoridae: Stilbonematinae) with an extraordinary reproductive potential from Belize, Central America. *Nematology*, in press.

Pires-dasilva, A. 2007. Evolution of the control of sexual identity in nematodes. *Seminars in Cell and Developmental Biology* **18**, 362–370.

Platt, H.M. & Zhang, Z.N. 1982. New species of marine nematodes from Loch Ewe, Scotland. *Bulletin of the British Museum (Natural History)/Zoology Series* **42**, 227–246.

Polz, M.F., Felbeck, H., Novak, R., Nebelsick, M. & Ott, J.A. 1992. Chemoautotrophic, sulfur-oxidizing symbiotic bacteria on marine nematodes: morphological and biochemical characterization. *Microbial Ecology* (*Historical Archive*) **24**, 313–329.

Polz, M.F., Distel, D.L., Zarda, B., Amann, R., Felbeck, H., Ott, J.A. & Cavanaugh, C.M. 1994. Phylogenetic analysis of a highly specific association between ectosymbiotic, sulfur-oxidizing bacteria and a marine nematode. *Applied and Environmental Microbiology* **60**, 4461–4467.

Polz, M.F., Harbison, C. & Cavanaugh, C.M. 1999. Diversity and heterogeneity of epibiotic bacterial communities on the marine nematode *Eubostrichus dianae*. *Applied Environmental Microbiology* **65**, 4271–4275.

Polz, M., Ott, J.A., Bright, M. & Cavanaugh, C. 2000. When bacteria hitch a ride. *American Malacological Society News* **66**, 531–539.

Pradillon, F., Schmidt, A., Peplies, J. & Dubilier, N. 2007. Species identification of marine invertebrate early stages by whole-larvae in situ hybridisation of 18S ribosomal RNA. *Marine Ecology Progress Series* **333**, 103–116.

Riemann, F., Thiermann, F. & Bock, L. 2003. *Leptonemella* species (Desmodoridae, Stilbonematinae), benthic marine nematodes with ectosymbiotic bacteria, from littoral sand of the North Sea island of Sylt: taxonomy and ecological aspects. *Helgoland Marine Research* **57**, 118–131.

Ronquist, F. & Huelsenbeck, J.P. 2003. MrBayes 3: Bayesian phylogenetic inference under mixed models. *Bioinformatics* **19**, 1572–1574.

Roy, T. & Gupta, A. 1975. Intersex or sex reversal amongst plant parasitic nematodes. *Acta Morphologica Neerlando–Scandinavica* **13**, 213–218.

Schiemer, F., Novak, R. & Ott, J.A. 1990. Metabolic studies on thiobiotic free-living nematodes and their symbiotic microorganisms. *Marine Biology* (*Berlin*) **106**, 129–137.

Schizas, N.V., Street, G.T., Coull, B.C., Chandler, G.T. & Quattro, J.M. 1997. An efficient DNA extraction method for small metazoans. *Molecular Marine Biology and Biotechnology* **6**, 381–383.

Stamatakis, A. 2006. RAxML-VI-HPC: maximum likelihood-based phylogenetic analyses with thousands of taxa and mixed models. *Bioinformatics* **22**, 2688–2690.

Stamatakis, A., Hoover, P. & Rougemont, J. 2008. A rapid bootstrap algorithm for the RAxML Web servers. *Systematic Biology* **57**, 758–771.

Steiner, G. 1923. Intersexes in Nematodes. *Journal of Heredity* **14**, 147–158.

Tamura, K., Peterson, D., Peterson, N., Stecher, G., Nei, M. & Kumar, S. 2011. MEGA5: Molecular Evolutionary Genetics Analysis using maximum likelihood, evolutionary distance, and maximum parsimony methods. *Molecular Biology and Evolution* **28**, 2731–2739.

Tchesunov, A. V., Ingels, J., Popova, E. V. 2012. Marine free-living nematodes associated with symbiotic bacteria in deep-sea canyons of north-east Atlantic Ocean. Journal of the Marine Biological Association of the United Kingdom **92**, 1257–1271.

Tchesunov, A.V. 2013. Marine free-living nematodes of the subfamily Stilbonematinae (Nematoda, Desmodoridae): taxonomic review with descriptions of a few species from the Nha Trang Bay, Central Vietnam. *Meiofauna Marina* **20**, 71–94.

Urbancik, W., Bauer-nebelsick, M. & Ott, J.A. 1996*a*. The ultrastructure of the cuticle of Nematoda. *Zoomorphology* **116**, 51–64.

Urbancik, W., Novotny, V. & Ott, J.A. 1996*b*. The ultrastructure of the cuticle of Nematoda. II. The cephalic cuticle of Stilbonematinae (Adenophorea, Desmodoridae). *Zoomorphology* **116**, 65–75.

van Megen, H., van Den Elsen, S., Holterman, M., Karssen, G., Mooyman, P., Bongers, T., Holovachov, O., Bakker, J. & Helder, J. 2009. A phylogenetic tree of nematodes based on about 1200 full-length small subunit ribosomal DNA sequences. *Nematology* **11**, 927–950.

Vitiello, P. 1974. Nouvelles espèces de Desmodorida (Nematoda) des côtes de Provence. *Tethys* **5**, 137–146.

Winnepenninckx, B., Backeljau, T. & De wachter, R. 1995. Phylogeny of protostome worms derived from 18S rRNA sequences. *Molecular Biology and Evolution* **12**, 641–649.

Zhuo, K., Liao, J., Cui, R. & Li, Y. 2009. First record of female intersex in *Hirschmanniella shamimi* Ahmad, 1972 (Nematoda: Pratylenchidae), with a checklist of intersexes in plant nematodes. *Zootaxa* **1973**, 61–68.

List of abbreviations in figures

a = amphidial fovea
b = pharyngeal bulbus
bac = bacteria
c = pharyngeal corpus
ccs = central conical setae
cg = corpus gelatum
cgo = caudal gland opening
cl = cloaca
cs = cephalic seta
fa = amphidial fovea fovea
fp = finger-like papillae
g = gut
gso = glandular sensory organ
i = pharyngeal isthmus
ls = labial sensillae
lss = long somatic setae
na = non-striated tail tip
p = sucker shaped papillae
pcs = precloacal setae
ss = somatic setae
scs = subcephalic seta
sp = spiculum
ss = somatic setae
ts = terminal seta
vel = velum

Associate Editor: Adrian Glover

Chapter 5

Growth in width and FtsZ ring longitudinal positioning in a gammaproteobacterial symbiont

Authors Nikolaus Leisch, Jolanda Verheul, Niels R. Heindl, Harald R. Gruber Vodicka, Nika Pende, Tanneke den Blaauwen and Silvia Bulgheresi

Keywords -

Publication status Article published in Current Biology **22**(19): R831-832

Detailed description of NL's contribution

a. carried out the electron microscopy

b. contributed to the sacculus purification and imaging

c. performed the immunofluorescence staining

d. analyzed data and prepared the figures

e. wrote parts of the manuscript, edited and approved the manuscript

Magazine
R831

Growth in width and FtsZ ring longitudinal positioning in a gamma-proteobacterial symbiont

Nikolaus Leisch[1], Jolanda Verheul[2], Niels R. Heindl[1], Harald R. Gruber-Vodicka[3], Nika Pende[1], Tanneke den Blaauwen[2], and Silvia Bulgheresi[1,4]

Rod-shaped bacteria usually grow in length and place their FtsZ ring and division site at midcell, perpendicular to their long axis [1,2]. Here, we provide morphometric and immunocytochemical evidence that a nematode-associated gammaproteobacterium [3,4] grows in width, sets a constricting FtsZ ring parallel to its long axis, and divides longitudinally by default. Remarkably, the newly described FtsZ ring appears to be not only 90° shifted with respect to model rods, but also elliptical and discontinuous. This reveals an unexpected versatility of the gammaproteobacterial cytokinetic machinery.

On the basis of electron microscopy analysis, Polz *et al.* [3] provided the first evidence that the gammaproteobacterium attached to the surface of the marine nematode *Laxus oneistus* grows in width and divides longitudinally. They also hypothesized that this ectosymbiont does so in order to relay host attachment to both its daughter cells. Here, we extend this seminal ultrastructural analysis [3] and provide experimental evidence that FtsZ-based symmetrical longitudinal fission is the default reproductive strategy adopted by the ectosymbiont. This rod-shaped bacterium has neither been isolated, nor found free-living in the environment. Its cells adhere to the nematode surface with one of their poles and form a monoculture of laterally packed, upright rods [3]. A C-type lectin secreted onto the cuticle by the nematode mediates ectosymbiont attachment, as well as ectosymbiont–ectosymbiont aggregation [5,6].

By measuring the length and width of 4,004 cells, we show that the ectosymbiont grows in width, not in length (Figure 1A,B), unlike most other rod-shaped bacteria or non-polarized eukaryotic cells [2]. All the applied electron microscopy methods (Figure S1 in the Supplemental Information available online with this article) show that septation starts and progresses synchronously at both poles, involves both the membrane and a peptidoglycan layer (sacculus), and terminates with a deeply constricted cell.

In the model gammaproteobacterium *Escherichia coli*, the tubulin homolog FtsZ is essential for transverse fission [1,7]. After self-assembling into a membrane-associated ring positioned at midcell, the FtsZ ring starts to constrict at the leading edge of the

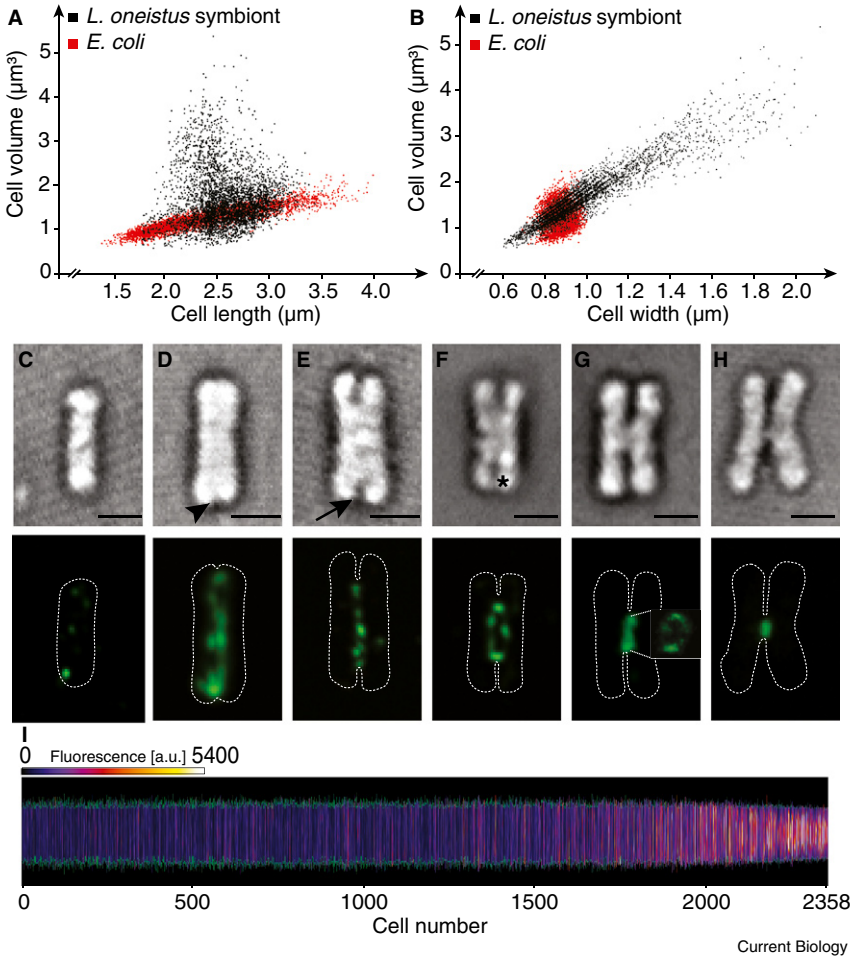

Figure 1. Growth in width and FtsZ longitudinal positioning in a nematode-associated bacterium. Volumes plotted versus length (A) or width (B) of *L. oneistus* ectosymbiont (black) or *E. coli* (red) cells. (A) Cell length shows a direct linear correlation to cell volume in *E. coli* (n = 5,021), but not in the ectosymbiont (n = 4,004). (B) Cell width shows a direct linear correlation to cell volume in the ectosymbiont, but not in *E. coli*. (C–H) Confocal laser scanning microscopy images showing FtsZ (green) localization in non-dividing (C) and dividing (D–H) *L. oneistus* ectosymbiont cells. For each division stage the representative localization pattern observed in >25 cells is displayed (bottom), with the corresponding differential contrast image (top). In an ectosymbiont not displaying any membrane constriction (C), FtsZ fluorescence concentrates at one pole. In a symbiont with polar indentations, FtsZ appears as a medially localized elliptical ring (D), which constricts at later fission stages (E–G) and to a maximum immediately before separation of cell daughters (H). Insert in (G) shows a lateral view of the FtsZ ring. Arrowheads point to slight polar indentations, arrows to readily visible constrictions, asterisks to deep constrictions. Dashed lines represent cell outline. Scale bar is 1 µm. (I) Cell length and longitudinal FtsZ fluorescence profiles of 2,358 ectosymbiont cells sorted by increasing cell width, from left to right. The green outline represents the cell length and the heat map represents the FtsZ fluorescence intensity of each cell along its length. The leftmost bar represents the thinnest cell, the rightmost bar the widest cell. The calibration bar displays FtsZ fluorescence intensity in arbitrary units (a.u.).

Current Biology Vol 22 No 19
R832

inner cell membrane, which results in cytokinesis. The product of the ectosymbiont *fts*Z gene, identified in a genome draft and validated by PCR, is 59% identical and 72% similar to *E. coli* K12 *fts*Z. In accordance with the 16S rRNA gene-based phylogeny [8], the ectosymbiont FtsZ protein clusters with proteins from basal Gammaproteobacteria of the family Chromatiaceae (Figure S2A). We examined ectosymbiont FtsZ expression by probing membrane-immobilized protein extracts with a monoclonal anti-FtsZ antibody and we specifically detected a single protein of the apparent molecular weight expected for the FtsZ monomer (~40 kDa; Figure S2B). In immunostained ectosymbiont cells that did not display any sign of septation, FtsZ fluorescence concentrates at one pole (Figure 1C). In cells that have just initiated division, as indicated by slight polar indentations (Figure 1D), FtsZ appears as an elliptical ring that constricts along with the cell envelope as its ingression proceeds (Figure 1E,F). Remarkably, FtsZ fluorescence does not appear homogenous throughout the elliptical ring, and gaps can be detected in 3D reconstructions (Movie S1). The FtsZ ellipse is reduced to a ring (Figure 1G) and to a dot in maximally constricted cells i.e. immediately before separation of the daughter cells (Figure 1H). We conclude that, despite the 90° shift in division plane orientation with respect to model rod-shaped bacteria, an FtsZ-based constricting ring is longitudinally positioned in dividing cells.

We recorded the FtsZ fluorescence of 2,358 immunolabelled ectosymbiont cells and we could observe an increase in FtsZ fluorescence in the center of the long axis as the cells widen (Figure 1I). Moreover, the thinner cells appear less fluorescent than the thicker cells, suggesting that the increase in FtsZ fluorescence is not solely due to a shift of FtsZ signal from the periphery to the center of the long axis, but also to an increase in its concentration. We conclude that FtsZ longitudinal positioning invariably follows growth in width and that longitudinal fission is the ectosymbiont's default reproduction mode.

FtsZ ring positioning in Gammaprotebacteria depends on the periodic and MinE-driven oscillation of MinC and MinD along the long axis of the cell [1,2]. We identified the *min*CDE genes in our ectosymbiont genome draft and, as in the case of FtsZ, the MinCDE proteins phylogenetically cluster together with those of the Chromatiaceae (data not shown). The ectosymbiont gene repertoire suggests that MinCDE-based spatial regulation of the FtsZ ring may potentially mediate either transverse or longitudinal fission.

From a cell biological point of view, default longitudinal positioning of a constricting FtsZ ring reveals an unsuspected plasticity of the mechanisms underlying gammaproteobacterial growth and division. In particular, the ectosymbiont FtsZ ring appears to be not only 90° shifted with respect to model rod-shaped bacteria, but elliptical and discontinuous.

From a symbiosis-centered perspective, it is intriguing to speculate that ectosymbiont longitudinal fission may be induced by signals produced by the nematode host, similarly to host-induced cytokinesis inhibition in insect and plant endosymbionts [9,10].

Supplemental Information

Supplemental Information includes experimental procedures, two figures and one movie and can be found with this article online at http://dx.doi.org/10.1016/j.cub.2012.08.033.

Acknowledgements

This work was supported by the Austrian Science Fund (FWF) projects P22470 (N.L., N.R.H, N.P. and S.B.) and P20394 (H.R.G) and is contribution 926 from the Carrie Bow Cay Laboratory, Caribbean Coral Reef Ecosystem Program, National Museum of Natural History, Washington, DC. We thank Jacqueline Montanaro, Siegfried Reipert, Norbert Vischer, Ronald Breedijk, Henk van Veen, the Core Facility for Cell Imaging and Ultrastructural Research of the University of Vienna and the van Leeuwenhoek Centre for Advance Microscopy, Amsterdam for technical support, Mark Blaxter for generating the metagenomic reads, Gerhard Herndl for making computational resources available, and Lawrence Rothfield, Joerg A. Ott, Michael Glotzer, Jürgen Kleine-Vehn and Wolfgang Miller for fruitful discussions and for comments on the manuscript.

References

1. Adams, D.W., and Errington, J. (2009). Bacterial cell division: assembly, maintenance and disassembly of the Z ring. Nat. Rev. Microbiol. *7*, 642–653.
2. Oliferenko, S., Chew, T.G., and Balasubramanian, M.K. (2009). Positioning cytokinesis. Genes Dev. *23*, 660–674.
3. Polz, M.F., Felbeck, H., Novak, R., Nebelsick, M., and Ott, J.A. (1992). Chemoautotrophic, sulfur-oxidizing symbiotic bacteria on marine nematodes: Morphological and biochemical characterization. Microb. Ecol. (Historical Archive) *24*, 313–329.
4. Polz, M.F., Distel, D.L., Zarda, B., Amann, R., Felbeck, H., Ott, J.A., and Cavanaugh, C.M. (1994). Phylogenetic analysis of a highly specific association between ectosymbiotic, sulfur-oxidizing bacteria and a marine nematode. Appl. Environ. Microbiol. *60*, 4461–4467.
5. Bulgheresi, S., Schabussova, I., Chen, T., Mullin, N.P., Maizels, R.M., and Ott, J.A. (2006). A new C-type lectin similar to the human immunoreceptor DC-SIGN mediates symbiont acquisition by a marine nematode. Appl. Environ. Microbiol. *72*, 2950–2956.
6. Bulgheresi, S., Gruber-Vodicka, H.R., Heindl, N.R., Dirks, U., Kostadinova, M., Breiteneder, H., and Ott, J.A. (2011). Sequence variability of the pattern recognition receptor Mermaid mediates specificity of marine nematode symbioses. ISME J. *5*, 986–998.
7. Bi, E.F., and Lutkenhaus, J. (1991). FtsZ ring structure associated with division in *Escherichia coli*. Nature *354*, 161–164.
8. Bayer, C., Heindl, N.R., Rinke, C., Lücker, S., Ott, J.A., and Bulgheresi, S. (2009). Molecular characterization of the symbionts associated with marine nematodes of the genus *Robbea*. Environ. Microbiol. Reports *1*, 136–144.
9. Login, F.H., Balmand, S., Vallier, A., Vincent-Monégat, C., Vigneron, A., Weiss-Gayet, M., Rochat, D., and Heddi, A. (2011). Antimicrobial peptides keep insect endosymbionts under control. Science *334*, 362–365.
10. Mergaert, P., Uchiumi, T., Alunni, B., Evanno, G., Cheron, A., Catrice, O., Mausset, A.-E., Barloy-Hubler, F., Galibert, F., Kondorosi, A., *et al.* (2006). Eukaryotic control on bacterial cell cycle and differentiation in the Rhizobium–legume symbiosis. Proc. Natl. Acad. Sci. USA *103*, 5230–5235.

[1]University of Vienna, Department of Genetics in Ecology, Althanstrasse 14, 1090 Vienna, Austria. [2]Swammerdam Institute of Life Sciences, Faculty of Science, University of Amsterdam, Science Park 904, 1098 XH Amsterdam, The Netherlands. [3]University of Vienna, Department of Marine Biology, Althanstrasse 14, 1090 Vienna, Austria. [4]Medical University of Vienna, Center for Anatomy & Cell Biology, Währingerstrasse 10, 1090 Vienna, Austria.
*E-mail: silvia.bulgheresi@univie.ac.at

Supplemental Information

Growth in width and FtsZ ring longitudinal positioning in a gammaproteobacterial symbiont

Nikolaus Leisch, Jolanda Verheul, Niels R. Heindl, Harald R. Gruber-Vodicka, Nika Pende, Tanneke den Blaauwen and Silvia Bulgheresi

Supplemental Experimental Procedures

Nematode collection

L. oneistus individuals were collected in October 2010 in approximately 1 m depth from a shallow water back-reef sand bar off Carrie Bow Cay, Belize (16°48´11 N, 88°04´55 W). The worms were extracted from the sand by gentle swirling in seawater and by pouring the latter onto a 63-µm-pore-size sieve. The meiofauna retained by the sieve was transferred into a Petri dish. Single nematodes were identified based on morphological features under a dissecting microscope and picked by hand. For electron microscopy nematodes were pre-fixed with 2.5% (vol/vol) glutaraldehyde in a 0.1 M sodium cacodylate buffer for 12-16 h at 4°C, rinsed three times in 0.1 M sodium cacodylate, and stored in this buffer at 4°C. For immunofluorescence, batches of 50 nematodes each were fixed in methanol. For DNA extraction, batches of 500 nematodes were flash frozen in liquid N_2. All samples were deep-frozen for transportation and storage except those fixed for electron microscopy.

Ectosymbiont collection and *E. coli* strain

Batches of 500 freshly collected *L. oneistus* were incubated for 3 min in an $MgSO_4$ solution isotonic to seawater to induce ectosymbiont dissociation. Dissociated symbionts were collected by 2 min centrifugation at 6 krpm. After removal of the supernatant, bacterial pellets were rinsed 3 times in filter-sterilized seawater and deep-frozen for shipping and storage. Deep-frozen ectosymbiont pellets were used for cell

size measurement, as well as for peptidoglycan extraction and visualization. The wild type *E. coli* K12 strain MC4100 was grown to steady state in minimal glucose medium and fixed while shaking at the growth temperature of 28°C before harvesting by centrifugation for imaging [S1].

Bacterial cell measurements

Images of non-permeabilized cells were taken with a BX-Olympus wide-field fluorescence microscope immediately after thawing, and analyzed with Coli-Inspector, a plug-in for ImageJ (http://simon.bio.uva.nl/objectj/, under examples). Cell outlines were automatically traced and both the length and width of each cell were automatically measured using a segmented line. The average cell width was calculated from projected area (A) and axis length (L) assuming a cylinder with hemispherical caps. Cell volume was calculated assuming two hemispheres connected by a cylinder. Automatic tracing was manually double-checked and false signals removed (e.g. multiple cells counted as one). For *E. coli*: n= 5,021; width range= 0.67 - 0.99 µm, mean width= 0.87 +/- 0.04; length range= 1.41 - 3.99 µm, mean= 2.36 +/- 0.47. For ectosymbiont cells: n=4,004; width range= 0.6 - 2.1 µm, mean= 0.99 +/- 0.23; length range= 1.80 - 3.50 µm; mean= 2.60 +/- 0.27.

In the graphic visualization of FtsZ fluorescence of 2,358 immunostained ectosymbiont cells, each bar represents an individual bacterial cell, whereas the intensity of FtsZ fluorescence is displayed as color ranging from dark blue to white. The length of the individual cells is indicated in green. The cells were sorted from left to right by increasing width. The cell length ranges between 1.77 and 3.54 µm (mean= 2.68 +/- 0.29). The cell width ranges between 0.5 and 1.98 µm (mean= 0.87 +/- 0.24).

Electron Microscopy

For scanning electron microscopy (SEM), bacteria were dissociated from the nematodes by mild sonication and the cell suspension was allowed to settle on poly-L-lysine-covered coverslips for 2 h. After being post-fixed for 4 h at room temperature in 0.1 M

sodium cacodylate buffer supplemented with 1% (vol/vol) osmium tetroxide, the samples were dehydrated in a graded alcohol series. They were then transferred into pure acetone and critical point dried with a CPD 300 unit (Leica) after which the coverslips where mounted on stubs and gold sputtercoated (AGAR B7340). Images were taken with an XL20 (Philips) in the Microscope Control program (Version 7.00, FEI).

For Transmission Electron Microscopy (TEM), pre-fixed specimens were high pressure frozen with an HPM 100 (Leica) and further processed in the freeze substitution unit AFS2 (Leica). Substitution was performed at -90° for 110 h using acetone supplemented with 2% (vol/vol) osmium tetroxide as substitution medium. Afterwards, the samples were rinsed twice with pure acetone, slowly warmed up to room temperature and embedded in Epon resin. Sections were cut on an UC7 ultra microtome (Leica), mounted on formvar-coated copper slot grids (Agar Scientific) and stained with 0.5% (wt/vol) uranyl acetate (Leica) for 15 min and with 2 % (wt/vol) lead citrate (Leica) for 7 min. Sections were viewed on a Zeiss EM-902 and images were recorded with an Olympus SharpEye camera system using the AnalySIS 5.0 program.

Peptidoglycan isolation

Bacterial pellets were thawed, resuspended in 100 µl H_2O and slowly dripped into 350 µl 4% (vol/vol) SDS in H_2O at 99° C. After boiling for 1 h the suspension was spun down in an airfuge Beckman ultracentrifuge at 30 psi for 30 min, washed twice with H_2O containing 0.01% (vol/vol) SDS and the pellet was dissolved in 20 µl of the same solution. The obtained bacterial sacculi were allowed to settle on a freshly carbon-coated copper 400 mesh grid (EMS) for 15 min, air-dried and sputter-coated with Platinum at a 25° angle. The samples were viewed on a CM10 Transmission Electron Microscope (Philips) equipped with a Megaview II soft imaging system at 110 kVolt.

***L. oneistus* ectosymbiont genome draft assembly and annotation**

Two lanes of Illumina GAII read sets were quality trimmed to a minimal phred quality score of 20 and filtered for adapter contamination using the nesoni package (available at

vicbioinformatics.com/nesoni.shtml). We assembled the read sets using velvet 1.2.0.3 [S2] with multiple kmer size settings (23, 33 and 47). We roughly identified symbiont contigs in each assembly by their coverage and %GC signatures. The selected contigs were merged using the graph accordance assembly (GAA) tool [S3]. The set of merged contigs was BLASTx searched (E value cutoff of 1×10^{-50}) [S4] for gammaproteobacterial contigs as implemented in geneious 5.5 [S5] using a custom database of 30 representative gammaproteobacterial genomes. For each cell division gene (*fts*Z, *min*C, *min*D and *min*E) only one contig was identified, annotated by the RAST server [S 6] and deposited in GenBank (JQ780823-JQ780826).

FtsZ-based phylogenetic analysis

The sequence of the cell division gene *fts*Z was extracted from the available, fully sequenced gammaproteobacterial genomes based on the submitted GenBank annotations. For *Chromatiaceae* genome drafts, including that of the *L. oneistus* ectosymbiont (available at http://rast.nmpdr.org/rast.cgi upon request), the contigs were annotated using the RAST server [S6], coding sequences were extracted, and predicted protein translations were aligned using MAFFT. The optimal substitution model for the protein alignment was evaluated with MrModeltest, and WAG+G+I was chosen. Phylogeny was reconstructed using PHYML, and node support in the tree was calculated using aLRT with an aLRT score ≥ 80% considered statistically significant.

Antibodies and Western blots

We used a mouse monoclonal antibody [S7] that recognizes a C-terminal epitope of *E. coli* FtsZ (the most C-terminal 15 aa of *E. coli* are identical to those of the ectosymbiont FtsZ except for a single aa). For Western blots, proteins were separated by reduced sodium dodecyl sulfate (SDS)-polyacrylamide gel electrophoresis (PAGE) on NuPAGE 4-12% Bis-Tris pre-cast gels (Invitrogen). They were then transferred to Hybond ECL nitrocellulose membranes (Amersham Biosciences). Membranes were blocked 30 min in phosphate-buffered saline (PBS) containing 5% (wt/vol) nonfat milk (PBSM) at room temperature and probed overnight at 4°C with mouse monoclonal anti-FtsZ antibody

(1:500) in PBSM (and without as a negative control). Blots were subsequently incubated for 30 min at room temperature with a horseradish peroxidase-conjugated anti-mouse secondary antibody (1:2,000; Amersham Biosciences) in PBSM. Protein-antibody complexes were visualized using ECL Plus detection reagents and films (Amersham Biosciences).

Immunostaining

Immunostaining was performed as described [S8]. Briefly, fixed *L. oneistus* individuals were rehydrated and washed in PBS containing 0.1% Tween 100 (washing solution). Bacterial peptidoglycan was permeabilized by incubation for 30 min with 0.1% (wt/vol) lysozyme. Blocking was carried out for 1 h in washing solution containing 2% (wt/vol) bovine serum albumin (blocking solution). Worms were incubated overnight under gentle agitation at 4°C in blocking solution with FITC-conjugated anti-FtsZ Fabs. Unbound primary antibody was removed by three washing steps in washing solution. Bacteria were dissociated from the nematodes by brief sonication and mounted in Vectashield (Molecular Probes). Images were recorded on a Nikon A1 confocal microscope.

Figure S1

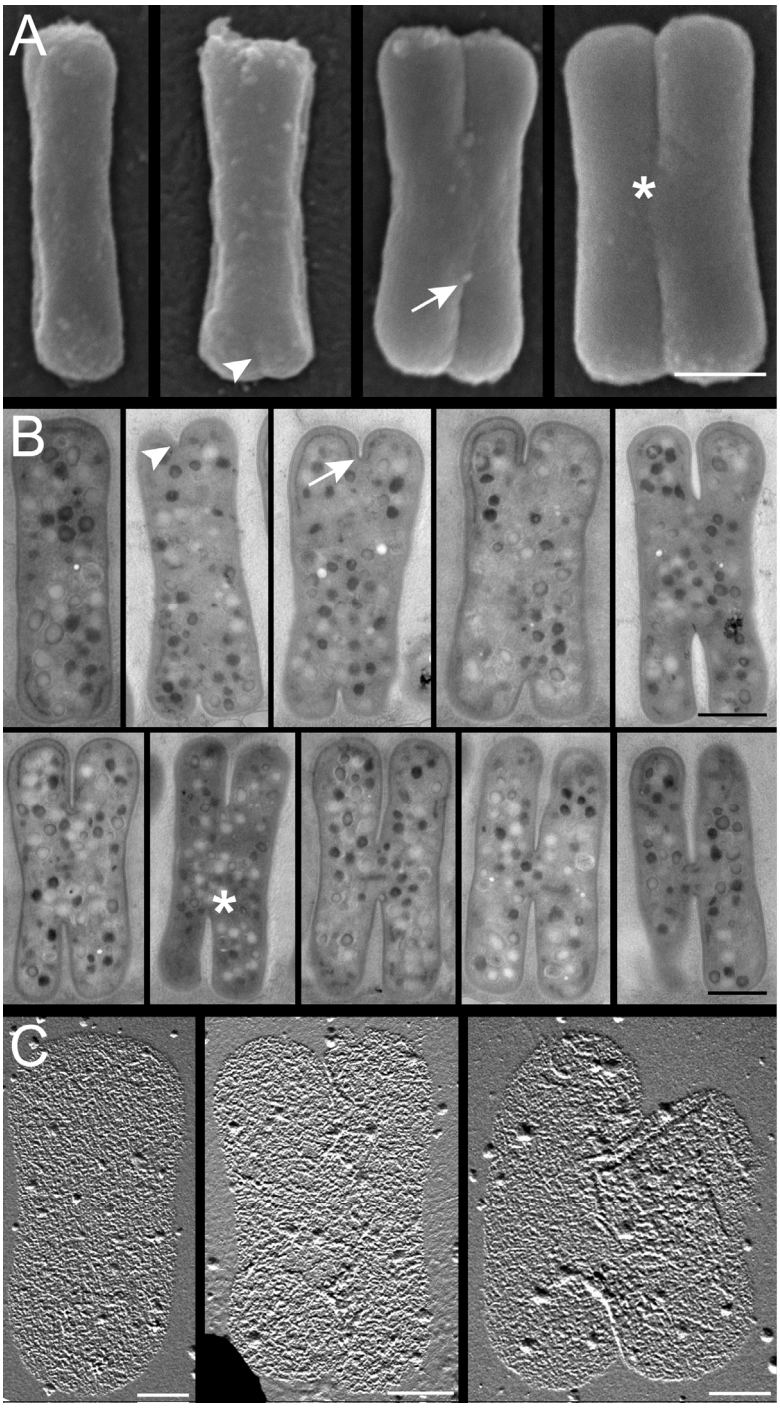

Figure S1. Electron microscopic analysis of the *L. oneistus* ectosymbiont membrane and peptidoglycan layer.

Scanning (A) and transmission (B) electron micrographs displaying increasing degree of membrane invagination are arranged from left to right and top to bottom. Arrowheads point to slight polar indentations, arrows to readily visible constrictions, asterisks to deep constrictions. Scale bar 1 µm. (C) Peptidoglycan sacculi extracted from a non-dividing (right) and from two dividing symbionts (middle and left). No signs of fission are visible in the non-dividing symbiont (right), whereas readily visible and deep constrictions appear at the poles of dividing symbionts (middle and left). Scale bar 500 nm.

Figure S2

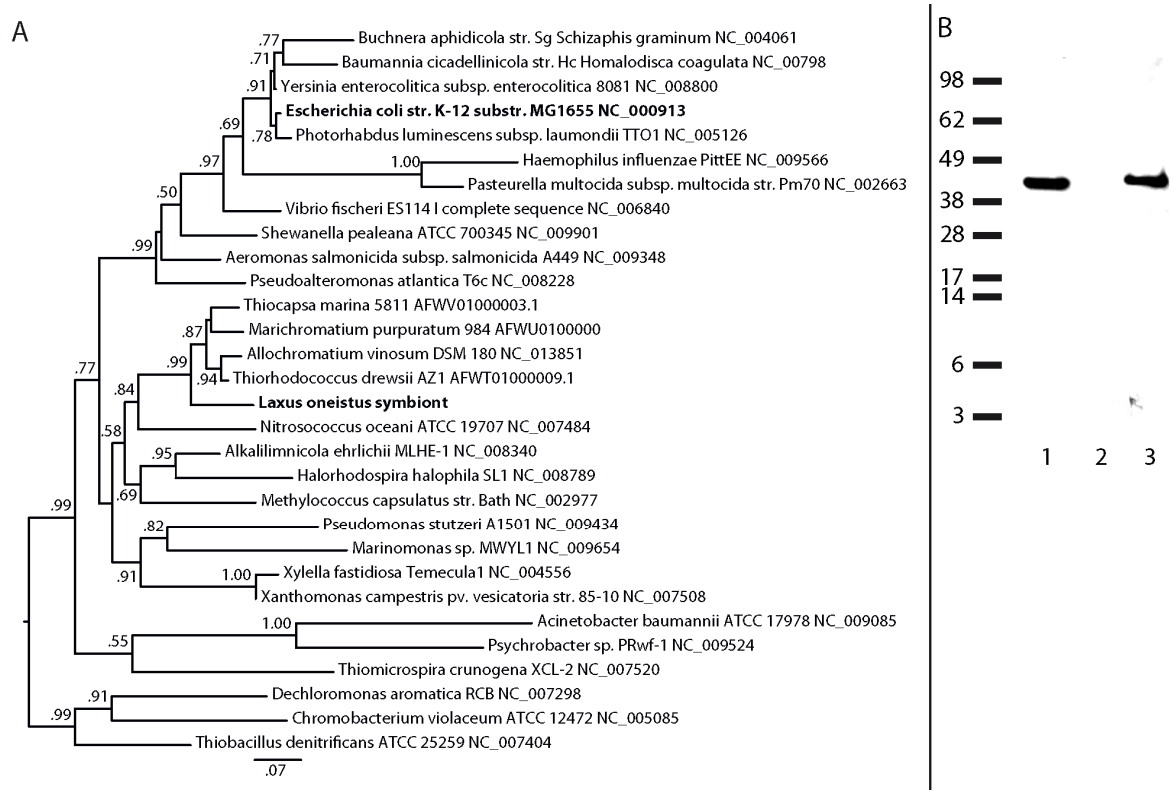

Figure S2. Phylogeny and expression of the ectosymbiont FtsZ protein.

(A) Gammaproteobacterial FtsZ protein-based phylogeny. The analysis is based on a MAFFT amino acid alignment (484 aa positions) and estimated under the WAG+G+I

model using ML analysis (PHYML) with node support calculated by aLRT. Scale bar represents 20% estimated sequence divergence. Deltaproteobacterial sequences were used as outgroup. (B) Western blots of bacterial protein extracts. *E. coli* protein extracts (lane 1) and *L. oneistus* ectosymbiont protein extracts (lanes 2 and 3) probed with a mouse monoclonal anti *E. coli* FtsZ (lane 1 and 3, respectively) and secondary antibody alone (lane 2). Numbers indicate apparent MW expressed in KDa.

Supplemental References

S1. Den Blaauwen, T., Aarsman, M.E., Vischer, N.O., and Nanninga, N. (2003). Penicillin-binding protein PBP2 of *Escherichia coli* localizes preferentially in the lateral wall and at mid-cell in comparison with the old cell pole. Mol. Microbiol. *47*, 539-547.

S2. Zerbino, D.R., and Birney, E. (2008). Velvet: Algorithms for de novo short read assembly using de Bruijn graphs. Genome Res. *18*, 821-829.

S3. Yao, G., Ye, L., Gao, H., Minx, P., Warren, W.C., and Weinstock, G.M. (2012). Graph accordance of next-generation sequence assemblies. Bioinformatics *28*, 13-16.

S4. Altschul, S.F., Gish, W., Miller, W., Myers, E.W., and Lipman, D.J. (1990). Basic local alignment search tool. J. Mol. Biol. *215*, 403-410.

S5. Drummond, A., Ashton, B., Buxton, S., Cheung, M., Cooper, A., Heled, J., Kearse, M., Moir, R., Stones-Havas, S., Sturrock, S., *et al.* (2010). Geneious v5.1, available from http://www.geneious.com/.

S6. Aziz, R.K., Bartels, D., Best, A.A., DeJongh, M., Disz, T., Edwards, R.A., Formsma, K., Gerdes, S., Glass, E.M., Kubal, M., *et al.* (2008). The RAST server : rapid annotations using subsystems technology. BMC Genomics *9*, 75.

S7. Voskuil, J.L., Westerbeek, C.A., Wu, C., Kolk, A.H., and Nanninga, N. (1994). Epitope mapping of *Escherichia coli* cell division protein FtsZ with monoclonal antibodies. J. Bacteriol. *176*, 1886-1893.

S8. Bulgheresi, S., Schabussova, I., Chen, T., Mullin, N.P., Maizels, R.M., and Ott, J.A. (2006). A new C-type lectin similar to the human immunoreceptor DC-SIGN mediates symbiont acquisition by a marine nematode. Appl. Environ. Microbiol. *72*, 2950-2956.

Chapter 6

Non-ring FtsZ mediated cell constriction in a longitudinal dividing gammaproteobacterial symbiont

Authors Nikolaus Leisch, Nika Pende, Jolanda Verheul, Tanneke den Blaauwen and Silvia Bulgheresi

Keywords binary fission, bacterial cell growth, MONTS, symbiosis

Publication status Manuscript is ready for submission to Environmental Microbiology

Detailed description of NL's contribution

a. collected material on two field trips to Carrie Bow Caye (Belize)

b. carried out the electron microscopy

c. performed the immunofluorescence staining

d. performed all morphometric, fluorescent profile and statistical analyses

e. analyzed data and prepared the figures

f. wrote the manuscript

Abstract

The molecular basis of bacterial cell division has mostly been studied in model bacteria. Yet, the vast majority of microorganisms are not cultivable and their reproduction modes are almost unexplored. Here, we investigated binary fission in a *Gammaproteobacterium* attached to the cuticle of the marine nematode *Robbea hypermnestra*. We showed that this symbiont grows in width and divides longitudinally, a division mode only described of the *Laxus oneistus* symbiont so far. However, the cell poles of the *R. hypermnestra* symbiont are not invaginating synchronously. The basal, nematode-attached pole constricts earlier than the apical one. We visualized septation progression by Electron Microscopy. Moreover, immunostaining of the *R. hypermnestra*-associated bacterium with an anti-FtsZ antibody revealed that FtsZ-mediated constriction at the basal pole precedes apical one. Our results show that non-ring FtsZ can initiate septation, which in turn leads to an asynchronously progressing division. This is the first report of non-ring FtsZ-mediated constriction in a gammaproteobacterial cell.

Introduction

Most prokaryotes grow and divide by a process called binary fission; the cell doubles in size and divides into two equal daughter cells. The major cytoskeletal protein responsible for the division is FtsZ. This guanosine triphosphatase (GTPase) is the prokaryotic homologue of the eukaryotic cytoskeletal protein tubulin. It is a highly conserved protein, which is involved in cytokinesis in most prokaryotes and plastids (Margolin 2005). It initiates cell division by polymerizing into linear protofilaments, forming the so-called Z-ring underneath the cytoplasmic membrane (Bi and Lutkenhaus 1991, Adams and Errington 2009). The Z-ring therefore provides the location of the division site andrecruits additional

division proteins to form the so called “divisome” (de Boer 2010, Erickson et al. 2010). *In vitro* it can exert a contractile force which could lead to constriction of the cell envelope during cytokinesis (Mingorance et al. 2010, Osawa and Erickson 2013). In the rod-shaped model organisms *Escherichia coli* and *Bacillus subtilis*, the placement of the Z-ring has been studied extensively. Two negative regulator systems have been identified, on the one hand, nucleoid occlusion which blocks Z-ring formation over the chromosome (also referred to as nucleoid) to avoid truncating the DNA (Wu and Errington 2012). On the other hand, the Min system, which inhibits FtsZ polymerization at the cell poles as this would lead to DNA-free mini-cells. (reviewed in Lutkenhaus 2007). However, the mechanisms of cell growth and division have been investigated only in few cultivable model organisms, calling for broadening cell biological studies to non-model organisms (Den Blaauwen 2013, Goley 2013). Based mostly on electron-microscopic observations, it has been hypothesized that a number of bacterial symbionts of marine nematodes (Polz et al. 1992, Bayer et al. 2009), a marine ciliate (Fenchel and Finlay 1989), a marine oligochaete (Giere and Krieger 2001) and a deep-sea mussel (Zielinski et al. 2009) can divide along their longitudinal axis. Recently, it was shown that the rod-shaped symbiont of the marine nematode *Laxus oneistus* (referred to as Los from here on out), grows in width instead of length and divides via FtsZ-based fission along its length axis by default (Leisch et al. 2012). As Los, the symbiont of the closely related nematode *Robbea hypermnestra* (previously referred to as *Robbea* sp.3) is a basal gammaproteobacterium (Bayer et al. 2009). It is rod-shaped, attaches with one pole to the cuticle of its host thus forming a monolayer (Figure 1 A) and appears bright white in incident light, which is most likely due to elemental sulphur inclusions. The same has been observed for multiple stilbonematid ectosymbionts, and elemental sulphur was detected using HPLC and Raman microspectroscopy (Polz et al.

1992, Himmel et al. 2009). Additionally, the symbiont of *R. hypermnestra* (Rhs) encodes the *aprA* gene, which is a key enzyme in the sulphur metabolism (Bayer et al. 2009). All this evidence supports the hypothesis that Rhs, like all characterized stilbonematid ectosymbionts, is a chemoautotrophic sulphur-oxidizing bacterium. Experiments using symbiont specific fluorescence in situ hybridization – probes showed that the association is mono-specific, as in each worm carries a virtually pure cell culture (Bayer et al. 2009, Ott et al. 2014).

We investigated the morphology and growth of Rhs, as well as the molecular mechanisms underlying its division. We characterized the symbiont using morphometric analysis based on light microscopy and documented growth and division using scanning electron microscopy. Furthermore, we demonstrated that an anti-FtsZ antibody, raised against *E. coli* FtsZ, recognized Rhs FtsZ. Finally, by immunostaining the different division stages of Rhs as well as quantifying them, we could show that Rhs divides longitudinally, but the division progress is temporally disconnected between the two poles. The basal pole, i.e. the pole that is in contact with the nematode, starts to constrict earlier than the apical pole, which in turn leads the septum to constrict terminally in the apical most 30% of the cell.

Material and Methods

Ectosymbiont collection and *E. coli* strain

Sediment samples were collected on multiple field trips (12/2011, 03/2013, 03/2014) in approximately 1m depth from a sand bar off Carrie Bow Caye, Belize (16°48'11.01"N, 88° 4'54.42"W). Specimens of *R. hypermnestra* were extracted from the sediment by stirring the sand in seawater and pouring the supernatant through a 63 µm mesh sieve. The retained material was transferred into a Petri dish and single nematodes handpicked using pipettes under a dissecting microscope. *R. hypermnestra* was identified according to (Ott et al. 2014). For DNA extraction, Western Blotting and immunostaining, nematodes were fixed in methanol and transported and stored at -20°C. For Scanning Electron Microscopy (SEM) the samples were fixed according to (Montanaro et al.) with PHEM-buffered glutaraldehyde (2.5%) overnight at 4°C, rinsed twice with washing buffer (4.5X PHEM) and transported and stored in washing buffer at 4°C. The wild type E. coli K12 strain MC4100 was grown to steady state in minimal glucose medium and kept at 28°C and agitated during fixation before harvesting by centrifugation (den Blaauwen et al. 2003).

Electron Microscopy

Whole worms were post fixed with 1% osmium tetroxide for 2h at 4°C. Bacteria were dissociated from the nematodes by mild sonication, the supernatant transferred on a glass slide coated with poly-L-lysine for attachment, before post fixation as described above. The samples were further dehydrated with a graded ethanol series, followed by pure acetone and critical point drying with a CPD 300 unit (Leica). Finally, they were mounted on stubs and gold coated with an AGAR B7340 sputtercoater unit. Images were acquired

with a XL20 (Philips) using the Microscope control program (version 7.00, FEI).

DNA extraction and homology cloning of *Robbea hypermnestra* ectosymbiont *ftsZ* gene

Genomic DNA was extracted from three single *R. hypemnestra* nematodes as previously described (Schizas et al. 1997). 2 µl of DNA were used as template in each 50 µl PCR reaction. A 1182 nt-long fragment was amplified using specific Rhs *ftsZ* genes primers RssftsZF (5'- ATGTTTGAACTAATGGATACCAATGG -3') and RssftsZR (5' – TTAGTCCGCCTGACGGCGCAGAAA -3'). Touchdown PCR conditions were as follows: 94°C for 3 min, followed by 8 cycles at 94°C for 45 s, 58°C to 50°C for 45 s, 72°C for 75 s, followed by 27 cycles 94°C for 45 s, 50°C for 45 s, 72°C for 75 s, and a final elongation step at 72°C for 10 min. We randomly picked and fully sequenced six clones containing the *R. hypemnestra ftsZ* gene fragment in both directions. Sequences were aligned and compared with CodonCode Aligner 3.7.1 software (CodonCode Corporation, Dedham, MA, USA).

Western Blot

For Western Blots, proteins from dissociated ectosymbionts were separated by reduced sodium dodecyl sulfate (SDS) - polyacrylamide gel electrophoresis (PAGE) on NuPAGE 4-12% Bis-Tris pre-cast gels (Invitrogen), followed by transfer to Hybond ECL nitrocellulose membranes (Amersham Biosciences). Membranes were blocked 45 minutes in phosphate-buffered saline (PBS) containing 5% (wt/vol) nonfat milk (PBSM) at room temperature and incubated overnight at 4°C with a rabbit polyclonal anti-E. coli FtsZ antibody in PBSM. For the negative control, the primary antibody was omitted at this step. After three washing

steps in PBSM to remove unbound antibody, the blots were incubated for 1 h at room temperature with a horseradish peroxidase-conjugated anti-rabbit secondary antibody (1:5,000; Amersham Biosciences) in PBSM. Protein-antibody complexes were visualized using ECL Plus detection reagents and films (Amersham Biosciences).

Immunofluorescence

Fixed nematodes were rehydrated and washed in PBS containing 0.1% Tween 20 (PBT), followed by permeabilization of the bacterial peptidoglycan by incubation for 10 min with 0.1% (wt/vol) lysozyme at 37°C. Blocking was carried out for 1 h in PBT containing 2% (wt/vol) bovine serum albumin (blocking solution) at room temperature. Rhs were immunostained with a 1:500 dilution of rabbit polyclonal anti-*E. coli* FtsZ antibody (Koppelman et al. 2004) in blocking solution overnight under gentle agitation at 4°C. For the negative control, the primary antibody was omitted for this step. The samples were washed three times in PBT to remove unbound primary antibody and incubated with secondary Alexa555 conjugated anti-rabbit antibody (Molecular Probes) at a 1:500 dilution in blocking solution for 1 h at room temperature. Unbound secondary antibody was removed by three washing steps in PBT and to dissociate Rhs, worms were sonicated for 40 s in the tubes prior mounting. One µl of the bacterial solution was mixed with 0.5 µl of mounting medium Vectashield (Vector Labs).

Cell size and fluorescence measurement

Cell suspensions were applied on an 1% agarose covered microscopy slide (Koppelman et al. 2004) and imaged using a Nikon Eclipse 50i microscope equipped with either a DS-Fi1 camera (Nikon) or a MFCool camera (Jenoptik). Epifluorescence images were acquired

using the NIS Elements F 3.22 software (Nikon) or the ProgRes Capture Pro 2.8.8 software (Jenoptik) and processed using the public domain program ImageJ (Schneider et al. 2012) and the analysis tool Coli Inspector (van der Ploeg et al. 2013). Cell outlines were traced and cell length and width were measured automatically. Automatic tracing was manually double-checked and errors removed (e.g. multiple cells counted as one). For the average fluorescence profiles, cells were chosen based on phase-contrast images, each cell was resampled to the same length and the fluorescent intensities added up and averaged. Data analysis was performed using Excel 2010 (Microsoft Corporation) and SigmaPlot 12.0.0.182 (Systat Software). Graphs were created with SigmaPlot and figures were compiled using Photoshop CS6 and Illustrator CS 6 (Adobe Systems Inc.).

Results

Longitudinal fission of the rod-shaped bacteria attached to the cuticle of the nematode *R. hypermnestra* was initially hypothesized by (Bayer et al. 2009) based on electron microscopic observations. Here, we extended the morphological analysis and documented sequential stages of binary fission as it progressed along the symbionts longitudinal axis. Cells in progressing stage of division from left to right are shown in (Figure 1 A - F). SEM analysis showed that the cell envelope started to ingress in the middle of the basal, but not of the apical pole (Figure 1 A, C arrowheads). Once the septation had progressed along the length axis, the apical pole started to ingress (Figure 1 A, D arrows). From here onwards septation progressed along the length axis (Figure 1 E), leading to two identical daughter cells (Figure 1 F).

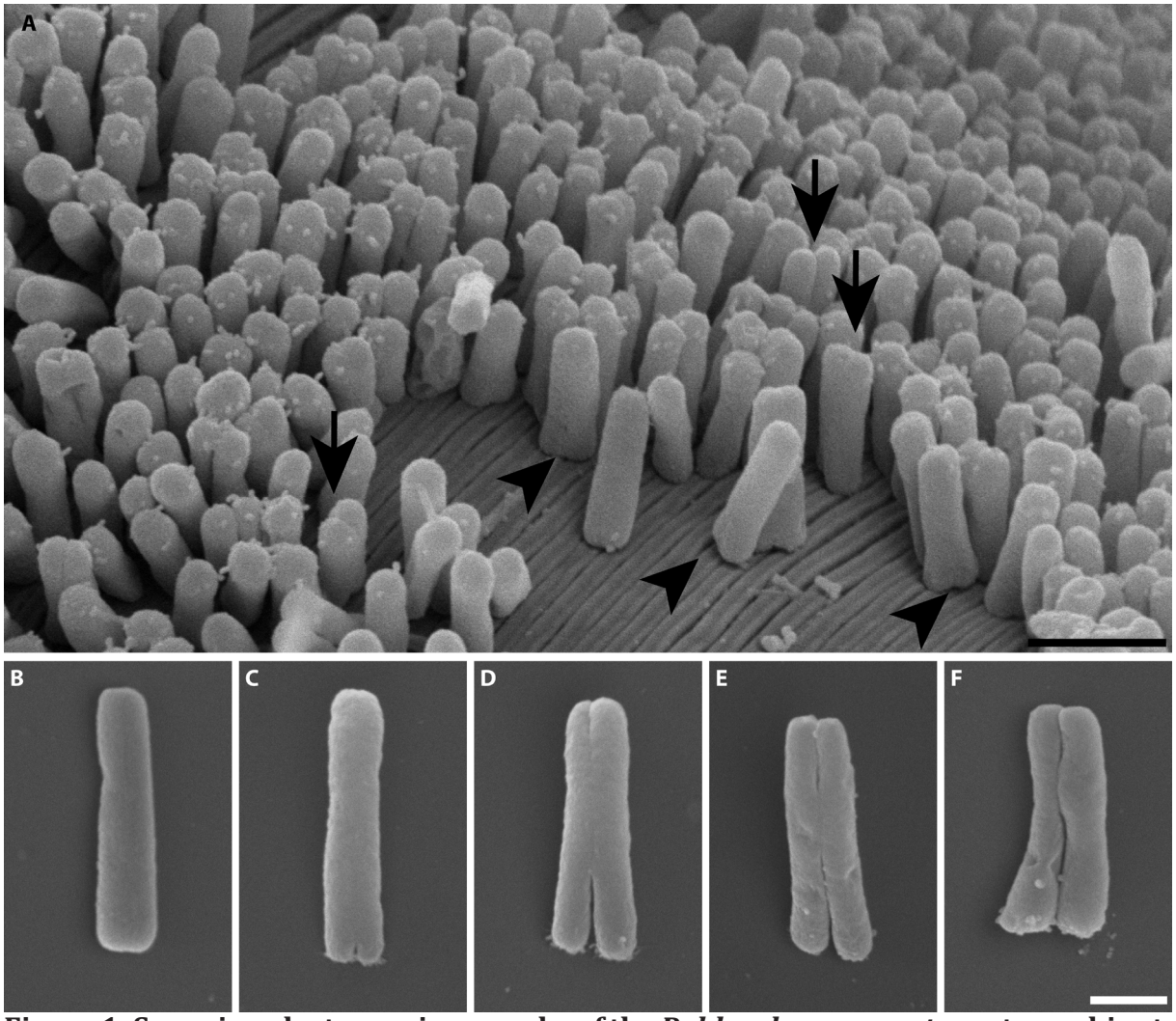

Figure 1: Scanning electron micrographs of the *Robbea hypermnestra* ectosymbiont. (A) shows the rod-shaped symbiont cells attached to the nematode cuticle in a monolayer, as to form a simple columnar epithelium. (B-F) shows representative cells of sequential stages of division from left to right. Single cells were oriented, so that the basal (nematode-attached) pole points downwards and all cells were recorded at the same magnification. Arrowheads indicate basal constriction and arrows point to cells with readily visible constriction at both poles. Scale bar is 5 µm in (A) and 1 µm in (F).

To clarify if Rhs grows in width (as suggested by the ultrastructural analysis), we took morphometric measurements of hundreds of Rhs cells (n=1691). For comparison, we recorded measurements of Los cells (n=950) and *E. coli* cells grown to steady state (n=3189). Using the cell area as a measurement of growth, we plotted it against either cell length or cell width and the resulting scatter plot was analysed using linear regression analysis. Plotting the cell length against the cell area resulted in hardly any correlation

in Rhs (Figure 2 A, R^2 = 0.089, p<0.001), little correlation in Los (Figure 2 B, R^2= 0.282, p<0.001) and a very strong correlation in *E. coli* (Figure 2 C, R^2=0.922, p<0.001). The reverse was true in the plot showing cell width plotted against the cell area. A strong correlation between width increase and area increase could be observed for Rhs (Figure 2 D, R^2=0.614, p< 0.001) and Los (Figure 2 E, R^2=0.528, p<0.001), whilst *E. coli* (Figure 2 F, R^2=0.001, p=0.17) showed none. All regression analyses, except for *E. coli* width versus area (Figure 2 F), were statistically significant. This clearly showed that Rhs, similarly to Los and contrary to *E. coli*, grows predominantly in width.

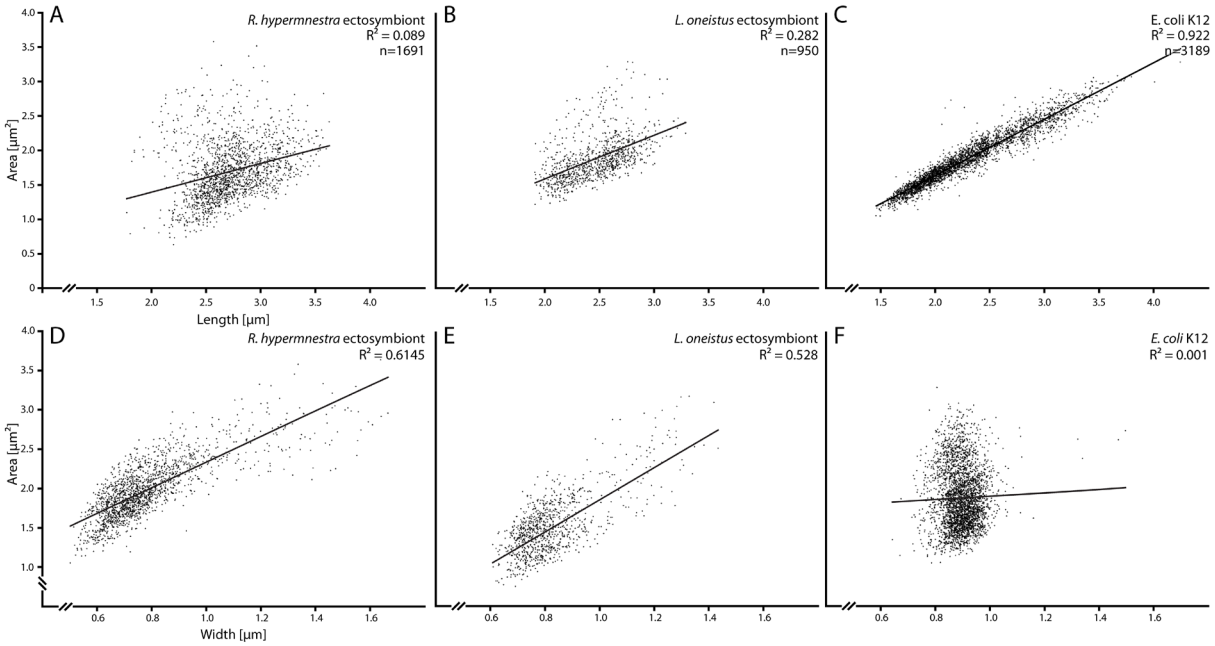

Figure 2: Morphometric comparison of Rhs, Los, and *E. coli*.
Cell area plotted against either length of (A) Rhs, (B) Los or (C) *E. coli* cells or width of (D) Rhs, (E) Los or (F) *E. coli* cells. Rhs and Los show, unlike *E. coli*, no to little correlation between length and cell area. Both Rhs and Los show a strong correlation between cell width and cell area, whilst *E. coli* shows none. Regression line and R^2 values of the simple linear regression analysis are shown for each plot.

To assess if Rhs longitudinal cell division is FtsZ based, we sought to homology clone Rhs *ftsZ* gene. PCR resulted in a *ftsZ* gene fragment endcoding for 1182bp, with 62% identity and 75% similarity to *E. coli* K12 *ftsZ,* and 88% identity and 91% similarity to Los *ftsZ*.

We confirmed Rhs FtsZ expression by probing membrane-immobilized bacterial protein extracts with an anti- E*. coli* FtsZ antibody. This detected a single, specific band (Figure 3) ~40kDa, the predicted molecular weight of *E. coli* FtsZ, which we interpreted to be the ectosymbiont FtsZ monomer.

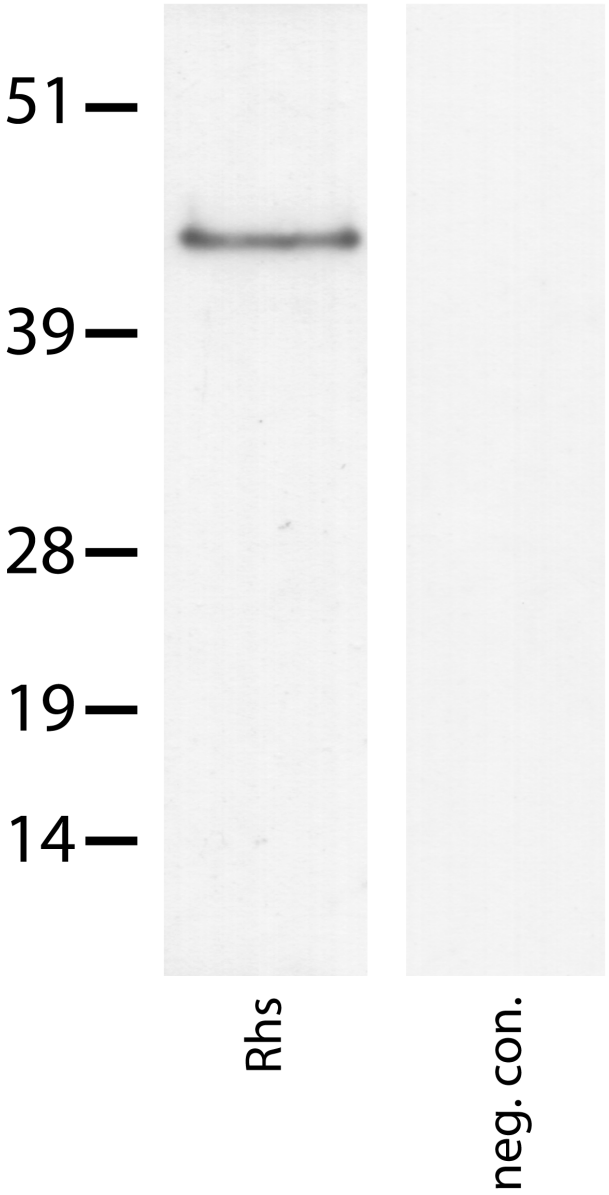

Figure 3: Western Blot of bacterial protein extracts.
Rhs protein extracts probed with rabbit polyclonal anti E.coli FtsZ (Koppelman et al. 2004) (lane Rhs) and secondary antibody alone (Lane neg. con.) Numbers indicate apparent MW expressed in kDa.

We immunostained Rhs FtsZ and examined its localization pattern by calculating average fluorescence profiles based on epifluorescence images. We divided the cells into four distinct stages: cells showing no sign of constriction (stage 0) (Figure 4 A), cells showing only basal constriction (stage 1) (Figure 4 B), cells showing constriction on both poles (stage 2) (Figure 4 C) and highly constricted cells (stage 3) (Figure 4 D). In stage 0 cells non-ring FtsZ was detected throughout the whole cell (Figure 4 A and I magenta line; n=31). In stage 1 cells a patch of non-ring FtsZ was visible at the basal, constricting pole (Figure 4 B) together with a higher overall level of FtsZ signal along the cell length (Figure 4 I, blue line; n=28). In stage 3 cells, we detected a line of FtsZ signal connecting the two leading edges of the constriction (Figure 4 C) corresponding to a ring-like structure (an example is shown in Fig. 4 E-H). In the average fluorescence profile of the stage 2 cells (Figure 4 I, green line; n=31) the slight peaks at ~25% and ~90% of the cell length represented the basal and apical end of the Z-ellipse, respectively, and indicated that the apical constriction trailed behind the basal. Stage 3 cells had a highly constricted Z-ring (Figure 4 D) and their profile indicated that the constriction would eventually terminate in the apical-most 30% of the cell (Figure 4 I, yellow line; n=22). The FtsZ signal in the apical part of these cells was higher compared to the signal seen in the stage 1 cells, most likely due to the formation of a full Z-ring at the later stage. We conclude that this gammaproteobacterium divides longitudinally by means of a constricting Z-ring. Remarkably this is preceded by non-ring FtsZ-mediated constriction at the basal pole.

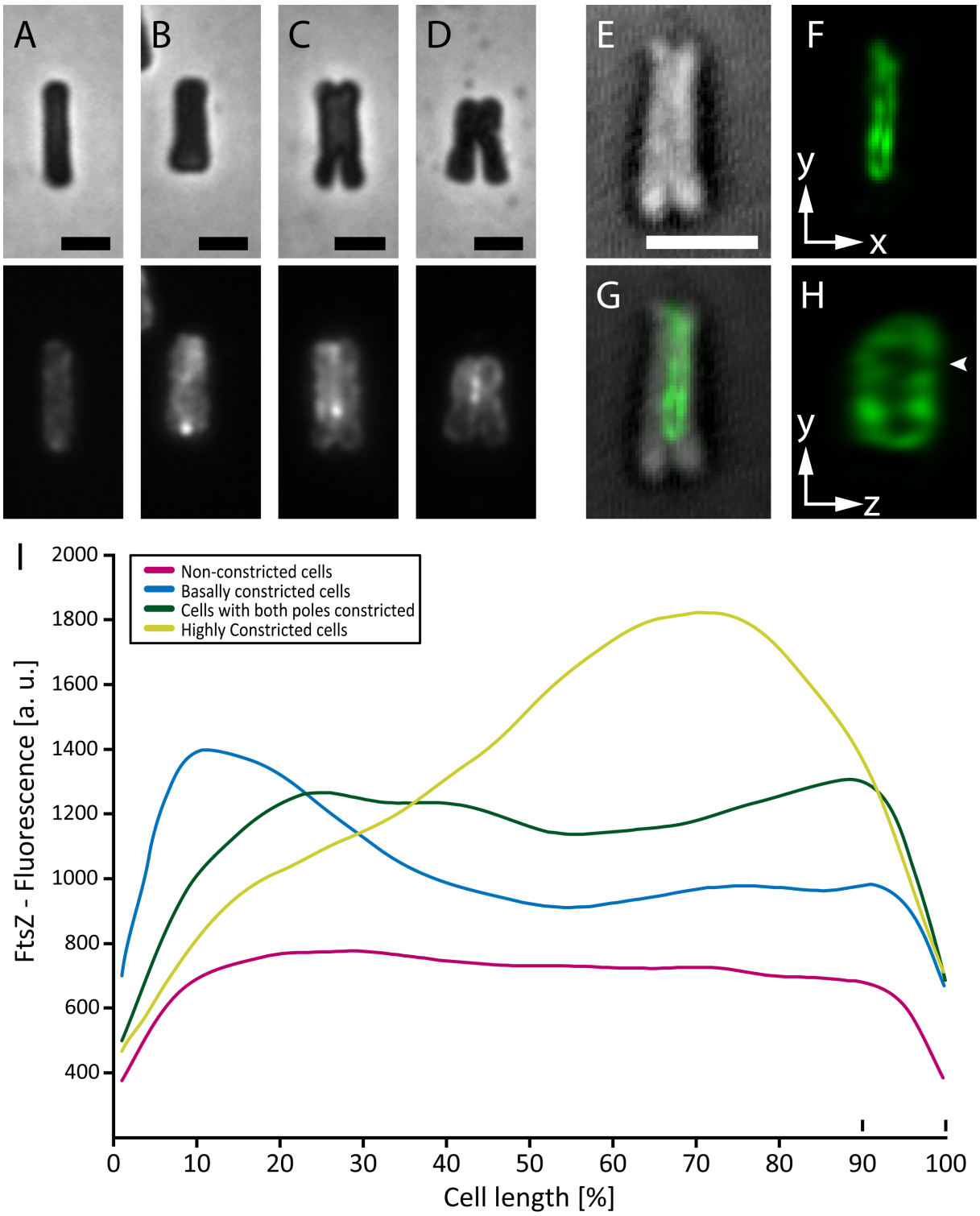

Figure 4: FtsZ localization pattern in Rhs cells

(A-D) show representative phase-contrast (upper row) and FtsZ epifluorescence (lower row) images of (A) a non-dividing cell, (B) a cell with only the basal pole constricted, (C) a cell with two invaginating poles and (D) of a highly constricted cell. (E-H) shows confocal laser scanning images of a cell with both poles constricting and a fully formed Z-ellipse. (E) is the differential contrast image and (F) is a Z-projection of the FtsZ fluorescence stack. (G) shows an overlay of (E) and (F) and (H) is the Z-projection (F) rotated by 90°, the arrowhead indicates a gap in the Z-ellipse. (I) are average fluorescence profiles of non-

dividing cells (magenta line; n= 31; corresponds to (A)), cells with basally located furrow (blue line; n=28; corresponds to (B)), cells showing constriction on both poles (green line; n=31; corresponds to (C)) and highly constricted cells (yellow line; n=22; corresponds to (D)). FtsZ fluorescence is expressed in arbitrary units (a.u.) and plotted along the cell length expressed in percentage. Scale bars are 1µm in (A-D) and 2 µm in (E).

Discussion

This study describes the growth mode and a form of longitudinal division that is exhibited by the gammaproteobacterial symbiont of *Robbea hypermnestra*. Similar to the closely related Los, it grows predominantly in width and only little length variation is observed. Like most prokaryotes it uses the tubulin homologue FtsZ to divide; however, non-ring FtsZ initiates division at the basal pole of the cell and a Z-ring can only be observed at a later stage when the apical pole has started to divide as well. Due to this delay, the termination site of the constriction is shifted towards the apical pole and we termed this "asynchronous division".

Rhs division mode is similar to that seen in Los, the first gammaproteobacterial example of longitudinal division (Leisch et al. 2012). In Los a Z-ellipse, spanning the whole length of the cell, is assembled prior to constriction of the cell wall. In contrast, in Rhs septation is initiated when non-ring FtsZ leads to localized invagination. Similar furrows have been observed in the cyanelles of the glaucophyte *Cyanophora paradoxa* (Sato et al. 2007, Sato et al. 2009) and temperature sensitive *E. coli* with mutations in either the *rodA* and/or *pbp2* genes (Begg and Donachie 1985, Begg and Donachie 1998, Zaritsky et al. 1999). If either of these genes is inactivated, *E. coli* cells become spherical (Begg and Donachie 1998). In the rodA mutant KLB24 Septation starts from a single point of the sphere, with localized invagination growing further outward and eventually encompassing the whole cell (Lutkenhaus and Addinall 1996, Begg and Donachie 1998, de Pedro et al. 2001). A study

analysing the FtsZ localization pattern in these cells reported three kinds of fluorescence patterns. Cells with no signs of septation show a single spot, two spots connected by an arc are found in slightly constricted cells and fully formed rings can be seen in further constricted cells. It was suggested that the spot represents the initial point from which FtsZ polymerization starts. The increased diameter of these spherical cells might not allow the formation of a complete Z-ring, which is why in the intermediate stage only an Z-arc can be observed (Lutkenhaus and Addinall 1996). Rhs is the first microbe in which this is the default division mechanism and the cause might be similar to the one in the spherical *E. coli* mutants. Due to the increased circumference, the Z-ellipse can initially not be formed and the localized invagination is a way of reducing the circumference until a full Z-ellipse can be formed. Los doesn't show such a way of dividing but analysis of the morphometric data shows a highly significant difference between Rhs and Los in length (Rhs 2.72 μm ± 0.30, Los 2.47 ± 0.27; Mann-Whitney Rank Sum Test, p = <0. 001) and width (Rhs 0.79 μm ± 0.18, Los 0.82 ± 0.13; Mann-Whitney Rank Sum Test, p = <0.001), which might be the reason why they show this two different septation mechanisms.

Due to the limits of resolution and the high cytosolic FtsZ background we could not clarify the transition from non-ring FtsZ accumulation to the FtsZ-ellipse with the present epifluorescence data set. A super resolution approach using e.g. 3D-structured illumination microscopy could reveal how the Z-ellipse is formed in detail.

Rhs appears to first invaginate at the basal pole, strongly indicating a polarity to the cell. Using electron microscopic analysis, no obvious morphological adaptation could be found (e.g. holdfast). In model organisms the heterogeneous distribution of specific phospholipids along the cell membrane was shown to influence the localization of proteins (Mileykovskaya and Dowhan 2005, Matsumoto et al. 2006). Visualizing the distribution of

cardiolipin with the fluorescent dye 10-N-nonyl acridine orange should provide insight into Rhs polarity.

Also in unicellular eukaryotes, longitudinal fission has been reported for euglenid protists, such as Trypanoplasma (Pecková and Lom 1990), Trypanosoma (reviewed in Field and Carrington 2009), and Euglena (Gillot and Triemer 1978). In contrast, their cell envelope constricts at one pole only, instead of both poles, as seen in Rhs.

Heterogeneous distribution of molecules along the bacterial cell envelope could be triggered by the host with whom Rhs lives in a tight symbiotic relationship. Eukaryotic organisms can dramatically influence the cell cycle of their symbionts. Weevils of the genus *Sitophilus* use the peptide ColA and its bacteriostatic and bactericidal properties to keep their endosymbiont population under control (Login et al. 2011). Similarly, in the legume-Rhizobium bacteria symbiosis, the morphological differentiation and cell division of the symbiont can be controlled by host peptides (reviewed in Kondorosi et al. 2013) Furthermore, all investigated stilbonematid ectosymbionts show drastic deviations from the cell division known from model organisms (e.g. longitudinal division, size independent division (Leisch et al. 2012, Pende et al. 2014)). Therefore, the asynchronous division of Rhs may be caused by its symbiotic lifestyle. Successful establishment of an ectosymbiont culture will allow us to address the points mentioned above, understand the underlying mechanisms and investigate the extent of influence the symbiotic lifestyle has on this bacterium.

Acknowledgements

This work was supported by the Austrian Science Fund (FWF) project P22470-B17 (N.L. and S.B.), an uni:docs fellowship from the University of Vienna (N.P.) and the Ph.D. completion grant 2014 of the University of Vienna (N.L.). We are very grateful to the Core

Facility Cell Imaging and Ultrastructure Research of the University of Vienna for technical support. This work is contribution XXX from the Carrie Bow Cay Laboratory, Caribbean Coral Reef Ecosystem Program, National Museum of Natural History, Washington, DC.

References

Adams, D. W. and J. Errington (2009). "Bacterial cell division: assembly, maintenance and disassembly of the Z ring." Nature Reviews Microbiology **7**(9): 642-653.

Bayer, C., N. R. Heindl, C. Rinke, S. Lücker, J. A. Ott and S. Bulgheresi (2009). "Molecular characterization of the symbionts associated with marine nematodes of the genus *Robbea*." Environmental Microbiology Reports **1**(2): 136-144.

Begg, K. J. and W. D. Donachie (1985). "Cell shape and division in *Escherichia coli*: experiments with shape and division mutants." Journal of Bacteriology **163**(2): 7.

Begg, K. J. and W. D. Donachie (1998). "Division Planes Alternate in Spherical Cells of *Escherichia coli*." Journal of Bacteriology **180**(9).

Bi, E. F. and J. Lutkenhaus (1991). "FtsZ ring structure associated with division in *Escherichia coli*." Nature **354**(6349): 161-164.

de Boer, P. A. (2010). "Advances in understanding *E. coli* cell fission." Current Opinion in Microbiology **13**(6): 730-737.

de Pedro, M. A., W. D. Donachie, J.-V. Höltje and H. Schwarz (2001). "Constitutive Septal Murein Synthesis in *Escherichia coli* with Impaired Activity of the Morphogenetic Proteins RodA and Penicillin-Binding Protein 2." Journal of Bacteriology **183**(14): 4115-4126.

Den Blaauwen, T. (2013). "Prokaryotic cell division: flexible and diverse." Current Opinion in Microbiology **16**: 738-744.

den Blaauwen, T., M. E. G. Aarsman, N. O. E. Vischer and N. Nanninga (2003). "Penicillin binding protein PBP2 of *Escherichia coli* localizes preferentially in the lateral wall and at mid cell in comparison with the old cell pole." Molecular Microbiology **47**(2): 539-547.

Erickson, H. P., D. E. Anderson and M. Osawa (2010). "FtsZ in bacterial cytokinesis: cytoskeleton and force generator all in one." Microbiology and Molecular Biology Reviews **74**(4): 504-528.

Fenchel, T. and B. Finlay (1989). "Kentrophoros: a mouthless ciliate with a symbiotic kitchengarden." Ophelia: International Journal of Marine Biology **30**(2): 75-93.

Field, M. C. and M. Carrington (2009). "The trypanosome flagellar pocket." Nature Reviews Microbiology **7**(11): 775-786.

Giere, O. and J. Krieger (2001). "A triple bacterial endosymbiosis in a gutless oligochaete (Annelida): ultrastructural and immunocytochemical evidence." Invertebrate Biology **120**(1): 41-49.

Gillot, M. and R. Triemer (1978). "The ultrastructure of cell division in *Euglena gracilis*." Journal of Cell Science **31**: 25-35.

Goley, E. D. (2013). "Tiny cells meet big questions: a closer look at bacterial cell biology." Molecular Biology of the Cell **24**(8): 1099-1102.

Himmel, D., L. C. Maurin, O. Gros and J.-L. L. Mansot (2009). "Raman microspectrometry

sulfur detection and characterization in the marine ectosymbiotic nematode *Eubostrichus dianae* (Desmodoridae, Stilbonematidae)." Biology of the cell / under the auspices of the European Cell Biology Organization **101**(1): 43-54.

Kondorosi, E., P. Mergaert and A. Kereszt (2013). "A Paradigm for Endosymbiotic Life: Cell Differentiation of Rhizobium Bacteria Provoked by Host Plant Factors." Microbiology **67**(1): 611-628.

Koppelman, C., M. E. G. Aarsman, J. Postmus, E. Pas, A. O. Muijsers, D. Scheffers, N. Nanninga and T. den Blaauwen (2004). "R174 of *Escherichia coli* FtsZ is involved in membrane interaction and protofilament bundling, and is essential for cell division." Molecular Microbiology **51**(3): 645-657.

Leisch, N., J. Verheul, N. R. Heindl, H. R. Gruber-Vodicka, N. Pende, T. den Blaauwen and S. Bulgheresi (2012). "Growth in width and FtsZ ring longitudinal positioning in a gammaproteobacterial symbiont." Current Biology **22**(19): R831-832.

Login, F. H., S. Balmand, A. Vallier, C. Vincent-Monegat, A. Vigneron, M. Weiss-Gayet, D. Rochat and A. Heddi (2011). "Antimicrobial peptides keep insect endosymbionts under control." Science **334**(6054): 362-365.

Lutkenhaus, J. (2007). "Assembly dynamics of the bacterial MinCDE system and spatial regulation of the Z ring." Annual Review of Biochemistry **76**: 539-562.

Lutkenhaus, J. and S. G. Addinall (1996). "FtsZ-spirals and -arcs determine the shape of the invaginating septa in some mutants of *Escherichia coli*." Molecular Microbiology **22**(2): 231-237.

Margolin, W. (2005). "FtsZ and the division of prokaryotic cells and organelles." Nature Reviews Molecular Cell Biology **6**(11): 862-871.

Matsumoto, K., J. Kusaka, A. Nishibori and H. Hara (2006). "Lipid domains in bacterial membranes." Molecular Microbiology **61**(5): 1110-1117.

Mileykovskaya, E. and W. Dowhan (2005). "Role of membrane lipids in bacterial division-site selection." Current Opinion in Microbiology **8**(2): 135-142.

Mingorance, J., G. Rivas, M. Vélez, P. Gómez-Puertas and M. Vicente (2010). "Strong FtsZ is with the force: mechanisms to constrict bacteria." Trends in Microbiology **18**(8): 348-356.

Montanaro, J., N. Leisch, D. Gruber, A. Inic-Kanada, S. Belij, E. Stein, N. Bintner, A. Ladurner and T. Barisani-Asenbauer "Preserving ultrastructure and morphology of tissue using PHEM buffered fixatives." Journal of Microscopy **under review**.

Osawa, M. and H. P. Erickson (2013). "Liposome division by a simple bacterial division machinery." Proceedings of the National Academy of Sciences of the United States of America **110**(27): 11000-11004.

Ott, J. A., H. R. Gruber-Vodicka and N. Leisch (2014). "Phylogenetic confirmation of the genus Robbea (Nematoda: Desmodoridae, Stilbonematinae) with the description of three new species." Systematics and Biodiversity **12**(4): 434-455.

Pecková, H. and J. Lom (1990). "Growth, morphology and division of flagellates of the genusTrypanoplasma (Protozoa, Kinetoplastida) in vitro." Parasitology Research **76**.

Pende, N., N. Leisch, H. R. Gruber-Vodicka, N. R. Heindl, J. A. Ott, T. Den Blaauwen and S.

Bulgheresi (2014). “Size-independent symmetric division in extraordinarily long cells.” Nature communications **5**: 4803.

Polz, M., H. Felbeck, R. Novak, M. Nebelsick and J. A. Ott (1992). “Chemoautotrophic, sulfur-oxidizing symbiotic bacteria on marine nematodes: Morphological and biochemical characterization.” Microbial Ecology **24**(3): 313-329.

Sato, M., Y. Mogi, T. Nishikawa, S. Miyamura, T. Nagumo and S. Kawano (2009). “The dynamic surface of dividing cyanelles and ultrastructure of the region directly below the surface in Cyanophora paradoxa.” Planta **229**(4): 781-791.

Sato, M., T. Nishikawa, H. Kajitani and H. Kawano (2007). “Conserved relationship between FtsZ and peptidoglycan in the cyanelles of *Cyanophora paradoxa* similar to that in bacterial cell division.” Planta **227**(1): 177-187.

Schizas, N. V., G. T. Street, B. C. Coull, G. T. Chandler and J. M. Quattro (1997). “An efficient DNA extraction method for small metazoans.” Molecular Marine Biology and Biotechnology **6**(4): 381-383.

Schneider, C. A., W. S. Rasband and K. W. Eliceiri (2012). “NIH Image to ImageJ: 25 years of image analysis.” Nature Methods **9**(7): 671-675.

van der Ploeg, R., J. Verheul, N. O. Vischer, S. Alexeeva, E. Hoogendoorn, M. Postma, M. Banzhaf, W. Vollmer and T. den Blaauwen (2013). “Colocalization and interaction between elongasome and divisome during a preparative cell division phase in *Escherichia coli*.” Molecular Microbiology **87**: 1074-1087.

Wu, L. J. and J. Errington (2012). “Nucleoid occlusion and bacterial cell division.” Nature Reviews Microbiology **10**(1): 8-12.

Zaritsky, A., A. Van Geel, I. Fishov, E. Pas, M. Einav and C. L. Woldringh (1999). "Visualizing multiple constrictions in spheroidal *Escherichia coli* cells." Biochimie **81**(8-9): 897900.

Zielinski, F. U., A. Pernthaler, S. Duperron, L. Raggi, O. Giere, C. Borowski and N. Dubilier (2009). "Widespread occurrence of an intranuclear bacterial parasite in vent and seep bathymodiolin mussels." Environmental Microbiology **11**(5): 1150-1167.

Chapter 7

Size-independent symmetric division in extraordinarily long cells.

Authors Nika Pende*, Nikolaus Leisch*, Harald R. Gruber Vodicka, Niels R. Heindl, Jörg A. Ott, Tanneke den Blaauwen and Silvia Bulgheresi

*these authors contributed equally

Keywords binary fission, bacterial cell growth, symbiosis, marine sulfur-oxidizing bacteria, filamentous bacteria, Gammaproteobacteria

Publication status Article published in Nature Communications **5**: 4803

Detailed description of NL's contribution

a. collected material on two field trips to Carrie Bow Caye (Belize)

b. sequenced 16S rRNA genes of the *E. fertilis* symbiont

c. performed the electron microscopy

d. performed the immunofluorescence staining of the *E. fertilis* symbiont

e. performed all morphometric, fluorescent profile and statistical analyses

f. analyzed data and prepared the figures

g. wrote parts of the manuscript, edited and approved the manuscript

nature COMMUNICATIONS

ARTICLE

Received 12 Jun 2014 | Accepted 24 Jul 2014 | Published 15 Sep 2014

DOI: 10.1038/ncomms5803 OPEN

Size-independent symmetric division in extraordinarily long cells

Nika Pende[1,*], Nikolaus Leisch[1,*], Harald R. Gruber-Vodicka[2], Niels R. Heindl[1], Jörg Ott[3], Tanneke den Blaauwen[4] & Silvia Bulgheresi[1,5]

Two long-standing paradigms in biology are that cells belonging to the same population exhibit little deviation from their average size and that symmetric cell division is size limited. Here, ultrastructural, morphometric and immunocytochemical analyses reveal that two *Gammaproteobacteria* attached to the cuticle of the marine nematodes *Eubostrichus fertilis* and *E. dianeae* reproduce by constricting a single FtsZ ring at midcell despite being 45 µm and 120 µm long, respectively. In the crescent-shaped bacteria coating *E. fertilis*, symmetric FtsZ-based fission occurs in cells with lengths spanning one order of magnitude. In the *E. dianeae* symbiont, formation of a single functional FtsZ ring makes this the longest unicellular organism in which symmetric division has ever been observed. In conclusion, the reproduction modes of two extraordinarily long bacterial cells indicate that size is not the primary trigger of division and that yet unknown mechanisms time the localization of both DNA and the septum.

[1] Department of Ecogenomics and Systems Biology, University of Vienna, Althanstrasse 14, 1090 Vienna, Austria. [2] Department of Symbiosis, Max Planck Institute for Marine Microbiology, Celsiusstrasse 1, D-28359 Bremen, Germany. [3] Department of Limnology and Biooceanography, University of Vienna, Althanstrasse 14, 1090 Vienna, Austria. [4] Department of Bacterial Cell Biology, Swammerdam Institute of Life Sciences, Faculty of Science, University of Amsterdam, Science Park 904, 1098 XH Amsterdam, the Netherlands. [5] Center for Anatomy and Cell Biology, Medical University of Vienna, Währingerstrasse 10, 1090 Vienna, Austria. * These authors contributed equally to this work. Correspondence and requests for materials should be addressed to S.B. (email: silvia.bulgheresi@univie.ac.at).

The spatial control of bacterial growth, division and morphology—as well as the mechanisms of DNA organization and segregation—has been investigated only in a handful of cultivable organisms so far[1]. Given the overwhelming phylogenetic and morphological diversity of microbes, our current knowledge on their cell biology likely represents only a tiny piece of the overall picture. This is regrettable given that the void in antibiotics discovery[2], coupled with an increasing awareness about the role of uncultivable, non-pathogenic microbes in animal health, implies major applied benefits from studying how environmental bacteria reproduce.

Most known bacteria are between 0.4 and 2 μm in diameter, and 0.5 and 5 μm in length. Model rod-shaped bacteria control their overall size by varying their cell length, which, in turn, is under control of the division apparatus[3,4]. *Escherichia coli*, for example, can grow into long, aseptate filaments with regularly spaced nucleoids following mutations in filamentous temperature sensitive (*fts*) genes, which direct the assembly of the division apparatus[5]. Although these *E. coli* mutants cannot build a functional constricting ring and finally lyse, DNA replication and chromosome segregation continue unaffected for several generations.

The metabolic status of the cell may also affect bacterial length: *Bacillus subtilis* is longer when incubated in a nutrient-rich medium and shorter when nutrients are limited[6,7]. In the former case, *B. subtilis* accumulates a metabolite that induces a glucosyltransferase. This, in turn, inhibits FtsZ polymerization so that cell division is delayed and the cells grow longer[8]. In a striking example of convergent evolution, the size of *E. coli* is similarly linked to nutrient availability by a different but functionally analogous glucosyltransferase[9–12].

With the sole exception of the giant surgeonfish gut symbiont[13], the molecular basis of the reproduction of naturally occurring long to giant bacteria (longest length between 10 and 750 μm) is unexplored. Many of them are marine sulphur-oxidizing bacteria (SOBs) and contain large nitrate and sulphur inclusions that reduce the volume of their active cytoplasm[14]. Here we investigated the molecular mechanisms underlying the reproduction mode of two extraordinarily long bacteria coating the newly described nematode species *Eubostrichus fertilis* (Fig. 1a–d and Supplementary Fig. 1a)[15] and *E. dianeae*[16,17] (Supplementary Fig. 1b; hereafter we refer to these filamentous bacteria as Efs and Eds, respectively). Eds contains strongly refracting spherical cytoplasmic inclusions[17] and Raman microspectrometry proved that at least some of these contain elemental sulphur[18,19]. Although these data suggest that Eds may store and oxidize sulphur, previous 16S ribosomal RNA (rRNA) gene-based analyses of the *E. dianeae*-associated bacterial community did not yield any SOB 16S rRNA gene sequence[20]. As for *E. fertilis*, crescent-shaped bacteria are attached with both poles to their nematode host so that their long axis is always parallel to the host's anterior–posterior axis. This, combined with their shifted alignment to one another around the worm circumference, confers a rope-like appearance (Fig. 1a), similar to that observed for *E. cf. parasitiferus*[16,17], *E. topiarius*[21] and *Adelphus rolandi*[22]. Although DNA staining of *E. cf. parasitiferus*-associated bacteria revealed several nucleoids in each cell[17], binary fission was detected neither in these, nor in Eds cells. It was therefore hypothesized that both ectosymbionts elongate without dividing, possibly due to nematode-secreted inhibitors[17].

This study was designed to determine how supersized bacteria associated with two *Eubostrichus* nematodes reproduce on their respective hosts.

Results

One bacterial phylotype coats each nematode species. To molecularly identify the filamentous bacteria coating *E. fertilis* and *E. dianeae,* we extracted genomic DNA (gDNA) from single symbiotic worms and constructed bacterial 16S rRNA gene libraries. Based on BLASTN search, we identified three and seven SOB 16S rRNA sequences in the *E. fertilis* and *E. dianeae* libraries, respectively. We compared these SOB sequences to those of other stilbonematid and oligochaete symbionts, as well as to those of bacteria belonging to the *Chromatiaceae* and other uncultured *Gammaproteobacteria* that are >95% similar to the symbionts. The resulting 16S rRNA gene-based phylogenetic tree (Fig. 2) shows that the representative SOB sequences, each obtained either from the *E. fertilis* or the *E. dianeae* 16S rRNA gene library (GenBank accession numbers KF278590 and KF278587, respectively) belong to the Marine Oligochaete and Nematode Thiotrophic Symbionts (MONTS) cluster of *Gammaproteobacteria*[23] and are most closely related to *E. topiarius*-associated bacteria. To confirm that the MONTS 16S rRNA sequences obtained in our libraries originated from Efs and Eds, we applied fluorescence *in situ* hybridization (FISH) probes specifically targeting those sequences (probe Efs1057 and

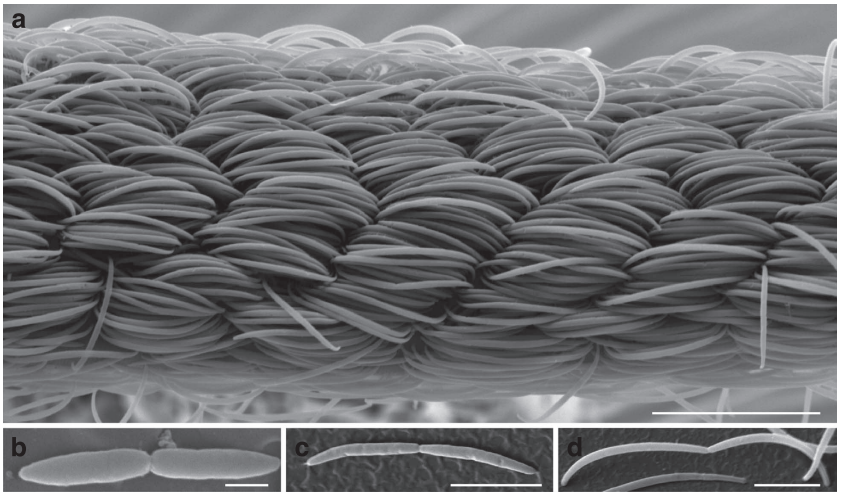

Figure 1 | Scanning electron microscope (SEM) micrographs of the *E. fertilis* ectosymbiont. (**a**) Central portion of the bacterial coat and (**b**–**d**) single constricted Efs cells of different lengths. Scale bar, 20 μm in **a**, 1 μm in **b** and 5 μm in **c**,**d**.

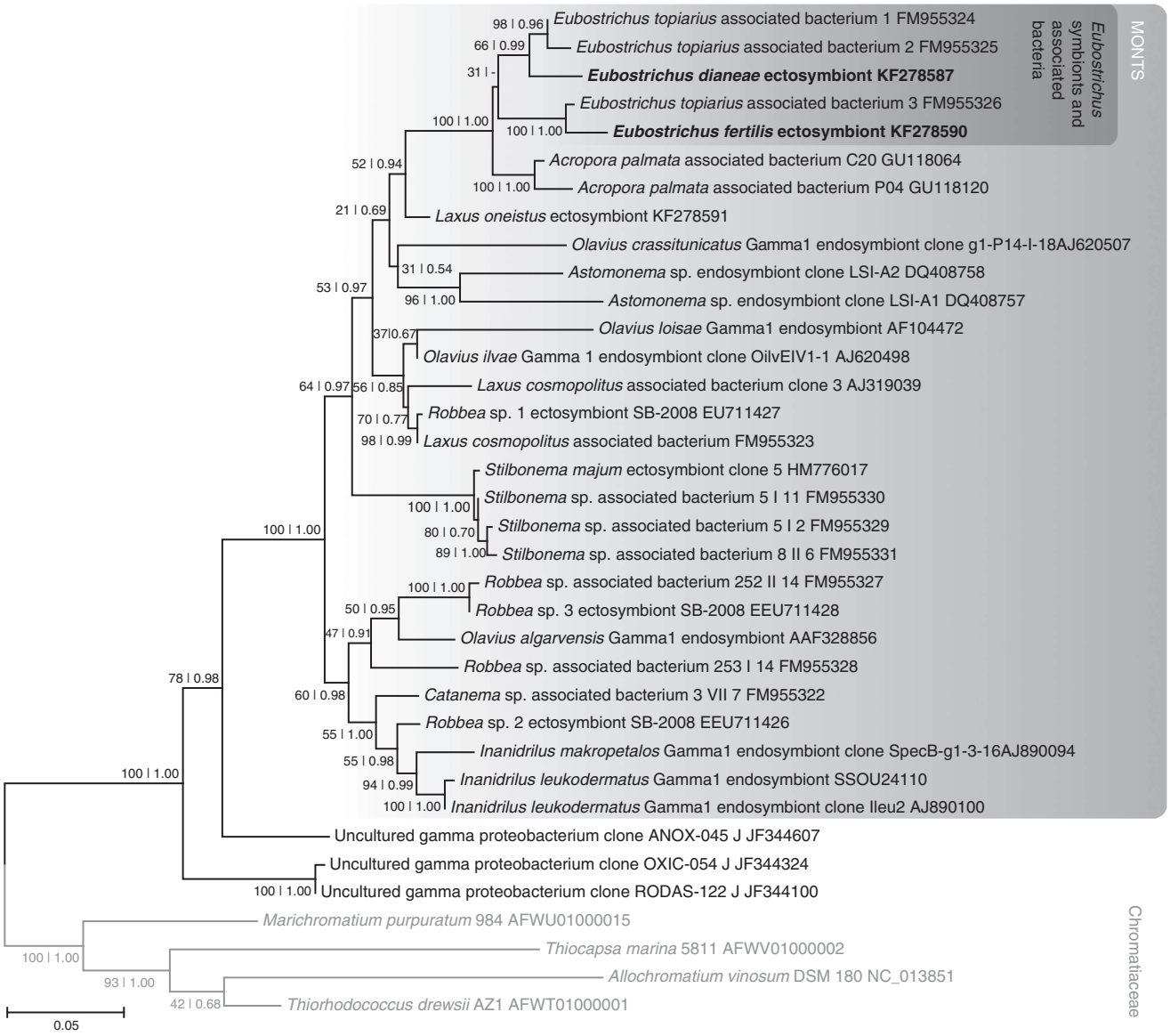

Figure 2 | Gammaproteobacterial 16S rRNA gene tree based on the most likely RAxML tree (GTR + I + G model of substitution). Rapid bootstrapping (RAxML) and posterior probability (MrBayes) node support is given for all nodes. The minus symbol (–) instead of a posterior probability in the *Eubostrichus*-associated bacteria cluster indicates that this node was not resolved in the MrBayes consensus. The *Chromatiaceae* outgroup is indicated with grey font colour. Scale bar represents the mean number of nucleotide substitutions per site. GenBank accession numbers are indicated after the names of the sequences.

Eds214, respectively) to whole mount *Eubostrichus* nematodes. All bacteria attached to the host surface were triple stained by the bacterial probe EUB338, by the *Gammaproteobacteria*-specific probe GAM42a and by the respective MONTS-specific probes (Fig. 3 and Supplementary Fig. 2). This confirms that the MONTS 16S rRNA gene sequences obtained in our libraries originated from the filamentous bacteria coating *E. fertilis* and *E. dianeae*. Moreover, given that all bacteria detected by the *Eubacteria*-specific probe were also detected by the *Gammaproteobacteria*- and MONTS-specific probe, the non-MONTS 16S rRNA gene sequences identified in our libraries, including those attributable to *Deltaproteobacteria* (Supplementary Fig. 2) did not originate from cuticle-associated bacteria. In conclusion, Efs and Eds are two novel distinct MONTS phylotypes, each one associated with the respective host species. The phylogenetic placement of Eds and Efs is consistent with that observed for all marine nematode ectosymbionts characterized by full 16S rRNA-gene cycle so far[24–26]. Moreover, given that Efs and Eds were the only bacteria detected on the surface of their respective hosts, these newly characterized stilbonematid ectosymbioses also appear to be monospecific.

The nematode symbionts express the tubulin homologue FtsZ. In the model gammaproteobacterium *E. coli*, cell division is initiated by polymerization of the tubulin homologue FtsZ into a ring (the Z-ring) and its subsequent constriction[27–29]. In *E. coli* cells, the ring is usually positioned at midcell, perpendicular to the longitudinal axis[30]. After the self-assembly the Z-ring starts to constrict, thereby directing the division of the cell, which results in two equal daughter cells. Given that FtsZ mediates binary fission in all known *Gammaproteobacteria*, including the longitudinally dividing MONTS associated with *Laxus*

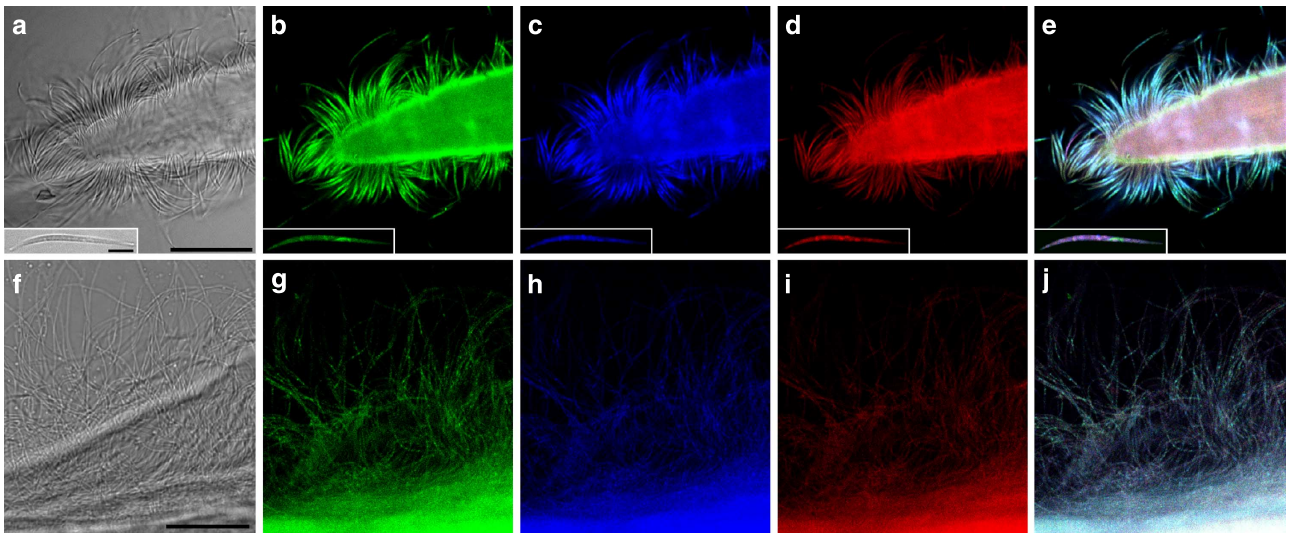

Figure 3 | FISH/laser-scanning confocal microscopy (LSCM) of ectosymbionts attached to the worm surface. Images of the Efs coat are shown in **a**–**e** and images of the Eds coat in **f**–**j**. **a** and **f** are the corresponding bright field images of **b**–**e** and **g**–**j**, respectively. Each single symbiont is triple stained with specific probes targeting *Eubacteria* (**b** and **g**), *Gammaproteobacteria* (**c** and **h**), and the symbiont (Efs1027 and Eds214, respectively; **d** and **i**). (**e**) and (**j**) are overlay pictures of (**b**–**d**) and (**g**–**i**), respectively. A single Efs cell is shown in the insets in (**a**–**e**). Scale bar, 25 μm for all images and 5 μm for the insert.

oneistus[31], and it is part of the genetic repertoire of three additional MONTS (genome drafts available upon request at http://rast.nmpdr.org/rast.cgi), we hypothesized that Efs and Eds also express the *fts*Z gene. By using degenerate PCR primers on gDNA extracted from single symbiotic nematodes, we homology cloned Efs and Eds *fts*Z-gene fragments. The predicted Efs FtsZ protein fragment (322 amino acids) had 83% sequence identity with that of the *L. oneistus ecto*symbiont, and 67% with that of *E. coli* K12, whereas the corresponding sequence identities for the predicted Eds FtsZ protein fragment (336 amino acids) were 84% and 66%, respectively. The *Eubostrichus* symbiont FtsZ proteins cluster with other MONTS FtsZ proteins in our phylogenetic reconstruction (Supplementary Fig. 3). To assess if the *Eubostrichus* ectosymbionts express FtsZ, a commercially available anti-*E. coli* FtsZ antibody was tested on Western blots of protein extracted from host-dissociated ectosymbionts. This resulted in the specific detection of protein bands of ~40 kDa, the predicted molecular weight of *E. coli* FtsZ (Supplementary Fig. 4). In conclusion, both Efs and Eds express the cell division protein FtsZ and their genes are phylogenetically related to the *L. oneistus* ectosymbiont FtsZ and form a 16S rRNA gene-concordant cluster.

Symmetric FtsZ-based fission in 4 to 45 μm-long Efs cells. Morphometric analysis of 2,731 Efs cells showed a length range of 3.54–44.55 μm and a width range of 0.38–1.21 μm (Table 1; Supplementary Fig. 5) and scanning electron microscopy (SEM) analysis revealed constricted cells of lengths ranging from 6.1 to 23.2 μm (Fig. 1b–d). Consistently, Efs cell length distribution indicated that most length values are similarly represented in the population (Supplementary Fig. 5). To test the hypothesis that Efs cells can divide at any length, we immunostained them with an anti-FtsZ antibody and analyzed its localization pattern. FtsZ rings appeared in 77/662 cells (11.6%) between 3.5 and 45 μm long (Fig. 4a,b,d,f and Supplementary Fig. 6). Unsegregated DNA localized at midcell in cells with homogeneous FtsZ staining (Fig. 4e left plot and representative image in Fig. 4c), whereas DNA was already segregated in cells with mid-cell (non-ring) FtsZ accumulation (Fig. 4e, middle plot). In cells showing a Z-ring (e.g. insert Fig 4d insert), we observed symmetric DNA segregation both in terms of localization and of fluorescence signal intensity (Fig. 4e, rightmost plot). Of note, in these cells, the DNA signal was often highly fragmented as if originating from several nucleoids (see for example Fig. 4b or Supplementary Fig. 6b,n). Mid-cell membrane constriction in correspondence with mid-cell FtsZ signal indicates that FtsZ polymerized into a functional constricting ring (Fig. 4f). FtsZ fluorescence profiles of 662 cells aligned from the shortest to longest (left to right in Supplementary Fig. 7a–d) did neither indicate a continuous FtsZ fluorescence accumulation at midcell, nor a continuous DNA partitioning pattern as Efs lengthens. However, most of the cells displaying mid-cell FtsZ signal (62.3%; Supplementary Table 1) were 15–30-μm long. We conclude that Efs cells divide by FtsZ-based fission and may symmetrically segregate the DNA at virtually every length leading to a 10-fold variation in cell length.

Table 1 | Size measurements of the *Eubostrichus fertilis* and the *Eubostrichus dianeae* symbionts.

	Eubostrichus fertilis symbiont ($n = 2,731$)		*Eubostrichus dianeae* symbiont ($n = 2,743$)	
	length (μm)	width (μm)	length (μm)	width (μm)
Minimum	3.54	0.38	16.46	0.41
Maximum	44.55	1.21	120.22	1.40
Mean	16.23	0.60	49.70	0.75
s.d.	7.06	0.08	14.70	0.12

Symmetric FtsZ-based fission in up to 120-μm-long Eds cells. Each Eds filament is attached to the nematode host by one of its poles (Supplementary Fig. 1b,d). Morphometric analysis of 2,743 Eds cells showed a length range 16.5–120.2 μm and a width range of 0.4–1.4 μm (Table 1), albeit most cells are ~50-μm long (Supplementary Fig. 5). To assess if Eds divides via FtsZ-based fission, we immunostained it with an anti-FtsZ antibody and

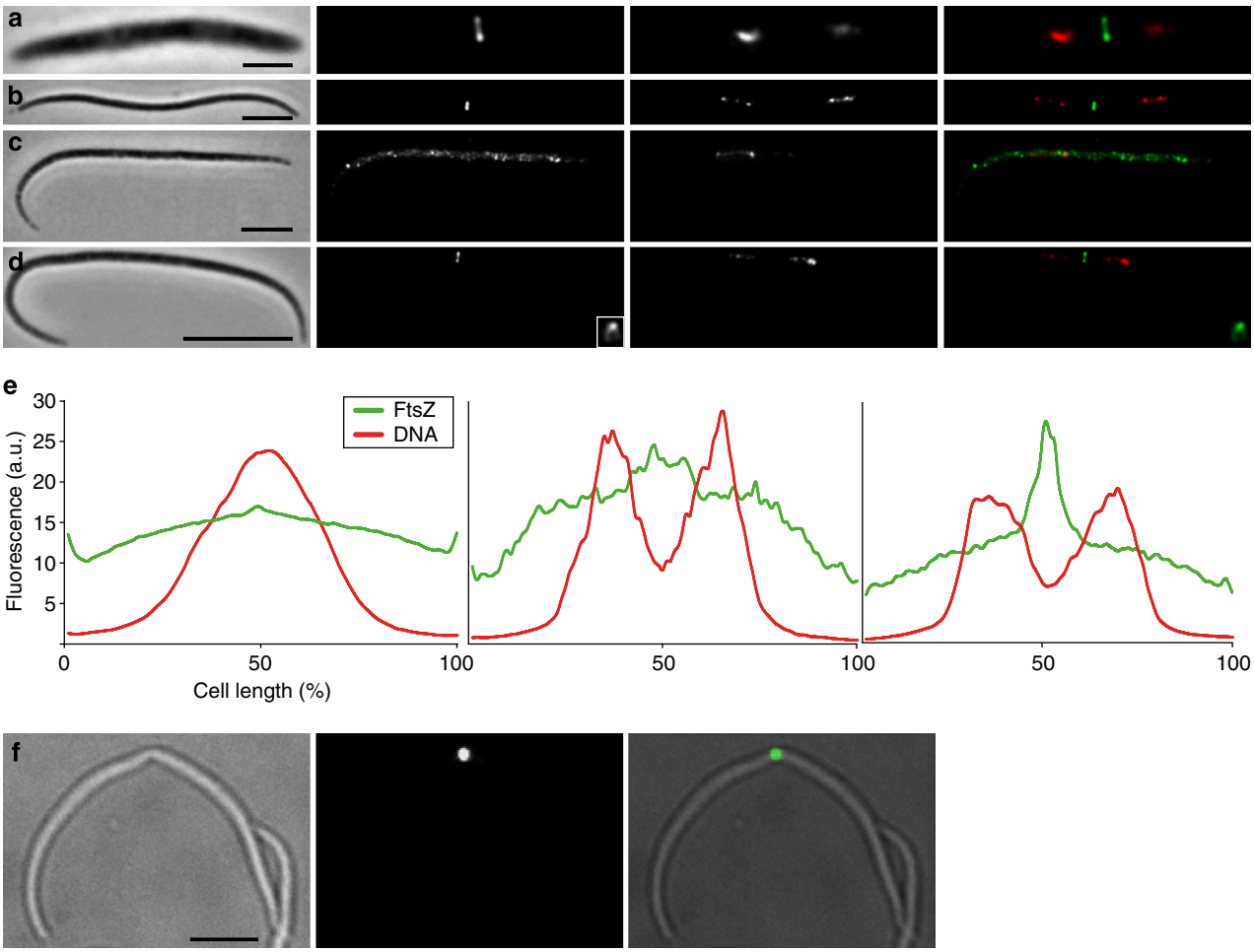

Figure 4 | FtsZ and DNA localization pattern in Efs cells. (**a**–**d**) From left to right, phase contrast, FtsZ fluorescence, DNA fluorescence and FtsZ (green)/DNA (red) overlay images of immunostained Efs cells of different lengths (**a**,**b** and **d** have FtsZ rings and segregated DNA, **c** has neither mid-cell FtsZ accumulation nor segregated DNA). Insets in **d** show an LSCM image of an FtsZ ring from a different cell. **e** shows average fluorescence profiles of 549 cells displaying neither FtsZ mid-cell accumulation nor DNA segregation (left), 36 cells with both non-ring FtsZ accumulation at mid-cell (middle) and segregated DNA, and 77 cells with FtsZ rings and segregated DNA (right). FtsZ fluorescence (green) and DNA fluorescence (red) expressed in arbitrary units (a.u.) are plotted along the cell length expressed in percentage. LSCM images of an immunostained Efs constricted cell are shown in **f**, from left to right bright field, FtsZ fluorescence and overlay. Scale bars. 2 μm in **a**, 5 μm in **b**,**c** and **f** and 10 μm in **d**.

analyzed its localization pattern. In the shortest cells, FtsZ was homogenously distributed throughout the cell, whereas unsegregated DNA localized at midcell (Fig. 5a–d, the shortest cells correspond to the bars occupying—approximately—the leftmost third of the profile; representative single cell in Fig. 5e and leftmost plot in h). In the medium length cells, FtsZ fluorescence accumulated in a central portion of the cell between the segregated DNA (central third of each profile in Fig. 5a–d, representative image in f and central plot in h). In the longest cells, FtsZ appeared as a sharp, mid-cell band and DNA was further segregated into the two prospective daughter cells (rightmost third of each profile in Fig. 5a–d, representative image in g and rightmost plot in h). Notably, and as observed for Efs, only a small fraction of the Eds cells displayed FtsZ rings (87/772, 11.27%). However, all of them were longer than 30 μm, indicating that the propensity of Eds to divide increases as it lengthens (Supplementary Table 1). Plotting the DNA fluorescence emitted by 301 cells with non-segregated DNA (representative image in Supplementary Fig. 8b) and by 237 cells with segregated DNA (representative image in Supplementary Fig. 8c) against the cell length confirmed symmetric partitioning of the DNA into the two prospective daughter cells (Supplementary Fig. 8a). As observed in Efs cells displaying FtsZ rings, the DNA signal was often highly fragmented as if originating from several nucleoids (Supplementary Fig. 8c). Further, confocal microscopy revealed that mid-cell FtsZ polymerizes into a circular ring in Eds and that this is functional as it can drive cell membrane constriction (Fig. 5i). We conclude that the gammaproteobacterium Eds, despite its extraordinary length, divides transversally and symmetrically by means of a single, constricting FtsZ ring placed at midcell.

Discussion

In this study we investigated the reproduction modes of two naturally occurring supersized bacteria at the molecular level. This is the only such study besides that on the firmicute symbiont inhabiting the surgeonfish gut[13], and the first one involving environmental sulphur-oxidizing *Gammaproteobacteria* (as shown by our 16S rRNA gene-based phylogeny). Although previous morphological studies suggested that *Eubostrichus*-associated filamentous bacteria do not divide[17], we provided morphometric and immunocytochemical evidence that both Efs and Eds undergo binary fission. As shown by FISH with specific probes targeting their rRNA genes, only Efs and Eds are

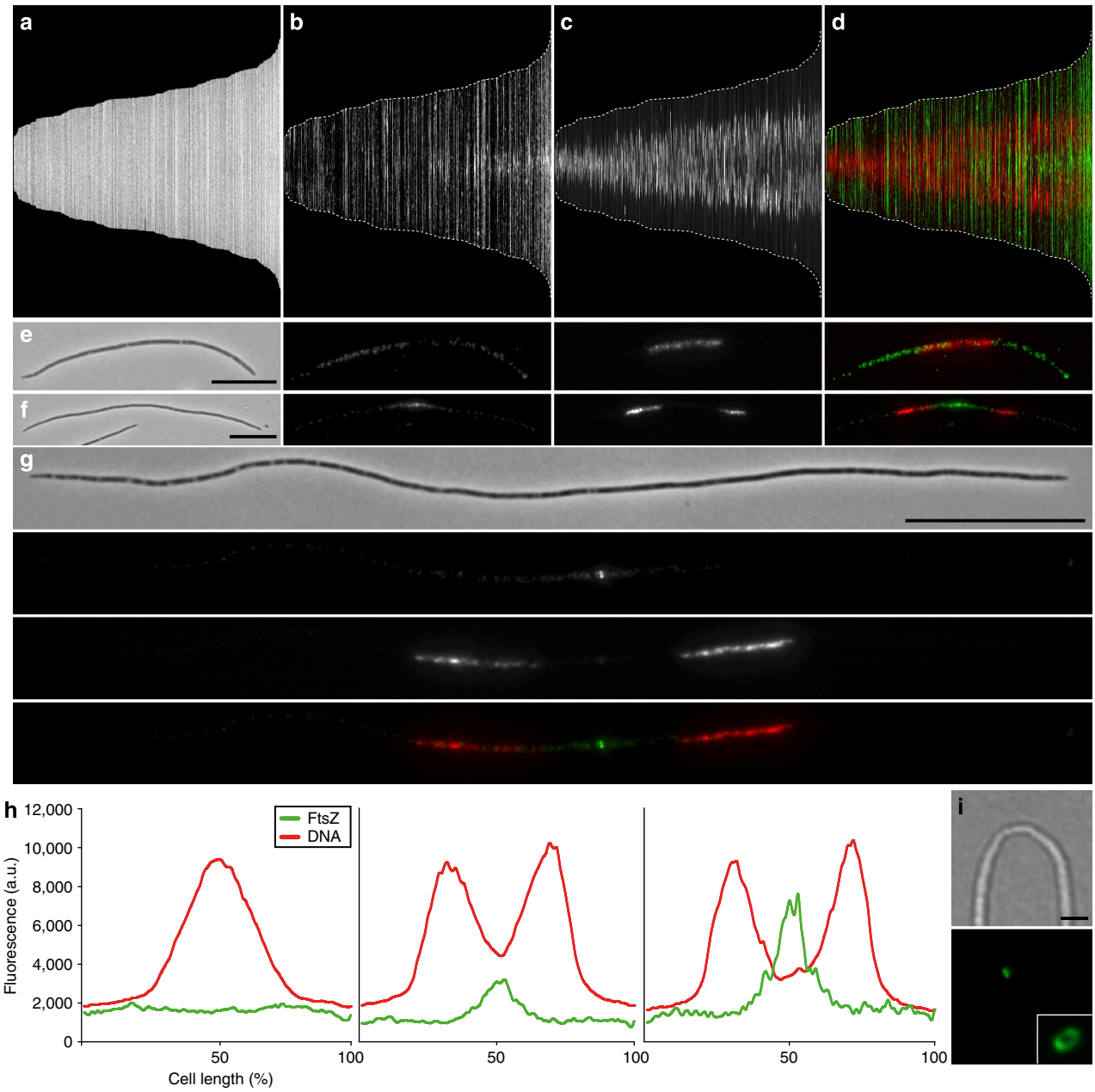

Figure 5 | FtsZ and DNA localization pattern in Eds cells. Cell length, FtsZ fluorescence, DNA fluorescence and overlay of FtsZ (green) and DNA (red) fluorescence of 562 Eds cells are represented in **a**–**d**, respectively. Cells are sorted by increasing cell length from left to right that is, the leftmost bar represents the shortest and the rightmost bar the longest cell. Cell length ranges from 16.46 to 82.54 µm (mean 43.16 ± 12.30). Dotted white line in **b**–**d** indicates the cell outline. (**e**–**g**) Phase contrast, FtsZ fluorescence, DNA fluorescence and FtsZ (green)/DNA (red) overlay images of immunostained Eds cells of different lengths displayed from left to right in **e** and **f** and top to bottom in **g**. **h** shows average fluorescence profiles of 301 cells with homogeneous FtsZ staining and non-segregated DNA (left), 189 cells with FtsZ accumulation at mid-cell and segregated DNA (middle), and 54 cells with FtsZ rings and segregated DNA (right). FtsZ fluorescence (green) and DNA fluorescence (red) expressed in arbitrary units (a.u.) are plotted along the cell length in percentage. LSCM images of a constricted immunostained Eds cell is shown in **i**, bright field and corresponding FtsZ fluorescence below. Inset shows an LSCM image of a FtsZ ring from a different cell. Scale bars, 10 µm in **e** and **f**, 20 µm in **g** and 2 µm in **i**.

detectable on the surface of their respective hosts. Therefore, each nematode is carrying a virtually pure bacterial cell culture. This enabled us to analyze the localization pattern of the key division protein FtsZ and of the DNA in hundreds of symbiont cells. The fact that Eds appears to be the only bacterium coating its host seems to contradict a former study[20], which suggested a high level of bacterial diversity associated with the nematode. However, all 16S rRNA gene sequences obtained in that first study originated from bacteria commonly found in marine environments; given the lack of whole nematode FISH-based evidence, these sequences likely originated from bacteria localized on nematode regions other than the cuticle (for example, the gut). Alternatively (or in addition), environmental bacteria non-stably associated with *E. dianeae* may also have been represented in the previously reported 16S rRNA gene library. Although our libraries were not extensively sequenced, they also contained non-MONTS 16S rRNA gene sequences (see Methods). Despite their heterogeneity, we could identify only a single MONTS phylotype (GenBank

KF278587) and this appeared to be the only one present on the nematode cuticle by FISH. The lack of SOB sequences in the library constructed by Polz *et al.*[20] could be due to a PCR bias, which we might have circumvented by using a shorter and more degenerate universal forward primer (616F instead of 27F). In conclusion, although we cannot exclude that bacteria other than Eds may occasionally be found on the *E. dianeae* surface, all nematode-coating bacteria visualized in our FISH analysis belong to a single MONTS phylotype. We observed the same for *E. fertilis*, suggesting high host-symbiont specificity for this newly described association as well.

The fact that there are no FtsZ rings overlapping with strong DNA signal is consistent with what is observed in *E. coli* and probably due to the phenomenon of nucleoid occlusion[32]; however, Efs and Eds DNA did not occupy the first and the last 20% of the cell length at any cell stage (Figs 4e and 5h and Supplementary Fig. 8), suggesting yet unknown mechanisms excluding DNA from the poles and preventing FtsZ polymerization in the first and the last 20% of the *Eubostrichus* ectosymbiont cells. Besides nucleoid occlusion, a second negatively acting mechanism, the Min system, dictates the selection of division sites in model bacteria[5]. In *E. coli*, the FtsZ inhibitor MinC, driven by the MinD and MinE proteins, oscillates back and forth between the two cell poles. As a consequence, MinC concentration is highest at the poles and lowest near midcell. As the cell elongates, the concentration near the cell's centre is reduced until it becomes so low that FtsZ can polymerize and constrict the cell. Therefore, cell length is determined by the amount of MinC so that larger amounts produce longer cells[33]. The complete *min* operon is present in all the MONTS genomes sequenced so far (ref. 31 and genomic data available upon request for three additional MONTS at http://rast.nmpdr.org/rast.cgi), whereas there is no genomic evidence of another well-described FtsZ-positioning system, the DivIVA system. However, the analysis of symbiont MinC localization pattern is needed to draw conclusions about the involvement of the Min system in *Eubostrichus* ectosymbionts FtsZ-ring positioning.

Besides marine nematode *ecto*symbionts, several oversize *endo*symbionts have been described, such as legume-nodulating *Alphaproteobacteria*[34], the gammaproteobacterium associated with *Sitophilus* weevils[35], the bacteroidete *Sulcia* inhabiting sharpshooters[36] and the firmicute *Epulopiscium* spp. thriving in the surgeonfish gut[37]. In the first two systems, host-secreted antimicrobial peptides (nodule-specific cysteine-rich peptides[38] and Coleopterycin-A[39], respectively) inhibit bacterial fission but not genome replication, which results in polyploidy. By blocking bacterial reproduction, hosts may better control the number and location of their endosymbionts[34,39]. The factors that trigger *Epulopiscium* sp. morphotype B extreme growth are still elusive, but polymerization of two polar FtsZ rings results in two intracellular daughter cells. These grow within the mother cell cytoplasm and are eventually released by perforating the mother cell envelope. Surprisingly, only a small portion of the mother DNA is passed on to the offspring[13,40], as reviewed in ref. 41. The fragmentation of the DNA staining frequently observed in *Eubostrichus*-associated filaments suggests that they are polyploid (as is the case for all aforementioned oversize endosymbionts) and that chromosomes are segregated prior to and independently from septation. This is consistent with the hypothesis that condensation resolution should be sufficient to segregate replicated sister chromosomes before cytokinesis[42]. However, more sensitive techniques such as FISH with *ori*C-specific probes are needed to determine the maximum genome copy numbers and the segregation dynamics in dividing Efs and Eds.

FtsZ immunostaining of *Eubostrichus*-coating bacteria revealed that, despite their large size and the likely presence of multiple genomes, they divide by symmetric transverse fission. Therefore, in contrast to all aforementioned endosymbionts that grow to extraordinary sizes because they either do not divide or they do so atypically, *Eubostrichus*-coating bacteria may become outstandingly long due to a delay in canonical binary fission. Given that Eds and Efs have not been isolated yet, we do not know whether nematode-secreted molecules mediate this delay or whether this delay is intrinsic to the bacteria. In the first case, Eds and Efs would represent the first bacteria whose growth is under host control in an *ecto*symbiosis, a form of association commonly considered less intimate than *endo*symbiosis. Besides cultivation, morphometric analysis of ectosymbionts associated with juvenile nematodes might reveal a correlation between bacterial length and host developmental stage.

It is intriguing to speculate that a similar mechanism coordinating *B. subtilis* or *E. coli* size with metabolic state (see Introduction) is at work in *Eubostrichus* symbionts. The FtsZ and DNA profiles of the crescent-shaped Efs, which are attached to its host with both poles, showed that it may divide at virtually any cell length between 3 and 45 µm. The bacterial coat is highly ordered (Fig. 1a) with the short crescent-shaped cells being proximal (that is, close to the host surface) and the long crescents being distal (Supplementary Fig. 1a,c). Their chemosynthetic metabolism relies on the diffusion of reduced sulphur compounds (for example, H_2S) and oxygen. If we assume that the distal Efs cells have better access to them and grow faster, less nutrients will be available for the proximal ones, which will therefore grow slower. Given that Eds filaments are monopolarly attached to their host (Supplementary Fig. 1b,d), the accessibility to sulphide and oxygen does not differ among them so that they may all experience the same growth rate. The ecological advantage of the two different bacterial coat architectures remains to be determined and might be due to differences in the physiology and/or behaviour of the two *Eubostrichus* hosts.

Taken together, this first molecular study of the reproduction of two environmental *Gammaproteobacteria* showed that they may vary over 12 times in cell length, largely exceeding the size variation observed in model bacteria, and that they can divide by FtsZ-based symmetric binary fission up to a length of 120 µm. This implies that novel molecular machineries may time cell division and position the genome and division plane in *Gammaproteobacteria*, a class of several ecologically and medically important bacteria.

Methods

Nematode collection. Specimens of *E. fertilis* and *E. dianeae* were collected in December 2011/January 2012 and in March/April 2014 in ~1 m depth from a sand bar off Twin Cays, Belize (16° 49′ 25.74″ N, 88° 6′ 21.18″ W). The nematodes were extracted from the sand by stirring the sand in seawater and pouring the supernatant through a 63-µm-pore-size mesh sieve. The content of the net was transferred into a Petri dish and single individuals were then picked by hand using fine tweezers under a dissecting microscope. *E. dianeae* identity was assessed morphologically according to the study by Hopper *et al.*[16] and molecularly according to the study by Kampfer *et al.*[43] This nematode has also been referred to as *E. dianae* in the literature. To establish *E. fertilis* identity, eukaryotic 18S rRNA gene libraries were constructed using the same two gDNA extractions employed for constructing bacterial 16S rRNA gene libraries (see below). *E. fertilis* 18S rRNA gene-based phylogenetic placement is published elsewhere[15]. For gDNA extraction, Western blotting, FISH and immunostaining, nematodes were fixed in methanol and stored at −20°C for transportation and storage. For SEM, nematodes were fixed with 2.5% glutaraldehyde and stored at 4 °C.

Scanning electron microscopy. Worms were either directly post-fixed with 1% osmium tetroxide for 2 h at room temperature, or the bacteria were first dissociated from the nematodes by mild sonication, allowed to settle on poly-L-lysine treated coverslips and then post-fixed. The samples were dehydrated in a graded ethanol series, transferred into pure acetone and critical point dried with a CPD 300 unit (Leica). After mounting, either whole worms or the bacteria-coated coverslips on stubs were gold-sputtercoated with an AGAR B7340 sputtercoater unit. Images were taken with a XL20 (Philips) using the Microscope control programme (version 7.00, FEI).

gDNA extraction, PCR and cloning of 16S rRNA genes. For the construction of the *E. dianeae* and *E. fertilis* 16S rRNA gene libraries gDNA was extracted from two single *E. dianeae* and two single *E. fertilis* nematodes as previously described[44]. gDNA (2 µl) were used as template in each 50 µl PCR reaction. Fragments (1,499-nucleotide (nt)-long) of bacterial 16S rRNA genes were amplified by PCR with primers 616V (5′-AGAGTTTGATYMTGGCTC-3′)[45] and 1492R (5′-GGYT ACCTTGTTACGACTT-3′)[46]. Cycling conditions for the 16S rRNA gene amplification were as follows: 94 °C for 4 min followed by 35 cycles of 94 °C for 45 s, 49 °C for 30 s, 72 °C for 90 s and a final elongation of 72 °C for 10 min. We randomly picked and fully sequenced eight clones from the two *E. fertilis* 16S rRNA gene libraries. Three belonged to members of the MONTS[23] cluster, two were from *Desulfobulbaceae*, one from *Oceanospirillales*, one from *Staphylococcus* and one from an unclassified bacterium. We randomly picked and fully sequenced 31 clones from the two *E. dianeae* 16S rRNA gene libraries. Thirteen clones were from sulphur-reducing *Deltaproteobacteria*, seven belonged to members of the MONTS cluster, three were from *Cytophaga*, five from *Rhodospirillales* and three from unclassified bacteria. Sequences were assembled with CodonCode Aligner 3.7.1 software (CodonCode Corporation, Dedham, MA, USA).

Homology cloning of *Eubostrichus* ectosymbiont *ftsZ* genes. gDNA was extracted from a single *E. fertilis* and a single *E. dianeae* as described above for the amplification of rRNA genes. For homology cloning of the Eds *fts*Z gene, a 1,106 nt-long fragment was amplified using degenerate primers ftsz1F (5′-GCVGTVA-TYAARGTBATCGG-3′) and ftsZ2.1R (5′-GCYGGRATRTCSAGRTAATC-3′). For homology cloning of the Efs *fts*Z gene, an additional amplification step was performed on the 1,106 nt-long ftsz1F-ftsZ2.1R fragment with the nested primer ftsZ1Fnes1 (5′-ATCAAGGTTATCGGGGT-3′). Touchdown PCR conditions for both degenerate and nested PCRs were as follows: 94 °C for 3 min, followed by 8 cycles at 94 °C for 45 s, 58–50 °C for 45 s, 72 °C for 75 s, followed by 27 cycles 94 °C for 45 s, 50 °C for 45 s, 72 °C for 75 s, and a final elongation step at 72 °C for 10 min. The Efs *fts*Z-gene fragment was directly sequenced in both directions. The Eds *fts*Z-gene fragment was cloned as described above for the rRNA genes and four clones containing the Eds *fts*Z-gene fragment were fully sequenced in both directions. All the sequences were aligned and compared with CodonCode Aligner 3.7.1 software. We obtained a 967 nt-long sequence for Efs (GenBank accession number KF453620) and a 1.007 nt-long sequence for Eds (KF453619).

16S rRNA gene-based phylogenetic analysis. A bacterial 16S rRNA gene dataset was constructed by adding sequences from GenBank with >95% identity to Efs and Eds using BLASTN[47] and selected *Chromatiaceae* as an outgroup. The sequences were aligned with MAFFT Q-INSi[48]. To reconstruct the phylogenetic relations of the symbionts we used the GTR + G + I model with maximum likelihood (RAxML[49]) and Bayesian inference (MrBayes[50]) based algorithms. To evaluate node stability we performed a rapid bootstrapping analysis (RAxML, 200 runs; ref. 51) and used posterior probabilities (MrBayes, two million generations, burnin of 25%).

Fluorescence *in situ* hybridization (FISH). By using the arb PROBE_DESIGN tool (the arb software package[52]; Table 2), we designed two FISH probes (Eds214 and Efs1057) specific to the SOBs identified in the *E. fertilis* and *E. dianeae* 16S rRNA gene libraries (GenBank accession numbers KF278590 and KF278587, respectively). In addition, we designed a probe (SRB64) targeting the *Deltaproteobacteria* identified in the *E. dianeae* 16S rRNA gene library (GenBank accession number KJ877189). We confirmed their specificity by comparing them with all available sequences in GenBank, the arb-silva 114 database[53] and RDP (Ribosomal Database Project) rel.10.32 (ref. 54). The Eds214 probe has 0/3/1357 non-target hits in RDP allowing for 0/1/2 mismatches, the Efs1057 0/12/3725 and the SRB64 probe 2/493/677. All probes were fluorescently labelled on their 5′ end (Thermo Fisher Scientific, Ulm, Germany). FISH was performed on *Eubostrichus* nematodes according to the study by Manz *et al.*[55] and as applied in the study by Bulgheresi *et al.*[25,26]. A detailed overview of all probes and formamide concentrations used in the different experiments is given in Table 2. To determine stringent hybridization conditions, a formamide series was conducted for all the probes (10, 15, 20, 25, 30, 35, 40 and 50%; refer to Table 2 for optimal incubation time, formamide percentage and probe concentrations). Nematodes were mounted in Vectashield (Vector Labs, Burlingame, CA, USA). When performing FISH with SRB64, bacteria were dissociated from *E. dianeae* cuticle prior to mounting. Dissociation was performed to ensure that all the bacteria attached to the cuticle would be equally prone to visual inspection, that is, to ensure that the signal emanating from putative normal-sized *Deltaproteobacteria* would not be masked by the numerically dominant, giant Eds cells. Symbiotic nematodes or dissociated symbionts were examined using a Leica TCS-SP2 confocal laser-scanning microscope combined with an inverted DM-IRE2 microscope (Leica Microsystems, Heidelberg, Germany). The EUB338 probe is from the study by Amann *et al.*[56], Gam42a and Beta42a from the study by Manz *et al.*[55] FISH probe names refer to their target on the *E. coli* 16S rRNA, numbering according to [57].

Bacterial cell size and fluorescence measurements. Cells were immobilized on 1% agarose and photographed using a Leica TCS-SP2 confocal laser-scanning microscope combined with an inverted DM-IRE2 microscope (Leica Microsystems) or a Nikon Eclipse 50i microscope equipped with either a DS-Fi1 camera (Nikon) or a MFCool camera (Jenoptik). Epifluorescence images were acquired using the NIS Elements F 3.22 software (Nikon) or the ProgRes Capture Pro 2.8.8 software (Jenoptik) and processed using the public domain programme ImageJ[58] in combination with the analysis tool Coli-Inspector[59]. Cell outlines were traced and cell length and width were measured automatically. Automatic tracing was manually double-checked and errors removed (for example, multiple cells counted as one). In the fluorescence profiles each bar represents a single bacterial cell, and the intensity of fluorescence is displayed as intensity of the respective colour (Ftsz in green and DNA in red in the overlay). The cells were sorted by increasing length from left to right. For the average fluorescence profiles, each cell was resampled to the same length and the intensities then averaged. For the fluorescence profiles, data were acquired from a single immunostaining. For the morphometric analysis and the length histograms, data from multiple experiments were pooled.

Western Blotting, immunostaining and DNA staining. For Western blots, Efs and Eds protein extracts—obtained from dissociated ectosymbionts—were separated by reduced SDS–polyacrylamide gel electrophoresis (PAGE) on NuPAGE 4–12% Bis-Tris pre-cast gels (Invitrogen). They were then transferred to Hybond ECL nitrocellulose membranes (Amersham Biosciences). Membranes were blocked for 45 min in phosphate-buffered saline (PBS) containing 5% (wt/vol) nonfat milk

Table 2 | Probes used for FISH.

Probe	Specificity	Sequence/5′ modification	Target RNA	Position*	Formamide percentage/ incubation time (h)/ probe concentration (ng µl^{-1})	Reference
EUB338	Most bacteria	5′-GCTGCCTCCCGTAGGAGT-3′ Fluorescein	16S	338–355	40%/12/3.8	Amann *et al.*[56]
GAM42a	*Gammaproteobacteria*	5′-GCCTTCCCACATCGTTT-3′ Cy5	23S	1,027–1,043	40%/12/2.4	Manz *et al.*[55]
BETA42a	*Betaproteobacteria*	5′-GCCTTCCCACTTCGTTT-3′ Cy3	23S	1,027–1,043	40%/12/2.4	Manz *et al.*[55]
Eds214	*E. dianeae* ectosymbiont	5′-GCTCATCATCATAGCGGAA-3′ Cy3	16S	214–235	40%/12/2.4	This study
Eds214mis	One mismatch to the *E. dianeae* ectosymbiont	5′-GGCTCATCATCTTAGCGGAAG-3′ Cy3	16S	214–235	40%/12/2.4	This study
SRB64	Sulphate-reducing *Deltaproteobacteria* identified in the 16S rRNA gene library	5′-TGCAAGCAACCCCTTTCTCGTT-3′ Fluorescein	16S	64–86	40%/12/3.8	This study
Efs1027	*E. fertilis* ectosymbiont	5′-TCACCGCGCTCCCAAGG-3′ Cy3	16S	1,027–1,044	30%12/2.4	This study
Efs1027mis	One mismatch to the *E. fertilis* ectosymbiont	5′-TCACCGCGCACCCAAGG-3′ Cy3	16S	1,027–1,044	30%12/2.4	This study

FISH, fluorescence *in situ* hybridization.
*16S rRNA position, *E. coli* numbering[57].

(PBS Milk (PBSM)) at room temperature and probed overnight at 4 °C with a commercially available rabbit polyclonal anti-*E. coli* FtsZ antibody (Agrisera, Sweden; 1:400) in PBSM (and without, as a negative control). Unbound primary antibody was removed by three washing steps in PBSM and blots were subsequently incubated for 1 h at room temperature with a horseradish peroxidase-conjugated anti-rabbit secondary antibody (1:5,000; Amersham Biosciences) in PBSM. Protein–antibody complexes were visualized using ECL Plus detection reagents and films (Amersham Biosciences).

Immunostaining was performed as described[31]. Briefly, fixed nematodes were rehydrated and washed in PBS containing 0.1% Tween 20 (PBT, washing solution). Bacterial peptidoglycan was permeabilized by incubation for 20 min with 0.1% (wt/vol) lysozyme at 37 °C. Blocking was carried out for 1 h in PBT containing 2% (wt/vol) bovine serum albumin (blocking solution) at room temperature. Efs and Eds were both immunostained with a 1:200 dilution of commercially available rabbit polyclonal anti-*E. coli* FtsZ antibody (Agrisera) in blocking solution overnight under gentle agitation at 4 °C or in blocking solution alone. Unbound primary antibody was subsequently removed by three washing steps in PBT and secondary Alexa555 conjugated anti-rabbit antibody (Molecular Probes, USA) applied at a 1:500 dilution in blocking solution for 1 h at room temperature. Unbound secondary antibody was removed by three washing steps in PBT and DNA was stained with YOYO-1 Iodide (Molecular Probes) dissolved in a Tris-EDTA buffer supplemented with 50 mM potassium citrate, 0.1% Triton-X100 and 0.1 g l^{-1} of RNAseA according to the study by Marie *et al.*[60] To dissociate Efs and Eds, worms were sonicated for 40 s in the tubes prior to mounting. Bacterial solution (1 µl) was mixed with 0.5 µl of mounting medium Vectashield (Vector Labs).

References

1. Goley, E. D. Tiny cells meet big questions: a closer look at bacterial cell biology. *Mol. Biol. Cell* **24,** 1099–1102 (2013).
2. Silver, L. Challenges of antibacterial discovery. *Clin. Microbiol. Rev.* **24,** 71–109 (2011).
3. Chien, A. C., Hill, N. S. & Levin, P. A. Cell size control in bacteria. *Curr. Biol.* **22,** R340–R349 (2012).
4. Marshall, W. F. *et al.* What determines cell size? *BMC Biol.* **10,** 101 (2012).
5. Errington, J., Daniel, R. A. & Scheffers, D. J. Cytokinesis in bacteria. *Microbiol. Mol. Biol. Rev.* **67,** 52–65 (2003).
6. Pierucci, O., Helmstetter, C. E., Rickert, M., Weinberger, M. & Leonard, A. C. Overexpression of the dnaA gene in *Escherichia coli* B/r: chromosome and minichromosome replication in the presence of rifampin. *J. Bacteriol.* **169,** 1871–1877 (1987).
7. Sargent, M. G. Control of cell length in *Bacillus subtilis*. *J. Bacteriol.* **123,** 7–19 (1975).
8. Weart, R. B. *et al.* A metabolic sensor governing cell size in bacteria. *Cell* **130,** 335–347 (2007).
9. Trueba, F. J. & Woldringh, C. L. Changes in cell diameter during the division cycle of *Escherichia coli*. *J. Bacteriol.* **142,** 869–878 (1980).
10. Zaritsky, A., Woldringh, C. L., Helmstetter, C. E. & Grover, N. B. Dimensional rearrangement of *Escherichia coli* B/r cells during a nutritional shift-down. *J. Gen. Microbiol.* **139,** 2711–2714 (1993).
11. Hill, N. S., Buske, P. J. & Levin, P. A. A moonlighting enzyme links *Escherichia coli* cell size with cenral metabolism. *PLoS Genet.* **9,** e1003663 (2013).
12. Grover, N. B. & Woldringh, C. L. Dimensional regulation of cell-cycle events in *Escherichia coli* during steady-state growth. *Microbiology* **147,** 171–181 (2001).
13. Angert, E. R. & Clements, K. D. Initiation of intracellular offspring in *Epulopiscium*. *Mol. Microbiol.* **51,** 827–835 (2004).
14. Schulz, H. N. & Jorgensen, B. B. Big bacteria. *Annu. Rev. Microbiol.* **55,** 105–137 (2001).
15. Ott, J. A., Leisch, N. & Gruber-Vodicka, H. R. *Eubostrichus fertilis* n. sp., a new marine nematode (Desmodoridae, Stilbonematinae) with an extraordinary reproductive potential from Belize, Central America. *Nematology* doi:10.1163/15685411-00002807 in the press.
16. Hopper, B. E. & Cefalu, R. C. Free-living marine nematodes from Biscayne-Bay, Florida. V. Stilbonematinae: contributions to the taxonomy and morphology of the genus *Eubostrichus* Greeff and related genera. *Trans. Am. Microsc. Soc.* **92,** 578–591 (1973).
17. Polz, M., Felbeck, H., Novak, R., Nebelsick, M. & Ott, J. Chemoautotrophic, sulphur-oxidizing symbiotic bacteria on marine nematodes: morphological and biochemical characterization. *Microb. Ecol.* **24,** 313–329 (1992).
18. Himmel, D., Maurin, L. C., Gros, O. & Mansot, J. L. Raman microspectrometry sulphur detection and characterization in the marine ectosymbiotic nematode *Eubostrichus dianae* (Desmodoridae, Stilbonematidae). *Biol. Cell.* **101,** 43–54 (2009).
19. Maurin, L. C., Himmel, D., Mansot, J. L. & Gros, O. Raman microspectrometry as a powerful tool for a quick screening of thiotrophy: an application on mangrove swamp meiofauna of Guadeloupe (F.W.I.). *Mar. Environ. Res.* **69,** 382–389 (2010).
20. Polz, M. F., Harbison, C. & Cavanaugh, C. M. Diversity and heterogeneity of epibiotic bacterial communities on the marine nematode *Eubostrichus dianae*. *Appl. Environ. Microbiol.* **65,** 4271–4275 (1999).
21. Berger, E. C., Urbancik, W. & Ott, J. A. *Eubostrichus topiarius* sp.n. a new free-living marine species of Stilbonematinae (Nematoda: Desmodoridae) from a shallow subtidal sand bottom. *Nematologica* **42,** 521–536 (1996).
22. Ott, J. A. A new symbiotic, marine nematode *Adelphos rolandi* gen.n. sp.n. (Stilbonematinae), from the Caribbean Sea. *Ann. Nat. Hist. Mus. Wien* **99,** 417–422 (1997).
23. Heindl, N. R. *et al.* First detection of thiotrophic symbiont phylotypes in the pelagic marine environment. *FEM Microbiol. Ecol.* **77,** 223–227 (2011).
24. Polz, M. F. *et al.* Phylogenetic analysis of a highly specific association between ectosymbiotic, sulphur-oxidizing bacteria and a marine nematode. *Appl. Environ. Microbiol.* **60,** 4461–4467 (1994).
25. Bayer, C. *et al.* Molecular characterization of the symbionts associated with marine nematodes of the genus *Robbea*. *Environ. Microbiol. Rep.* **1,** 136–144 (2009).
26. Bulgheresi, S. *et al.* Sequence variability of the pattern recognition receptor Mermaid mediates specificity of marine nematode symbioses. *ISME J.* **5,** 986–998 (2011).
27. Bi, E. F. & Lutkenhaus, J. FtsZ ring structure associated with division in *Escherichia coli*. *Nature* **354,** 161–164 (1991).
28. Addinall, S. G. & Holland, B. The tubulin ancestor, FtsZ, draughtsman, designer and driving force for bacterial cytokinesis. *J. Mol. Biol.* **318,** 219–236 (2002).
29. den Blaauwen, T., de Pedro, M. A., Nguyen-Disteche, M. & Ayala, J. A. Morphogenesis of rod-shaped sacculi. *FEMS Microbiol. Rev.* **32,** 321–344 (2008).
30. Adams, D. W. & Errington, J. Bacterial cell division: assembly, maintenance and disassembly of the Z ring. *Nat. Rev. Microbiol.* **7,** 642–653 (2009).
31. Leisch, N. *et al.* Growth in width and FtsZ ring longitudinal positioning in a gammaproteobacterial symbiont. *Curr. Biol.* **22,** R831–R832 (2012).
32. RayChaudhuri, D., Gordon, G. S. & Wright, A. How does a bacterium find its middle? *Nat. Struct. Biol.* **7,** 997–999 (2000).
33. De Boer, P., Crossley, R. E. & Rothfield, L. I. Roles of MinC and MinD in the site-specific septation block mediated by the MinCDE system of *Escherichia coli*. *J. Bacteriol.* **174,** 63–70 (1992).
34. Mergaert, P. *et al.* Eukaryotic control on bacterial cell cycle and differentiation in the Rhizobium-legume symbiosis. *Proc. Natl Acad. Sci. USA* **103,** 5230–5235 (2006).
35. Nardon, P. & Wicker, C. La symbiose chez le genre Sitophilus (Coleoptere *Curculionide*): principaux aspects morphologiques, physiologiques et genetiques [bacterie symbiotique]. *Annee Biol.* **20,** 327–373 (1981).
36. Wu, D. *et al.* Metabolic complementarity and genomics of the dual bacterial symbiosis of sharpshooters. *PLoS Biol.* **4,** e188 (2006).
37. Mendell, J. E., Clements, K. D., Choat, J. H. & Angert, E. R. Extreme polyploidy in a large bacterium. *Proc. Natl Acad. Sci. USA* **105,** 6730–6734 (2008).
38. Van de Velde, W. *et al.* Plant peptides govern terminal differentiation of bacteria in symbiosis. *Science* **327,** 1122–1126 (2010).
39. Login, F. H. *et al.* Antimicrobial peptides keep insect endosymbionts under control. *Science* **334,** 362–365 (2011).
40. Miller, D. A., Suen, G., Clements, K. D. & Angert, E. R. The genomic basis for the evolution of a novel form of cellular reproduction in the bacterium *Epulopiscium*. *BMC Genomics* **13,** 265 (2012).
41. Angert, E. R. DNA replication and genomic architecture of very large bacteria. *Annu. Rev. Microbiol.* **66,** 197–212 (2012).
42. Wang, X., Montero Llopis, P. & Rudner, D. Organization and segregation of bacterial chromosomes. *Nat. Rev. Genet.* **14,** 191–203 (2013).
43. Kampfer, S., Sturmbauer, C. & Ott, J. A. Phylogenetic analysis of rDNA sequences from adenophorean nematodes and implications for the adenophorea-secernentea controversy. *Invertebr. Biol.* **117,** 29–36 (1998).
44. Schizas, N. V., Street, G. T., Coull, B. C., Chandler, G. T. & Quattro, J. M. An efficient DNA extraction method for small metazoans. *Mol. Mar. Biol. Biotechnol.* **6,** 381–383 (1997).
45. Juretschko, S. *et al.* Combined molecular and conventional analyses of nitrifying bacterium diversity in activated sludge: *Nitrosococcus mobilis* and *Nitrospira*-like bacteria as dominant populations. *Appl. Environ. Microbiol.* **64,** 3042–3051 (1998).
46. Kane, M. D., Poulsen, L. K. & Stahl, D. A. Monitoring the enrichment and isolation of sulfate-reducing bacteria by using oligonucleotide hybridization probes designed from environmentally derived 16S rRNA sequences. *Appl. Environ. Microbiol.* **59,** 682–686 (1993).
47. Altschul, S. F., Gish, W., Miller, W., Myers, E. W. & Lipman, D. J. Basic local alignment search tool. *J. Mol. Biol.* **215,** 403–410 (1990).
48. Katoh, K., Kuma, K.-I., Toh, H. & Miyata, T. MAFFT version 5: improvement in accuracy of multiple sequence alignment. *Nucleic Acids Res.* **33,** 511–518 (2005).
49. Stamatakis, A. RAxML-VI-HPC: maximum likelihood-based phylogenetic analyses with thousands of taxa and mixed models. *Bioinformatics* **22,** 2688–2690 (2006).
50. Ronquist, F. & Huelsenbeck, J. MrBayes 3: Bayesian phylogenetic inference under mixed models. *Bioinformatics* **19,** 1572–1574 (2003).

51. Stamatakis, A., Hoover, P. & Rougemont, J. A rapid bootstrap algorithm for the RAxML Web servers. *Syst. Biol.* **57,** 758–771 (2008).
52. Ludwig, W. *et al.* ARB: a software environment for sequence data. *Nucleic Acids Res.* **32,** 1363–1371 (2004).
53. Pruesse, E. *et al.* SILVA: a comprehensive online resource for quality checked and aligned ribosomal RNA sequence data compatible with ARB. *Nucleic Acids Res.* **35,** 7188–7196 (2007).
54. Cole, J. *et al.* The Ribosomal Database Project: improved alignments and new tools for rRNA analysis. *Nucleic Acids Res.* **37,** D141 D145 (2009).
55. Manz, W., Amann, R., Ludwig, W., Wagner, M. & Schleifer, K.-H. Phylogenetic oligodeoxynucleotide probes for the major subclasses of proteobacteria: problems and solutions. *Syst. Appl. Microbiol.* **15,** 593–600 (1992).
56. Amann, R. I., Krumholz, L. & Stahl, D. A. Fluorescent-oligonucleotide probing of whole cells for determinative, phylogenetic, and environmental studies in microbiology. *J. Bacteriol.* **172,** 762–770 (1990).
57. Brosius, J., Palmer, M. L., Kennedy, P. J. & Noller, H. F. Complete nucleotide sequence of a 16S ribosomal RNA gene from *Escherichia coli*. *Proc. Natl Acad. Sci. USA* **75,** 4801–4805 (1978).
58. Schneider, C. A., Rasband, W. S. & Eliceiri, K. W. NIH Image to ImageJ: 25 years of image analysis. *Nat. Methods* **9,** 671–675 (2012).
59. van der Ploeg, R. *et al.* Colocalization and interaction between elongasome and divisome during a preparative cell division phase in *Escherichia coli*. *Mol. Microbiol.* **87,** 1074–1087 (2013).
60. Marie, D., Vaulot, D. & Partensky, F. Application of the novel nucleic acid dyes YOYO-1, YO-PRO-1, and PicoGreen for flow cytometric analysis of marine prokaryotes. *Appl. Environ. Microbiol.* **62,** 1649–1655 (1996).

Acknowledgements

This work was supported by the Austrian Science Fund (FWF) project P22470-B17 (N.L., N.P., N.R.H. and S.B.), an uni:docs fellowship from the University of Vienna (N.P.), Marie-Curie Intra-European Fellowship PIEF-GA-2011-301027 CARISYM (H.R.G.-V.) as well as by the National Science Foundation Nemasym Research Network grant to S. Patricia Stock (NSF-IOS 0840932). We are very grateful to the Core Facility Cell Imaging and Ultrastructure Research of the University of Vienna for technical support. We thank the Schleper Group of the Department of Ecogenomics and Systems Biology and the Laboratory of Genome Dynamics, the Medical University of Vienna (particularly Wolfgang Miller) for inspiring discussions. This work is contribution 966 from the Carrie Bow Cay Laboratory, Caribbean Coral Reef Ecosystem Programme, the National Museum of Natural History, Washington, DC.

Author contributions

The study was designed by S.B. Samples were collected by N.P, N.L., N.R.H., J.O. and S.B. DNA extraction and PCR were performed by N.P., N.L. and N.R.H. Phylogenetic analysis was performed by H.R.G.-V. Immunostaining was performed by N.P. and N.L. Image analysis was performed by N.L., T.dB. and N.P. FISH and Western blots were performed by N.P. Statistical analysis was done by N.L. Confocal microscopy was performed by S.B. The manuscript was written by S.B. and corrected by N.L, N.P, H.R.G-V., J.O. and T.dB.

Additional information

Supplementary Information accompanies this paper at http://www.nature.com/naturecommunications

Competing financial interests: The authors declare no competing financial interests.

Reprints and permission information is available online at http://npg.nature.com/reprintsandpermissions/

How to cite this article: Pende, N. *et al.* Size-independent symmetric division in extraordinarily long cells. *Nat. Commun.* 5:4803 doi: 10.1038/ncomms5803 (2014).

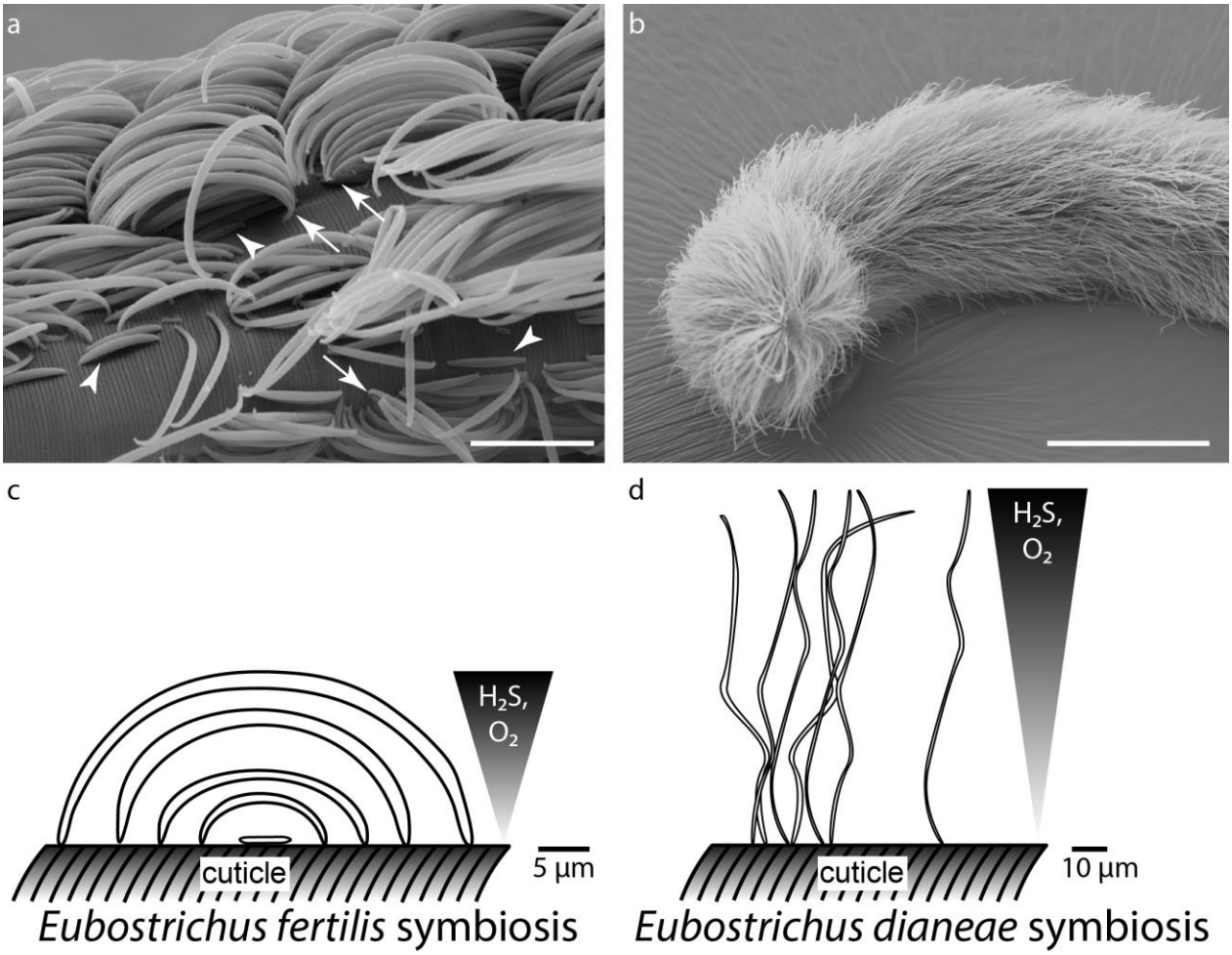

Supplementary Fig.1 The bacterial coats of *E. fertilis* and *E. dianeae*. (a) Scanning electron micrograph of the *E. fertilis* symbiosis. The bacterial coat was mechanically disturbed to show the proximal to apical arrangement of short (arrowheads) versus long crescent-shaped cells (arrows). (b) Scanning electron micrograph of the *E. dianeae* symbiosis (anterior end of the nematode). Bacterial filaments are attached with one pole to the nematode. (c-d) Sketches *of E. fertilis* and *E. dianeae* bacterial coat architectures (left and right, respectively) with proposed gradient of H_2S availability in the space between the sand and the host cuticle. Scale bar is 5 µm in (a) and 100 µm in (b).

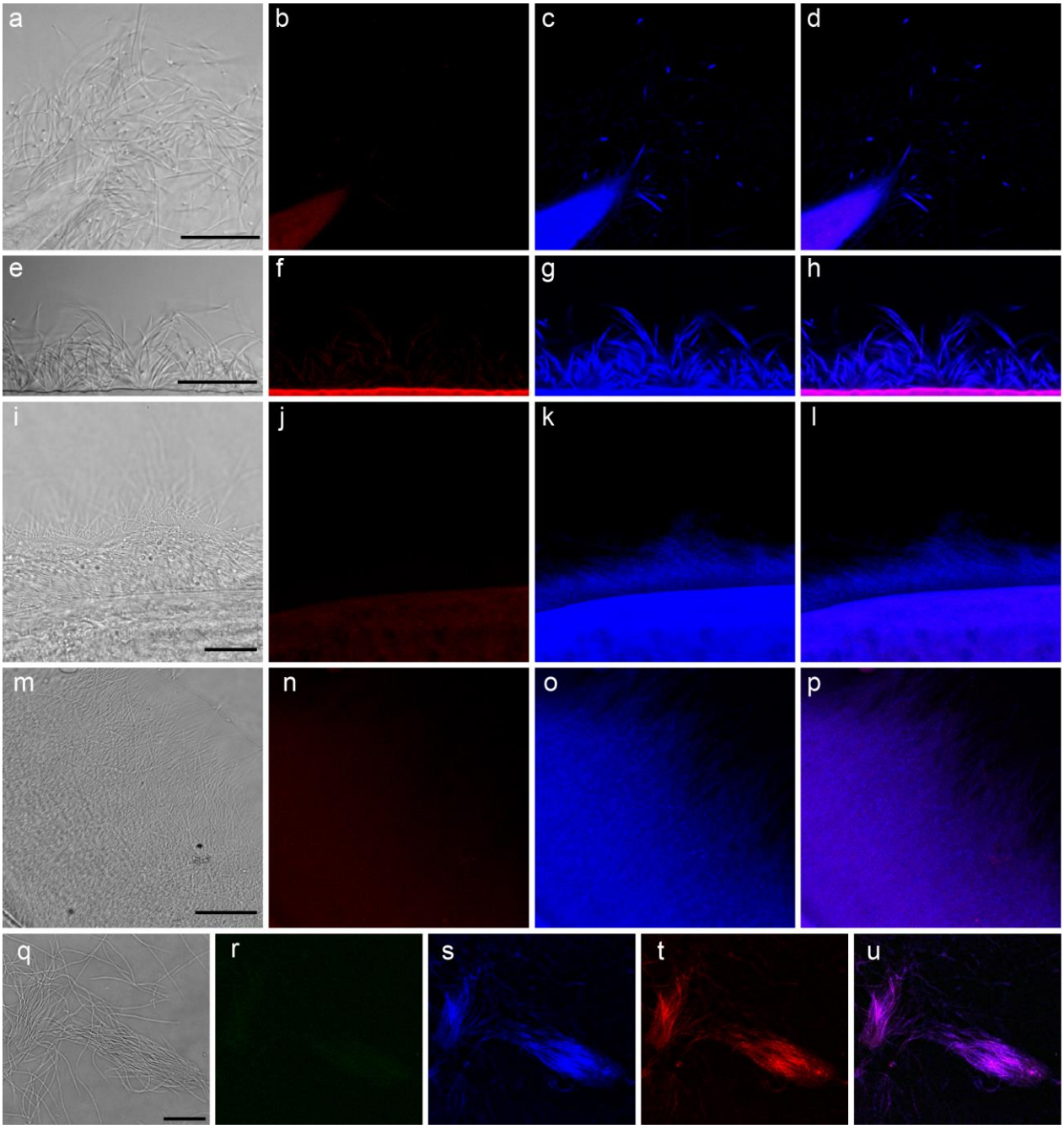

Supplementary Fig.2 FISH LSCM of *E. fertilis* (a-h) and *E. dianeae* (i-u) ectosymbionts attached to the worm surface. Bright field images (a, e, i, m) of ectosymbionts stained with a *Gammaproteobacteria*-specific probe (c, g, k, o), but neither with a *Betaproteobacteria*-specific probe (b and j) or very weakly with probes carrying a single nucleotide mismatch with the respective specific ones ((f and n), Efs1027mis and Eds214mis, respectively, see Table 1). d, h, l, and p are overlay pictures of (b-c), (f-g), (j-k) and (n-o), respectively. (q-u) shows bacteria detached from the *E. dianeae* surface that are stained with an Eds-specific probe (Eds214; (t)) and a *Gammaproteobacteria*-specific probe (s), but not with a probe targeting sulphate-reducing Deltaproteobacteria (SRB64; (r)). (q) is the corresponding bright field image and (u) the overlay of the images shown in (q-t). Scale bar is 25 µm in all images.

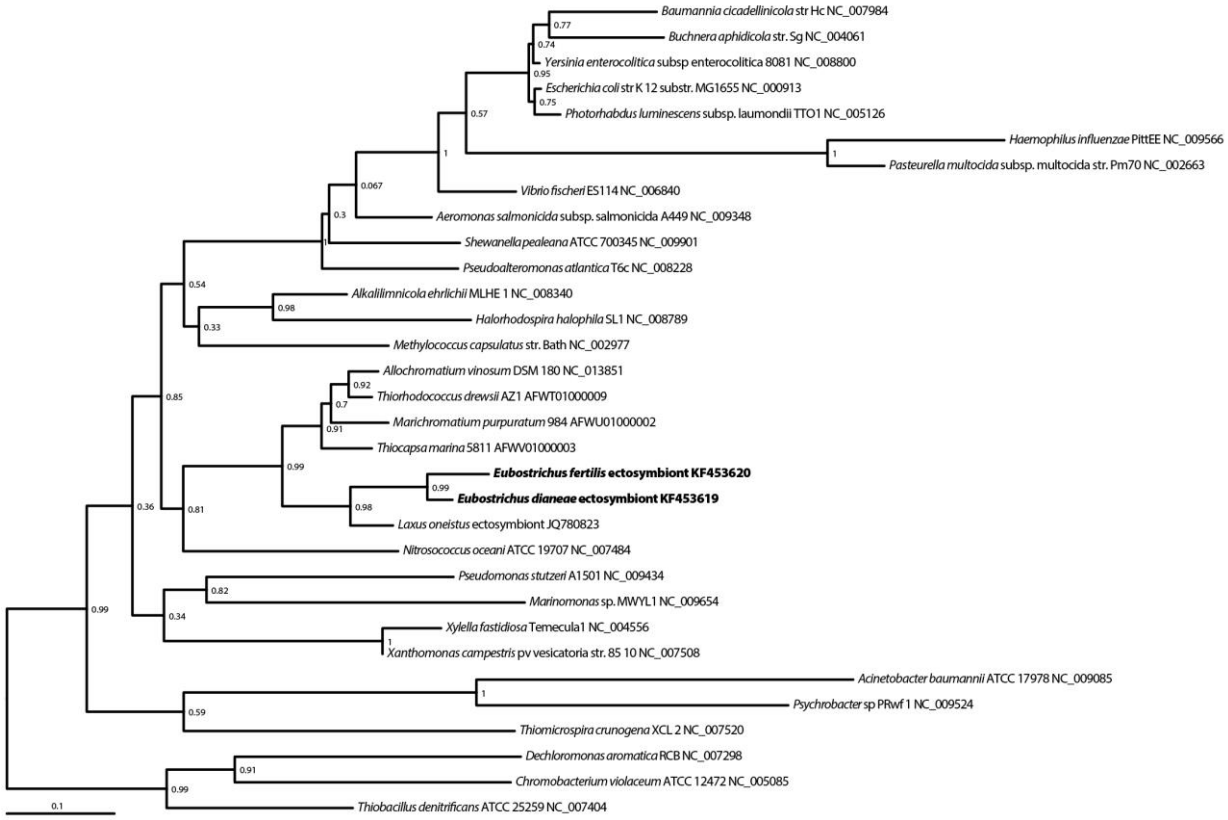

Supplementary Fig.3 Gammaproteobacterial FtsZ tree-based on the most likely PHYML tree (WAG model of substitution) using an amino acid alignment of 473 positions. aRLT node support is given for all nodes. Scale bar represents the mean number of amino acid substitutions per site. GenBank accession numbers are indicated after the names of the organisms.

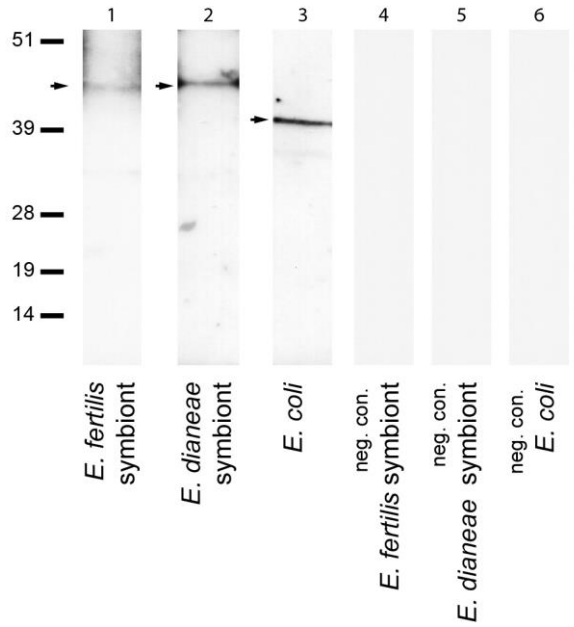

Supplementary Fig.4 Western blots of symbiont protein extracts. Efs (lanes 1 and 4), and Eds (lanes 2 and 5) and *E. coli* (lane 3 and 6) protein extracts either probed with a commercially available rabbit polyclonal anti-*E.coli* FtsZ antibody (Agrisera, Sweden; lanes 1-3) or with the secondary antibody only (lanes 4-6). Numbers indicate apparent MW expressed in kDa. Arrows indicate protein bands detected by the rabbit polyclonal anti-*E.coli* FtsZ antibody (Agrisera, Sweden).

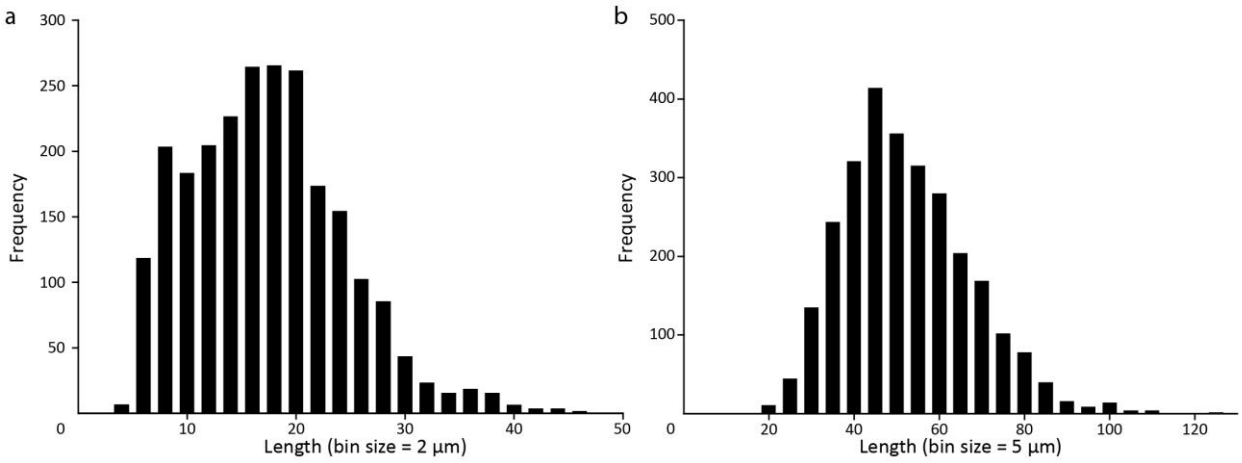

Supplementary Fig.5 Length size distributions of Efs and Eds cells. (a) Histogram showing the length size distribution of 2,371 Efs cells (bin size of 2 μm) and (b) histogram showing the length size distribution of 2,743 Eds cells (bin size of 5 μm).

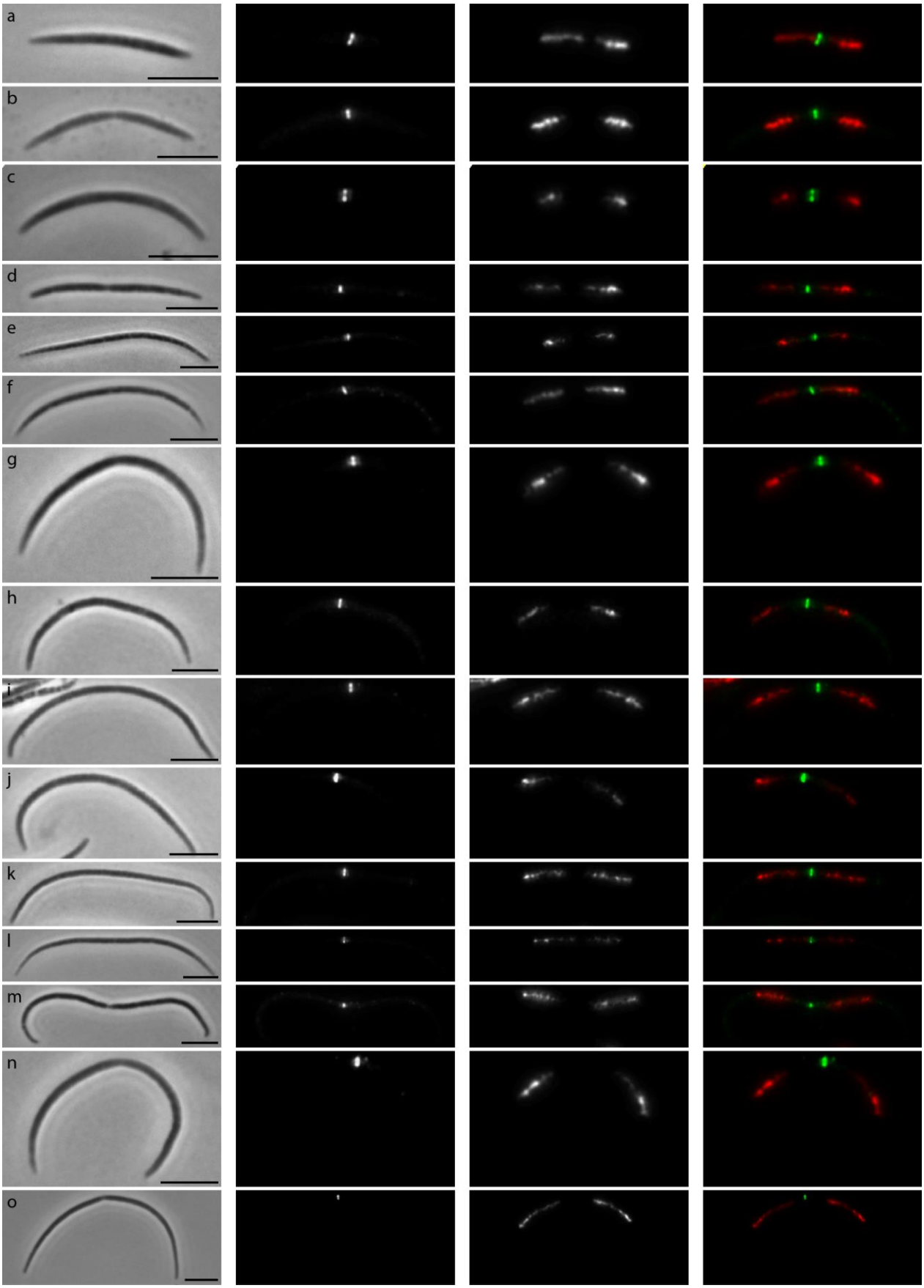

Supplementary Fig.6 FtsZ and DNA localization patterns of dividing Efs cells are shown in a-o. From left to right, phase contrast, FtsZ and DNA localization and an overlay of FtsZ (green) and DNA (red) localization. Cells are sorted by increasing length from top to bottom. Scale bar is 5 μm in each image.

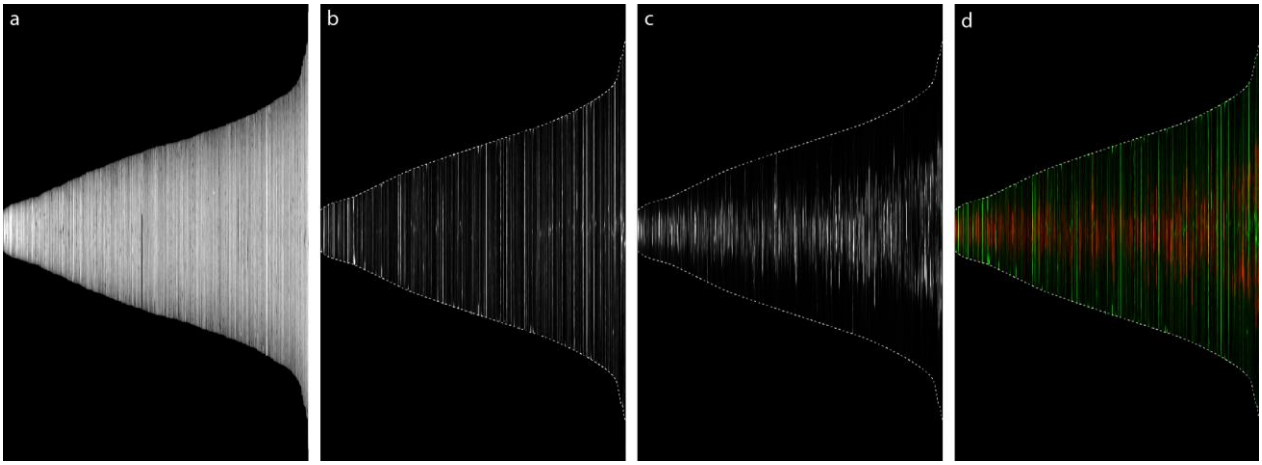

Supplementary Fig.7 FtsZ and DNA localization pattern in Efs cells. Cell length, FtsZ fluorescence, DNA fluorescence and overlay of FtsZ (green) and DNA (red) fluorescence, of 662 Efs cells are shown in (a – d) respectively. Cells are sorted by increasing cell length from left to right i.e. the leftmost bar represents the shortest and the rightmost bar the longest cell. Cell length ranges from 4.23 to 45.25 μm (mean 17.19 +/- 7.52). Dotted white line in (b-d) indicates the cell outline.

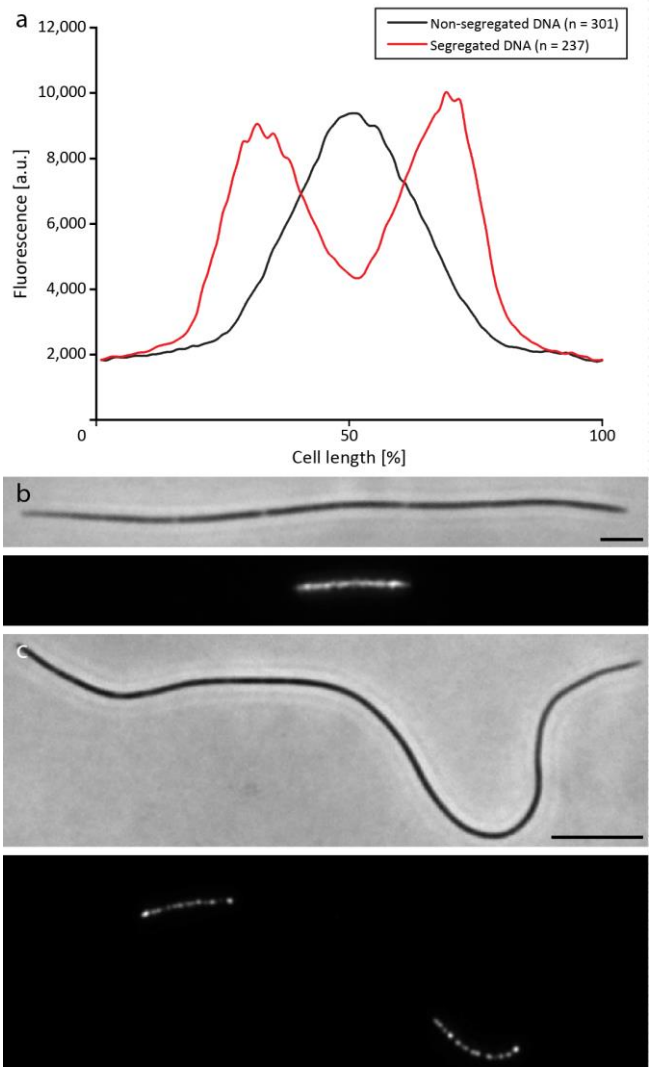

Supplementary Fig.8 DNA distribution along the Eds cell length. (a) shows an average fluorescence profile of 538 Eds cells. Black shows DNA localization in cells with non-segregated DNA (n=301) and red shows DNA localization in cells with segregated DNA (n=237) plotted along the length of the cell in percentage. (b) and (c) shows representative phase contrast and fluorescence images, from top to bottom, of cells bearing non-segregated and segregated DNA, respectively. Scale bar is 5 μm in (b) and 10 μm in (c).

Supplementary Table 1: Size distribution of cells having an FtsZ-ring.

Length size classes of Efs cells [µm]	**Total**	**0-15**	**15-30**	**30-45**	
# of Efs cells with a Z-ring	77	16	48	13	
% of cells with a Z-ring / size class		20.8	62.3	16.9	
Length size classes of Eds cells [µm]		**0-35**	**35-70**	**70-105**	**105-140**
# of Eds cells with a Z-ring	87	0	75	11	1
% of cells with a Z-ring / size class		0	86.2	12.6	1.1

Chapter 8

Conclusive Discussion

The results outlined in this thesis represent the first steps in understanding the life cycle of symbiotic bacteria that colonize the surface of a free-living marine nematode. By understanding growth and division mode of the four different strains we aimed to identify conserved paradigms of the gammaproteobacterial cell division machinery. These will eventually contribute to a better understanding of the fundamental process of the bacterial cell cycle and its evolution. This thesis provides the first answers to these questions and gives additional insight into these unique animal/bacteria partnerships. Chapter 2 describes a method used in all the subsequent chapters to preserve and visualize this symbiosis, especially the bacterial partners, using electron microscopy. Chapters 3 and 4 consist of zoological descriptions of four stilbonematid hosts, with two of them being central for the subsequent chapters. They include detailed morphological characterization and molecular analysis of their phylogeny. Chapters 5 - 7 form the core of this thesis, as they characterize the reproduction modes of four closely related basal *Gammaproteobacteria* (Figure 4). I aimed to determine the default direction of growth and mode of division, and to elucidate the molecular mechanisms underlying the latter. Each individual chapter contains a discussion of the methods used and the findings obtained in their individual context. Accordingly, this conclusive discussion does not repeat the individual discussions, but considers selected pertinent topics, open questions, and an outlook on future research.

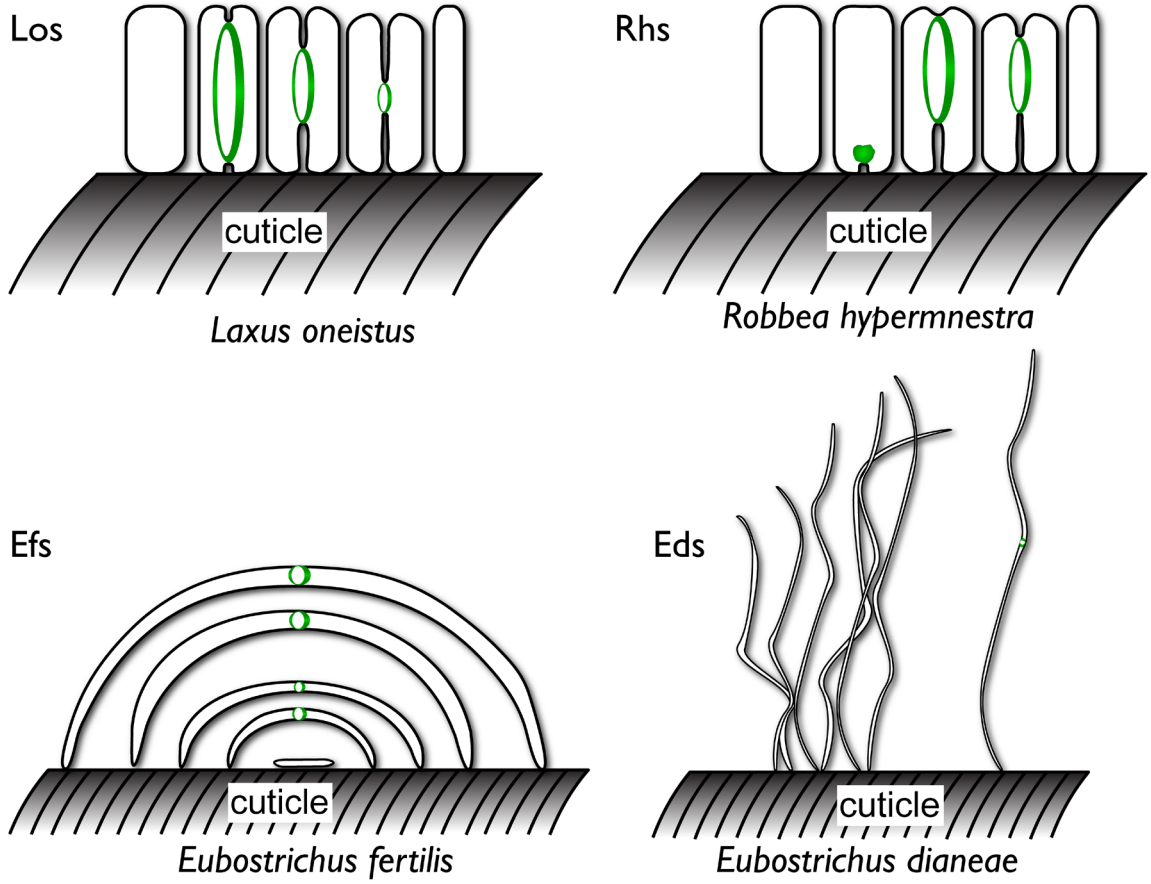

Figure 4: Overview of the four characterized symbionts, their arrangement on the host and their division mode. (A) Los in progressing stage of division from left to right, (B) Rhs in progressing stage of division from left to right, (C) Efs as it is arranged on the nematode cuticle with the longest cells furthermost on the outside and the shortest closest to the cuticle and (D) Eds of increasing length from left to right, with a dividing cell rightmost. FtsZ is indicated in green.

8.1. Growth and division of symbiotic rod-shaped bacteria

"*To be brutally honest, few people care that bacteria have different shapes. Which is a shame, because the bacteria seem to care very much.*" (Young 2006) This slightly tongue-in-cheek statement is not only the beginning of an excellent and thorough review on bacterial shape (Young 2006), but also points towards some of the core questions that are tackled in the field of bacterial cell biology: Why does a certain bacterium have a certain shape? What are the benefits of a certain shape and what are the mechanisms that confer this shape?

Microorganisms have a wide variety of cell morphologies; however, similar forms have arisen in different lineages, indicating that shape and its adaptation are undergoing

evolutionary selection. As bacteria solely depend on diffusion for the uptake of nutrients, respiration and any form of communication with their environment, the surface area-to-volume ratio is an important factor (reviewed in Young 2007). By adopting a rod-shaped morphology, the surface-to-volume ratio stays almost constant as the cell elongates; when compared with a sphere of the same volume, the rod-shaped cells surface area is about 20% bigger. Based on the work on *E. coli* and *B. subtilis*, it is also thought that the process of cell division may benefit from the rod-shaped morphology. The length axis defines a transverse axis for the polarity of the Min-protein gradient and, therefore, for the FtsZ localization and septation (reviewed in Young 2006, Chang and Huang 2014).

The work with the rod-shaped symbionts Los and Rhs presented in this thesis (Leisch et al. 2012) challenges the classical view of how we see rod-shaped bacteria. On the first glance longitudinal division is simply achieved by rotation of the Z-ring by 90°, but when considering the underlying mechanisms, many questions arise.

8.1.1. How is growth in width achieved?

The growth of bacteria like *E. coli* requires elongation of the sacculus. This bag-like macromolecule is located in the periplasmic space between cytosolic and outer membrane. It is the stress-bearing component that maintains cell shape and counteracts the intracellular turgor pressure and external osmotic changes. It is composed of sugar strands (glycans) that are cross-linked with peptides, hence the name peptidoglycan (PG). Growth of the sacculus takes place by cleavage of the cross-link followed by insertion of new peptidoglycan strands (reviewed in Typas et al. 2012). A recent high-resolution atomic force microscopy (AFM) study showed that the sacculus of *E. coli* is - contrary to what has been assumed before - highly disordered and consists of differentiated bands running circumferentially. By insertion of new strands into these bands, the cell will elongate (Turner et al. 2013). How is this achieved in cells that are growing in width instead of length, like Los and Rhs? Are these differentiated bands aligned parallel to the length axis instead of perpendicularly to direct growth into the width axis? A high-resolution

approach using AFM and electron cryotomography is necessary to clarify the fundamental architecture of the sacculus. This, combined with high-pressure liquid chromatography to determine the chemical composition of the sacculus, should help us to understand the growth mode of these cells.

The widely conserved actin homologue MreB plays a central role in cell elongation. It interacts with membrane-embedded proteins which interact with proteins on the external side of the membrane (e.g. PBPs); these are involved in synthesizing and modifying peptidoglycan (reviewed in Shih and Rothfield 2006). Inhibition of MreB (e.g. by incubation with the antibiotic A22) leads to the loss of the rod-shaped morphology and the transition to a spherical cell (Bean et al. 2009). MreB polymers rotate circumferentially along the cell wall, depending on cell wall synthesis (Teeffelen et al. 2011), and localize to areas of negative curvature where PG synthesis is mediated; as a result the cell is straightened. This, coupled with the re-direction of growth away from the cell pole, leads to the maintenance of the rod-shape (Ursell et al. 2014). Given the tight link between peptidoglycan and MreB, it is necessary to elucidate the orientation and movement of MreB to understand how bacteria that mainly grow in width accomplish growth and cell shape maintenance. Immunolabelling of Los MreB and analysis of cells treated with the MreB polymerization inhibitor A22 are planned for the near future. This will be complemented by pulse and pulse-chase experiments using fluorescently labelled PG precursors and vital membrane stains (see e.g. Pogliano et al. 1999, Kuru et al. 2012, Siegrist et al. 2013, Ursell et al. 2014) to visualize areas of PG incorporation (growth) and provide information about the generation time.

8.1.2. What are the prerequisites of longitudinal division?

The results of the studies on the rod-shaped symbionts (Leisch et al. 2012, Leisch et al. in preparation) clearly show that there is a viable second plane of division (parallel to the longitudinal axis instead of perpendicular) which allows for growth, DNA segregation and eventually leads to equally sized daughter cells.

In *E. coli*, the MinCDE system plays an important role in placing the Z-ring. Min D and E drive the oscillation from pole to pole and MinC is the active FtsZ inhibitor. Integrated over time, the inhibitory effect of MinC is highest at the poles, allowing the Z-ring formation at mid-cell (reviewed in de Boer 2010). To support Z-ring placement in the middle of the width axis, this system would need to oscillate from side-to-side instead. Intriguingly, a recent study by Zieske and Schwille (2014) showed, using a cell-free approach, that an increase in width can lead to a change of Min oscillation from parallel to the length axis to perpendicular to the length axis. Preliminary Los MinD immunostaining showed patches of MinD fluorescence at both poles prior to the formation of the Z-ring (Figure 5A). In cells showing non constricted (Figure 5B) and constricted (Figure 5C and D) Z-rings, multiple patches of MinD fluorescence were randomly distributed throughout the whole cell. We never observed the expected, one cell half-only pattern. Therefore, these experiments need to be expanded (by e.g. higher resolution imaging using structured illumination

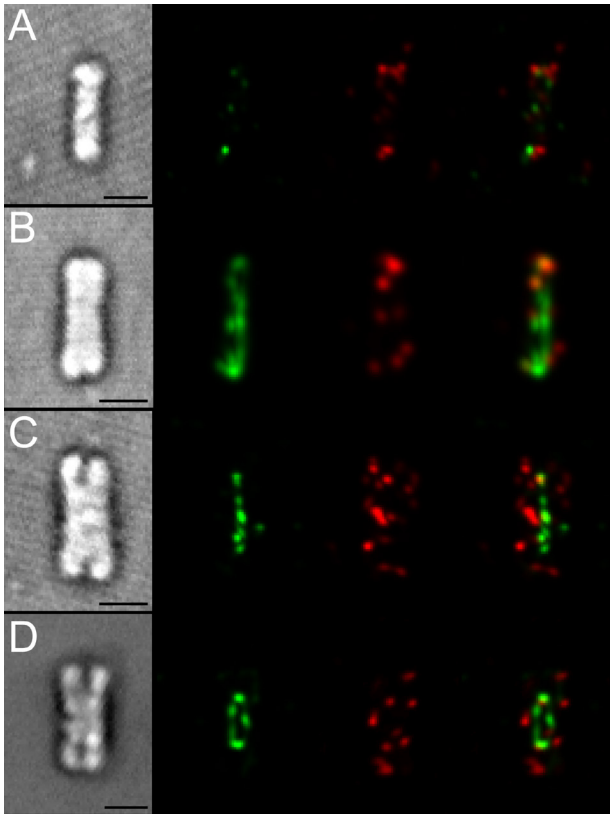

Figure 5: Localization pattern of FtsZ and MinD in Los cells in progressing stages of division from top to bottom. Leftmost row shows transmitted light, second to fourth row are average intensity projections of FtsZ fluorescence (green), MinD fluorescence (red) and an overlay of both. Scale bar is 1µm.

microscopy, as well as co-localization analysis of FtsZ with MinC, the actual FtsZ inhibitor) to obtain a better understanding of the Z-ring placement.

The second negative regulator system that assists Z-ring localization is the NO system. The nucleoid is the region of the cell in which the chromosome is being constrained by chromosome folding (e.g. via supercoiling or nucleoid-associated proteins). In *E. coli* SlmA binds to the nucleoid through DNA-binding domains and affects FtsZ polymerization (Wu and Errington 2012). This means in turn that the localization pattern of the nucleoid can influence the Z-ring placement, and a more longitudinal orientation and localization of the nucleoid might facilitate the longitudinal division (see Figure 6).

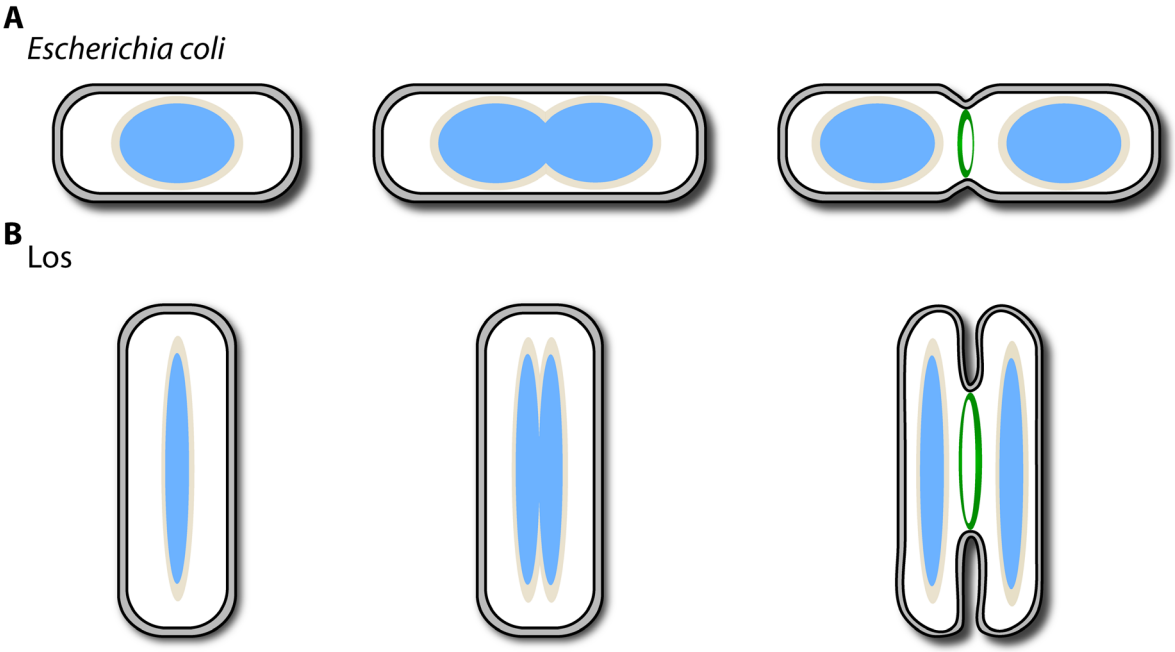

Figure 6: Schematic nucleoid localization in *E. coli* and hypothetical nucleoid localization in Los. (A) shows drawings of *E. coli* cells in progressing stages of division from left to right, the location of the nucleoid (blue) and the area of nucleoid occlusion (cream). (B) shows drawings of Los cells in progressing stages of division from left to right, the proposed location of the nucleoid (blue) and the area of nucleoid occlusion (cream).

To put this division mode into perspective, it is necessary to study the chromosome localization in Los and Rhs to see to which extent it is involved in Z-ring placement. Unfortunately, attempts to visualize the DNA in these cells by using nucleic acid stains have

been met with little success. Further trials, using anti double-stranded DNA antibodies for immunofluorescence analysis and serial sectioning of high-pressure frozen symbionts for transmission electron microscopic analysis, are already ongoing.

Like in most prokaryotes, the division of all our symbionts is mediated by the protein FtsZ. Already shortly after the description of the Z-ring by Bi and Lutkenhaus (1991) it was postulated that FtsZ could act as a force generator. This is based on the observation that no motor molecules can be found in bacteria and that FtsZ protofilaments can undergo a change from a straight to a curved conformation, which could generate force (reviewed in Erickson et al. 2010). In an *in vitro* approach it was shown that lipid vesicles can be deformed by FtsZ (Osawa et al. 2008) and even septated (Osawa and Erickson 2013). Based on the data available for this protein (e.g. detailed crystal structure characterization), theoretical models have been postulated which indicate that FtsZ could indeed generate the force needed to drive septation (reviewed in Ying et al. 2013, Meier and Goley 2014). In Los, a Z-ellipse assembles which constricts and eventually becomes a Z-ring (see (Leisch et al. 2012) Figure 1C-H). Unlike *E. coli*, where the ring constricts radially (i.e. the diameter of

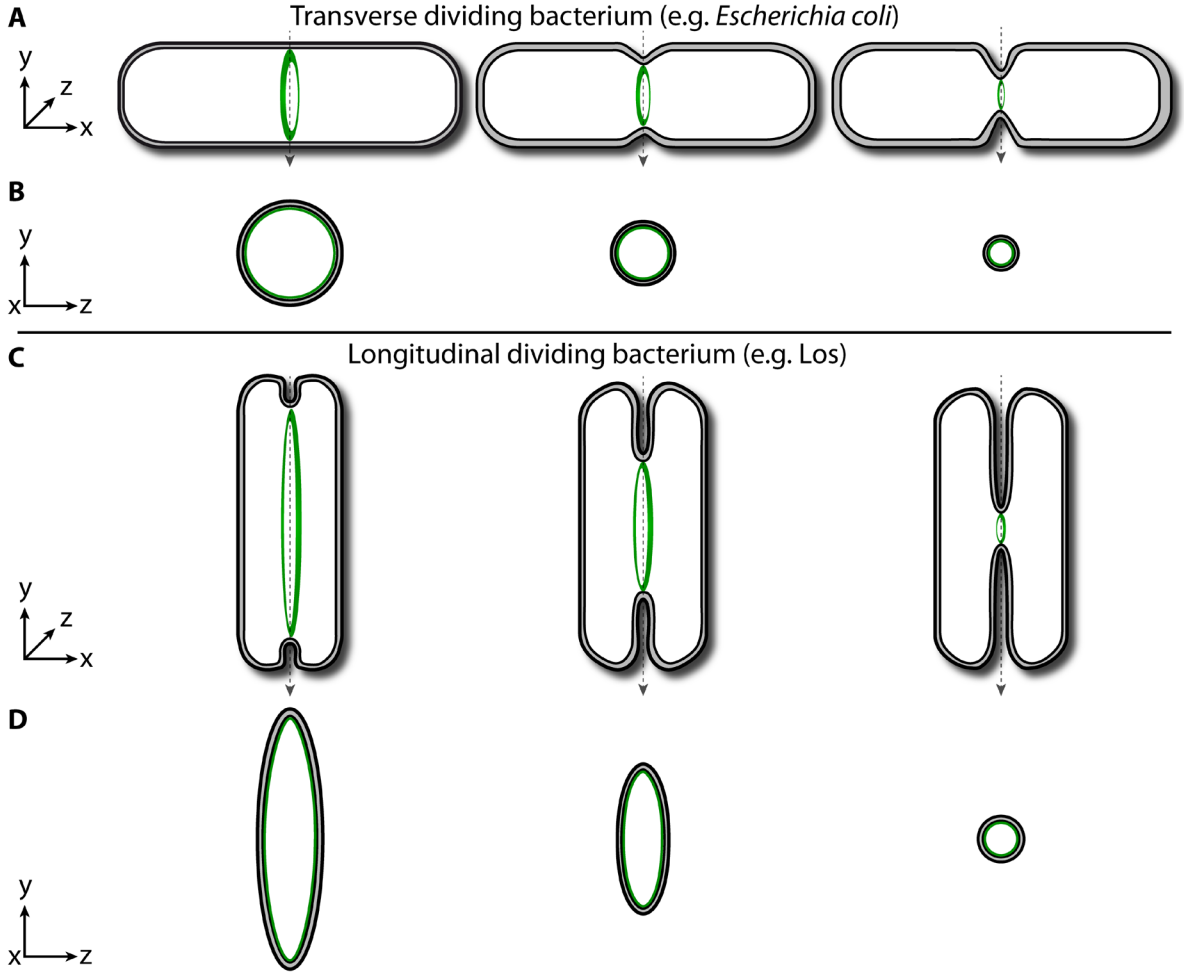

Figure 7: Schematic representation of the Z-ring in transverse and longitudinal dividing bacteria. (A) shows rod-shaped cells in progressing stages of transverse division from left to right, (B) is the corresponding view rotated by 90° (the section plane is indicated by the grey arrow). (C) shows rod-shaped cells in progressing stages of longitudinal division from left to right. (D) is the corresponding view rotated by 90° (the section plane is indicated by the grey arrow). FtsZ is indicated in green.

the ring structure is reduced evenly), the Z-ellipse of Los constricts only in one dimension until a ring structure has been achieved and constriction continues radially (see Figure 7).

A switch from ellipse to ring necessitates a reduction of the longer axis of the ellipse, the transverse axis. Such a phenomenon has not been reported so far, and how this is achieved and if this is due to localized constriction along the y-axis of the ellipse or if it is a consequence of the cell geometry, still needs to be understood.

Analysis of the genome drafts of longitudinally dividing and filamentous MONTS (genome drafts are available at http://rast.nmpdr.org/rast.cgi upon request) shows that key proteins,

which mediate growth and division in model organisms, are present (e.g. FtsABIKLQWZ, MinCDE, MreBCD, ParAB, RodA, ZapA, ZipA). We compared phylogenetic trees based on protein sequence (e.g. FtsZ, MinCDE see e.g. (Leisch et al. 2012) Supplementary Figure 2) with trees based on the 16S rRNA gene which were highly similar. This indicates that the FtsZ and MinCDE proteins of the symbionts are not highly diverging but conserved, as reported for most prokaryotes (reviewed in Margolin 2005, Lutkenhaus 2007). Furthermore, Western blot experiments indicated that important key components of the growth and Z-ring positioning machinery like MreB and MinD are expressed (unpublished data). Taken all this together, it appears that the different division modes described are not due to highly divergent, dedicated cell division proteins. Instead it appears that *ad hoc* control of the rather conserved gammaproteobacterial cell division machinery may result in a specific, probably host-tailored division mode, a hypothesis which still needs to be experimentally verified. Heterologous expression of symbiont cell division proteins, such as MinCDE and FtsZ for further purification and characterization studies (e.g. crystal structure analysis and FtsZ polymerization assays), as well as complementation studies in *E. coli* are underway.

We cannot exclude the possibility of additional factors that could act as positive or negative regulators of the Z-ring (like the ones found in e.g. *Myxococcus xanthus* (Treuner-Lange et al. 2013) or *Streptomyces coelicolor* (Willemse et al. 2011)). However, given the close phylogenetic relationship of all four symbionts, their identical ecological niche and the occurrence in the same habitat, it is rather unlikely that a single factor (or a factor for each symbiont) conveys these species-specific modifications. On the other hand, it has been shown that eukaryotic hosts of many symbiotic associations are capable of influencing the symbionts' cell cycle drastically (e.g. Van de Velde et al. 2010, Login et al. 2011).

8.2. Symbiotic lifestyle and its impact on the symbiont cell cycle

Research in the last few decades has shown how important symbiotic associations are

in every ecological niche (McFall-Ngai 2008, McFall-Ngai et al. 2013). One important aspect of these relationships is the control of the host when it comes to the localization and proliferation of the symbiont/s, to avoid e.g. being overgrown, accumulation of toxic metabolites from the symbiont, and so forth.

In the squid-*Vibrio* symbiosis the host expels ~90% of the symbionts colonizing its light organ every day at dawn (Lee and Ruby 1994). This reduction of symbionts interrupts their quorum-sensing induced bioluminescence and seeds the environment with symbionts that can be acquired by the host's offspring (reviewed in McFall-Ngai 2014).

In the legume-rhizobia symbiosis, nodule-specific cysteine-rich peptides target the symbionts and lead to drastic morphological changes like elongation, together with genome re-duplication, weakening of the cell membranes and inhibition of bacterial cytokinesis (Van de Velde et al. 2010). Similarly, weevils of the genus *Sitophilus* carry an endosymbiotic *Gammaproteobacterium* that supplements the diet of its host with vitamins (Heddi et al. 1999). The weevil expresses an antimicrobial peptide, coleoptericin-A (ColA), which leads to filamentous symbiont cells that carry multiple genomes and are not able to undergo cell division. Additionally, ColA has bactericidal properties, implying a role in the insect's defense against microbial infections, aside from regulating symbiont number and localization (Login et al. 2011).

In the giant tubeworm *Riftia pachyptila,* detailed analyses of the trophosome have shown multiple morphotypes of its symbiont, ranging from rods to small cocci and big cocci. Each of these morphotypes can be found predominately in a specific region of a trophosome lobule, when viewed as a cross-section. The central zone harbors rod-shaped bacteria which show a high rate of division and only few cases of cell lysis; progressing towards the periphery, small cocci followed by big cocci are found. The cocci show only few division stages but cell lysis occurs often. It has therefore been hypothesized that the central rod-shaped bacteria function as "stem cells" by dividing and replenishing the symbiont pool. The symbiont cells that are pushed outwards are inhibited in division and grow into cocci,

and eventually will be lysed in what the authors termed the “degenerative zone” (Bright and Sorgo 2003). The mechanisms that facilitate the inhibition of cytokinesis and the morphological changes are still unknown.

The Stilbonematid symbiosis also appears to be under strict control. Each species investigated so far showed only association with a single phylotype of symbiont (Polz et al. 1994, Bayer et al. 2009, Bulgheresi et al. 2011, Pende et al. 2014). One of the key players in this specificity that could be identified so far is the calcium dependent C-type lectin Mermaid and its isoforms. Experiments on *Laxus oneistus* and *Stilbonema majum* showed that it is secreted by the worm in the symbiont-covered region, and some of its isoforms exhibit different affinities for the different symbionts (Bulgheresi et al. 2006, Bulgheresi et al. 2011). Most likely together with their symbionts, these worms manage to exclude any other bacterium from growing on their cuticle. Recently, two putative binding proteins from the lipopolysaccharide-binding protein (LBP) / bactericidal permeability-increasing (BPI) superfamily have been shown to be expressed in *L. oneistus*. Members of this superfamily are associated with the recognition and killing of gram-negative bacteria in vertebrates and invertebrates. Immunolocalization studies showed that in *L. oneistus*, the two putative proteins Lo-BPI1 and Lo-BPI2 are secreted throughout the whole nematode and also localize with the ectosymbiont. The symbionts seem not to be affected; together with the Mermaids, these proteins could be responsible for recruiting the correct symbiont and exclude other prokaryotes (Bauer 2012).

The symbiont localization pattern on *Laxus oneistus* cuticle exemplifies best how strongly regulated colonization is. The anterior end (Figure 8A, arrowhead) is completely symbiont

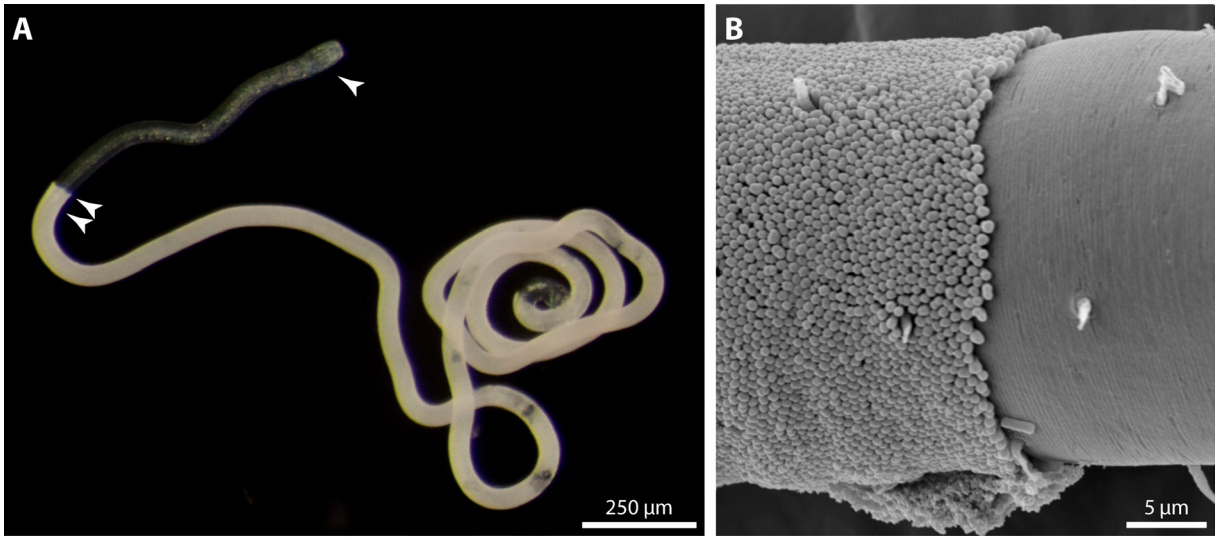

Figure 8: Habitus of *Laxus oneistus* and onset of its bacterial coat. (A) Shows the habitus of *Laxus oneistus* under incident light, the arrowhead points to the translucent anterior end, the double arrows to the onset of the bacterial coat which gives the worm its white color (Image courtesy of U. Dirks) (B) shows a scanning electron micrograph of the onset of the bacterial coat.

free, and the bacterial coverage starts at a gender-specific distance from the anterior end (Figure 8A, double arrows) at a clearly defined onset (Figure 8B). Furthermore, the diameter of the worm decreases by the length of the symbiont at this point. As a result, the worm's diameter stays constant despite being covered by the bacteria (Ott et al. 1995).

The glandular sensory organs (GSO) are complex epidermal glands and consist of two types of gland cells, a sensory cell and an epidermal cell, and are connected via the hollow setae to the outside. They are arranged in regular intervals throughout the whole body and secrete extracellular mucus that covers worm and symbiont (Nebelsick et al. 1992, Bauer-Nebelsick et al. 1995) and the Mermaid isoforms which confer symbiont attachment (Bulgheresi et al. 2006, Bulgheresi et al. 2011). The high numbers of GSOs, their gland cells and the fact that they are in contact with the environment via the hollow setae makes them the obvious starting point for further studies about whether the host influences the symbionts morphology and cell cycle and how. The use of comparative "Omics" in nematode systems (between symbiotic and non-symbiotic tissues, species and/or developmental stages) revealed convergent evolution and identified genes that convey host specificity, as well as microbial-eukaryotic lateral gene transfer (reviewed in

Murfin et al. 2012). *L. oneistus* is a good candidate to conduct such an "Omics" approach. By extracting RNA, proteins and metabolites from the GSOs located in the posterior, symbiotic body region and from the anterior, aposymbiotic region, nematode genes that are specifically expressed in the symbiotic region might be identified and screened for candidates that could be involved in symbiont control (e.g. PG-binding proteins or bacteriostatic/bacteriocidal compounds). A *L. oneistus* transcriptome is already available and will be helpful for the transcript annotation (accessible under http://genepool-blast.bio.ed.ac.uk/partigene/2008075_SilviaBulgheresi/) (Bulgheresi 2011).

Stable isotope experiments indicate that the worms metabolism is fueled by its autotrophic bacteria (Ott et al. 1991). Inducing longitudinal division (Los and Rhs) or filamentation (Efs and Eds) could be a strategy to increase bacterial biomass and therefore the fitness of the association (by being aligned perpendicular to the host surface, a higher amount of Los and Rhs cells can be attached, than if the symbionts were arranged parallel). Additionally, it was proposed that the symbiont can act as a protective mantel for the worm, considering that hydrogen sulfide is toxic for metazoans (Hentschel et al. 1999). Both *E. fertilis* and *E. dianeae* are predominantly found in a habitat with high sulfide concentrations. Carrying a higher bacterial biomass could be the factor which allowed them to colonize and persist in this environment.

We owe the discovery of these variations of canonical binary fission to the fact that these bacteria live in a mono-specific symbiotic association. Each worm carries a virtually pure culture of symbionts that are all exposed to the same environmental conditions. This fact, paired with their high abundances in their respective habitats, makes these associations highly useful model organisms to study multiple aspects of symbiotic interactions. While many symbioses are similarly constituted of only two partners, the stilbonematid system is unique as the association with the ectosymbiont persists throughout the whole nematodes life cycle, which includes four molting events (Ott et al. 1995). This aspect of the symbiosis allows us to tackle questions about eukaryote-prokaryote interactions (e.g. how is the association initiated? How is the ectosymbiont population maintained despite

the molting events? How are the symbionts kept under control?). Their location on the outside of the worm, combined with state of the art imaging techniques, should allow us to answer some of these questions. The advances in fluorescence microscopy over the last few years allows for resolution below the diffraction limit, reduced photo-toxicity and rapid 3D image acquisition (e.g. Gao et al. 2014) Therefore, imaging live worms-associated symbionts is now feasible.

By sampling this symbiotic association we can also obtain what is usually considered a paradox, a pure culture of environmental bacteria. This aspect is what allowed us to get the first insight into the life cycle of these bacteria, despite the fact that they are still uncultivable. Over the course of this thesis, the sampling and symbiont recovery techniques have been refined to a point where we can perform multiple experiments (e.g. morphometric analysis, 16S identification, immunofluorescence staining) with the population of a single worm.

One bottleneck that prevents broader comparative studies between multiple species is the fact that an overwhelming majority of bacteria found in the environment cannot be cultivated so far (Schloss and Handelsman 2004). However, the last few years saw the emergence of so called “high-throughput” cultivation methods. By separating single cells into gel microdroplets (Zengler et al. 2002), porous hollow fiber membranes (Aoi et al. 2009) or the wells of a chip (Nichols et al. 2010) and incubating these (where possible) under *in situ* conditions, many phylogenetic novel and so far uncultivated microbes can be eventually transitioned to grow on standard plates or in liquid culture. Future studies are needed to apply these methods in order to establish a culture of at least one member of the MONTS to further the understanding of the molecular mechanisms of cell division in detail. Establishing a MONTS culture would also allow us to explore to which extent the eukaryotic host influences the bacterial morphology and how they would grow and divide when the host is not present. This would allow us to see if e.g. the rod-shaped symbionts revert back to transverse fission when not host-associated.

The fact that all four of these closely related symbionts show such differences in their cell division raises the question: “How canonical is canonical binary fission?” It should also prompt us to re-evaluate how much we can generalize our findings from model-organisms to other bacterial species.

References

Aarsman, M. E., A. Piette, C. Fraipont, T. M. Vinkenvleugel, M. Nguyen-Distèche and T. den Blaauwen (2005). "Maturation of the *Escherichia coli* divisome occurs in two steps." Molecular Microbiology **55**(6): 1631-1645.

Adams, D. W. and J. Errington (2009). "Bacterial cell division: assembly, maintenance and disassembly of the Z ring." Nature Reviews Microbiology **7**(9): 642-653.

Amann, R. I., W. Ludwig and K. H. Schleifer (1995). "Phylogenetic identification and in situ detection of individual microbial cells without cultivation." Microbiology and Molecular Biology Reviews **59**(1): 143-169.

Angert, E. R. (2005). "Alternatives to binary fission in bacteria." Nature Reviews Microbiology **3**(3): 214-224.

Aoi, Y., T. Kinoshita, T. Hata, H. Ohta, H. Obokata and S. Tsuneda (2009). "Hollow-fiber membrane chamber as a device for in situ environmental cultivation." Applied and Environmental Microbiology **75**(11): 3826-3833.

Bailey, M. W., P. Bisicchia, B. T. Warren, D. J. Sherratt and J. Männik (2014). "Evidence for Divisome Localization Mechanisms Independent of the Min System and SlmA in *Escherichia coli*." PLoS genetics **10**(8): e1004504.

Bauer-Nebelsick, M., M. Blumer, W. Urbancik and J. A. Ott (1995). "The glandular sensory organ of Desmodoridae (Nematoda) - ultrastructure and phylogenetic implications." Invertebrate Biology **114**(3): 211-219.

Bauer, L. (2012). Molekulare Charakterisierung und Lokalisationsmuster zweier putativer Bakterien-permeabilisierender Proteine (BPI) eines marinen symbiotischen Nematoden (Molecular charaterisation and localization pattern of two putative bacteria-permeabilising proteins (BPI) of a marine symbiotic nematode). Thesis to

obtain Magister (Msc), University of Vienna, supervised by J. Ott and S. Bulgheresi, http://othes.univie.ac.at/21863/.

Bayer, C., N. R. Heindl, C. Rinke, S. Lücker, J. A. Ott and S. Bulgheresi (2009). "Molecular characterization of the symbionts associated with marine nematodes of the genus *Robbea*." Environmental Microbiology Reports **1**(2): 136-144.

Bean, G. J., S. T. Flickinger, W. M. Westler, M. E. McCully, D. Sept, D. B. Weibel and K. J. Amann (2009). "A22 disrupts the bacterial actin cytoskeleton by directly binding and inducing a low-affinity state in MreB." Biochemistry **48**(22): 4852-4857.

Bernhardt, T. G. and P. A. de Boer (2005). "SlmA, a nucleoid-associated, FtsZ binding protein required for blocking septal ring assembly over Chromosomes in *E. coli*." Molecular Cell **18**(5): 555-564.

Betzig, E., G. H. Patterson, R. Sougrat and O. W. Lindwasser (2006). "Imaging intracellular fluorescent proteins at nanometer resolution." Science **313**: 1642-1645.

Bi, E. F. and J. Lutkenhaus (1991). "FtsZ ring structure associated with division in *Escherichia coli*." Nature **354**(6349): 161-164.

Boucher, D. H., S. James and K. H. Keeler (1982). "The ecology of mutualism." Annual Review of Ecology and Systematics **13**: 315-347.

Bramkamp, M., R. Emmins, L. Weston, C. Donovan, R. A. Daniel and J. Errington (2008). "A novel component of the division-site selection system of *Bacillus subtilis* and a new mode of action for the division inhibitor MinCD." Molecular Microbiology **70**(6): 1556-1569.

Bright, M. and S. Bulgheresi (2010). "A complex journey: transmission of microbial symbionts." Nature Reviews Microbiology **8**(3): 218-230.

Bright, M., J. Klose and A. D. Nussbaumer (2013). "Giant tubeworms." Current Biology **23**(6): R224-R225.

Bright, M. and A. Sorgo (2003). "Ultrastructural reinvestigation of the trophosome in adults of *Riftia pachyptila* (Annelida, Siboglinidae)." Invertebrate Biology **122**(4): 347-368.

Bulgheresi, S. (2011). "Calling the roll on Laxus oneistus immune defense molecules." Symbiosis **55**(3): 127-135.

Bulgheresi, S., H. R. Gruber-Vodicka, N. R. Heindl, U. Dirks, M. Kostadinova, H. Breiteneder and J. A. Ott (2011). "Sequence variability of the pattern recognition receptor Mermaid mediates specificity of marine nematode symbioses." The ISME journal **5**(6): 986-998.

Bulgheresi, S., I. Schabussova, T. Chen, N. P. Mullin, R. M. Maizels and J. A. Ott (2006). "A New C-Type Lectin Similar to the Human Immunoreceptor DC-SIGN Mediates Symbiont Acquisition by a Marine Nematode." Applied and Environmental Microbiology **72**(4): 2950-2956.

Bulloch, W. (1960). The history of bacteriology. London, Oxford University Press.

Carballido-López, R. (2006). "The bacterial actin-like cytoskeleton." Microbiology and Molecular Biology Reviews **70**(4): 888-909.

Cavanaugh, C. M., S. L. Gardiner, M. L. Jones, H. W. Jannasch and J. B. Waterbury (1981). "Prokaryotic cells in the hydrothermal vent tube worm *Riftia pachyptila* Jones: possible chemoautotrophic symbionts." Science **213**(4505): 340-342.

Chalfie, M., Y. Tu, G. Euskirchen, W. W. Ward and D. C. Prasher (1994). "Green fluorescent protein as a marker for gene expression." Science **263**(5148): 802-805.

Chang, F. and K. C. Huang (2014). "How and why cells grow as rods." BMC biology **12**(54).

de Boer, P. A. (2010). "Advances in understanding *E. coli* cell fission." Current Opinion in Microbiology **13**(6): 730-737.

de Boer, P. A., R. E. Crossley, A. R. Hand and L. I. Rothfield (1991). "The MinD protein is a membrane ATPase required for the correct placement of the *Escherichia coli* division site." The EMBO journal **10**(13): 4371-4380.

de Boer, P. A. J., R. E. Crossley and L. I. Rothfield (1989). "A division inhibitor and a topological specificity factor coded for by the minicell locus determine proper placement of the division septum in *E. coli*." Cell **56**(4): 641-649.

den Blaauwen, T., M. A. de Pedro, M. Nguyen-Disteche and J. A. Ayala (2008). "Morphogenesis of rod-shaped sacculi." FEMS Microbiology Reviews **32**(2): 321-344.

Douglas, A. E. (2011). "Lessons from studying insect symbioses." Cell host & microbe **10**(4): 359-367.

Dubilier, N., C. Bergin and C. Lott (2008). "Symbiotic diversity in marine animals: the art of harnessing chemosynthesis." Nature Reviews Microbiology **6**(10): 725-740.

Dyall, S. D., M. T. Brown and P. J. Johnson (2004). "Ancient Invasions: From Endosymbionts to Organelles." Science **304**(5668): 253-257.

Erickson, H. P., D. E. Anderson and M. Osawa (2010). "FtsZ in bacterial cytokinesis: cytoskeleton and force generator all in one." Microbiology and Molecular Biology Reviews **74**(4): 504-528.

Errington, J. (2003). "Dynamic proteins and a cytoskeleton in bacteria." Nature Cell Biology **5**: 175-178.

Felbeck, H., J. J. Childress and G. N. Somero (1981). "Calvin-Benson cycle and sulphide oxidation enzymes in animals from sulphide-rich habitats." Nature **293**: 2.

Fenton, A. K. and K. Gerdes (2013). "Direct interaction of FtsZ and MreB is required for septum synthesis and cell division in *Escherichia coli*." The EMBO journal **32**: 1953-1965.

Gao, L., L. Shao, B. C. Chen and E. Betzig (2014). "3D live fluorescence imaging of cellular dynamics using Bessel beam plane illumination microscopy." Nature protocols **9**: 1083-1101.

Gilson, P. R. and P. L. Beech (2001). "Cell division protein FtsZ: running rings around bacteria, chloroplasts and mitochondria." Research in Microbiology **152**(1): 3-10.

Gustafsson, M. G. L. (2005). "Nonlinear structured-illumination microscopy: wide-field fluorescence imaging with theoretically unlimited resolution." Proceedings of the National Academy of Sciences of the United States of America **102**(37): 13081-13086.

Heddi, A., A. M. Grenier, C. Khatchadourian, H. Charles and P. Nardon (1999). "Four intracellular genomes direct weevil biology: nuclear, mitochondrial, principal endosymbiont, and Wolbachia." Proceedings of the National Academy of Sciences of the United States of America **96**(12): 6814-6819.

Hentschel, U., E. C. Berger, M. Bright, H. Felbeck and J. A. Ott (1999). "Metabolism of nitrogen and sulfur in ectosymbiotic bacteria of marine nematodes(Nematoda, Stilbonematinae)." Marine Ecology Progress Series **183**: 149-158.

Hill, N. S., P. J. Buske and P. A. Levin (2013). "A moonlighting enzyme links *Escherichia coli* cell size with cenral metabolism." PLoS genetics **9**(7): e1003663.

Himmel, D., L. C. Maurin, O. Gros and J. L. Mansot (2009). "Raman microspectrometry sulfur detection and characterization in the marine ectosymbiotic nematode *Eubostrichus dianae* (Desmodoridae, Stilbonematidae)." Biology of the Cell **101**(1): 43-54.

Hu, Z. and J. Lutkenhaus (2000). "Analysis of MinC reveals two independent domains involved in interaction with MinD and FtsZ." Journal of Bacteriology **182**(14): 3965-3971.

Hu, Z. and J. Lutkenhaus (2003). "A conserved sequence at the C-terminus of MinD is

required for binding to the membrane and targeting MinC to the septum." Molecular Microbiology **47**(2): 345-355.

Hu, Z., C. Saez and J. Lutkenhaus (2003). "Recruitment of MinC, an Inhibitor of Z-Ring Formation, to the Membrane in *Escherichia coli*: Role of MinD and MinE." Journal of Bacteriology **185**(1): 196-203.

Joyce, E. P. and B. K. Daniel (2008). "MinJ (YvjD) is a topological determinant of cell division in *Bacillus subtilis*." Molecular Microbiology **70**(5): 1166-1179.

Kuru, E., H. Hughes, P. J. Brown and E. Hall (2012). "In situ probing of newly synthesized peptidoglycan in live bacteria with fluorescent D-amino acids." Angewandte Chemie **51**(50): 12519-12523.

Lackner, L. L., D. M. Raskin and P. A. De Boer (2003). "ATP-Dependent Interactions between *Escherichia coli* Min Proteins and the Phospholipid Membrane In Vitro." Journal of Bacteriology **185**(3): 735-749.

Lee, K.-H. and E. G. Ruby (1994). "Effect of the squid host on the abundance and distribution of symbiotic Vibrio fischeri in nature." Applied and Environmental Microbiology **60**(5): 1565-1571.

Leisch, N., N. Pende, J. Verheul, T. Den Blaauwen and S. Bulgheresi (in preparation). "Non-ring FtsZ-mediated cell constriction in a longitudinal dividing gammaproteobacterial symbiont."

Leisch, N., J. Verheul, N. R. Heindl, H. R. Gruber-Vodicka, N. Pende, T. den Blaauwen and S. Bulgheresi (2012). "Growth in width and FtsZ ring longitudinal positioning in a gammaproteobacterial symbiont." Current Biology **22**(19): R831-832.

Login, F. H., S. Balmand, A. Vallier, C. Vincent-Monegat, A. Vigneron, M. Weiss-Gayet, D. Rochat and A. Heddi (2011). "Antimicrobial peptides keep insect endosymbionts

under control." Science **334**(6054): 362-365.

Lutkenhaus, J. (2007). "Assembly dynamics of the bacterial MinCDE system and spatial regulation of the Z ring." Annual Review of Biochemistry **76**: 539-562.

Madigan, M. T., J. M. Martinko, P. V. Dunlap and D. P. Clark (2008). Brock - Biology of microorganisms. San Francisco, Benjamin Cummings.

Maloy, S. and M. Schaechter (2006). "The era of microbiology: a golden phoenix." International microbiology : the official journal of the Spanish Society for Microbiology **9**(1): 1-7.

Margolin, W. (2005). "FtsZ and the division of prokaryotic cells and organelles." Nature Reviews Molecular Cell Biology **6**(11): 862-871.

Marston, A. L. and J. Errington (1999). "Selection of the midcell division site in *Bacillus subtilis* through MinD-dependent polar localization and activation of MinC." Molecular Microbiology **33**(1): 84-96.

Marston, A. L., H. B. Thomaides, D. H. Edwards, M. E. Sharpe and J. Errington (1998). "Polar localization of the MinD protein of *Bacillus subtilis* and its role in selection of the mid-cell division site." Genes & Development **12**(21): 3419-3430.

Matsumoto, K., J. Kusaka, A. Nishibori and H. Hara (2006). "Lipid domains in bacterial membranes." Molecular Microbiology **61**(5): 1110-1117.

McFall-Ngai, M. (2008). "Are biologists in 'future shock'? Symbiosis integrates biology across domains." Nature Reviews Microbiology **6**(10): 789-792.

McFall-Ngai, M. (2014). "Divining the Essence of Symbiosis: Insights from the Squid-Vibrio Model." PLoS Biology **12**(2): e1001783.

McFall-Ngai, M., M. G. Hadfield, T. C. Bosch, et al. (2013). "Animals in a bacterial world, a new imperative for the life sciences." Proceedings of the National Academy of

Sciences of the United States of America **110**(9): 3229-3236.

Meier, E. L. and E. D. Goley (2014). "Form and function of the bacterial cytokinetic ring." Current Opinion in Cell Biology **26**: 19-27.

Mileykovskaya, E. and W. Dowhan (2005). "Role of membrane lipids in bacterial division-site selection." Current Opinion in Microbiology **8**(2): 135-142.

Mingorance, J., G. Rivas, M. Vélez, P. Gómez-Puertas and M. Vicente (2010). "Strong FtsZ is with the force: mechanisms to constrict bacteria." Trends in Microbiology **18**(8): 348-356.

Moriya, S., R. A. Rashid, C. D. A. Rodrigues and E. J. Harry (2010). "Influence of the nucleoid and the early stages of DNA replication on positioning the division site in *Bacillus subtilis*." Molecular Microbiology **76**(3): 634-647.

Murfin, K. E., A. R. Dillman, J. M. Foster, S. Bulgheresi, B. E. Slatko, P. W. Sternberg and H. Goodrich-Blair (2012). "Nematode-bacterium symbioses—cooperation and conflict revealed in the "Omics" age." The Biological Bulletin **223**: 85-102.

Myers, G. (2012). "Why bioimage informatics matters." Nature Methods **9**: 659-660.

Nanninga, N. (1991). "Cell division and peptidoglycan assembly in *Escherichia coli*." Molecular Microbiology **5**(4): 791-795.

Nebelsick, M., M. Blumer, R. Novak and J. Ott (1992). "A new glandular sensory organ in *Catanema sp.* (Nematoda, Stilbonematinae)." Zoomorphology **112**(1): 17-26.

Nichols, D., N. Cahoon, E. M. Trakhtenberg, L. Pham, A. Mehta, A. Belanger, T. Kanigan, K. Lewis and S. S. Epstein (2010). "Use of Ichip for High-Throughput In Situ Cultivation of "Uncultivable" Microbial Species." Applied and Environmental Microbiology **76**(8): 2445-2450.

Noffke, N., D. Christian, D. Wacey and R. M. Hazen (2013). "Microbially induced sedimentary

structures recording an ancient ecosystem in the ca. 3.48 billion-year-old Dresser Formation, Pilbara, Western Australia." Astrobiology **13**(12): 1103-1124.

Osawa, M., D. E. Anderson and H. P. Erickson (2008). "Reconstitution of contractile FtsZ rings in liposomes." Science **320**(5877): 792-794.

Osawa, M. and H. P. Erickson (2013). "Liposome division by a simple bacterial division machinery." Proceedings of the National Academy of Sciences of the United States of America **110**(27): 11000-11004.

Osteryoung, K. W. (2001). "Organelle fission in eukaryotes." Current Opinion in Microbiology **4**(6): 639-646.

Ott, J., M. Bright and S. Bulgheresi (2004). "Symbioses between marine nematodes and sulfur-oxidizing chemoautotrophic bacteria." Symbiosis **36**: 103-126.

Ott, J. A., M. Bauer-Nebelsick and V. Novotny (1995). "The genus *Laxus* Cobb, 1894 (Stilbonematinae: Nematoda) Description of two new species with ectosymbiotic chemoautotrophic bacteria." Proceedings of the Biological Society of Washington **108**(3): 508-527.

Ott, J. A., R. Novak, F. Schiemer, U. Hentschel, M. Nebelsick and M. F. Polz (1991). "Tackling the Sulfide Gradient: A Novel Strategy Involving Marine Nematodes and Chemoautotrophic Ectosymbionts." Marine Ecology **12**(3): 261-279.

Pace, N. R., D. A. Stahl, D. J. Lane and G. J. Olsen (1986). The Analysis of Natural Microbial Populations by Ribosomal RNA Sequences. Advances in Microbial Ecology. K. C. Marshall. New York, Springer US. **9:** 1-55.

Pende, N., N. Leisch, H. R. Gruber-Vodicka, N. R. Heindl, J. A. Ott, T. Den Blaauwen and S. Bulgheresi (2014). "Size-independent symmetric division in extraordinarily long cells." Nature communications **5**: 4803.

Pinho, M. G., M. Kjos and J.-W. Veening (2013). "How to get (a)round: mechanisms

controlling growth and division of coccoid bacteria." Nature Reviews Microbiology **11**(9): 601-614.

Pogliano, J., N. Osborne, M. D. Sharp, A. Abanes-De Mello, A. Perez, Y.-L. Sun and K. Pogliano (1999). "A vital stain for studying membrane dynamics in bacteria: a novel mechanism controlling septation during Bacillus subtilis sporulation." Molecular Microbiology **31**(4): 1149-1159.

Polz, M., H. Felbeck, R. Novak, M. Nebelsick and J. A. Ott (1992). "Chemoautotrophic, sulfur-oxidizing symbiotic bacteria on marine nematodes: Morphological and biochemical characterization." Microbial Ecology **24**(3): 313-329.

Polz, M. F., D. L. Distel, B. Zarda, R. Amann, H. Felbeck, J. A. Ott and C. M. Cavanaugh (1994). "Phylogenetic analysis of a highly specific association between ectosymbiotic, sulfur-oxidizing bacteria and a marine nematode." Applied and Environmental Microbiology **60**(12): 4461-4467.

Potluri, L. P., S. Kannan and K. D. Young (2012). "ZipA Is Required for FtsZ-Dependent Preseptal Peptidoglycan Synthesis prior to Invagination during Cell Division." Journal of Bacteriology **194**(19): 5334-5342.

Raskin, D. M. and P. de Boer (1997). "The MinE Ring: An FtsZ-Independent Cell Structure Required for Selection of the Correct Division Site in *E. coli*." Cell **91**(5): 685-694.

Raskin, D. M. and P. A. de Boer (1999). "Rapid pole-to-pole oscillation of a protein required for directing division to the middle of *Escherichia coli*." Proceedings of the National Academy of Sciences of the United States of America **96**(9): 4971-4976.

Rodrigues, C. D. and E. J. Harry (2012). "The Min system and nucleoid occlusion are not required for identifying the division site in *Bacillus subtilis* but ensure its efficient utilization." PLoS genetics **8**(3): e1002561.

Schloss, P. D. and J. Handelsman (2004). "Status of the microbial census." Microbiology and

Molecular Biology Reviews **68**(4): 686-691.

Sharp, K. H., S. K. Davidson and M. G. Haygood (2007). "Localization of *'Candidatus* Endobugula sertula' and the bryostatins throughout the life cycle of the bryozoan *Bugula neritina*." The ISME journal **1**(8): 693-702.

Shen, B. and J. Lutkenhaus (2010). "Examination of the interaction between FtsZ and MinCN in *E. coli* suggests how MinC disrupts Z rings." Molecular Microbiology **75**(5): 1285-1298.

Shih, Y.-L. L. and L. Rothfield (2006). "The bacterial cytoskeleton." Microbiology and Molecular Biology Reviews **70**(3): 729-754.

Siegrist, M. S., S. Whiteside, J. C. Jewett, A. Aditham, F. Cava and C. R. Bertozzi (2013). "(D)-amino acid chemical reporters reveal peptidoglycan dynamics of an intracellular pathogen." ACS chemical biology **8**(3): 500-505.

Tchesunov, A. V. (2013). "Marine free-living nematodes of the subfamily Stilbonematinae (Nematoda, Desmodoridae): taxonomic review with descriptions of a few species from the Nha Trang Bay, Central Vietnam." Meiofauna Marina **20**: 71-94.

Teeffelen, V. S., S. Wang, L. Furchtgott, K. C. Huang, N. S. Wingreen, J. W. Shaevitz and Z. Gitai (2011). "The bacterial actin MreB rotates, and rotation depends on cell-wall assembly." Proceedings of the National Academy of Sciences of the United States of America **180**(38): 15822-15827.

Treuner-Lange, A., K. Aguiluz, C. van der Does, et al. (2013). "PomZ, a ParA like protein, regulates Z ring formation and cell division in *Myxococcus xanthus*." Molecular Microbiology **87**(2): 235-253.

Turner, R. D., A. F. Hurd, A. Cadby, J. K. Hobbs and S. J. Foster (2013). "Cell wall elongation mode in Gram-negative bacteria is determined by peptidoglycan architecture." Nature communications **4**: 1496.

Typas, A., M. Banzhaf, C. Gross and W. Vollmer (2012). "From the regulation of peptidoglycan synthesis to bacterial growth and morphology." Nature Reviews Microbiology **10**(2): 123-136.

Ursell, T. S., J. Nguyen, R. D. Monds, A. Colavin, G. Billings, N. Ouzounov, Z. Gitai, J. W. Shaevitz and K. C. Huang (2014). "Rod-like bacterial shape is maintained by feedback between cell curvature and cytoskeletal localization." Proceedings of the National Academy of Sciences of the United States of America **111**(11): E1025–E1034.

Van de Velde, W., G. Zehirov, A. Szatmari, et al. (2010). "Plant peptides govern terminal differentiation of bacteria in symbiosis." Science **327**(5969): 1122-1126.

Vaughan, S., B. Wickstead, K. Gull and S. G. Addinall (2004). "Molecular evolution of FtsZ protein sequences encoded within the genomes of archaea, bacteria, and eukaryota." Journal of Molecular Evolution **58**(1): 19-29.

Weart, R. B., A. H. Lee, A. C. Chien, D. P. Haeusser, N. S. Hill and P. A. Levin (2007). "A metabolic sensor governing cell size in bacteria." Cell **130**(2): 335-347.

Willemse, J., J. W. Borst, E. de Waal, T. Bisseling and G. P. van Wezel (2011). "Positive control of cell division: FtsZ is recruited by SsgB during sporulation of *Streptomyces*." Genes & Development **25**(1): 89-99.

Woese, C. R. and G. E. Fox (1977). "Phylogenetic structure of the prokaryotic domain: the primary kingdoms." Proceedings of the National Academy of Sciences of the United States of America **74**(11): 5088-5090.

Wu, L. J. and J. Errington (2004). "Coordination of Cell Division and Chromosome Segregation by a Nucleoid Occlusion Protein in *Bacillus subtilis*." Cell **117**(25): 915-925.

Wu, L. J. and J. Errington (2012). "Nucleoid occlusion and bacterial cell division." Nature Reviews Microbiology **10**(1): 8-12.

Ying, L., H. Jen, Z. Lingyun, C. Yiwen, S. Weina, H. Kerwyn Casey, W. Hong-Wei and Y. Sheng (2013). "FtsZ Protofilaments Use a Hinge-Opening Mechanism for Constrictive Force Generation." Science **341**(6144): 392-395.

Young, K. D. (2006). "The Selective Value of Bacterial Shape." Microbiology and Molecular Biology Reviews **70**(3): 660-703.

Young, K. D. (2007). "Bacterial morphology: why have different shapes?" Current Opinion in Microbiology **10**(6): 596-600.

Young, K. D. (2010). "Bacterial shape: two-dimensional questions and possibilities." Annual Review of Microbiology **64**: 223-240.

Yu, X. C. and W. Margolin (1999). "FtsZ ring clusters in min and partition mutants: role of both the Min system and the nucleoid in regulating FtsZ ring localization." Molecular Microbiology **32**(2): 315-326.

Zengler, K., G. Toledo, M. Rappé, J. Elkins, E. J. Mathur, J. M. Short and M. Keller (2002). "Cultivating the uncultured." Proceedings of the National Academy of Sciences of the United States of America **99**(24): 15681-15686.

Zieske, K. and P. Schwille (2014). "Reconstitution of self-organizing protein gradients as spatial cues in cell-free systems." eLife.

Appendix

Appendix 1 - Summary in English

Research in the area of bacterial cell biology over the last two decades showed that the majority of all prokaryotes possess tubulin and actin homologues, and both growth and cell division are highly complex and orchestrated processes, governed by protein machineries that localize at precise sub-cellular locations. Many prokaryotes engage in symbiotic association with eukaryotic hosts, which allows them to e.g. utilize additional energy resources, access to additional habitats, or increase their locomotion. The free-living marine nematodes of the sub-family Stilbonematinae live in such an association. Each species' cuticle is covered by a single gammaproteobacterial phylotype, which is arranged in a species-specific manner. The worm's movement transports the bacteria through both sulfide- and oxygen-rich sediments, essential components to enable the bacterial chemoautotrophic metabolism which will eventually feed the host.

The main goal of this thesis was to characterize growth and division of Stilbonematid symbionts, gain insights into the life cycle of these basal *Gammaproteobacteria,* understand how the symbiotic lifestyle might influence them and shed light on what the conserved paradigms in bacterial cell division are. In addition, novel host-symbiont systems were taxonomically and morphologically characterized.

This thesis describes the growth and division mode of two rod-shaped symbionts (the symbiont of *Laxus oneistus*, termed Los, and the symbiont of *Robbea hypermnestra*, termed Rhs) and two filamentous symbionts (the symbiont of *Eubostrichus fertilis*, termed Efs, and the symbiont of *Eubostrichus dianeae*, termed Eds). We applied automated digital image analysis, scanning and transmission electron microscopy to isolated cells, and conducted immunostaining experiments to elucidate the sub-cellular localization pattern of the cell division protein FtsZ. Our data showed that the rod-shaped cells of Los and Rhs grow in width instead of length and we demonstrated that their default way of dividing is along their longitudinal axis as. However, while in Los a single Z-ellipse spans the whole length of the cell and constricts synchronously, in Rhs the nematode-attached pole starts

invagination earlier than the apical pole. This is mediated by a non-ring accumulation of FtsZ and the Z-ellipse only gets formed later in the division process. The two filamentous symbionts Efs and Eds divide by binary fission, but Efs can divide at virtually any length between 4 and 45 µm. In comparison, Eds can grow up to 120 µm long and positions the Z-ring precisely at mid-cell. Additionally, as both worms and symbionts cannot be cultivated, the adaptation of a buffer for the chemical fixation of marine invertebrates and their symbionts for electron microscopy is reported. It doesn't utilize toxic components and results in better ultrastructural preservation. Many of the stilbonematid species still lack a formal description; to contribute to a more complete picture of the species and their distribution, and to allow proper identification, four new stilbonematid species were described. Due to its high abundance *Eubostrichus fertilis* was an ideal candidate for the symbiont characterization. The description of *Robbea hypermnestra*, host of one of the symbionts characterized, together with that of two more members of the genus *Robbea*, allowed us to corroborate the previously debated genus *Robbea*.

To conclude, all four investigated symbionts show pronounced deviations from the canonical bacterial cell division mode found in bacterial model organisms. This thesis provides the framework for future research of the cell biology underlying these deviations, and it emphasizes the need to expand the field of bacterial cell division to a broader range of non-model organisms.

Appendix 2 – Deutsche Zusammenfassung

Die Forschung in der bakteriellen Zellbiologie hat in den letzten zwei Dekaden gezeigt, dass die Mehrheit aller Prokaryoten über Tubulin- und Aktin - Homologe verfügen. Sowohl Zellwachstum als auch Zellteilung sind hoch komplexe Vorgänge, welche von Proteinmaschinerien, die präzise an sub-zellulären Positionen lokalisieren, organisiert werden. Viele Prokaryoten leben in einem symbiotischen Verhältnis mit eukaryotischen Wirten, welche ihnen z.B erlauben zusätzliche Energiequellen zu nutzen, oder zusätzliche Habitate zu erschließen. Die freilebenden marinen Fadenwürmer der Sub-Familie Stilbonematinae leben in solch einer Symbiose. Jede Wurmart trägt auf ihrer Kutikula artspezifische Bakterien desselben gammaproteobakteriellen Phylotyps. Durch die Bewegung des Wurmes werden die Bakterien durch Sulfid- und Sauerstoff-reiche Sedimente transportiert, die essentiellen Komponenten für den chemoautotrophen Metabolismus der Bakterien, welcher letztendlich den Wirt ernährt.

Das Hauptziel dieser Arbeit war die Charakterisierung des Wachstums und der Zellteilung der Stilbonematiden Symbionten um Einblick in den Lebenszyklus dieser basalen Gammaproteobakterien zu erhalten und zu sehen wie der symbiotische Lebenswandel die Bakterien beeinflussen könnte. Weiters sollte untersucht werden was die grundlegenden konservierten Faktoren der bakteriellen Zellteilung sind.

In dieser Arbeit werden Zellwachstum und Teilungsmodus von zwei stäbchenförmigen Bakterien (der Symbiont von *Laxus oneistus*, genannt Los und der Symbiont von *Robbea hypermnestra*, genannt Rhs) und zwei filamentartigen Bakterien (der Symbiont von *Eubostrichus fertilis*, genannt Efs und der Symbiont von *Eubostrichus dianeae*, genannt Eds) charakterisiert. Automatisierte digitale Bildanalyse, Raster- und Transmissionselektronenmikroskopie und Immunofärbe-Methoden um die subzelluläre Positionierung des Zellzeilungsprotein FtsZ zu visualisieren, wurden eingesetzt. Hierbei zeigte sich, dass die stäbchenförmigen Zellen von Los und Rhs in die Breite statt in die Länge wachsen und sich der Länge nach teilen. Während sich jedoch in Los die Z-Ellipse

gleichmäßig zusammenzieht, kommt es bei Rhs zuerst zur Einschnürung an dem Zellpol, der mit dem Wurm in Kontakt steht. Diese Einschnürung wird durch Nicht-ringförmige FtsZ Akkumulation verursacht. Erst später wird die Z-Ellipse gebildet. Die filamentösen Symbionten Efs und Eds teilen sich mittels binärer Zellteilung, jedoch teilt sich Efs in jeder Länge zwischen 4 und 45µm. Eds hingegen wird bis zu 120µm lang und positioniert den Z-Ring präzise in der Zellmitte. Da diese Würmer und ihre Symbionten nicht kultiviert werden können, wurde außerdem ein Puffer für die chemische Fixierung von Invertebraten und ihrer Symbionten für die Elektronenmikroskopie adaptiert. Der Puffer enthält keine toxischen Komponenten und ermöglicht bessere ultrastrukturelle Erhaltung. Viele der Stilbonematiden sind noch nicht formal beschrieben. Um einen besseren Überblick über die verschiedenen Arten zu geben und um eine korrekte Identifizierung der Arten zu ermöglichen, wurden vier neue Spezies beschrieben. Aufgrund der hohen Abundanz war *Eubostrichus fertilis* ideal, um die Charakterisierung der Symbionten durchzuführen. Die Beschreibung von *Robbea hypermnestra*, des Wirts einer der untersuchten Symbionten, gemeinsam mit der Beschreibung zwei weiterer Arten konnte die bisher fragliche Gattung *Robbea* bestätigen.

Alle vier untersuchten Symbionten zeigen ausgeprägte Abweichungen von der bakteriellen Zellteilung welche in Modellorganismen dokumentiert wurde. Diese Arbeit schafft den Rahmen für zukünftige tiefergehende Studien über die Zellbiologie die diesen Abweichungen zugrunde liegt und zeigt die Notwendigkeit auf, das Feld der bakteriellen Zellbiologie auf Nicht-Modellorganismen auszudehnen.

Appendix 3 - Acknowledgements

A bit over three years ago, I decided that "I'll do a Ph.D.", but looking back at this journey I came to realize that I couldn't be where I am today without the help and support of many people. Therefore, I'd like to take the chance of saying thanks to all of you!

First and foremost many, many thanks to Silvia Bulgheresi, you initially offered me this amazing chance and were there every step of the way for discussion, guidance, advice and supervision. Thanks for all the help, the patience as well as all the non-scientific fun we had. Your unending enthusiasm for science is time and time again inspiring. A big thank is also due to Christa Schleper for all the advice and support she gave me during my Ph.D. studies

Many, many thanks go to Tanneke den Blaauwen for all the help and support I received from you. Without your help I'd probably still be at square one of this puzzle. Thanks for welcoming me to your lab in Amsterdam over and over again, answering any question at any day or night time and in general showing a lot of patience with a marine biologist from a landlocked country, dabbling in bacterial cell biology. I'm also greatly indebted to Jolanda Verheul for all your help and guidance in the lab and on the microscopes. One can't but be infected by your enthusiasm for science (and music), and I enjoyed working with you every single time I visited.

I'm very grateful to Jörg Ott, not only for introducing me to the fascinating world of symbiotic meiofauna but also for all his help tackling the (sometimes tricky) hosts again and again.

Thanks also go the whole shallow water symbiosis group and all its past and present members, Ulrich Dirks, Lisa Bauer, Harald Gruber-Vodicka, Nika Pende and Amir Schmidt.

Every single one of you somehow contributed to this work. Be it in the lab, in the field or during the times outside of the lab.

I also want to extend my thanks to Wolfang Miller and his group for the excellent meetings we shared.

A big thanks to the "old office gang" Clarissa Schwab, Melina Kerou and Michaela Stieglmeier for all the help during the last years as well as all the non-scientific discussion on movies, music, politics and TV series we had.

Many, many thanks also go to Andreas Angermayr and Alice Sorgo for welcoming me again and again in your home, whenever my work led me to Amsterdam. You guys managed to make each of my stays memorable and I still owe you big time for that!

Thanks are also due to Melina Kerou, Michaela Stieglmeier, Manuela Ceccoli and Nika Pende for reading my thesis and pointing out all my mistakes to me.

I had the privilege to work with many great people in the Ecogenomics department: not only were you doing great science, but you were also great colleagues and friends. Thanks to Romana Bittner for fighting the lab chaos every single day; many thanks to the Cripsr group, you guys not only do amazing stuff (still not sure I got it properly) but you also know how to have a good time both in the lab and outside! Thanks also to everyone else for all the talks we had, the interesting discussions as well as all the fun. I'm also grateful to Tim Urich for his support and guidance in the last years.

Thanks also to the "Bier-um-Vier" regulars, Michala Stieglmeir, Tim Urich, Melina Kerou, Pierre Offre, Isabelle Zink and everyone else who joined; make sure to keep the tradition alive!

I'd also like to thank Jacqueline Montanaro for delightful discussions about electron microscopy.

I'm very grateful to the colleagues from the Smithsonian Institute for the chance of working

on the marine station of Carrie Bow Caye, probably one of the best places in the world for a marine biologist to do his field work. Especially I'd like to thank Zach Foltz and Michael Jones for their tireless work behind the scenes to make each research stay as flawless as possible and big thanks as well to the station managers who took care of us and were supporting our science day in and day out.

I also want to thank my Ph.D. support team outside the confines of the University, Philipp Korntner and Mario Schimak for all the moral support when times were dire, the good advice you gave me and most importantly for all the non-scientific things we got to share. Thanks also have to go to an unnamed underwater volcano, whose (un)timely eruption eventually landed me in shallow water symbiosis research.

I'm also very thankful to my family who always supported my pursuit of science, the sea and its weird creatures. And last but not least I'd like to thank my otter half, Manuela Ceccoli, you were by my side all these years, supported me when things weren't going well and picked up my slack when my head was in the clouds of science again.

Appendix 4 – *Curriculum Vitae*

Mag. Nikolaus Leisch

Studies

2002-2010	M.Sc. Biology/Ecology with focus on marine biology, University of Vienna, Austria
	Master thesis "**Microanatomy of the trophosome region of the Platyhelminthes *Paracatenula* c.f. *polyhymnia***" under the supervision of Univ. Prof. Dr. Jörg Ott
Since 09/2011 -	Ph.D. Student at the Department of Ecogenomics and System Biology,
	University of Vienna, Austria on **„Marine nematode-bacteria symbiosis: New species and unexpected bacterial reproduction strategies"** under the supervision of Univ. Prof. Dr. Christa Schleper and Dr. Silvia Bulgheresi

Oral presentations

2012	"**Keeping in touch - Longitudinal fission in the *Laxus oneistus* ectosymbiont"** at the International Symposium for Microbial Ecology 14, Copenhagen, Denmark
2014	"**Longitudinal division in nematode-associated Gammaproteobacteria"** at the Academy Colloquium "50 Years of Fts: the A-Z of Bacterial Cell Division" of the Royal Netherlands Academy of Arts and Sciences in Amsterdam, The Netherlands (Talk in the master class for PhD Students)

Poster presentations

2012	**Keeping in touch - Longitudinal fission of the *Laxus oneistus* ectosymbiont** at the Symbiomics Field Workshop on Shallow Water Symbiosis, HYDRA Institute for Marine Sciences, Elba, Italy
2013	**Symmetric FtsZ-based fission in extraordinary long *Gammaproteobacteria*** at the 2013 Annual Meeting of the American Society for Cell Biology in New Orleans, USA
2014	**Reproduction strategies of stilbonematid ectosymbionts** at the 2nd Symbiomics Field Workshop, HYDRA Institute for Marine Sciences, Elba, Italy

Awards/Stipends

2012	Travel grants from the International Society for Microbial Ecology and the University of Vienna to participate at the ISME 14 in Copenhagen, Denmark
2013	Travel Grant from the University of Vienna to participate at the 2013 Annual Meeting of the American Society for Cell Biology in New Orleans, USA
2013/2014	Stipends from the University of Vienna for field work at the Carrie Bow Cay Field Station (Belize) of the Smithsonian National Museum of Natural History in March 2013 and March 2014
2014	Stipend from the Austrian Research Association (ÖFG) to conduct research at the University of Amsterdam and participate in the Academy Colloquium "50 Years of Fts: the A-Z of Bacterial Cell Division" of the Royal Netherlands Academy of Arts and Sciences in Amsterdam, The Netherlands
2014	Ph.D. completion grant from the University of Vienna
2014	The talk "Be fruitful, and multiply – Reproduction in the E. fertilis symbiosis", presented at the Science day at the Faculty of Life Sciences, Vienna, Austria, was selected as "Best PhD presentation".

Publications

H R Gruber-Vodicka, U Dirks, **N Leisch**, C Baranyi, K Stoecker, S Bulgheresi, N R Heindl, M Horn, C Lott, A Loy, M Wagner and J A Ott. ***Paracatenula*, an ancient symbiosis between thiotrophic Alphaproteobacteria and catenulid flatworms**. Proceedings of the National Academy of Science of the United States of America **108**(29): 12078-12083

N Leisch, U Dirks, H R Gruber-Vodicka, M Schmid, W Sterrer and J A Ott **Microanatomy of the trophosome region of *Paracatenula* cf. *polyhymnia* (Catenulida, Platyhelminthes) and its intracellular symbionts.** Zoomorphology **130**(4): 261-271

U Dirks, H R Gruber-Vodicka, **N Leisch**, W Sterrer and J A Ott **A new species of symbiotic flatworms, *Paracatenula galateia* sp. nov. (Platyhelminthes: Catenulida: Retronectidae) from Belize (Central America).** Marine Biology Research **7**(8): 769-777

U Dirks, H R Gruber-Vodicka, **N Leisch**, S Bulgheresi, B Egger, P Ladurner and J A Ott **Bacterial Symbiosis Maintenance in the Asexually Reproducing and Regenerating Flatworm *Paracatenula galateia*.** PLoS One **7**(4): e34709.

V Zheden, J von Byern, A Kerbl, **N Leisch**, Y Staedler, I Grunwald, A M Power, W Klepal **Morphology of the cement apparatus and the cement of the buoy barnacle *Dosima fascicularis* (Ellis & Solander, 1786) (Crustacea, Cirripedia, Thoracica, Lepadidae)** The Biological Bulletin **223**(2): 192-204

N Leisch, J Verheul, N R Heindl, H R Gruber-Vodicka, N Pende, T den Blaauwen and S Bulgheresi. **Growth in width and FtsZ ring longitudinal positioning in a gammaproteobacterial symbiont** Current Biology **22**(19): R831-R832

J A Ott, **N Leisch** and H R Gruber-Vodicka ***Eubostrichus fertilis* sp. n., a new marine nematode (Desmodoridae, Stilbonematinae) with an extraordinary reproductive potential from Belize, Central America.** Nematology **16**(7): 777-787

M Stieglmeier, A Klingl, R E J Alves, S Rittmann, M Melcher, **N Leisch** and Christa Schleper ***Nitrososphaera viennensis* sp. nov., an aerobic and mesophilic ammonia-oxidizing archaeon from soil and member of the novel archaeal phylum Thaumarchaeota** International Journal of Systematic and Evolutionary Microbiology **64**(8):2738-2752

J A Ott, H R Gruber-Vodicka, **N Leisch** and J Zimmermann **Phylogenetic confirmation of the genus *Robbea* GERLACH, 1956 (Nematoda: Desmodoridae, Stilbonematinae) with the description of three new species.** Systematics and Biodiversity **12**(4):434-455

N Pende*, **N Leisch***, H R Gruber-Vodicka, N R Heindl, J Ott, T den Blaauwen and S Bulgheresi **Size-independent symmetric division in extraordinarily long cells.** Nature Communications **5**: 4803

J Montanaro* and **N Leisch***, D Gruber, A Inic-Kanada, S Belij, E Stein, N Bintner, A Ladurner and T Barisani-Asenbauer **Preserving ultrastructure and morphology of tissue using PHEM buffered fixatives.** Journal of Microscopy (under review)

*these authors contributed equally